Adaptive Control for The Flying V

Master of Science Thesis

Rana Husain Ali Ul Haq

Delft University of Technology

TU Delft

Adaptive Control for The Flying V

Master of Science Thesis

by

Rana Husain Ali Ul Haq

to obtain the degree of Master of Science in Aerospace Engineering
at the Delft University of Technology
to be defended publicly on 7 January 2026 at 14:00

Student number:	4621271	
Project Duration:	10, 2023 - 12, 2025	
Graduation Committee:	Dr. ir. E. van Kampen	TU Delft, Main supervisor
	D. Atmaca MSc.	TU Delft, supervisor
	Dr. ir. C.C. de Visser	TU Delft, Chair
	Dr. M.J. Ribeiro	TU Delft, External Examiner
Institution:	Delft University of Technology	

Cover image of the Flying V image from: https://www.tudelft.nl/lr/flying-v

Background image used in the cover taken from:
https://pixabay.com/nl/photos/lucht-nederland-europa-nederlands-2165705/

An electronic version of this thesis is available at http://repository.tudelft.nl/

TU Delft

Contents

List of Figures

List of Tables

Nomenclature

List of Abbreviations

ABS Adaptive backstepping
AIDI adaptive IDI
ATM Air Traffic Management
BS Backstepping
CA Control Allocation
CAP Control Anticipation Parameters
CE Control Effectiveness
CFBS Command-Filtered Backstepping
CFD Computational Fluid Dynamics
CG Center of gravity
CLF Control Lyapunov Function
DB Dropback
DOF Degree of Freedom
EOM Equations of Motion
FAA International Air Transport Association
FAA Federal Aviation Administration
FC Fault Scenario
FCS Flight Control System
FEP Flight envelope protection
FS Full Scale
FTC Fault Tolerant Control
FTE Flight Test Experiments
FW Flying wing
IBS Incremental Backstepping
IDI Incremental Dynamic Inversion
INDI Incremental Nonlinear Dynamic Inversion
LTI Linear time-invariant
MIMO Multi-input and output
NDI Nonlinear Dynamic Inversion
OBS On-board Model
OS Overshoot
PID Proportional-Integral-Derivative
RLS Recursive Least Squares
RMS Root Mean Squared
SAF Sustainable Aviation Fuel
SMC Sliding Mode Control
SSFT Sub-Scale Flight Test
UAV Unmanned aerial vehicle
VLM Vortex Lattice Method
WTE Wind Tunnel Experiments

List of Symbols

α	Angle of attack	$^\circ$
β	Angle of sideslip	$^\circ$
V_t	Velocity	$\mathrm{m\,s^{-1}}$
V_a	Aerodynamic velocity vector	$\mathrm{m\,s^{-1}}$
h	Altitude	m
ρ	Density	$\mathrm{kg\,m^{-3}}$
$\bar{q}$	Dynamic pressure	Pa
V_∞	Freestream velocity	$\mathrm{m\,s^{-1}}$
M	Mach number	
t	Time	s
f	Generic scalar function	
$\mathbf{f}$	Generic vector function	
x	State variable	
$\mathbf{x}$	State vector	
u	Input variable	
$\mathbf{u}$	Input vector	
$\mathbf{e}$	Error	
ν	Virtual control input	
y	Output variable	
$\mathbf{y}$	Output vector	
θ	Generic parameter	
K	Generic gain constant	
A, B, C, D	State space matrices	
ω	Natural frequency	$\mathrm{rad/s}$
τ	Time constant	s
ζ	Damping ratio	
Δ	Incremental notation	
S	Wing surface Area	$\mathrm{m^2}$
b	Wing span	m
$\bar{c}$	Mean aerodynamic chord	m
m	Mass	kg
E	Earth reference frame	
B	Body reference frame	
a	Aerodynamic reference frame	
T	Transformation matrix	
$\mathbf{C}$	Rotation matrix	
C	Nondimensional aerodynamic coefficient	
X, Y, Z	Aerodynamic forces on x-y-z axis	N
L, M, N	Aerodynamic moments around x-y-z axis	N
F_X, F_Y, F_Z	Force around axis	N
M_X, M_Y, M_Z	Moment around axis	$\mathrm{N\,m}$
$\mathbf{x}$	Position vector	m
$\mathbf{v}$	Velocity vector	$\mathrm{m\,s^{-1}}$
$\mathbf{\Omega}$	Angular velocity matrix	$\mathrm{m\,s^{-1}}$
θ, ϕ, ψ	Attitude	$^\circ$
p, q, r	Rotational rates	$^\circ/\mathrm{s}$
$\dot{p}, \dot{q}, \dot{r}$	Rotational acceleration	$^\circ/\mathrm{s^2}$
I	Moment of Inertia	$\mathrm{kg \cdot m^2}$
$\mathbf{I}$	Moment of Inertia matrix	$\mathrm{kg \cdot m^2}$
δ	Control surface deflection	$^\circ$
$\mathbf{G}$	Control effectiveness matrix	

1

Introduction

This chapter serves as an introduction to the literature research and subsequent thesis that follows. The research context area is at first defined, where an introduction of the Flying V is described with the research activities to synthesize this new advanced aircraft design (1.1). Thereafter, the research motivation is defined (1.2) with the research scope defined in (1.3). The research objective and questions (1.4) describe the main objectives and questions to be answered in this research. At last, an outline of the research is described (1.5).

1.1. Research Context

Sustainability is a key commitment for future innovation and improvement of the aerospace industry. Regulatory bodies, institutions, and associations such as Federal Aviation Authority (FAA), European Parliament, International Air Transport Association (IATA) have established commitments and plans of working towards a Net-Zero sustainable Aviation by 2050 [1] [2] [3], through joint coordinated efforts by the industry and governments. The "Destination 2050" initiative outlines the potential route and strategy for establishing net zero CO_2 emissions by 2050. This Destination 2050 initiative presented a research report, which established four pillars of key innovations and measures necessary [1]:

1. Design improvements in aircraft and propulsion technologies
2. Use of sustainable aviation fuels (SAFs)
3. Implementing economic measures
4. Improvements in air traffic management (ATM) and aircraft operations

The interest in design improvements in aircraft or advanced aircraft design is motivated by the stagnation and asymptotic efficiency improvements for the traditional tube-and-wing configuration that has monopolized the past five decades of commercial aviation. Incremental steps were taken to improve efficiency, through improvements regarding disciplines such as aerodynamics, propulsion, structure, and avionics. These efficiency increases were compounded by constraints and demands such as higher payload capacity, passenger occupancy and producing less noise and emissions [2, 3]. The Destination "2050" project assigns projected emissions reduction across varying aircraft market segments, shown in Figure 1.1.

[1] IATA - Fly Net Zero: `https://www.iata.org/flynetzero`
[2] FAA - Aviation Climate Action Plan - `https://www.faa.gov/sustainability`
[3] European Union: Destination 2050 - `https://www.destination2050.eu/`

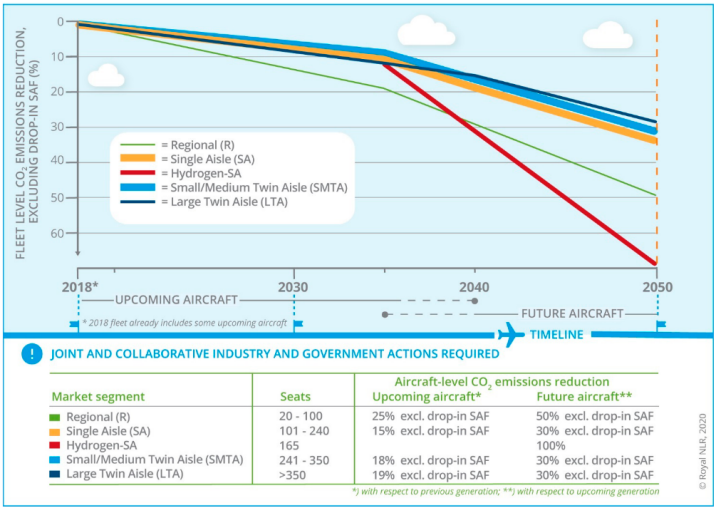

Figure 1.1: Projected emission reduction across varying aircraft market segments [1]

The realisation of these reductions can come through the use of new aircraft types that utilise hybrid-powered engines, but also have advanced aircraft configurations and designs such as C-wing, Box-Wing, joined wing, strut-braced wing (SBW), truss-braced wing (TBW), Blended Wing Body (BWB) and flying wing (FW) illustrated in Figure 1.2 & 1.3. The nature of their improved aerodynamic performance allows for drag minimisation or lift-to-drag maximisation when compared to conventional aircraft configuration. Thus, minimising environmental and noise footprint [1, 4].

(a) C-Wing (b) Box-Wing (c) Joined Wing

Figure 1.2: Advanced aircraft configurations set 1[4]

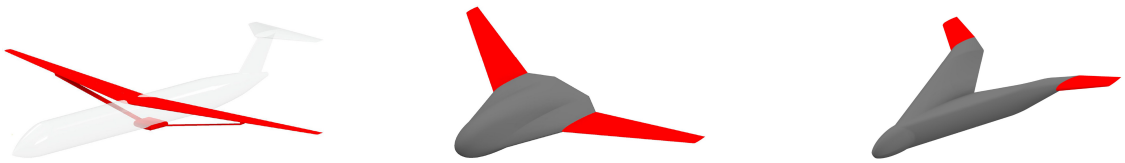

(a) strutt- & truss-braced wing design **(b)** Blended Wing Body (BWB) design **(c)** Flying Wing (FW) design

Figure 1.3: Advanced aircraft configuration set 2 [4]

Delft University of Technology (TU Delft) has multiple projects committed to further innovate and improve sustainability for aerospace and especially sustainable aviation [4]. One project aims to address the first pillar through an advanced aircraft design and configuration with the realization of a Flying wing (FW) concept, the Flying V.

The initial concept of the Flying V was first formed in 2013 at Airbus Future Projects in Hamburg by Benad [5], where a flying wing was designed consisting of two fuselage barrels in the shape of a V and a high sweep angle. Thus, creating a concept that allows for an efficient structure for a pressurized cabin with an aerodynamically favourable wing shape. Subsequent (feasibility) studies against a reference aircraft, A350-900 were conducted and a glider & powered version of the concept were

[4] sustainable aviation: `https://www.tudelft.nl/en/ae/sustainable-aviation`

constructed, thus demonstrating handling qualities and aerodynamic characteristics. Preliminary estimations determined 10 % higher lift-to-drag and 2% lower empty weight compared to an A350-900 [6, 7]. The proposed concept caught interest and studies followed at the TU Delft, where an aerodynamic optimization study was conducted, at cruising conditions with a Mach number of 0.85, altitude of 13000m and lift coefficient of 0.26. The study presented an estimation of 25 % higher lift-to-drag ratio compared to the NASA Common Research Model (CRM) [8, 9]. Some key changes with the aerodynamic optimization were made in regard to the wing platform and cabin cross-section of the conceptual design, as shown in Figure 1.4 & 1.5.

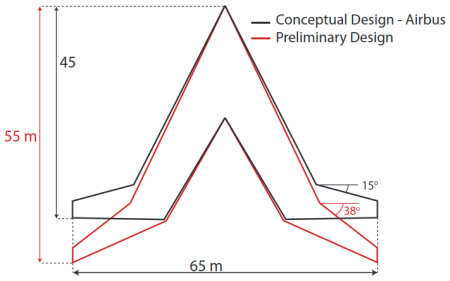

Figure 1.4: Updated aircraft planform [8]

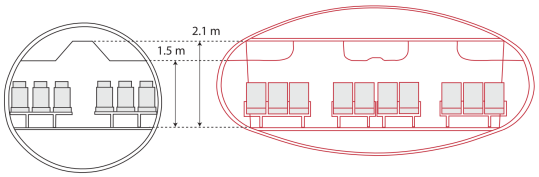

Figure 1.5: Cabin cross-section from cylindrical to oval [8]

Concurrently, a parameterization of the structural design was performed [10] with a study against an A350-like aircraft reference aircraft. The study showed a 17% lower Finite Element Method (FEM) weight where the sizing was done based upon different load cases and the maximum stress allowable assuming an all-aluminium structure [11]. The baseline set by the aerodynamic and structural analysis was used in a rudimentary design synthesis process, which resulted in estimations of a fuel burn reduction of 20% compared to a modern twin-aisle aircraft [7].
This presented grounded arguments to advance further and research the development of this aircraft by the TU Delft, The Flying V as shown in Figure 1.6 [5] as a concept art render, while adhering to the necessary certifications for realisation as a viable and more energy-efficient alternative to the conventional tube-and-wing design.

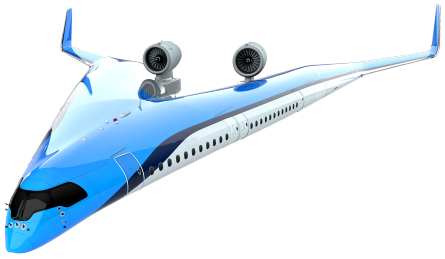

Figure 1.6: The Flying V aircraft conceptual render

1.2. Research Motivation

It can be observed that the design of the Flight Control System (FCS) is a multidisciplinary activity with significant effort and costs. A common design strategy in the civil and military domain of the aerospace industry is based on a divide and conquer approach, whereby a nonlinear control design task is decomposed into several linear sub-problems [12]. Where for the design of a nonlinear aircraft, linearized models are determined and used for control design at various operation points of the flight envelope. One classical method, which has been widely used and certified for FCS over the last decades, is gain-scheduling [12].

Gain scheduling adjusts the controller parameters based on the plant dynamics (aircraft) and auxiliary measurements such as altitude (h), Mach number (M), angle of attack (α). The method uses a lookup table and appropriate logic for selecting the designed control parameter to operate in that condition. Thus, sets of control parameters can be designed and scheduled over an envelope, to obtain

[5] Taken from `https://www.tudelft.nl/lr/flying-v/`

a global controller. However, frequent and rapid changes can lead to instability in addition to no logic for adjusting its strategy under the presence of changes in aircraft dynamics, which can occur due to causes such as component failure or atmospheric disturbances, thus the FCS cannot ensure optimal performance and handling qualities, thus significantly increasing pilot workload. The development and implementation of such a controller is also costly and requires significant research and effort, as the designed controller needs to be validated for a broad region of the flight envelope [13].

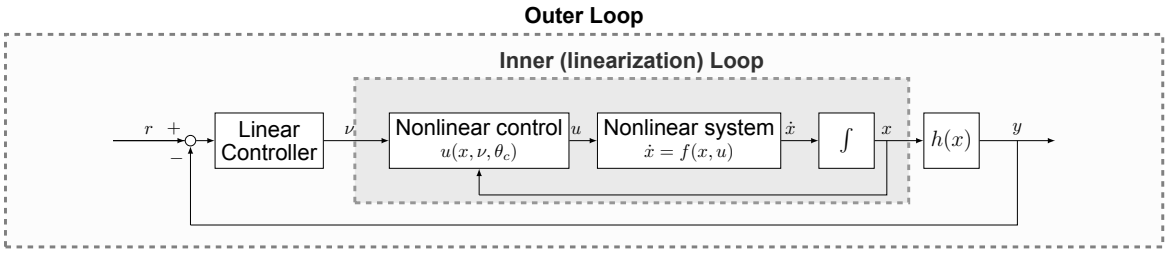

Figure 1.7: General block diagram for nonlinear control methods

One class of methods to overcome the significant effort that is demanded with gain-scheduling, are nonlinear control methods, such as Nonlinear Dynamic Version (NDI) or Backstepping (BS), which incorporate aircraft dynamics to handle the nonlinearities of the aircraft (*model-based*). Thus, by using the dynamics in its control design, these methods can provide a linearized inner loop system with a single outer loop linear controller for controlling the aircraft, as shown in Figure 1.7. Using such a technique can remove the need for gain-scheduling across the whole flight envelope [14]. NDI is based upon the principle of feedback linearization, where the controller feeds back the aircraft dynamics to the aircraft model for cancelling the nonlinearities. Backstepping is a method applicable for vehicles described in strict-feedback form and concerns a systematic Lyapunov-based recursive design method, which steps back toward the control input starting with a scalar equation that is separated by the largest number of integrators. In comparison to NDI, backstepping is more modular, as the control designer can choose which nonlinearities to deal with [15]. One real world application of NDI is for the Lockheed Martin F-35 FCS [16, 17].

However, these methods are reliant on the availability of an accurate aircraft model, which is not always feasible and can especially become a problem when the aircraft model is only known to a limited extent [18]. Incremental NDI (INDI) [19] and Incremental Backstepping (IBKS) [20] seek to address these limitations, by reducing the need for full model knowledge where only the control effectiveness part of the aircraft dynamics is modelled and rely on sensor measurements (*sensor-based*). Thus, improving its robustness against model parameter uncertainties compared to NDI & Backstepping [18, 21].

The latest version of the Flying V FCS uses a nonlinear control method, Incremental Nonlinear Dynamic Inversion (INDI) with Flight Envelope Protection (FEP), where the INDI control method is used for the stability, tracking performance and improve handling quality of the nonlinear Flying V aircraft model [22]. The Flight Envelope Protection system ensures safe operation and control within the flight envelope and limits by integrating the protection laws for the angle of attack, load factor and roll angle [23].

In the latest FCS several shortcomings were encountered and one of them was the uncertainty in the control surface effectiveness was introduced, which lead to saturation of the rudder. As INDI is still dependent on model information, and it can experience degraded performance if there exists a model mismatch. Moreover, time delays, noise and other uncertainties have an effect on stability. Research towards investigating the stability and robustness of INDI [18, 24] has motivated to the development of Hybrid-INDI, which uses complementary filters state estimations and sensor measurements of the aircraft [25] or to combine robust control methods has been conducted [18, 26]. Moreover, Adaptive nonlinear control methods based upon NDI, INDI, BS, IBS have been developed and used in the last decade and these methods adapt their control parameters to identify and account for uncertain or unmodeled dynamics and to design a fault-tolerant FCS.

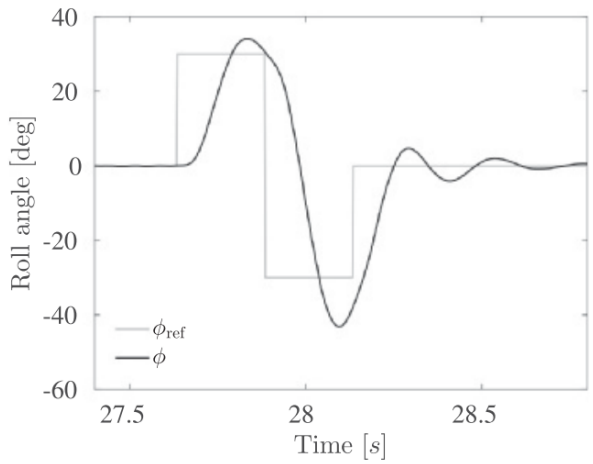

Figure 1.8: INDI CE underestimation results in slow response [27]

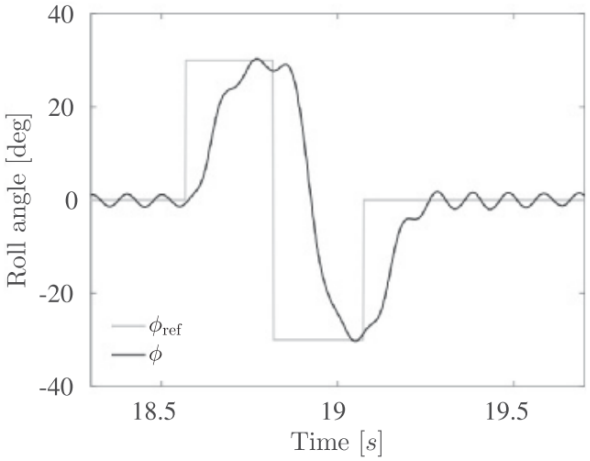

Figure 1.9: INDI CE overestimation results in oscillatory response [27]

A general overview of an Fault-Tolerant Flight Control (FTFC) is illustrated in Figure 1.10, whereby certain main components are presented. The development to create FTFC is motivated since Loss-of-Control (LOC-I) is one of the large reasons for aircraft incidents in commercial aviation [28]. For FTFC systems, adaptive control methods are described as a class of active reconfigurable flight control laws, which continuously adapts its control parameters to ensure the safe operation of the aircraft in case of faults and reduce the required pilot effort.

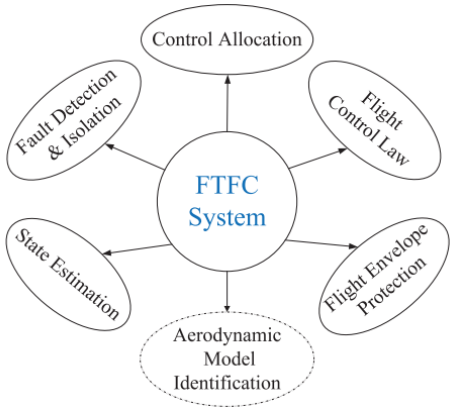

Figure 1.10: FTFC overview [29]

Modern adaptive control methods can be generally subdivided in two control schemes, which is the Direct Adaptive Control, shown in Figure 1.11 and Indirect Adaptive control, shown in Figure 1.12.

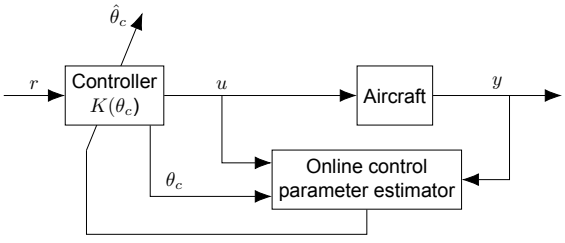

Figure 1.11: Direct adaptive control scheme

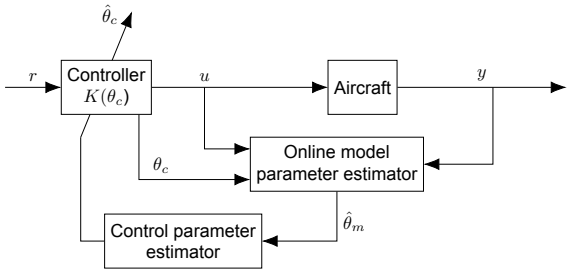

Figure 1.12: Indirect adaptive control scheme

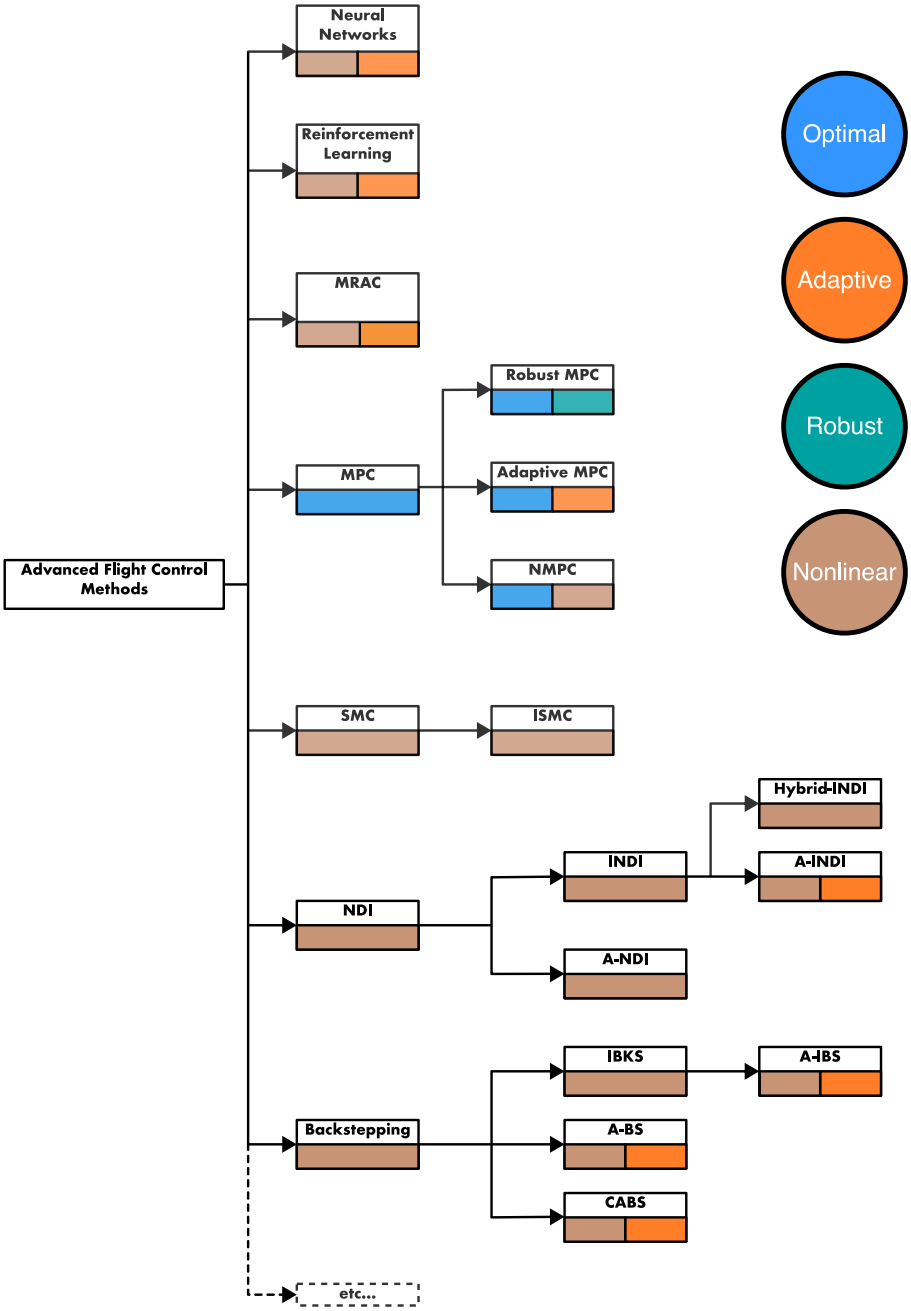

Figure 1.13: Class of methods overview gathered from preliminary research towards advanced flight control methods

1.3. Research Scope

To further focus the research and narrow down the scope, some initial decisions are made to focus on what areas to improve or adjust upon. As the current Flying V FCS already has components such as Control Allocation and Flight Envelope Protection, they will not be within the scope of research. The development of a Fault Detection & Isolation (FDI) system is also not within scope, because it primarily concerns methods to identify faults.

Scoping the area of adaptive control methods to focus on the selected class of methods as shown in Figure 1.13, which presents several state-of-the art methods concerning advanced flight control. Each respective method has been characterised with a property for which they are commonly applied for. As the research cannot cover all of adaptive methods due to time constraints, a selection of methods of interest have to be defined early in the research process. This selection is based on the line of research from the line of research towards advanced flight control methods, which have seen applications in active fault-tolerant control. Certain methods such as including intelligent control methods, like Neural Networks and Reinforcement Learning have their own adaptation and learning mechanisms, but there are challenges concerning certification and robustness, which can impede the priority of creating a compliant FCS first. Moreover, such methods require extensive amount of data and training, where optimality is also not guaranteed, and thus these methods fall out of the scope. Moreover, methods like Model Predictive Control (MPC) concerns calculating optimal control inputs and as such they have been primarily combined with nonlinear control method in the inner loop [30–32], however such methods are often trained offline and adapting online is often computationally heavy.
Therefore, the literature research towards adaptive flight control for the Flying V, will be focused on adaptive & nonlinear control methods that are within the field of Backstepping approaches and Nonlinear Dynamic Inversion approaches.

1.4. Research Objective & Questions

From section 1.2 it has been established that the Flying V configuration or design optimizations can introduce uncertainties, characteristics, and dynamics. The FCS used for the research is current nonlinear FCS using the INDI method with Flight Envelope Protection (FEP) [23]. The main contribution is to research and design an adaptive FCS and developing a fault-tolerant flight control system, which can learn and adapt to model uncertainties and faults, while adhering to the stability and handling qualities to safely operate the aircraft and The main research question is defined as:

How can an adaptive control method be applied for the Flight Control System (FCS) of the Flying V for improving its fault tolerance?

To answer the main research question, several sub-questions are formulated to scope and define the research work and objective for the literature research and master thesis project. These sub-questions are:

1. What are the results and lessons from previous research on developing the FCS for the Flying V?
   (a) What is the current state of handling qualities of the Flying V?
   (b) What are the latest development in aerodynamic modelling for the Flying V?
   (c) What is the current state of the Flying V simulation model?
   (d) What assumptions and uncertainty are present in the simulation model of the Flying V?
   (e) What are the specifications and requirements that apply to an FCS with an adaptive control method?
2. What evaluation metrics are suitable to assess the adaptive control method for the FCS?
   (a) What are the flying & handling qualities criteria, which have been evaluated for the FCS?
   (b) What assessment for evaluating model parameter uncertainties have been performed?
3. What advancements have there been in the applications of nonlinear & adaptive methods?
   (a) What methods have been implemented for fault-tolerant control?
   (b) What method is the most suitable for fulfilling the requirements for the Flying V?
4. How does the selected adaptive method satisfy the requirements for the Flying-V FCS?
   (a) How does the adaptive FCS compare in tracking qualities to a non-adaptive FCS?
   (b) How does the adaptive FCS cope with faults compared to the non-adaptive FCS?

To aid in the literature research, theory primarily about adaptive control will be investigated, specifically existing methods that may have been used for similar aircraft designs such as the blended wing body (BWB) and tailless aircraft as there could be an overlap in characteristics that may provide insight on what adaptive method is appropriate.

1.5. Thesis Outline

This thesis is organised with a main research paper and five additional chapters.

Following this introduction, the main research paper of this research is presented and for the development a literature study was conducted (Chapter 2-5), where in Chapter 2 will focus on recent Flying V research results with a particular focus on activities which are relevant for developing the FCS. The chapter ends with the expected specifications and developments for the FCS. Chapter 3 provides an overview of nonlinear & adaptive control methods with a review of the latest state-of-the-art research and applications and their respective advantages & disadvantages. The chapter ends with a summary and conclusion of what adaptive control method(s) could be the most applicable for the Flying V based on the specifications and their capabilities. With this literature research, a preliminary analysis was conducted in Chapter 4 to gain familiarity with the discussed technique and at last a conclusion of the Literature research in Chapter 5. Additional results were generated and presented in Chapter 6 with further details on the simulation models and simulation results concerning on-board model mismatch and structural faults. At last, a conclusion, and recommendation towards future work is given in Chapter 7.

Part I

Scientific Paper

Adaptive Incremental Dynamic Inversion for Fault-tolerant Flight Control of a Flying Wing

Rana Husain Ali Ul Haq *
Delft University of Technology, Kluyverweg 1, 2629HS, Delft, The Netherlands

Sustainability is a key commitment for future innovation and improvement of the aerospace industry and to realise active research is invested towards advanced and new aircraft designs such as the Flying V. The Flying V is a flying wing design for commercial aviation, promising higher efficiency against conventional tube-and-wing aircraft. The Flight Control System (FCS) has to be designed to prove the airworthiness of the aircraft. In this work, a fault-tolerant FCS is designed that includes an adaptive incremental dynamic inversion inner loop rate control law with an outer loop that consists of longitudinal C* control law and Rate Control Attitude Hold roll control laws for lateral control. Research and activities has led to an updated geometry design with aerodynamic data from RANS simulation, which requires tuning of its outer loop flight controls to be within level 1 handling quality. To investigate the fault tolerance of the aircraft with a structural fault case that results in a loss of effectiveness. It is shown that the adaptation allows the aircraft to cope with the faults and maintain satisfactory tracking performance.

I. Introduction

The Flying V is an advanced aircraft design of a Flying Wing (FW) concept researched at the Delft University of Technology. This aircraft design provides significant energy efficiency improvement for the realisation of a viable and more energy-efficient alternative to the conventional tube-and-wing design. The development of new advanced aircraft designs is a pillar of key innovations and necessary to further sustainability and improvement of the aerospace industry [1]. With the Flying V being an unconventional aircraft design, the research and development of the Flying V will result in many potential changes over time, such as from optimizations in regard to its aerodynamic design and structural design, engine placement or control surface adjustments, which will all introduce different characteristics of the aircraft. Such additions will go through testing and new data or requirements can be introduced over time as the aircraft matures from its baseline. The design and development of Flight Control System (FCS) has to be updated with these changes and is essential for the aircraft's airworthiness and compliance for certification.

Initial research towards the flying and handling qualities of the Flying V was performed with a linear aerodynamic model, estimated at a limited set of flight conditions, obtained using the Vortice Lattice Method (VLM) [2]. The VLM model was combined with wind tunnel data from Wind Tunnel Test Experiments (WTE) with a scaled Flying V model [3]. This combination was done to include the pitch break tendency at higher angle of attack that was captured with these experiments, as VLM does not capture these nonlinear phenomena. With this combined model, a study was performed to improve its handling qualities with by incorporating Incremental Nonlinear Dynamic Inversion (INDI), which is a sensor based control law that relies on an onboard Control Effectiveness (CE) model derived from aerodynamic parameters of the control surfaces, in the inner loop [4]. The implemented FCS was revised with outer loop controllers based on C* parameter for longitudinal control, roll rate command and sideslip compensation for directional control and augmented with Flight Envelope Protection (FEP) for angle of attack, load factor and roll angle protection [5]. Additionally, the FCS was tuned and evaluated to adhere to Level 1 Flying qualities with sensor dynamics. Numerical simulations revealed that the FCS is robust against aerodynamic uncertainties up to 20%, but its control effort increased with the aerodynamic uncertainty, which was especially apparent for the rudder where additional oscillations were observed due to low control authority resulting in degrading performance.
The VLM model and combined model were also used in various pilot-in-the-loop simulator studies and various manoeuvres were covered [6]. The FCS with FEP and compared with other FCS has been tested in a simulator pilot experiments, which confirmed the limited control authority due to control surface saturation, which was also observed in previously conducted piloted experiments [7–9].

*MSc. Student, Control and Simulation, Faculty of Aerospace Engineering

The Flying V's control surface layout provides redundant control effectors, which can provide control authority for pitch and roll, but limited control authority during manoeuvres could require additional pilot effort to maintain stability and in case of control surface failure, it can impede on the flight safety of the aircraft. One of the largest reasons for aircraft incidents is Loss-of-Control (LOC-I) in commercial aviation [10, 11], which has been trending downwards as Fly-by-Wire systems have become more advanced, and with further research and development towards Fault Tolerant Flight Control (FTFC) systems further reduction can be obtained. One class of FTFC design is active FTC, whereby adaptive control methods are employed to achieve reconfigurable flight control laws, which can continuously adapt its control parameters to ensure the safe operation of the aircraft by 'intelligent' and informed updates of its control effectiveness to utilise its control authority on the remaining control effectors in case of faults and thus reduce the required pilot effort [12, 13].
Adaptive INDI has seen recent advancements in the applications for drones [14], Vertical Take-off and Landing (VTOL) drones [15] and numerical simulations with an F-16 simulation model to achieve consistent handling qualities [16] and applied in [17] for fault tolerance of the Flying V. In [14] the Least Mean Squares (LMS) filter was implemented to perform online adaptation of its onboard CE model, as INDI with no adaptation had degraded performance due to CE model mismatch. In [16] CE inaccuracy due to uncertainties lead to varying handling quality and stability characteristics, which were improved through adaptation with LMS that corrected its onboard CE model. In [15] a parametric model using Multivariate B-spline to model its CE model was applied, which stored and adapt to new parameters online to identify the effectiveness. A two-step state and parameter estimation with Extended Kalman Filter (EKF) for state estimation and Recursive Least Squares (RLS) parameter estimation combined with variable forgetting factor has been applied in [17]. The adaptation of the CE model, which consists of coefficients from the aerodynamic model with respect to the dynamics in the inner loop. It was shown that the two-step parameter estimation would not determine the true estimation of its control effectiveness, but adaptation of its CE model would lead to other control surfaces compensating for the damaged control surface.

As the Flying V research is in constant development, a newer parametric geometry [18], which researched a family series of the Flying V, has been used to synthesise an aerodynamic model, for the full-scale aircraft with Reynolds-averaged Navier Stokes (RANS) simulations and VLM simulations [19].This new aerodynamic model provides more flight envelope points, determined at different angle of attacks, Mach numbers and altitudes and incorporates nonlinearities, which can estimate the occurrence of the pitch break at the various flight envelope points. Research has also been conducted towards control surface sizing and placement to satisfy certification requirements and achieve control authority for safe and operable flight [20].

The contributions of this paper are to investigate the possible performance degradation of the INDI inner rate control loop when faced with faults and use RLS to adapt the onboard CE model to cope with the fault and maintain accurate reference tracking performance. This research also uses the updated aerodynamic model and has updated the outer loop gain tuning routines.
The outline of the paper is as follows. In section II, a description of the simulation model of the Flying V is described, control surface layout (II.A), aerodynamic model & parameters (II.B), actuator model (II.C), airframe dynamics (II.D) and lastly sensor model (II.E). The FCS used in this paper is outlined in section III with a description of the outer loop controllers (III.A), the inner loop for rate control with INDI (III.B), The adaptive INDI implementation III.C), a description of how faults are injected (III.D) and lastly the tuning of outer loop controller (III.E). Finally, the simulation results are presented in Section IV, with the discussion and lastly the conclusion in Section V.

II. Flying V Simulation Model

The aircraft simulation model defines the dynamics used for this research where at first, the control surface layout, aerodynamic model and parameters used in the model are described, thereafter the actuator dynamics, formulation of the rigid-body equations of motions and lastly the sensor dynamics are defined.

A. Control Surface Layout

The control surface layout used for this simulation model considers inboard and outboard elevons located at the trailing edge of the wing ($\delta_{CS1}^{L/R}, \delta_{CS2}^{L/R}$) for the right and left sides respectively. The inner and outboard elevon can be used for pitch and roll control. A rudder ($\delta_{CS3}^{L/R}$) is integrated into the winglets on the right and left sides respectively for yaw (directional) control. The geometry of the design is shown in Figure 1, including an optimal engine distance first

estimated [21] and is still under investigation. The landing gear was not taken into account for the study.

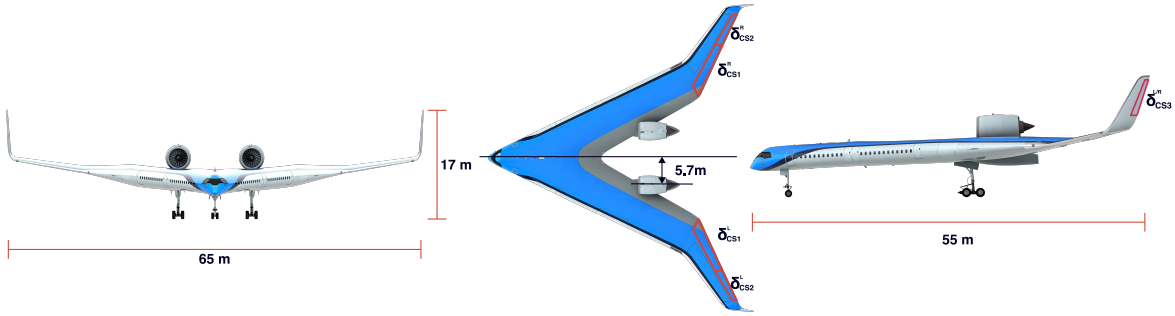

Fig. 1 Front, top and side view of the Flying V with (outer) dimensions and control surfaces

B. Aerodynamic Model & Aircraft Parameters

The aerodynamic model is from an early iteration of the study in [19], and is derived from a combination of RANS and VLM simulations at various flight envelope points from Mach (M) 0.2 to 0.7, height (h) 0m to 9750m. The model is a look-up table for force and moments in the body frame at various CG locations and consists of the dependencies as shown in Table 1.

Table 1 Force and moment aerodynamic coefficients, r and v denotes RANS and VLM simulations respectively, and i denotes inner elevon and o outer elevon. Adapted from [19]

at: $M/h/x_{cg}$	α	β	$\hat{p}$	$\hat{q}$	$\hat{r}$	$\delta_{e_{i/o}}$	$\delta_{a_{i/o}}$	δ_r
C_X	r					r	r	r
C_Y		r			v		r	r
C_Y	r			v		r		
C_l		r	v		v		r	r
C_m	r			v		r		
C_n		r	v		v		r	r

The aerodynamic coefficients for the control surfaces are modelled as ganged control surfaces with elevator deflection (δ_e), aileron deflection (δ_a) for the inner and outboard elevons. These respective aerodynamic coefficients will be split separately for each control surface with the assumption that the deflection of a single elevon will account for 50 % of the performance brought by the deflection of either both, as elevator, or asymmetrically, as aileron. The rudders on the winglet will be kept as they are. The tabulated aerodynamic data is also interpolated linearly.

The aircraft parameters concerning mass and CG are established in [18], assuming a family optimised Flying V, FV-1000 aircraft, which defines a Maximum Take-off Weight (MTOW) of 266 tonnes and a Maximum Landing Weight (MLW) 76% of its MTOW. The most forward (longitudinal) position of CG with MLW is at approximately 28.5m, distanced from the nose, and 29.1m at MTOW, the most aft position is 30.1m. The moment of inertia is determined through a lumped mass method as established in [2] and is a source of uncertainty as it has not been updated with the new geometry and aerodynamic model. The mean aerodynamic chord ($\bar{c}$) is 18m, the surface (S) is 898 m^2 and the span (b) is 65 m.

C. Actuators

The control surface actuators are modelled as an 2$^{\text{nd}}$ order system:

$$H_{act} = \frac{\omega_0^2}{s^2 + 2\zeta\omega_0 s + \omega_0^2} \tag{1}$$

The engine is modelled as a first order system with a maximum thrust of 379 kN [5]:

$$H_{eng}(s) = \frac{1}{0.2s + 1} \tag{2}$$

The elevon and rudder actuator dynamics and properties shown in Table 2 were based upon the actuator parameters defined for a large transport aircraft Boeing 747 [22, 23], which is changed from the actuator dynamics that were derived from more agile aircraft [5]:

Table 2 Control surface actuator limits and actuator parameters

	Inboard and outboard elevons ($\delta_{CS1}^{L/R}$ & $\delta_{CS2}^{L/R}$) min,max	Rudder ($\delta_{CS3}^{L/R}$) min, max
Position limits ($\dot{u}$) [deg]	-25,25	-30,30
Rate limits (u) [deg/s]	-40,40	-45,45
Natural frequency (ω_0) [rad/s]	35	35
Damping coefficient (ζ) [-]	0.8	0.8

D. Rigid Body Dynamics

The rigid body dynamics and aerodynamic coefficients are defined in the body-fixed reference frame ($\mathcal{F}_\mathcal{B}$) as shown in Figure 2.

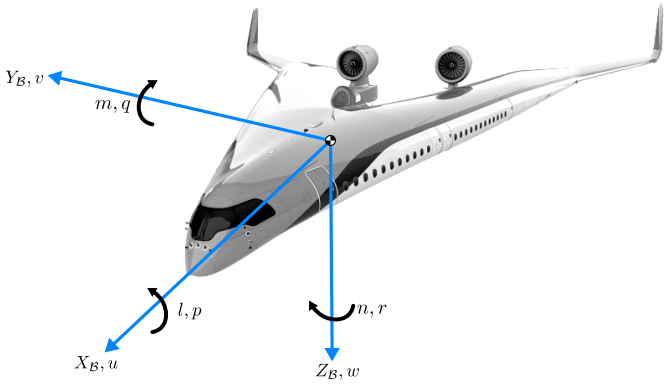

Fig. 2 Aircraft body axes and conventions. Adapted from [2]

The following assumptions are made to describe the equations of motion of the aircraft [3]; 1) The aircraft is a rigid body and has constant mass, 2) The Earth is flat and non-rotating and inertial reference frame, 3) There is zero wind and a perfect atmosphere, 4) The aircraft has a plane of symmetry such that $I_{xy} = I_{yz} = 0$ and thrust lies in the symmetry plane, 5) The gravitational acceleration is constant.
The forces acting on the aircraft consist of gravity, propulsion forces and aerodynamic forces. It is assumed that the distributed forces can be replaced with point forces that generate moments around the center of gravity. With the flat and non-rotating Earth assumption, the vehicle-carried normal Earth reference frame is similar to an inertial reference frame. The equation of motion for the simulation model describes a 6-Degree of Freedom (DOF) dynamic system and is formed by the translational dynamics, rotational dynamics, and the kinematics. The complete set of equations of motion for 6-DOF simulation is defined as:

$$
\begin{aligned}
\dot{x_E} &= (u\cos(\theta) + (v\sin(\phi) + w\cos(\phi))\sin(\theta))\cos(\psi) - (v\cos(\phi) - w\sin(\phi))\sin(\psi) \\
\dot{y_E} &= (u\cos(\theta) + (v\sin(\phi) + w\cos(\phi))\sin(\theta))\sin(\psi) + (v\cos(\phi) - w\sin(\phi))\cos(\psi) \\
\dot{z_E} &= -u\sin(\theta) + (v\sin(\phi) + w\cos(\phi))\cos(\theta) \\
\dot{u} &= vr - wq - g\sin(\theta) + \frac{F_X}{m} \\
\dot{v} &= wp - ur + g\sin(\phi)\cos(\theta) + \frac{F_Y}{m} \\
\dot{w} &= uq - vp + g\cos(\phi)\cos(\theta) + \frac{F_Z}{m} \\
\dot{p} &= \frac{I_{zz}}{I^*}M_X + \frac{I_{xz}}{I^*}M_Z + \frac{(I_{xx} - I_{yy} + I_{zz})I_{xz}}{I^*}pq + \frac{((I_{yy} - I_{zz})I_{zz} - I_{xz}^2)}{I^*}qr \\
\dot{q} &= \frac{M_Y}{I_{yy}} + \frac{(r^2 - p^2)I_{xz}}{I_{yy}} + \frac{(I_{zz} - I_{xx})}{I_{yy}}pr \\
\dot{r} &= \frac{I_{xz}}{I^*}M_X + \frac{I_{xx}}{I^*}M_Z + \frac{((I_{xx} - I_{yy})I_{xx} + I_{xz}^2)}{I^*}pq + \frac{(-I_{xx} + I_{yy} - I_{zz})I_{xz}}{I^*}qr \\
\dot{\phi} &= p + \sin(\phi)\tan(\theta)q + \cos(\phi)\tan(\theta)r \\
\dot{\theta} &= \cos(\phi)q - \sin(\phi)r \\
\dot{\psi} &= \frac{\sin(\phi)}{\cos(\theta)}q + \frac{\cos(\phi)}{\cos(\theta)}r
\end{aligned}
\tag{3}
$$

With I^* defined as followed:

$$
I^* = I_{xx} * I_{yy} - I_{xx}^2 \tag{4}
$$

The forces and moments are defined as followed:

$$
\begin{aligned}
F_X &= F^B_{X_{\text{aero}}} + F^B_{grav_X} + T_1 + T_2 \\
F_Y &= F^B_{Y_{\text{aero}}} + F^B_{grav_Y} \\
F_Z &= F^B_{Z_{\text{aero}}} + F^B_{grav_Z} \\
M_X &= M^B_{X_{\text{aero}}} \\
M_Y &= M^B_{Y_{\text{aero}}} - (T_1 + T_2)T_{dz} \\
M_Z &= M^B_{Z_{\text{aero}}} + (T_1 - T_2)T_{dy}
\end{aligned}
\tag{5}
$$

With T_1, T_2 the thrust force produced by the left and right engine and T_{dy}, T_{dz} are the respective moment arm lengths. The CG and reference position at which the aerodynamic forces act are described with x_{cg} and x_{ref} respectively. The body accelerations are calculated as:

$$
A_x = \frac{C_X}{m} - g\sin(\theta) \tag{6}
$$

$$
A_y = \frac{C_Y}{m} + g\sin(\phi)\cos(\theta) \tag{7}
$$

$$
A_z = \frac{C_Z}{m} + g\cos(\theta)\cos(\phi) \tag{8}
$$

With the 6-DOF simulation model an output state is also computed of 18 states are measured by the sensors.

E. Sensor Model

The sensors used in the Flying V simulation model are based upon the description provided in [5, 17], which based its sensor parameters on the specifications used in [24]. However, the baseline sensor parameter specifications would not obtain level 1 handling qualities for the Flying V, some adjustments were made to obtain that, and it is assumed that such sensors characteristics are obtainable. The sensor characteristics used for this research are shown in Table 3 .

Table 3 Sensor parameters, based on [24]

State	Noise (σ^2)	Bias	Delay [ms]	Sampling rate [Hz]	Filter time constant [s]
p, q, r [rad/s]	1.5×10^{-9}	3.0×10^{-5}	50	100	0.04
ϕ, θ, ψ [rad]	1.0×10^{-9}	4.0×10^{-3}	50	50	0.05
f_x, f_y, f_z [rad]	1.5×10^{-5}	2.5×10^{-3}	100	50	0.05
α, β [rad]	7.5×10^{-8}	3.0×10^{-3}	100	100	0.05
h [m]	4.5×10^{-3}	8.0×10^{-3}	150	20	0.05
V [m/s]	8.5×10^{-4}	2.5	150	20	0.05
δ_{CSi} [rad]	1.5×10^{-9}	2.5×10^{-5}	-	100	-

Additionally, noise and bias are also added to the control surface output, and these are assumed to be originated from the actuator sensors.

The model for the sensor dynamics and filtering is described in [5], where the sensors sample the state and are then filtered with a first order (discrete) filter, with their respective filter time constant. As the sensors do not provide direct measurements of the rotational accelerations $(\dot{p}, \dot{q}, \dot{r})$, to obtain these measurements a second order filter is applied on the gyroscope sensor, which measures the rotation rates (p, q, r) and are then computed with first order Euler differentiation. The filtering parameters for the second order filter are set to $\omega = 25$ and $\zeta = 0.75$.

III. Flight Control System Design

This section describes the baseline control architecture of the Flying V, which consist of inner loop rate control with INDI, outer loop controllers and at last tuning of the gains in the controller. The control architecture is derived from the implementation described in [5, 17], but Flight Envelope Protection (FEP) isn't implemented for this research. A complete overview of the controller is shown in Figure 3.

A. Outer Loop Control

This section will elaborate on the outer loop controllers and and is derived from the control structure as outlined in [5], where the outer loop control structure has several components, namely the:

1) C^* controller block with pitch reference model for longitudinal channel control, which has been adjusted in this research to not enable compensation near the pitch and roll attitude limits continuously, but only when it nears these limits.
2) A roll reference model for the roll channel control
3) Sideslip compensator for the yaw channel control
4) Linear Controller that computes a virtual control signal based on the references from the three aforementioned control blocks.
5) Speed controller to maintain the aircraft at the commanded trim speed
6) Pseudo-Control Hedging to prevent actuator wind-up by high (incremental) control commands

B. Incremental Nonlinear Dynamic Inversion (INDI) Rate Control

INDI is a nonlinear control law closely related to its model-based precursor, Nonlinear Dynamic Inversion (NDI), which aims to linearize a nonlinear system through the cancellation of nonlinear system dynamics with state feedback [25] and define a control law design where the inner loop behaves like an integrator, which can then be controlled by an outer loop linear controller, such as Proportional-Integral-Derivative (PID). One drawback of NDI is that it requires complete system knowledge and to overcome this drawback INDI uses sensor estimates for its control law design and reducing knowledge required of the system dynamics by using the control effectiveness (CE) model, thus requiring less model knowledge [26, 27]. This approach is derived derived for a nonlinear system through Taylor series expansion, at a current state and time point (x_0, u_0)

$$\mathbf{x} = \mathbf{f}(\mathbf{x}, \mathbf{u}) \tag{9}$$

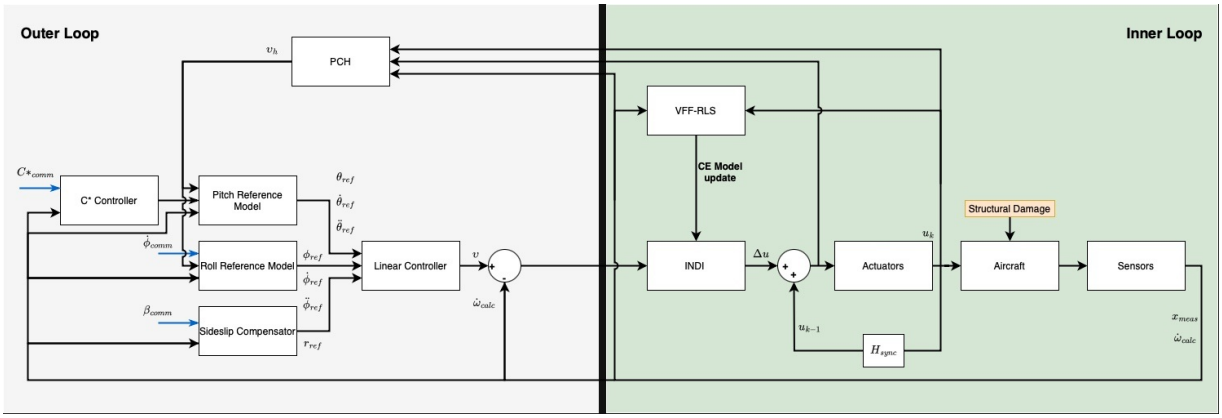

Fig. 3 Flight control system architecture. Modified from [17]

$$\dot{x} \approx f(x_0, u_0) + \frac{\partial f(x,u)}{\partial x}|_{x=x_0,u=u_0}(x - x_0) + \frac{\partial f(x,u)}{\partial u}|_{x=x_0,u=u_0}(u - u_0) \tag{10a}$$

$$\approx \dot{x}_0 + F((x_0, u_0))(x - x_0) + G(x_0, u_0)(u - u_0) \tag{10b}$$

$$\approx \dot{x}_0 + F((x_0, u_0))\Delta x + G(x_0, u_0)\Delta u \tag{10c}$$

Applying the time-scale separation principle, the linearisation is simplified and thereafter an incremental control law can be derived:

$$\dot{x} \approx \dot{x}_0 + G(x_0, u_0)\Delta u \tag{11}$$

$$\Delta u = G^{-1}(x_0, u_0)(\nu - \dot{x}_0) \tag{12}$$

Whereby $G(x_0, u_0)$ is the control effectiveness matrix, ν is the desired virtual reference from the outer loop controller and x_0 is the currently measured state estimate from the sensors and Δu is the incremental control command. By adding the previously measured control surface deflection, the control command to the actuators can be determined:

$$u = u_0 + \Delta u \tag{13}$$

For the application of INDI the following assumptions are implicitly made [26, 28, 29]:

1) Complete and accurate knowledge of states is available
2) Sensors to measure the acceleration $\mathbf{x}$ with sufficiently high sampling rate need to exist and be available
3) Sensor to measure the current control input (actuator) need to be available or estimated on the basis of a high-fidelity model of the actuator dynamics
4) Time-scale seperation where it is assumed that the state derivatives evolve faster than the state upon fast control action, which directly influences the dynamics of the rigid body
5) Fast control action is assumed, where the dynamics of the actuator (and control surface) evolve much faster than the states
6) Control effectiveness matrix is invertible

The derivation of INDI for rate control is obtained by first order Taylor Series approximation at the linearization state and input of the angular dynamics (ω) with the assumption of time-scale separation and sufficiently high sampling time:

$$\dot{\omega} = \mathbf{J^{-1}M} - \mathbf{J^{-1}}\Omega\mathbf{J}\omega \tag{14}$$

$$\dot{\omega} \approx \dot{\omega}_0 + F\Delta\mathbf{x} + G\Delta\mathbf{u} \tag{15}$$

$$\dot{\omega} \approx \dot{\omega}_0 + G\Delta\mathbf{u} \tag{16}$$

The control effectiveness matrix G is in Equation 18, with the control effectiveness coefficients ($C_{*_{\delta_{CS}^{L/R}}}$), which is the aerodynamics moment coefficients with respect to each control surface and rolling moment, are determined through the

linearization of the dynamics.

$$\Delta \mathbf{u} = G^{-1}(\omega_{des} - \omega_0) \tag{17}$$

$$G = \frac{\bar{q} * S}{\mathbf{I}} \begin{bmatrix} b & 0 & 0 \\ 0 & c & 0 \\ 0 & 0 & b \end{bmatrix} \begin{bmatrix} C_{l_{\delta^L_{CS1}}} & C_{l_{\delta^R_{CS1}}} & C_{l_{\delta^L_{CS2}}} & C_{l_{\delta^R_{CS2}}} & C_{l_{\delta_{CS3}}} \\ C_{m_{\delta^L_{CS1}}} & C_{m_{\delta^R_{CS1}}} & C_{m_{\delta^L_{CS2}}} & C_{m_{\delta^R_{CS2}}} & C_{m_{\delta_{CS3}}} \\ C_{n_{\delta^L_{CS1}}} & C_{n_{\delta^R_{CS1}}} & C_{n_{\delta^L_{CS2}}} & C_{n_{\delta^R_{CS2}}} & C_{n_{\delta_{CS3}}} \end{bmatrix} \tag{18}$$

$$C_{*_{\delta^{L/R}_{CS}}} = \frac{\partial C_m}{\partial \delta^{L/R}_{CSi}} \tag{19}$$

The control effectiveness is not squared and can not be inverted, for which there are more control surfaces available for generating a specific moment on the aircraft. A control allocation algorithm is used that makes the most effective choice on which control surface has been used, computed with the Moore-Penrose pseudoinverse [30] as:

$$\mathbf{P} = \mathbf{G}^T(\mathbf{G}\mathbf{G}^T)^{-1} \tag{20}$$

The incremental command is added with the previously known control surface deflection to form the commanded input to the actuators.

$$\mathbf{u} = \mathbf{u}_0 + \underbrace{\mathbf{P}(\mathbf{v} - \mathbf{x_0})}_{\Delta u} \tag{21}$$

One crucial aspect of applying INDI is its synchronization of the control deflections with the measurements of the sensors [26, 31, 32], as the control surface and sensor dynamics are not directly available, some latency occurs and if not accounted for, it can result in oscillatory response. To compensate for this, the sampling and filtering of the measurement from the actuators is performed with the same filtering as the body rate sensor, which is an 2^{nd} older filter, and a pure time delay to compensate for any difference between both sensors [26]. In this research, an additional time delay of $5ms$ is added.

C. Adaptive INDI Control Law

This section concerns the adaptation of control effectiveness through the correction with a scaling parameter, which is a lumped term that corrects for any mismatch between the onboard and real control effectiveness and has been employed in previous studies [16] and research presented by Swain & Manickavasagar in [13] used a FTC with Fault Detection and Identification for optimal control allocation by identifying a failure of a control surface through it's desired control demand and achieved control demand with a Kalman filter.

For this research's implementation each term in the control effectiveness matrix G is thus scaled as followed:

$$\tilde{G}_{ij} = \theta_{ij} G_{ij} \tag{22}$$

The prediction model is determined from the INDI control law, where the current on board model is used for the estimation and the prediction error is the residual of the incremental change of angular acceleration of the aircraft and the incremental deflection to achieve the desired change. The derivation of the residual is obtained through the following steps. First, the linearized equation of the angular dynamics with the assumption of time-scale separation is formulated.

$$\dot{\omega}_k \approx \dot{\omega}_{k-1} + \tilde{G}_{k-1}\Delta(u_k - u_{k-1}) \tag{23}$$

The previous angular acceleration as measured by the sensors $\dot{\omega}_{k-1}$ is brought to the left hand side, and an incremental change in angular acceleration is obtained.

$$\Delta\dot{\omega} = \dot{\omega}_k - \dot{\omega}_{k-1} = \tilde{G}_{k-1}\Delta\mathbf{u} \tag{24}$$

This incremental change on the left hand side should be proportional to the incremental change on the right hand side and thus the following residual is derived:

$$\epsilon = \Delta\dot{\omega}_{ij} - (\tilde{G}_{ij})_{k-1}\Delta\mathbf{u}_j \tag{25}$$

1. Recursive Least Squares

Recursive least squares algorithm has been used in various adaptive control studies for online identification and adaptation of control parameters. The algorithm can be formally described with three steps [33, 34]:

$$
\begin{aligned}
K_k &= P_{k-1}X_{k-1}(\lambda_k + X_{k-1}^T P_k X_{k-1})^{-1} \\
\hat{\theta}_k &= \hat{\theta}_{k-1} + K_k \epsilon_k \\
P_k &= \frac{1}{\lambda}(P_k - K_k X_{k-1} P_k)
\end{aligned}
$$

Where K is the gain, that corrects and updates the current parameter estimation. One main disadvantage of recursive identification is that when there is no excitation or "information richness" in the estimator, old information is continuously forgotten and this results in an exponentially growing covariance matrix, which could destabilise the system and parameter estimation. One solution is to employ a variable forgetting factor, which is tuned based on the information content (Σ_0) of the filter and continuously adjust the forgetting factor to keep the information content constant. This has the following formulation for the forgetting factor [34, 35]:

$$
\lambda = 1 - \frac{[1 - \phi_k K_k]\epsilon^2}{\Sigma_0} \tag{26}
$$

Setting the information constant can be done by expressing it with relation to the expected measurement noise with a nominal memory length (N_0) expressed as:

$$
\Sigma_0 = \sigma_0^2 N_0 \tag{27}
$$

Algorithm 1 Recursive least squares: parameter estimation

input: $\omega_{\mathbf{k}}, \omega_{\mathbf{k-1}}, \mathbf{U_k}, \mathbf{U_{k-1}}, \hat{\theta}_{\mathbf{k}}, \mathbf{P}_k, \lambda_k, C_{*_{\delta_{CS}^{L/R}}}$

initialization: $\hat{\theta}_{\mathbf{0}}, \mathbf{P}_0, \lambda_0, \mathbf{J}, \bar{q}, S, c, b$

while $k \leq N$ **do**

- $z_{k+1} = \dot{\omega}_k - \dot{\omega}_{k-1}$
- $\Delta\mathbf{U}_k = \mathbf{U}_k - \mathbf{U}_{k-1}$
- $\phi_{k+1} = \frac{\bar{q}*S}{\mathbf{I}} diag\left(\begin{bmatrix} b & c & b \end{bmatrix}\right) C_{*_{\delta_{CS}^{L/R}}} \Delta\mathbf{U}_k$
- $\epsilon_k = z_{k+1} - \phi_{k+1}^T \hat{\theta}_k$
- $\Delta\theta_{k+1} = \mathbf{0}^{3x5}$
- **for** $i \leq 3$ **do**
  - $K_{k+1} = \frac{P_k(i)\phi_{k+1}(i)}{(\lambda_k(i) + \phi_{k+1}^T P_k(i)\phi_{k+1}(i))}$
  - $\Delta\theta_{k+1}(i) = K_{k+1}\epsilon_k(i)$
  - $\lambda_k(i) = \max(\lambda_{\min}, \max(\lambda_{max}, 1 - (1 - \phi_{k+1}^T K_{k+1})\frac{e_k(i)^2}{\Sigma_0})$
  - $P_{k+1} = \lambda^{-1}\left(P_k - K_{k+1}\phi_{k+1}^T P_k\right)$
- **end for**
- **for** $j \leq 5$ **do**
  - $\Delta\bar{\theta}_{k+1}(j) = \frac{\sum_{i=0}^{3}\Delta\theta_{k+1}(i,j)}{3}$
  - **for** $i \leq 3$ **do**
    - **if** $|\Delta\theta_{k+1}(i,j) - \Delta\bar{\theta}_{k+1}(j)| >$ 1e-6 **then**
      - $\Delta\theta_{k+1}(i,j) = \Delta\bar{\theta}_{k+1}(j)$
    - **end if**
    - $\hat{\theta}_{k+1}(j) = \hat{\theta}_k(j) + \Delta\theta_{k+1}(j)$
  - **end for**
- **end for**

end while

By setting the value of, Σ_0 the filter adapts new information more quickly or slower, as the covariance matrix increases and becomes more sensitive. Thus, the speed of the adaptation is determined by how small of a value Σ_0 is set to, and a larger value increases the robustness of the parameter estimate. The variable forgetting factor also plays a crucial role for estimating sudden changes in CE, as new information becomes essential for the adaptation.
The RLS algorithm is applied in the adaptive control law, where it computes and adapts the correction parameter per row, which corresponds to all control surfaces per axis of the angular acceleration. One practical adjustment has been made with the correction parameter, which is that the respective update corresponding to each control surfaces is ensured to be proportionally similar. This is done by first storing the respective updates for each axis, and then applying that update if they conform to the same relative threshold, otherwise the mean correction for that control surface is applied and thus the magnitude of the correction is constrained for each row (axis moment) and column (control surface effectiveness). This also accounts for the noise that's present in the measurement by the sensors.

For the Flying V FCS, the virtual control hedge is subtracted for the pitch and roll reference model, but not sideslip compensator with respect to the yaw rate.

D. Fault injection

The simulation model has been updated to insert structural faults into the aircraft model. These faults are done through scaling, where the original aerodynamic coefficients for the control surface forces and moments are modified to introduce structural damage as described in [17]. Thus, the original coefficient of the respective control surface is scaled as following:

$$\tilde{C}_{*_{\delta_{CS}^{L/R}}} = \mu \cdot C_{*_{\delta_{CS}^{L/R}}} \tag{28}$$

With $\mu \in (1, 0)$, where 1 means it has full control effectiveness and 0 means that the control effectiveness is lost.

E. Tuning

The tuning of the gains in the outer loop control blocks are done through a multi-objective optimisation, as performed by Stougie [5]. However, the tuning routine was performed through trial-and-error with random sampling of gains until various objectives were minimized and constraints were satisfied. This section elaborates first on the bare-airframe dynamics at the selected flight condition, thereafter a new tuning routine through a Multi-Objective Parameter Synthesis (MOPS) is elaborated and at last the tuning results are presented.

1. Bare-airframe dynamic modes

Before the aircraft is tuned, the aircraft is trimmed at their respective flight conditions and the decoupled into longitudinal and lateral dynamics analyse the dynamic modes of the aircraft. The eigenvalues are shown in Figure 4 & 5 respectively, where it can be shown that at each respective flight condition, the phugoid is near the right half pole plane nearing instability with exception to the Takeoff condition where it is unstable. The Lateral eigenvalues reveal that the Dutch roll is also nearing instability, and all flight conditions have unstable spirals. This reveals that the bare-airframe dynamics require stability augmentation systems to fly the aircraft trimmed at the flight conditions.

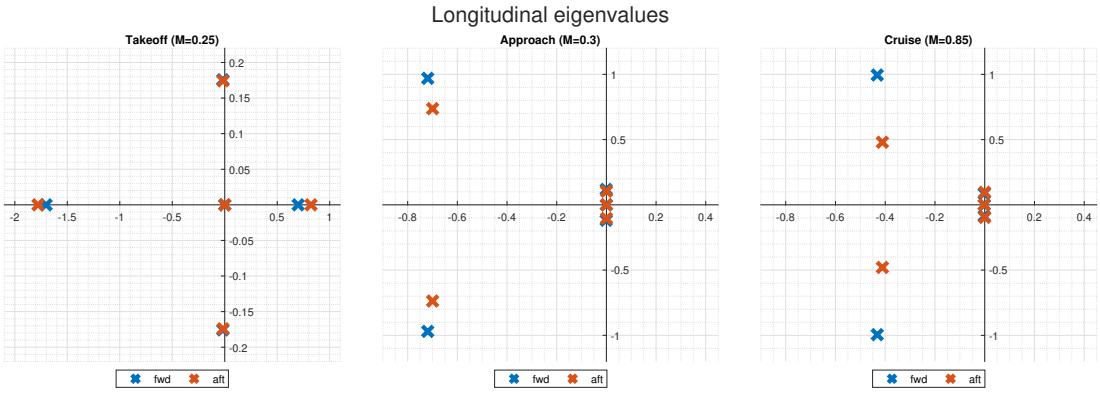

Fig. 4 Longtiudinal eigenvalues at forward and aft centre of gravity for three flight conditions

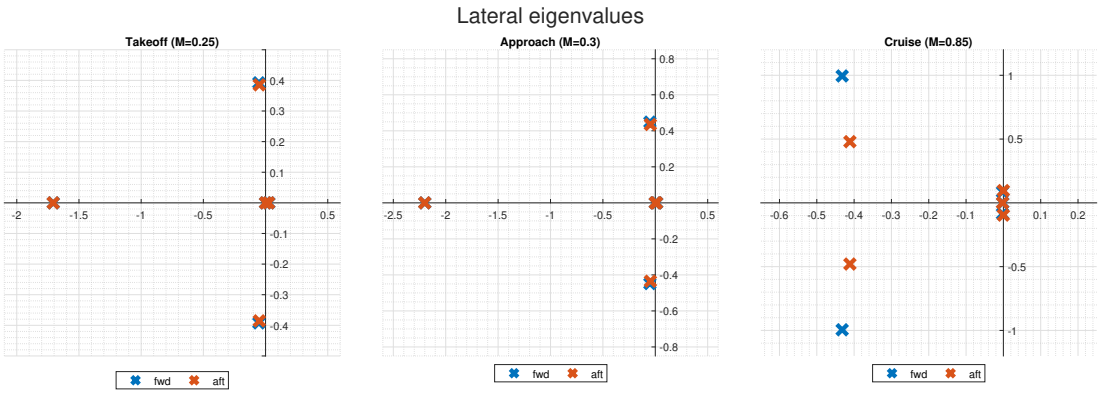

Fig. 5 Lateral eigenvalues at forward and aft centre of gravity for three flight conditions

This research will focus on the Approach flight condition, as it is a critical flight condition in aircraft operation.

2. Multi-Objective Parameter Synthesis tuning routine

The tuning of the gains in the outer loop control blocks are done through a multi-objective optimisation, extensively described by Stougie [36]. However, tuning was done through trial-and-error with random sampling of gains until various objectives were minimized and constraints were satisfied. This section elaborates the tuning routine with Multi-Objective Parameter Synthesis (MOPS) is elaborated and at last the tuning results are presented.

The optimisation method applied for the tuning is the *pattern search* optimisation in MATLAB [*], which is a direct search method that finds a set of points based on the current point at each iteration and approach an optimal point where the value of the objective function either decreases or remains the same for iteration. The optimisation is performed separately for the longitudinal and lateral design parameters, and the objective function is based upon the scoring for the following objectives [36]:

- The MIL-STD-179A flying and handling quality requirements [37–39]
- Stability margins, Gain and Phase, which is computed at the broken loop location just before the INDI control block in Figure 3 [40]
- Low Order Equivalent System (LOES) fit [37, 41]
- Attitude bandwidth for longitudinal control [42]
- Tracking performance with block inputs

For the tracking response, the following metrics are computed:

1) Root Mean Squared Error (RMSE), which quantifies the average error and penalises high deviations
2) $\delta_{CS_{activity}}$, which penalises high deflections, and thus high actuator rates
3) Risetime, Settlingtime, Overshoot all quantify the transient response to the tracking reference and obtained using the *stepinfo* function in MATLAB

$$RMSE = \sqrt{\sum_{i=0}^{N} \frac{(y_{r_i} - y_i)^2}{N}} \qquad \delta_{CS_{activity}} = \frac{\int_0^{T_{sim}} (\dot{\delta})^2}{T_{sim}} \tag{29}$$

The objectives are formulated to a composite scoring objective function where the constraints are either minimized or normalized, and then weighed proportionally to have a similar magnitude in the objective function. This weighing is defined according to trial and error. The level of flying qualities, are penalized proportionally depending on the thresholds of its flying quality with a weighed from 1 to 1000. Table 4 and 5 summarise all the objectives.

$$HQ_{i_{normalized}} = W_{FQ_i} * \left(\frac{HQ_{obtained} - HQ_{boundary}}{HQ_{desired}} \right)^2 \tag{30}$$

$$HQ_{i_{minimized}} = W_{FQ_i} * \left(HQ_{boundary} - HQ_{obtained} \right)^2 \tag{31}$$

$$\tag{32}$$

[*]https://nl.mathworks.com/help/gads/how-pattern-search-polling-works.html

The final objective is defined as a composite scoring between the handling quality and tracking performance as:

$$Score = HQScore + TQScore \tag{33}$$

The optimisation was performed until a minimum was found, however, due to the high computational time of the tuning the maximum evaluations for the optimisation was set at 320 function evaluations.

Table 4 Longitudinal tuning objectives [5, 40]

Longitudinal tuning objectives					
		Min		Max	
Description	**Type**	**B**	**C**	**B**	**C**
Response to C* block command of $\Delta C^* = 0.25$, T_{sim} = 35					
RMSE	Min		-		-
$CS_{activity}$	Min		-		-
x_{max}	Min		-		-
RS [s]	Min		-		-
ST [s]	Min		-		-
OS [%]	Min		10%		-
Linear Analysis					
GM v_q [dB]	Constr.		6		-
PM v_q [°]	Constr.		45		-
ω_{sp} [rad/s]	Constr.	-	0.87		-
ζ_{sp} [-]	Constr.		0.30 / 0.50		2.0 / 1.3
CAP [$g^{-1}s^{-2}$]	Constr.		0.085 / 0.16		3.6
$score_{LOES}$ [-]	Constr.		-		15

Table 5 Lateral tuning objectives [40]

Lateral tuning objectives					
		Min		Max	
Description	**Type**	**B**	**C**	**B**	**C**
Response to $\dot{\phi}$ block command of ±3°, $T_{sim} = 45s$					
RMSE	Min		-		-
$\Delta\beta$	Min		-		-
$CS_{activity}$	Min		-		-
x_{max}	Min		-		-
RS [s]	Min		-		-
ST [s]	Min		-		-
OS [%]	Min		10%		-
Linear Analysis					
GM v_p [dB]	Constr.		6		-
PM v_p [°]	Constr.		45		-
GM v_r [dB]	Constr.		6		-
PM v_r [°]	Constr.		45		-
$1/T_s$ [s^{-1}]	Constr.		-0.035 / -0.058		-
T_r [s]	Constr.		-		1.4 / 1.0
ω_{dr} [rad/s]	Constr.		0.5		-
ζ_{dr} [–]	Constr.		0.08		-
$\omega_{dr}\zeta_{dr}$ [rad/s]	Constr.		0.15 / 0.10		-
$score_{LOES}$ [–]	Constr.		-		15

The system is trimmed, and tuned for the approach condition (M=0.3, H=1km) with forward center of gravity (28.5) at MLW, and the results are presented in Table 6 and Table 7 for the longitudinal and lateral respectively, where the yellow coloured cells indicate criteria, which hasn't been fulfilled. The tracking of the references used in the tuning is shown in Figure 6 & 7.

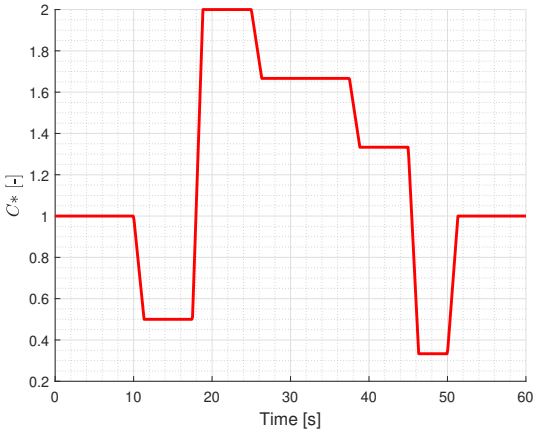

Fig. 6 Longitudinal C* tracking signal

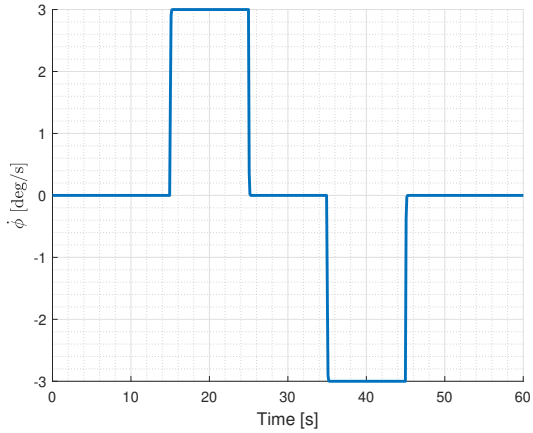

Fig. 7 Lateral $\dot{\phi}$ tracking signal

Table 6 Longitudinal tuning results

Description	Value
Linear analysis	
GM v_q [dB]	4.66
PM v_q [°]	51.18
ω_{sp} [rad/s]	1.39
ζ_{sp} [–]	0.65
CAP [$g^{-1}s^{-2}$]	0.32
$score_{LOES}$ [–]	2.53
Tracking quality	
OS	6.88 %
Risetime	0.48 s
Settlingtime	3.04 s
δ_{energy}	4.54 $\circ/s^2$

Table 7 Lateral tuning results

Description	Value
Linear Analysis	
GM v_p [dB]	5.93
PM v_p [°]	45.11
GM v_r [dB]	-7.62*
PM v_r [°]	42.35
$1/T_s$ [s^{-1}]	stable
T_r [s]	0.0793
ω_{dr} [rad/s]	7.26
ζ_{dr} [-]	2.48
$\omega_{dr}\zeta_{dr}$ [rad/s]	18.04
$score_{LOES}$ [–]	6.20
Tracking quality	
OS	12.832%
Risetime	1.19 s
Settlingtime	4.34 s
δ_{energy}	22.78 $\circ/s^2$

*smallest negative margin

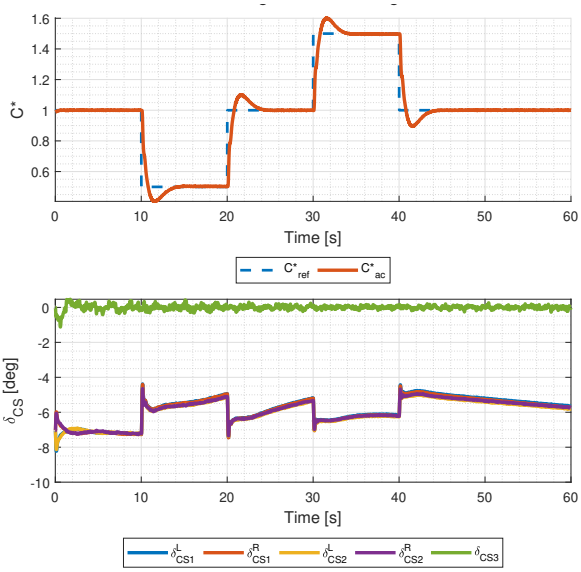

Fig. 8 Longitudinal tuned tracking response

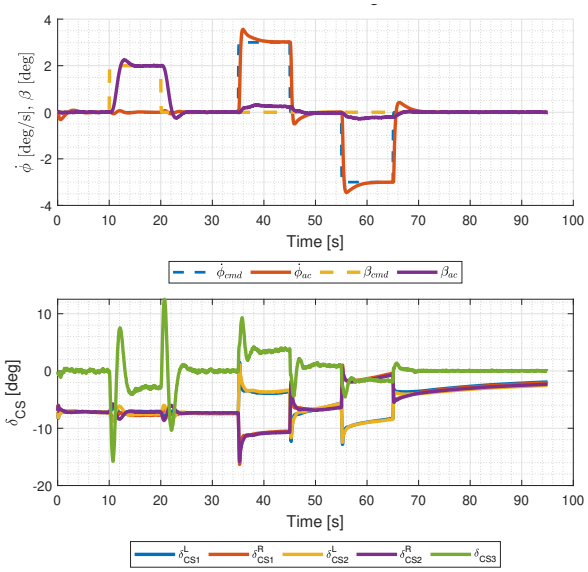

Fig. 9 Lateral tuned tracking response

IV. Results

In this section the numerical results are obtained for the approach flight condition at Mach = 0.3, Height = 1000m with a forward center of gravity. For the analysis the following tracking signals are used, for the C* command and roll rate command respectively, with a zero sideslip command. These signals are combined for longitudinal and lateral input tracking, shown in Figure 8 & 9.

An asymmetric structural fault is introduced as the inboard elevon has higher control authority for the longitudinal

channel and the outboard elevon has higher control authority for the roll channel, thus in a fault cause the healthy control surfaces are mainly responsible for reference tracking. The analysis was conducted in an incremental manner, where first a fault was introduced on the inboard elevon, left-hand side with increments of [1, 0.75, 0.5, 0.25, 0], where a value of 1 describes the control surface at full health and 0 means it has lost all of its effectiveness. Afterwards, a fault is introduced on the outboard elevon on the right-hand side, with the same increments. After the fault has been injected, a doublet signal is commanded for each elevon to excite the aircraft dynamics and create excitation for the parameter estimation.

The most severe case is presented when the respective faulty surfaces completely lose their effectiveness, which leads to degraded tracking, however with adaptation the tracking improves as shown by the results in Figure 10.

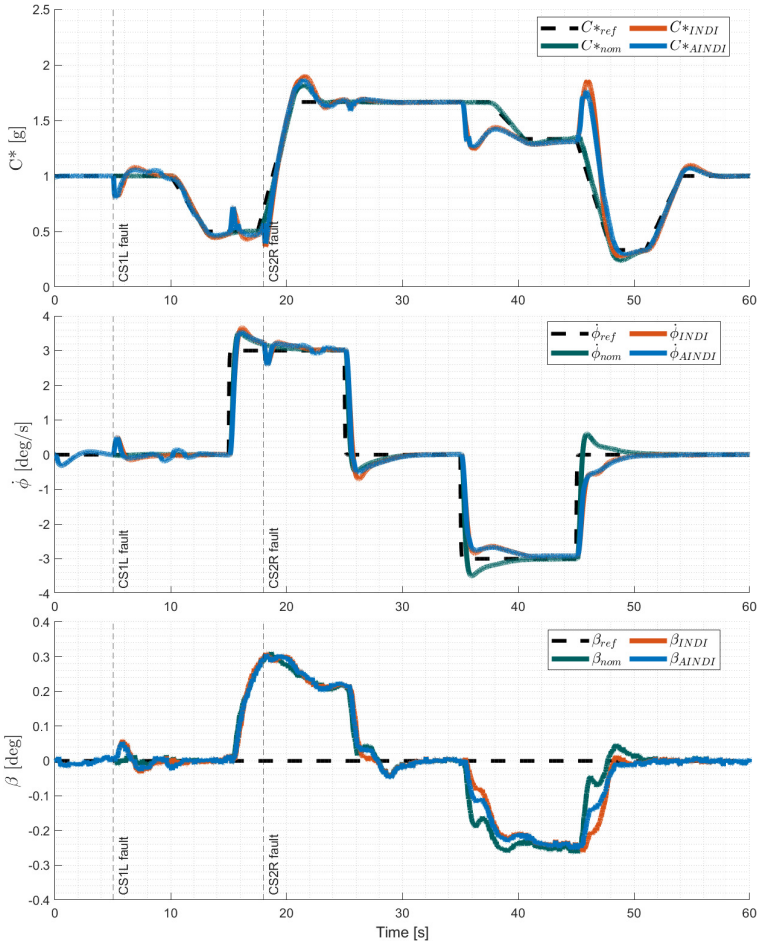

Fig. 10 C*, $\dot{\phi}$ and β control tracking comparison

The RMS for each tracking reference is shown in the Table 8, where it can be observed that the adaptive INDI is able to retain a lower RMSE compared to INDI in the presence of fault.

Table 8 RMSE of tracking responses

	Nominal		**Fault case**	
Tracking input	INDI	AINDI	INDI	AINDI
$\dot{\phi}$ [deg/s]	0.3233	0.3222	0.3877 (+20%)	0.3776 (+17%)
C*	0.0322	0.0313	0.1249 (+287%)	0.1129 (+260%)
β [deg]	0.1093	0.1095	0.1084 (−3%)	0.1072 (−2%)

In Figure 11 & 12 it can be observed that without adaptation, as the fault is introduced the control surfaces deflect

proportionally to the loss in effectiveness. However, with adaptation, the control surfaces are excited, and their deflection is changed as shown in Figure 13 & 14 due to the adaptation of its control effectiveness. This is further examined by the adaptation of the control effectiveness relative to the true control effectiveness of the aircraft dynamics shown in Figure 15, where the respective entries of the control effectiveness matrix correspond to the row and column respectively, here $\hat{G}(1,2)$ corresponds to the right hand inboard elevon control effectiveness estimation. It can be observed that the affected control surfaces on the left and right-hand side adjust proportionally, however as there is no excitation in the yaw channel, its control effectiveness does not show a significant difference as the change in sideslip angle was not perturbed significantly. The underestimation of the non-faulty CE terms lead to increased control effort by the respective control surfaces and thus account for the loss of effectiveness of the other control surfaces.

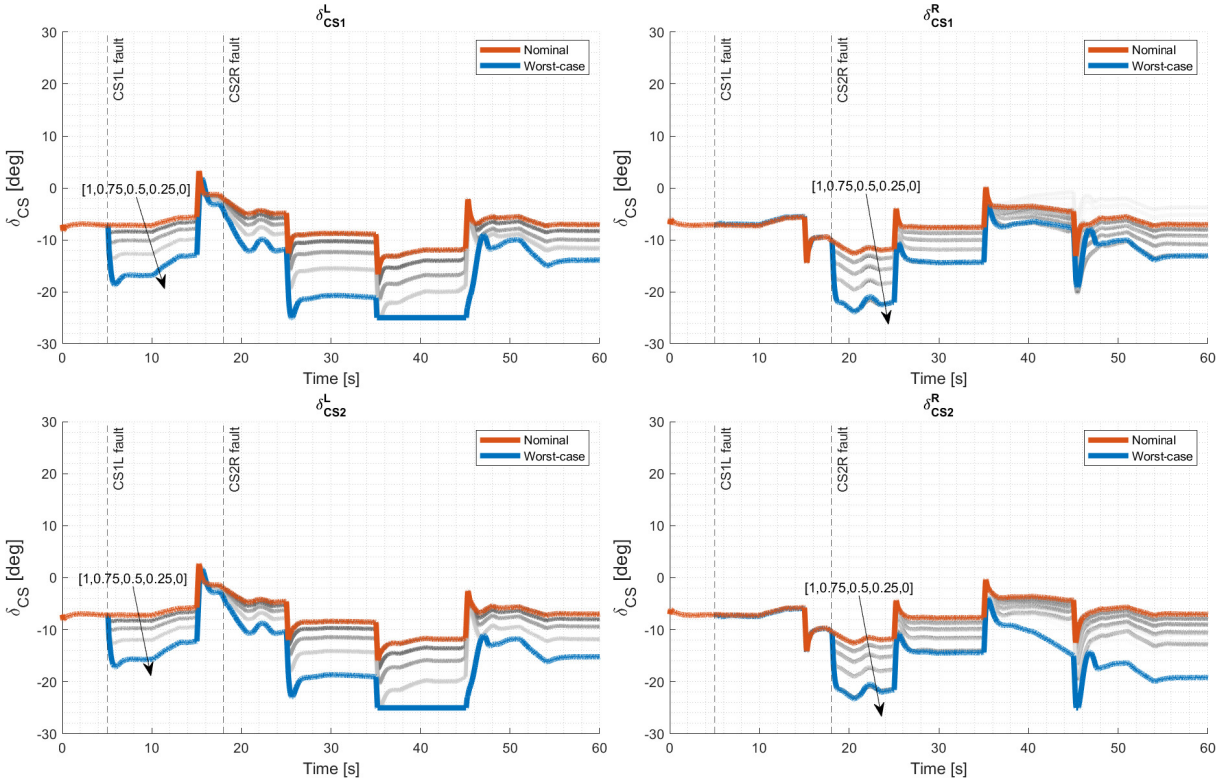

Fig. 11 INDI: Control surface deflection with fault on inboard elevon δ^L_{CS1} and outboard elevon δ^R_{CS2} in increments

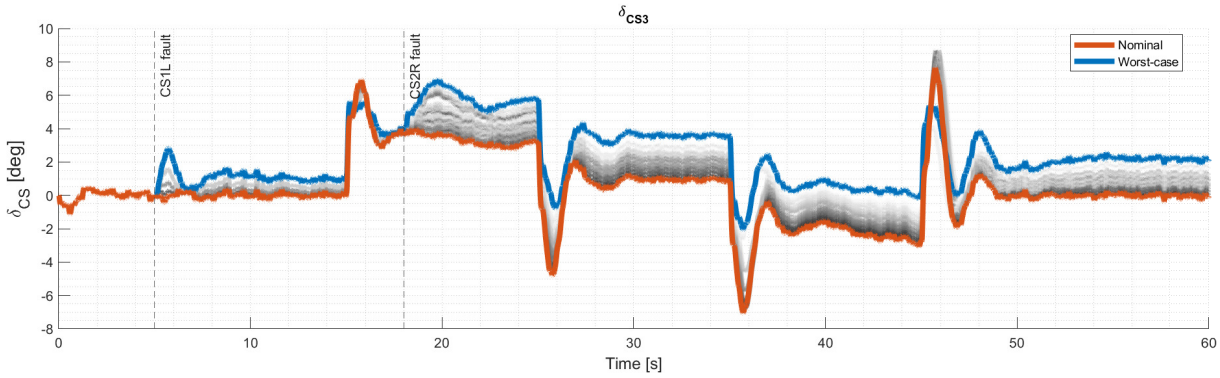

Fig. 12 INDI: Control surface deflection with fault on rudders δ_{CS3} in increments

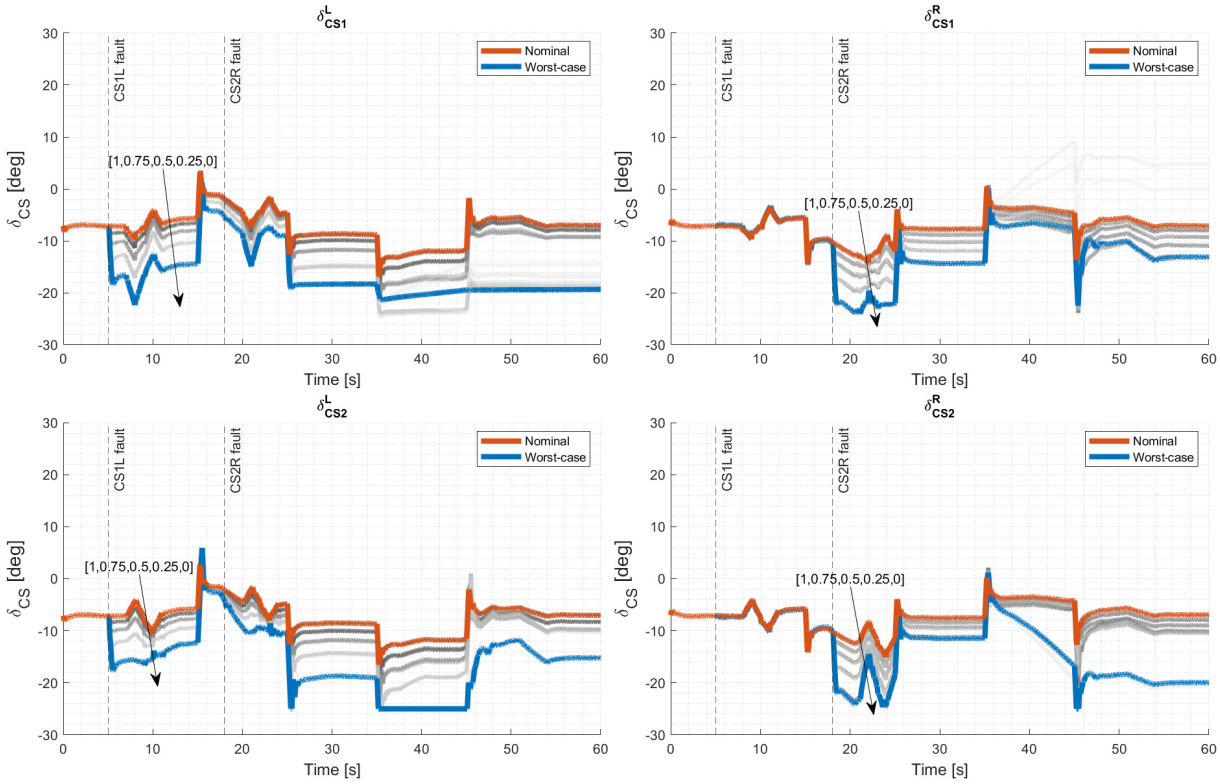

Fig. 13 AINDI: Control surface deflection with fault on inboard elevon δ^L_{CS1} and outboard elevon δ^R_{CS2} in increments

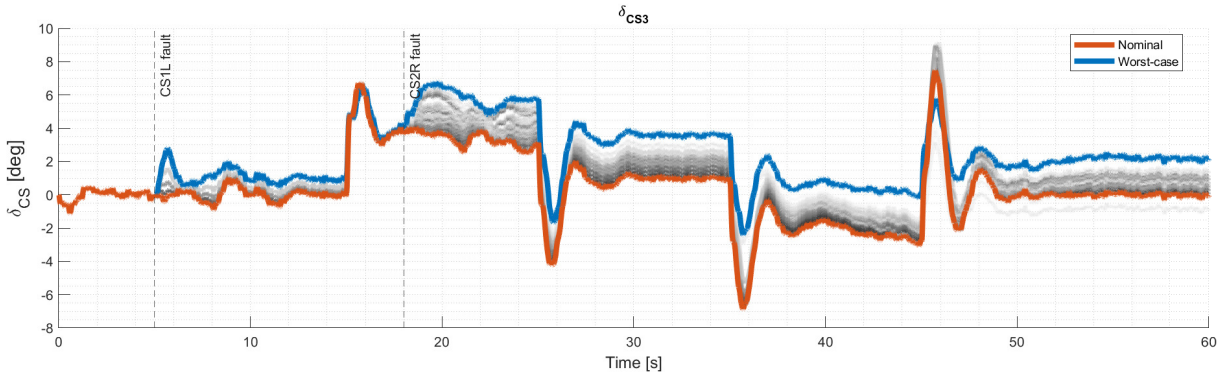

Fig. 14 AINDI: Control surface deflection with fault on rudders δ_{CS3} in increments

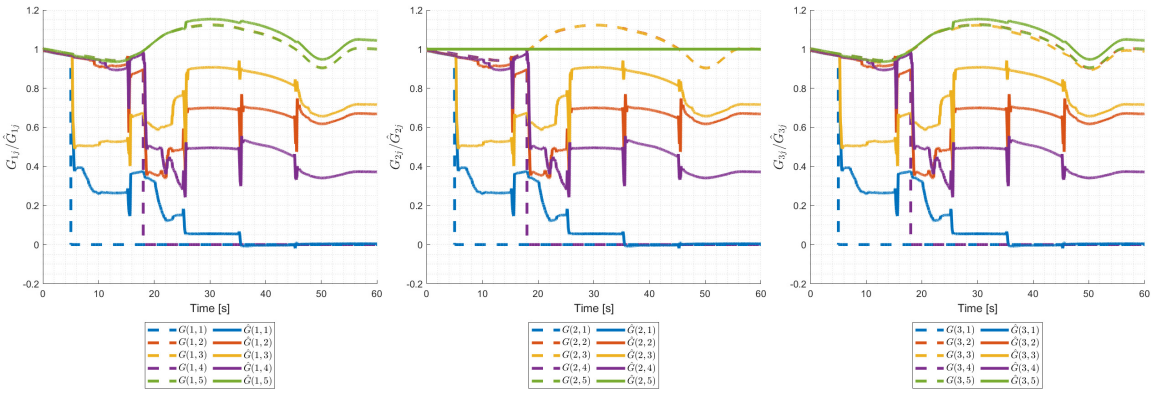

Fig. 15 Relative Control effectiveness estimation

V. Conclusion

In this research adaptive Incremental Nonlinear Dynamic Inversion (INDI) has been applied in the inner loop for rate control to adapt the onboard Control Effectiveness (CE) and account for model mismatches and faults. INDI has been known to be robust against model uncertainties, however in cases like limited control authority and faults, the concern of performance degradation could impede on safe and operable flight. These results establish how adaptation of the onboard CE used with INDI control law improves performance in the presence of faults such as loss of effectiveness. The CE model is adapted through a scaling parameter that corrects the currently estimated onboard model. This simple structure allows a generalisable implementation without prior-knowledge of the underlying model parameter structure, however, as non-linearities are not captured with this lumped correction term, different parameter models may be required. Further analysis of more challenging fault scenarios to observe how adaptation can maintain satisfactory performance tracking, where sensor faults and actuator faults can be performed. In addition, the excitation is triggered after the fault is injected, which is not known beforehand, with a doublet excitation signal. It is challenging to perform in a closed loop system without influencing the dynamics and potentially even destabilising the aircraft, thus the identification of an adaptation trigger and an optimal excitation could further improve accurate identification. Lastly, noise, disturbances and time delays and even loss of sensors influence the adaptations and needs to be analysed in further analysis.

References

[1] van der Sman, E., Peerlings, B., Kos, J., Lieshout, R., and Boonekamp, T., *Destination 2050*, Report, Netherlands Aerospace Centre NLR, 2021. URL `https://www.destination2050.eu/wp-content/uploads/2021/03/Destination2050_Report.pdf`.

[2] Cappuyns, T., *Handling Qualities of a Flying V Configuration*, MSc. Thesis, Delft University of Technology, 2019. URL `https://resolver.tudelft.nl/uuid:69b56494-0731-487a-8e57-cec397452002`.

[3] van Overeem, S., *Modelling, Control, and Handling Quality Analysis of the Flying-V*, MSc. Thesis, Delft University of Technology, 2022. URL `https://resolver.tudelft.nl/uuid:7fd04eec-41d4-4967-b246-89fdfac2446e`.

[4] van Overeem, S., Wang, X., and Van Kampen, E.-J., "Handling Quality Improvements for the Flying-V Aircraft using Incremental Nonlinear Dynamic Inversion," *AIAA SCITECH 2023 Forum*, American Institute of Aeronautics and Astronautics, Reston, Virginia, 2023. https://doi.org/10.2514/6.2023-0105.

[5] Stougie, J., Pollack, T., and Van Kampen, E.-J., "Incremental Nonlinear Dynamic Inversion control with Flight Envelope Protection for the Flying-V," *AIAA SCITECH 2024 Forum*, American Institute of Aeronautics and Astronautics, Reston, Virginia, 2024. https://doi.org/10.2514/6.2024-2565.

[6] Atmaca, D., Stroosma, O., and Van Kampen, E.-J., "Piloted Evaluation of Flying-V with Incremental Nonlinear Dynamic Inversion and Envelope Protection," *AIAA SCITECH 2025 Forum*, American Institute of Aeronautics and Astronautics, Reston, Virginia, 2025. https://doi.org/10.2514/6.2025-0973.

[7] Joosten, S., Stroosma, O., Vos, R., and Mulder, M., "Simulator Assessment of the Lateral-Directional Handling Qualities of the Flying-V," *AIAA SCITECH 2023 Forum*, American Institute of Aeronautics and Astronautics, Reston, Virginia, 2023. https://doi.org/10.2514/6.2023-0906, URL https://arc.aiaa.org/doi/10.2514/6.2023-0906.

[8] Torelli, R., Stroosma, O., Vos, R., and Mulder, M., "Piloted Simulator Evaluation of Low-Speed Handling Qualities of the Flying-V," *AIAA SCITECH 2023 Forum*, American Institute of Aeronautics and Astronautics, Reston, Virginia, 2023. https://doi.org/10.2514/6.2023-0907, URL https://arc.aiaa.org/doi/10.2514/6.2023-0907.

[9] Vugts, G., Stroosma, O., Vos, R., and Mulder, M., "Simulator Evaluation of Flightpath-oriented Control Allocation for the Flying-V," *AIAA SCITECH 2023 Forum*, American Institute of Aeronautics and Astronautics, Reston, Virginia, 2023. https://doi.org/10.2514/6.2023-2508, URL https://arc.aiaa.org/doi/10.2514/6.2023-2508.

[10] Boeing Commercial Airplanes, *Statistical Summary of Commercial Jet Airplane Accidents: Worldwide Operations 1959-2022*, The Boeing Company, Seattle, Washington, 2023. URL https://www.boeing.com/content/dam/boeing/boeingdotcom/company/about_bca/pdf/statsum.pdf.

[11] Airbus, *A Statistical Analysis of Commercial Aviation Accidents 1958 - 2024*, AIRBUS S.A.S., X00D17008863 Issue 9., Blagnac, 2025. URL https://accidentstats.airbus.com/wp-content/uploads/2025/02/20241325_A-Statistical-analysis-of-commercial-aviation-accidents-2025-links.pdf.

[12] Zhang, Y., and Jiang, J., "Bibliographical review on reconfigurable fault-tolerant control systems," *Annual Reviews in Control*, Vol. 32, No. 2, 2008, pp. 229–252. https://doi.org/10.1016/j.arcontrol.2008.03.008, URL https://linkinghub.elsevier.com/retrieve/pii/S1367578808000345.

[13] Christopher Edwards, Thomas Lombaerts, and Hafid Smaili, *Fault Tolerant Flight Control*, Lecture Notes in Control and Information Sciences, Vol. 399, Springer Berlin Heidelberg, Berlin, Heidelberg, 2010. https://doi.org/10.1007/978-3-642-11690-2.

[14] Smeur, E. J. J., Chu, Q., and de Croon, G. C. H. E., "Adaptive Incremental Nonlinear Dynamic Inversion for Attitude Control of Micro Air Vehicles," *Journal of Guidance, Control, and Dynamics*, Vol. 39, No. 3, 2016, pp. 450–461. https://doi.org/10.2514/1.G001490.

[15] Kanhai, P., *Adaptive control with Multivariate B-Splines and INDI*, MSc. Thesis, Delft University of Technology, 2022. URL https://resolver.tudelft.nl/uuid:fdd8e2fa-1372-4f79-aa05-6ab152e848e1.

[16] Smit, B., Pollack, T. S., and Kampen, E., "Adaptive Incremental Nonlinear Dynamic Inversion Flight Control for Consistent Handling Qualities," *AIAA Science and Technology Forum and Exposition, AIAA SciTech Forum 2022*, 2022. https://doi.org/10.2514/6.2022-1394.

[17] Atmaca, D., and Van Kampen, E.-J., "Fault Tolerant Control for the Flying-V Using Adaptive Incremental Nonlinear Dynamic Inversion," *AIAA SCITECH 2025 Forum*, American Institute of Aeronautics and Astronautics, Reston, Virginia, 2025. https://doi.org/10.2514/6.2025-0081.

[18] Oosterom, W., and Vos, R., "Conceptual Design of a Flying-V Aircraft Family," *AIAA AVIATION 2022 Forum*, American Institute of Aeronautics and Astronautics, Reston, Virginia, 2022. https://doi.org/10.2514/6.2022-3200, URL https://arc.aiaa.org/doi/10.2514/6.2022-3200.

[19] Asaro, S., and Vos, R., "Synthesis of the Aerodynamic Model of a Flying Wing Aircraft," *AIAA SCITECH 2025 Forum*, American Institute of Aeronautics and Astronautics, Reston, Virginia, 2025. https://doi.org/10.2514/6.2025-0852.

[20] Asaro, S., Atmaca, D., Van Kampen, E.-J., and Vos, R., "Control Surface Allocation Based on Offline Handling Quality Simulations for a Flying Wing Aircraft," *AIAA SCITECH 2025 Forum*, American Institute of Aeronautics and Astronautics, Reston, Virginia, 2025. https://doi.org/10.2514/6.2025-2475.

[21] van Empelen, S., *Engine Integration of the Flying V*, MSc. Thesis, Delft University of Technology, 2020. URL https://resolver.tudelft.nl/uuid:c519caf8-0eba-4633-a4f9-be37684417a8.

[22] NADZIEJKO, A., Ponchaud, J.-P., Moutinho, A., Saboo, S., and Shin, H.-S., "BENCHMARK REQUIREMENTS & PERFORMANCE METRICS," Tech. Rep. 723515-INCEPTION-D2.5, Cranfield University, INCEPTIOn, 2018.

[23] Pollack, T., Theodoulis, S., and van Kampen, E., "Commonalities between robust hybrid incremental nonlinear dynamic inversion and proportional-integral-derivative flight control law design," *Aerospace Science and Technology*, 2024. https://doi.org/10.1016/j.ast.2024.109377.

[24] Grondman, F., Looye, G., Kuchar, R. O., Chu, Q. P., and Van Kampen, E.-J., "Design and Flight Testing of Incremental Nonlinear Dynamic Inversion-based Control Laws for a Passenger Aircraft," *2018 AIAA Guidance, Navigation, and Control Conference*, American Institute of Aeronautics and Astronautics, Reston, Virginia, 2018. https://doi.org/10.2514/6.2018-0385.

[25] Slotine, J. J. E., and Li, W., *Applied Nonlinear Control*, Prentice-Hall, 1991. URL https://api.semanticscholar.org/CorpusID:106519536.

[26] van 't Veld, R. C., *Incremental Nonlinear Dynamic Inversion Flight Control*, MSc. Thesis, Delft University of Technology, 2016. URL https://resolver.tudelft.nl/uuid:f85a9c88-7bdb-42cd-a01c-aa85251d365c.

[27] Wang, S., *Incremental sliding mode flight control*, Doctoral Thesis, Delft University of Technology, 2019. URL https://resolver.tudelft.nl/uuid:c8259a08-bbee-4af0-b570-1350a2dd8d89.

[28] Acquatella, P. J., *Robust Nonlinear Spacecraft Attitude Control an Incremental Backstepping approach*, MSc. Thesis, Delft University of Technology, 2011. URL https://resolver.tudelft.nl/uuid:a56090a3-bbce-404b-8e4b-d0e9050b518a.

[29] Acquatella Bustillo, P., *Robust nonlinear attitude control of aerospace vehicles: An incremental nonlinear control approach*, Doctoral Thesis, Delft University of Technology, 2020. https://doi.org/10.4233/uuid:99d82992-080c-4c5d-8d40-4e62e62285c0.

[30] Durham, W., Bordignon, K. A., and Beck, R., *Aircraft Control Allocation*, Wiley, 2016. https://doi.org/10.1002/9781118827789.

[31] Luo, F., Zhang, J., and Jiang, B., "Robustness Analysis of Two Advanced Flight Control Laws: NDI and INDI," *Lecture Notes in Electrical Engineering*, Vol. 821 LNEE, Springer Science and Business Media Deutschland GmbH, 2022, pp. 660–668. https://doi.org/10.1007/978-981-16-7423-5{_}64.

[32] Pollack, T., and Van Kampen, E.-J., "Robust Stability and Performance Analysis of Incremental Dynamic Inversion-based Flight Control Laws," *AIAA SCITECH 2022 Forum*, American Institute of Aeronautics and Astronautics, Reston, Virginia, 2022. https://doi.org/10.2514/6.2022-1395.

[33] Lombaerts, T. J. J., *Fault Tolerant Flight Control*, Doctoral Thesis, Delft University of Technology, 2010. URL https://resolver.tudelft.nl/uuid:538b0174-fe84-43af-954d-02f256b2ec50.

[34] Campbell, S., Nguyen, N., Kaneshige, J., and Krishnakumar, K., "Parameter Estimation for a Hybrid Adaptive Flight Controller," *AIAA Infotech@Aerospace Conference*, American Institute of Aeronautics and Astronautics, Seattle, Washington, 2009. https://doi.org/10.2514/6.2009-1803.

[35] Fortescue, T., Kershenbaum, L., and Ydstie, B., "Implementation of self-tuning regulators with variable forgetting factors," *Automatica*, Vol. 17, No. 6, 1981, pp. 831–835. https://doi.org/10.1016/0005-1098(81)90070-4.

[36] Stougie, J., *Incremental Nonlinear Dynamic Inversion Control with Flight Envelope Protection for the Flying-V*, MSc. Thesis, Delft University of Technology, 2022. URL https://resolver.tudelft.nl/uuid:5d0a883c-bf58-4507-b688-6abccdca4842.

[37] Anonymous, "Flying Qualities of Piloted Aircraft," , 1990. MIL-STD-1797A, Department of Defense Interface Standard, originally issued January 30, 1990.

[38] Anonymous, "Flight Control Design–Best Practices," Tech. rep., NATO Research and Technology Organization (RTO), 2000.

[39] Cook, M. V., *Flight Dynamics Principles: A Linear Systems Approach to Aircraft Stability and Control*, Elsevier, 2012. https://doi.org/10.1016/C2010-0-65889-5.

[40] Anonymous, "Flight Control Systems – Design, Installation, and Test of Piloted Aircraft," , 2008. MIL-DTL-9490E, Department of Defense Detail Specification, issued April 22, 2008.

[41] Mitchell, D. G., and Hoh, R. H., "Low-Order Approaches to High-Order Systems: Problems and Promises," *Journal of Guidance, Control, and Dynamics*, Vol. 5, No. 5, 1982, pp. 482–489. https://doi.org/10.2514/3.56195.

[42] Mitchell, D. G., Klyde, D. H., Hoh, R. H., and Aponso, B. L., "Proposed Incorporation of Mission-Oriented Flying Qualities into MIL-STD-1797A," Technical Report WL-TR-94-3162, Wright Laboratory, Wright-Patterson Air Force Base, OH, USA, October 1994.

Part II

Literature Research

This part has already been graded

2

Flying V

This chapter concerns the description and literature review of research activities, which have contributed results in the interest of research and development for the Flying V's Flight Control System (FCS). These research activities are selected based on the main challenges identified in the research context Section 1.1, but also contributions that lead to new data or knowledge for developing the FCS. First an introduction of the Flying V is designed where the Full Scale model and Sub-Scale Flight Test Model are described (2.1). Thereafter, the description of aerodynamic modelling & system identification research results is described (2.2). Using the model subsequent flying & handling qualities research have been conducted (2.3) and the development for the Flying V's FCS will be described (2.4).

At last, a conclusion is provided where an answer to the following sub-questions will be determined and answered.

- What shortcomings and recommendations have been raised from previous research on developing the FCS for the Flying V?
  1. Which lessons can be learned from previous Flying V research?
  2. What is the current state of the Flying V simulation model?
  3. What are the uncertainty sources present in the current model of the Flying V?
  4. What are the specifications for the adaptive control FCS?

2.1. Flying V Design

In Section 1.1 a brief introduction of the Flying V was provided with respective key research activities. It was presented that the aerodynamic optimisation and structural analysis have converged to a preliminary design of the Flying V [2, 10, 11]. The top-level design requirements for the studies are outlined in Table 2.1. An engine-airframe study was conducted, which is essential given that the optimisation studies only considered the airframe alone. Aerodynamic simulations and a study on finding the optimal location were done, resulting in the location of the engine as illustrated in Figure 2.1 [33].

Parameter	Value	Unit
Length	55	[m]
Wingspan	65	[m]
Height	17	[m]
Pax	314	[-]
Fuel Capacity	140.000	[l]
Cargo Capacity	160	[m^3]
Design Mach Number	0.85	[l]
Cruise Altitude	43.000	[ft]

Table 2.1: Flying V Top level design parameters [34]

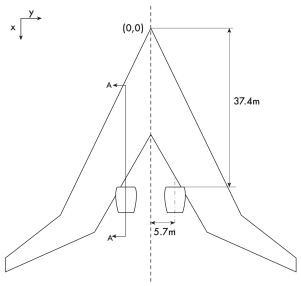

Figure 2.1: Recommended engine position. Taken from [33]

The preliminary design was used to investigate the handling qualities, for which a full-scale aerodynamic

model was developed with the Vortex Lattice Method (VLM) and a lumped mass model was used for the mass and moment of inertia estimation [34]. The design used for the study considers inboard and outboard elevons located at the trailing edge of the wing ($\delta_{CS1}^{L/R}, \delta_{CS2}^{L/R}$) for the right and left sides respectively. The inner and outboard elevon can be used for pitch and roll control. A rudder ($\delta_{CS3}^{L/R}$) is integrated into the winglets on the right and left sides respectively for yaw (directional) control. The geometry of the design is shown in Figure 2.2, but the landing gear was not taken into account for the study.

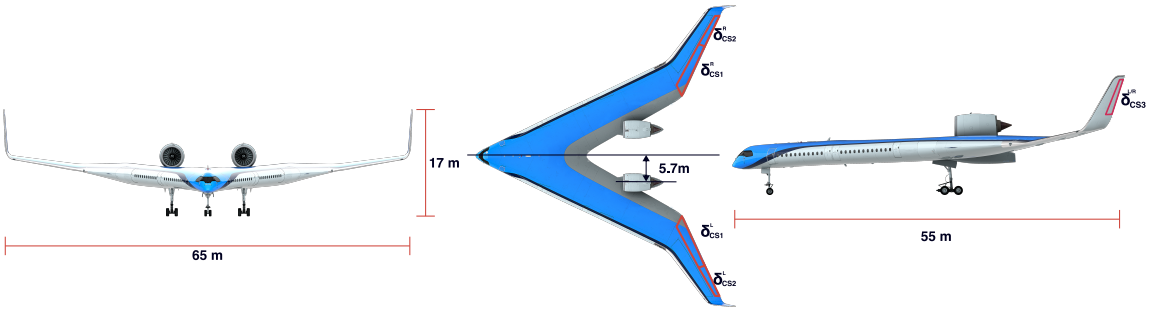

Figure 2.2: Front, top and side view of the Flying V with (outer) dimensions and control surfaces

Concurrently, for the development of a sub-scale model of the Flying V, a half-wing model was developed, that has an additional control surface on the wing and resulting to three control surfaces on the wing. The control surface design was motivated by the findings of a previous tailless aircraft study, where the need for extra control authority is one of the main challenges in the design phase of a flying wing configuration. Moreover, compared to conventional aircraft, the control surfaces of the Flying V will have to provide both longitudinal and lateral control authority [35, 36]. Initial experiments with the half did not have the wing with winglets nor were the engine airframe interactions included. This was investigated later with subsequent studies for winglet and rudder in study [37] and engine integration in [38]. The designs will be denoted as the Full Scale (FS) design and the Sub-Scale Flight Test (SSFT) design [1].

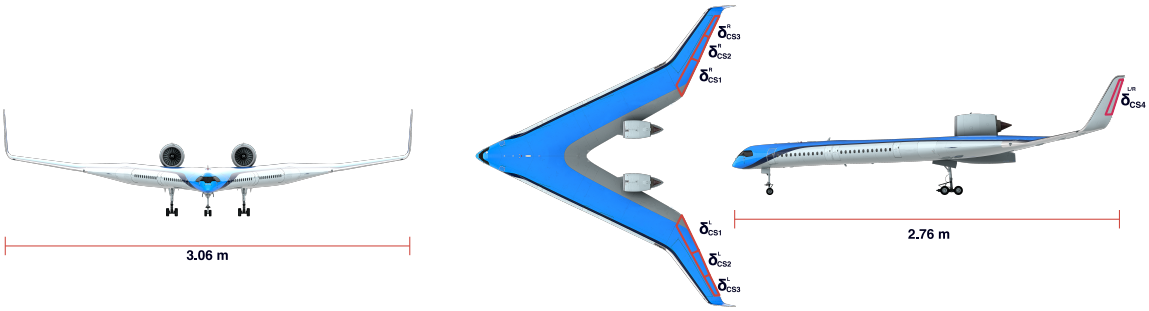

Figure 2.3: Front, top and side view of the Sub Scale Flight Test model with (outer) dimensions and control surfaces

Future studies have been performed concerning the optimisations have been performed and focus on aspects such as the outer wing [39], winglets [40], split flaps [41, 42]. Moreover based on the initial FS design a conceptual design for a Flying V Family has been developed [43] and an updated geometry design has been developed [44].

2.2. Aerodynamic Model & System Identification

Before describing the aerodynamic models & system identification studies, it is necessary to introduce in what reference frame the aerodynamic coefficients are defined in, which is the body-fixed reference frame ($\mathcal{F}_{\mathcal{B}}$) as shown in Figure 2.4.

[1] specifications taken from `https://www.tudelft.nl/en/ae/flying-v/flying-scale-model`

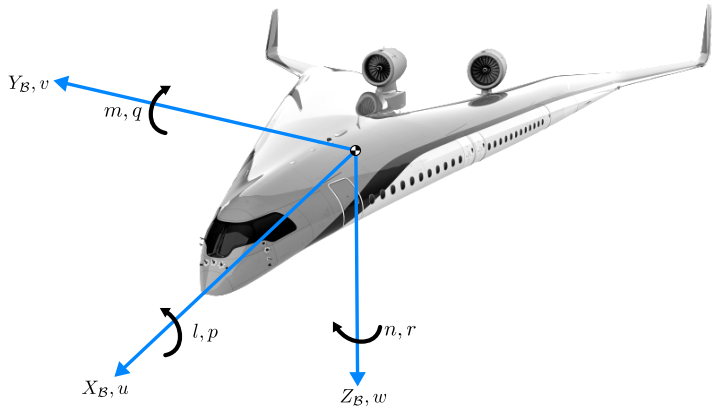

Figure 2.4: Aircraft body axes and conventions. Adapted from [34]

The origin of this reference frame is located at the aircraft's center of mass, and if the gravity field is constant, this origin coincides with the aircraft's center of gravity (CG). The body axes are defined as $X_\mathcal{B}$, which points forward and is in the symmetry plane of the aircraft, $Y_\mathcal{B}$, which is directed to the right wing of the aircraft and perpendicular to the symmetry plane and lastly $Z_\mathcal{B}$, which also lies in the symmetry plane and points downwards [45]. The body velocity (u, v, w) is described along each axis. The moment (l, m, n) and the angular rates (p, q, r) are also described about each axis. The forces and moments about each axis are non-dimensionalised and described as the following:

$$C_X = \frac{F_{X_\mathcal{B}}}{\bar{q}S} \qquad C_Y = \frac{F_{Y_\mathcal{B}}}{\bar{q}S} \qquad C_Z = \frac{F_{Z_\mathcal{B}}}{\bar{q}S} \tag{2.1}$$

$$C_l = \frac{M_{X_\mathcal{B}}}{\bar{q}Sb} \qquad C_m = \frac{M_{Y_\mathcal{B}}}{\bar{q}S\bar{c}} \qquad C_n = \frac{M_{Z_\mathcal{B}}}{\bar{q}Sb} \tag{2.2}$$

Where the dynamic pressure is defined as:

$$\bar{q} = \frac{1}{2}\rho_{air}V_\infty^2 \tag{2.3}$$

With the description of the aerodynamic coefficients outlined, first a brief theoretical background of system identification is described to understand the acquirement and process for creating an aerodynamic model (2.2.1). Thereafter, the research of the aerodynamic model for the Flying V is described (2.2.2. At last, the conclusion regarding the current state of Flying V aerodynamic models can be made (2.2.3).

2.2.1. Theoretical Background

Figure 2.5: Aerodynamic modelling procedure and phases. Adapted diagram from [46]

Initially, a Computational Fluid Dynamic (CFD) analysis is conducted, where the aerodynamic design of an aircraft is numerically analysed, and an aerodynamic model, which can be a discretized set of data, that defines the (static) aerodynamic coefficients at certain aircraft conditions (e.g. attitude & velocity, center of gravity, control deflections), can be estimated for characterising the aircraft's static and dynamic stability of the aircraft at certain operation points. However, the accuracy and completeness of this model are dependent on the CFD technique and analysis done, moreover, even with all computational resources available; wind tunnel tests and flight tests are the reliable source of aerodynamic

data, especially considering the nonlinear aerodynamic behaviour in flight. Thus, wind tunnel testing is used for further validation and investigation of the aerodynamics. However, dynamic characteristics of the aerodynamic coefficients can not be fully established in a wind tunnel test, as it concerns static conditions and operation points. Through flight testing, further investigation and gathering of flight test data is used to observe and capture data, where an identification process can be applied to develop a model that also captures dynamic characteristics of the aerodynamics [46, 47].

The identification process is referred to as system identification, which concerns itself with the determination of the mathematical model, in this case, the aerodynamic model, that gets identified through gathering experimental data. The framework of this process is also described as the Quad-M framework of flight vehicle system identification [47] as illustrated in Figure 2.6.

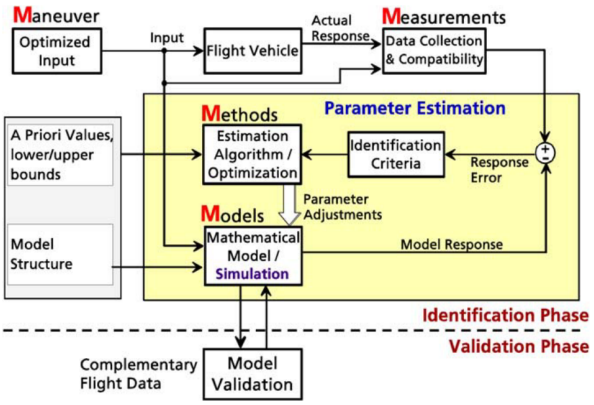

Figure 2.6: Quad M basics of flight vehicle system identification [**Jategaonkar2015FlightEdition**]

A general outline of this Quad-M is described as, where in the identification phase the following actions are applied:

- **Maneuver:** The selection and design of control input to excite the dynamic modes of the aircraft.
- **Measurements:** The aircraft states and response are gathered through measurements with sensors, which can have the presence of noise, bias and errors. Therefore selection and set-up of high-accuracy measurements of the aircraft response through the use of sensor instruments and filters is of great relevance. Using the measurement, state estimation techniques are used to determine the system's response and aircraft states.
- **Models:** The selection of the model that is used to parameterise the aircraft parameters.
- **Methods:** The selection of parameter estimation methods, concerns algorithms that are used to identify the parameters through the measurements and aircraft response, against the current model response.

Thereafter a validation phase is done, where the identified model is compared against known model information from previous measurements or tests. After such a process a mathematical formulation of the model can be defined:

$$\dot{\mathbf{x}} = \mathbf{f}(\mathbf{x}(\mathbf{t}), \mathbf{u}(\mathbf{t}), \boldsymbol{\Theta}) \tag{2.4}$$

$$\mathbf{y} = \mathbf{h}(\mathbf{x}(\mathbf{t}), \mathbf{u}(\mathbf{t}), \boldsymbol{\Theta}) \tag{2.5}$$

Where:

$$\begin{aligned} \mathbf{f}, \mathbf{h} &= \text{(nonlinear) system \& output equations} \\ \mathbf{x} &= \text{System states} \\ \mathbf{u} &= \text{Input} \\ \mathbf{y} &= \text{System output} \\ \boldsymbol{\Theta} &= \text{Unmodeled \& unknown parameters} \end{aligned}$$

2.2.2. Research

The aerodynamic model has been identified and developed through different sources. The first source concerns the Vortex Lattice Method (VLM), which describes a linearised aerodynamic model of the Full Scale aircraft. The second model is gathered using Wind Tunnel Experiments (WTE) on a half-wing sub-scale wing. The third model is determined through a flight test experiment with the SSFT aircraft. At last a combined model has been created using the linearised VLM model and WTE. For each model, research contributions for the model will be described with the respective assumptions and validity.

Vortex Lattice Method Model

A full-scale aerodynamic simulation model of the FS Flying V aircraft was determined through an aerodynamic analysis using ODILILA, which is an Airbus proprietary tool for Computational Fluid Dynamics (CFD) using the Vortex Lattice Method (VLM). The aircraft geometry is designed with the preliminary model, from previous studies, and translated into a parametric model that can be used with a lumped mass model for inertia estimations and a panel model, which is used for aerodynamic estimations, as illustrated in Figure 2.7. The tool takes the taper, twist, control surfaces, high lift devices and nacelles into account. One additional detail is that the ODILILA output has its own aerodynamic reference frame description, and thus a transformation from ODILILA's reference frame to the Flying V's body reference frame needs to be applied. The tool has inputs for different Center of gravity in (CG) in %MAC, aircraft velocity in Mach M, angle of attack (α), sideslip angle (β), normalized roll, pitch, yaw rate (p^*, q^*, r^*) and deflection of each control surface ($\delta^L_{CS_i}, \delta^R_{CS_i}$) [34].

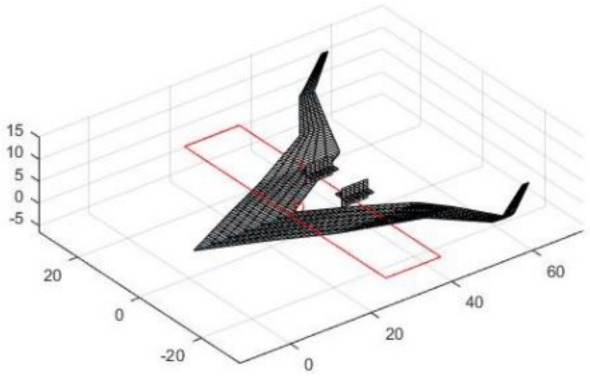

Figure 2.7: ODILILA panel method for the Flying V [34]

The generated output considers a range of aerodynamic coefficients across a range of low-velocity with Mach number ranging from 0.2 to 0.3 (approach) and 0.8 (cruise condition) for a range of angles of attacks (α). The model comes with limited validity as it makes several assumptions and choices, which are defined as follows [22, 34]:

- The VLM method assumes incompressible, inviscid and irrotational flow
- The atmospheric model does not include wing or wind shear or turbulence
- The model does not include the landing gears and fairing

The obtained VLM aerodynamic model describes a linear set of aerodynamic coefficients defined for:

- M : Mach number for approach conditions and cruise condition
- α : Angle of Attack angle range
- β: Side slip angle range
- $\hat{p}, \hat{q}, \hat{r}$: Non-dimensional Angular rates
- $\delta^{L/R}_{CS_i}$: Control surface deflection

The aerodynamic coefficients are defined as:

$$C_* = C_{*_0}(\cdot) + C_{*_\alpha}(\cdot) + C_{*_\beta}(\cdot) + C_{*_{p^*}}(\cdot) + C_{*_{q^*}}(\cdot) + C_{*_{r^*}}(\cdot) + \sum_{i=1}^{3} C^L_{*_{CSi}}(\cdot) + \sum_{i=1}^{3} C^R_{*_{CSi}}(\cdot) \tag{2.6}$$

$$\hat{p} = p\frac{c}{V} \qquad \hat{q} = q\frac{c}{V} \qquad \hat{r} = r\frac{c}{V} \tag{2.7}$$

Where C_* represents a specific force and moment coefficient ($C_X, C_Y, C_Z, C_l, C_m, C_n$) and $C_*(\cdot)$ contains the specific parameters relation for the respective coefficient(s). The model is used with interpolation to estimate coefficients between the datasets and extrapolation outside the dataset. The validity of the obtained model has been compared against the half-wing model WTE data, which is scaled for the Full Scale aircraft (Figure 2.8)

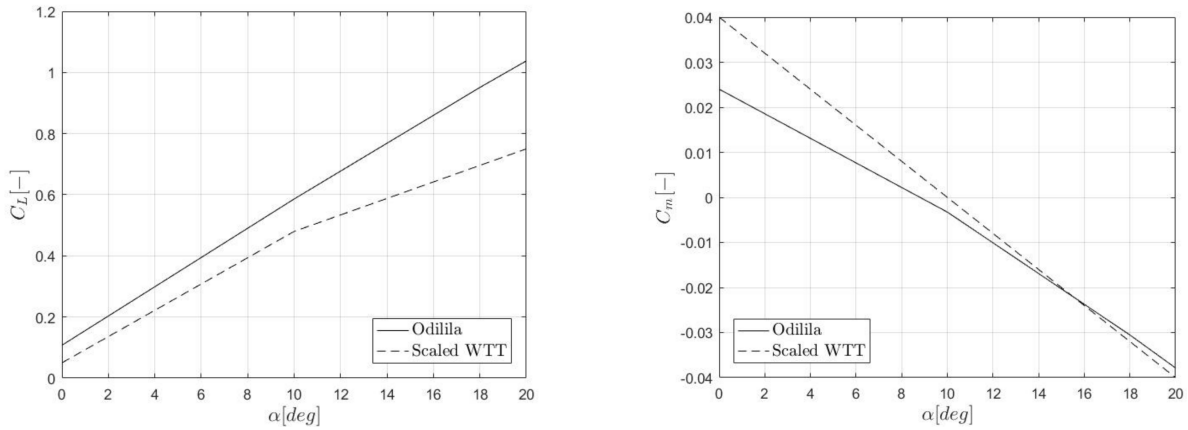

Figure 2.8: ODILILA comparison against Wind Tunnel Test Experiment (WTT). Left: Lift coefficient C_L. Right: Moment coefficient C_m [34]

It can be observed for the lift coefficient (C_L) comparison that up to an angle of attack of 10°, the slopes are similar, but after that, they diverge. For the moment coefficient (C_m) it can be observed the slopes are different at lower angle of attack values, but become similar at higher angle of attack values.

At the time of writing, a new aerodynamic model has been estimated of the full-scale Flying V with an updated geometry. This aerodynamic model has been estimated using Reynolds-Averaged Navier Stokes (RANS) method and VLM to estimate aerodynamic forces and moments contributions by the control surfaces.

Wind Tunnel Experiments

To demonstrate the flight capabilities and airworthiness of the Flying V, a Sub-Scale Flight Test (SSFT) aircraft for flight testing needs to be developed. Before such a model can be developed and designed, the flight characteristics of the aircraft have to be known, as the preliminary model was designed for cruise conditions only and no characteristics are known around approach speed and high angle of attack [48]. This is also done to ensure the safe operation of the SSFT model in flight tests.
Two Wind Tunnel Campaigns were set up [48, 49] and performed using a half-wing model, which was based on the preliminary geometry design and model obtained from previous studies, and has three control surfaces on the wing. Through the half-wing model as shown in Figure 2.9, the analysis of flow behaviour over the wing can be appropriately analysed, but the lift, drag, and moment results are different compared to a full-scale model. In the Wind Tunnel Test Experiments (WTE), the engine, winglet, and landing gear were not taken into consideration [48].
The first WTE campaign was focused on static tests for gathering static aerodynamic forces and moments with the purpose of aerodynamic model identification. The second campaign was focused on gathering information for system identification of the actuators on the control surfaces.

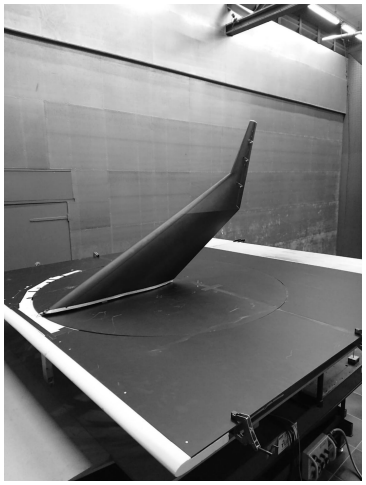

Figure 2.9: Half model wing test subject [48]

The maximum speed in the WTE was 30 m/s, thus compressibility effects are assumed to be small. For the test, different angle of attack, wind speed and control surface deflections are tested. The gathered experimental data plotted against the angle of attack is shown in Figure 2.10.

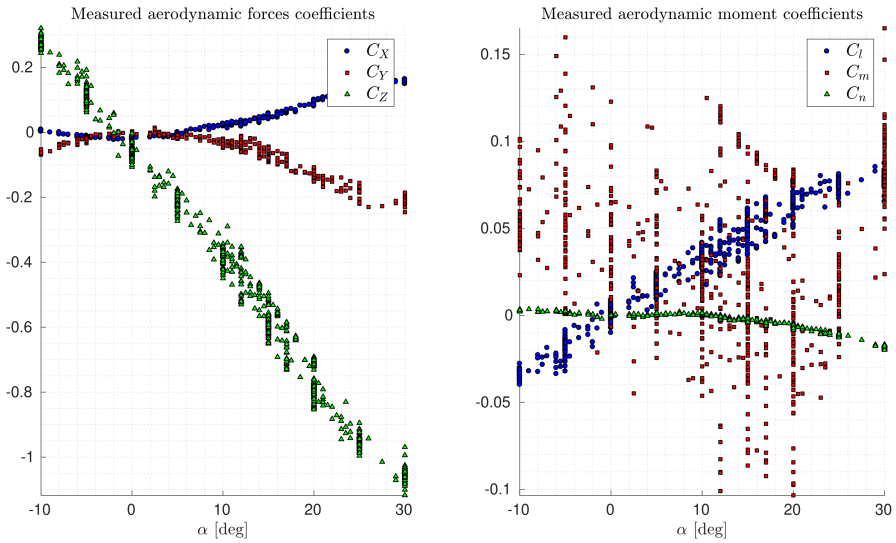

Figure 2.10: Measured aerodynamic forces and moment coefficients. Taken from [50]

With the experimental data gathered using these tests, an aerodynamic model identification study was performed [50], where the experimental dataset is split in an estimation and validation dataset. Figure 2.11 shows two cuts of the estimation convex hull of the dataset, and it can be seen that the validation samples fall into this convex hull also. The study used a stepwise regression technique for the aerodynamic model structure because it can find the strongest correlations between regressors and the dependent variable, while also allowing for the use of model types such as a polynomial model and a spline model. The aerodynamic model concerns an orthogonal polynomial model using Multivariate Orthogonal Functions, which is used to sort the regressors in order of significance for the already estimated model structure, and a non-orthogonal spline model. The spline model is developed to cope with the inability of polynomials to model the complete measured range of angle of attack.
For each model state vector is given by: $x = [\alpha, \hat{V}, \delta_1, \delta_2, \delta_3]$, where $\hat{V}$ is the wind speed normalized with respect to a reference speed and δ_i is the control surface deflection on the half wing model.

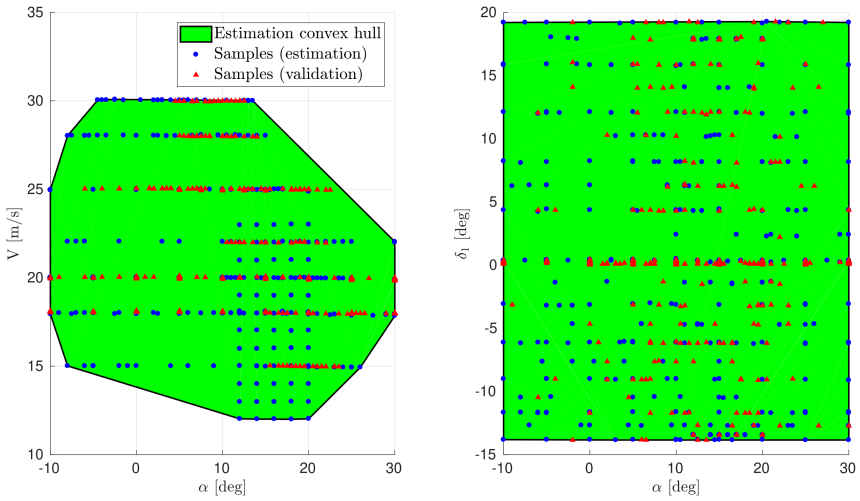

Figure 2.11: left shows $\alpha - V$ convex hull cut and right shows $\alpha - \delta_1$ cut. Taken from [50]

This aerodynamic model defined by the polynomial model is described as follows:

$$
\begin{aligned}
C_X &= C_{X0} + C_{X\alpha}\alpha + C_{X\alpha^2}\alpha^2 + C_{X\alpha^3}\alpha^3 + C_{X\alpha^4}\alpha^4 + C_{X\delta_1}\delta_1 + C_{X\delta_2}\delta_2 + \\
&\quad + C_{X\delta_3}\delta_3 + C_{X\delta_1^2}\delta_1^2 + C_{X\delta_2^2}\delta_2^2 + C_{X\hat{V}}\hat{V} + C_{X\hat{V}^2}\hat{V}^2 \\
C_Z &= C_{Z0} + C_{Z\alpha}\alpha + C_{Z\alpha^2}\alpha^2 + C_{Z\alpha^3}\alpha^3 + C_{Z\delta_1}\delta_1 + C_{Z\delta_2}\delta_2 + C_{Z\delta_3}\delta_3 + C_{Z\hat{V}}\hat{V} \\
C_l &= C_{l0} + C_{l\alpha}\alpha + C_{l\alpha^2}\alpha^2 + C_{l\alpha^3}\alpha^3 + C_{l\alpha^4}\alpha^4 + C_{l\delta_1}\delta_1 + C_{l\delta_2}\delta_2 + C_{l\delta_3}\delta_3 + C_{l\hat{V}}\hat{V} \\
C_m &= C_{m0} + C_{m\alpha}\alpha + C_{m\alpha^2}\alpha^2 + C_{m\alpha^3}\alpha^3 + C_{m\alpha^4}\alpha^4 + C_{m\delta_1}\delta_1 + C_{m\delta_2}\delta_2 + \\
&\quad + C_{m\delta_3}\delta_3 + C_{m\delta_1^2}\delta_1^2 + C_{m\delta_2^2}\delta_2^2 + C_{m\delta_1\delta_2}\left(\delta_1 \cdot \delta_2\right) + C_{m\alpha\delta_1^2}\left(\alpha \cdot \delta_1^2\right) + C_{m\alpha\delta_2^2}\left(\alpha \cdot \delta_2^2\right) + \\
&\quad + C_{m\alpha^2\delta_1}\left(\alpha^2 \cdot \delta_1\right) + C_{m\alpha^2\cdot\delta_2}\left(\alpha^2\delta_2\right) + C_{m\hat{V}}\hat{V} + C_{m\hat{V}\delta_1} \cdot \left(\hat{V} \cdot \delta_1\right) \\
C_n &= C_{n0} + C_\alpha\alpha + C_{\alpha^2}\alpha^2 + C_{\alpha^3}\alpha^3 + C_{\alpha^4}\alpha^4 + C_{\delta_1}\delta_1 + C_{\delta_2}\delta_2 + C_{\delta_1^2}\delta_1^2 + C_{\delta_2^2}\delta_2^2 + C_{\hat{V}}\hat{V}
\end{aligned}
\tag{2.8}
$$

The spline model is described as:

$$
\begin{aligned}
C_X &= C_{X\alpha}\alpha + C_{X\alpha^2}\alpha^2 + C_{X\delta_1}\delta_1 + C_{X\delta_2}\delta_2 + C_{X\delta_3}\delta_3 + C_{X\delta_4}\delta_4 + C_{X\hat{V}}\hat{V} + C_{X\hat{V}^2}\hat{V}^2 \\
&\quad + C_{X\alpha^2_{20}}\left(\alpha - \alpha_{20^\circ}\right)_+^2 \\
C_Z &= C_{Z0} + C_{Z\alpha}\alpha + C_{Z\delta_1}\delta_1 + C_{Z\delta_2}\delta_2 + C_{Z\delta_3}\delta_3 + C_{Z\tilde{V}}\tilde{V} + C_{Z\alpha^1_{11}}\left(\alpha - \alpha_{11}\right)_+ \\
&\quad + C_{Z\alpha^2_{17}}\left(\alpha - \alpha_{17^\circ}\right)_+^2 \\
C_l &= C_{l\alpha}\alpha + C_{l\delta_1}\delta_1 + C_{l\delta_2}\delta_2 + C_{l\delta_3}\delta_3 + C_{l\alpha^1_2}(\alpha - \alpha_{2^*})_+ + C_{l\alpha^2_{20}}\left(\alpha - \alpha_{20^\star}\right)_+^2 \\
&\quad + C_{l\delta_2\alpha_{14}}\delta_2\left(\alpha - \alpha_{14^\circ}\right)_+^0 + C_{l\delta_1\alpha_{23}}\delta_1\left(\alpha - \alpha_{23^\circ}\right)_+^0 \\
C_m &= C_{m0} + C_{m\alpha}\alpha + C_{m\delta_1}\delta_1 + C_{m\delta_2}\delta_2 + C_{m\delta_3}\delta_3 + C_{m\hat{V}}\hat{V} + C_{m\delta_1\delta_2}\delta_1\delta_2 + C_{m\delta_2\delta_3}\delta_2\delta_3 \\
&\quad + C_{m\delta_2^2}\delta_2^2 + C_{m\alpha\delta_2^2}\alpha\delta_2^2 + C_{m\alpha^2_{20}}\left(\alpha - \alpha_{20^\circ}\right)_+^2 + C_{m\alpha^2_{26}}\left(\alpha - \alpha_{26^\circ}\right)_+^2 + C_{m\delta_1\alpha_2}\delta_1\left(\alpha - \alpha_{2^*}\right)_+^0 \\
&\quad + C_{m\delta_1\alpha_{23}}\delta_1\left(\alpha - \alpha_{23^\circ}\right)_+^0 + C_{m\delta_2\alpha_{-7}}\delta_2\big(\alpha - \alpha_{7^\circ}\big)_+^0 + C_{m\delta_2\alpha_{14}}\delta_2\big(\alpha - \alpha_{14^\circ}\big)_+^0 + C_{m\delta_3\alpha_8\hat{\sigma}_3} \\
&\quad + \left(\alpha - \alpha_{8^\circ}\right)_+ \\
C_n &= C_{n0} + C_{n\alpha}\alpha + C_{n\alpha^2}\alpha^2 + C_{n\delta_1}\delta_1 + C_{n\delta_2}\delta_2 + C_{n\delta_2^2}\delta_2^2 + C_{n\hat{V}}\hat{V} + C_{n\alpha^1_8}(\alpha - \alpha_{8^\circ}) \\
&\quad + C_{n\alpha^2_5}(\alpha - \alpha_{5^\circ})^2
\end{aligned}
\tag{2.9}
$$

where α°_* is the angle of attack (in radians) where the knots are located (labelled in degrees for a better readability).

Figure 2.12 shows two slices from the polynomial and spline model of the pitching moment coefficient, along with the calculated prediction confidence bounds, and it can be observed in the figure that most data points fall within the calculated confidence bounds. Table 2.2 shows the fits that were achieved with each respective aerodynamic coefficient model, where the Residual Mean Square errors are determined for the estimation and validation dataset. Moreover, an analysis was done concerning the "local model quality" to determine how the model quality changes for different values of independent variables. It was determined that angle of attack was the variable of choice and the RMS is determined in segments of 5 degrees. The result is shown in Figure 2.13.

It has been shown that the spline model achieved better results than the polynomial model, however, the proposed spline implementation is rather limited as it only considers splines in the angle of attack dimension and does not consider continuity constraints at the knots. Thus, certain recommendations are provided for future spline-based methods, such as B-splines or Multivariate Simplex Splines [50].

Moreover, there are still limitations with the model as it does not consider:

- Biases in the estimations, as it is assumed that the measured data is free of systematic errors and errors in the independent variables due to no previous validated data of the Flying V being available.
- Winglets, landing gear and engine interaction
- No rudder control
- Not valid for lateral aerodynamic forces C_Y

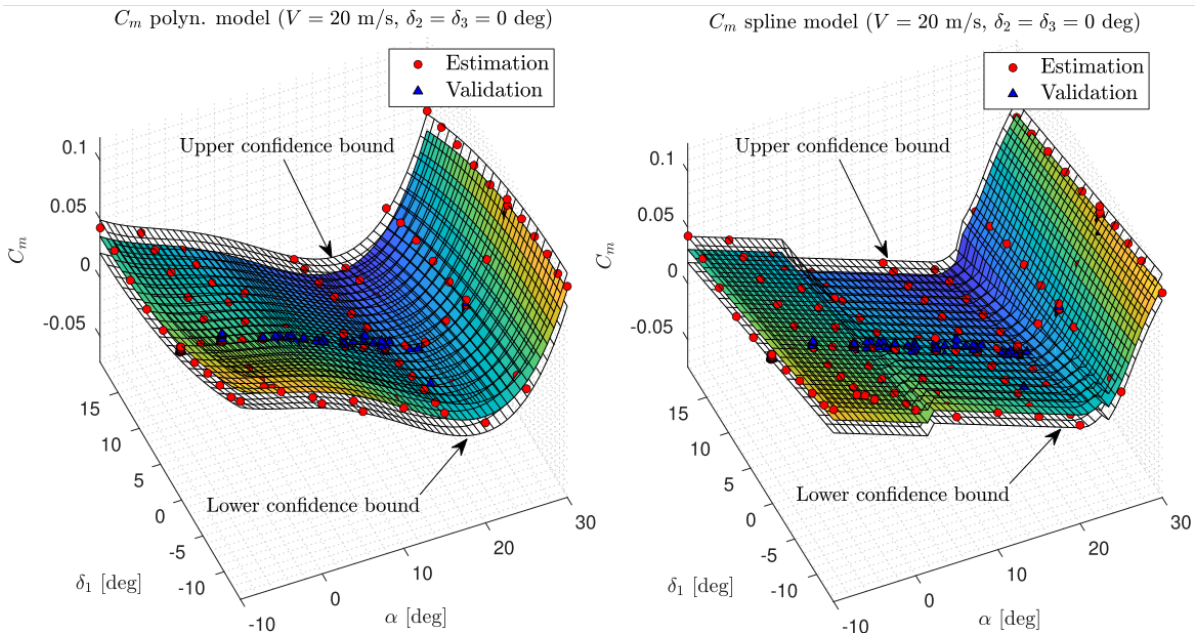

Figure 2.12: $\alpha - \delta_1$ slice for the pitching moment coefficient C_m with Polynomial and spline model respectively. Taken from [51]

Aerodynamic coefficient	RMS$_{rel}$ (est.)		RMS$_{rel}$ (Val.)	
	Polynomial	Spline	Polynomial	Spline
C_X	1.42 %	1.99 %	2.42 %	1.97 %
C_Z	1.42 %	0.75 %	2.38 %	0.96 %
C_m	2.54 %	2.13 %	7.24 %	2.75 %
C_l	1.18 %	1.11 %	4.59 %	1.25 %
C_n	2.25 %	2.03 %	2.74 %	2.28 %

Table 2.2: RMS for the estimation and validation dataset with the Polynomial and Spline aerodynamic model. Data taken from [50]

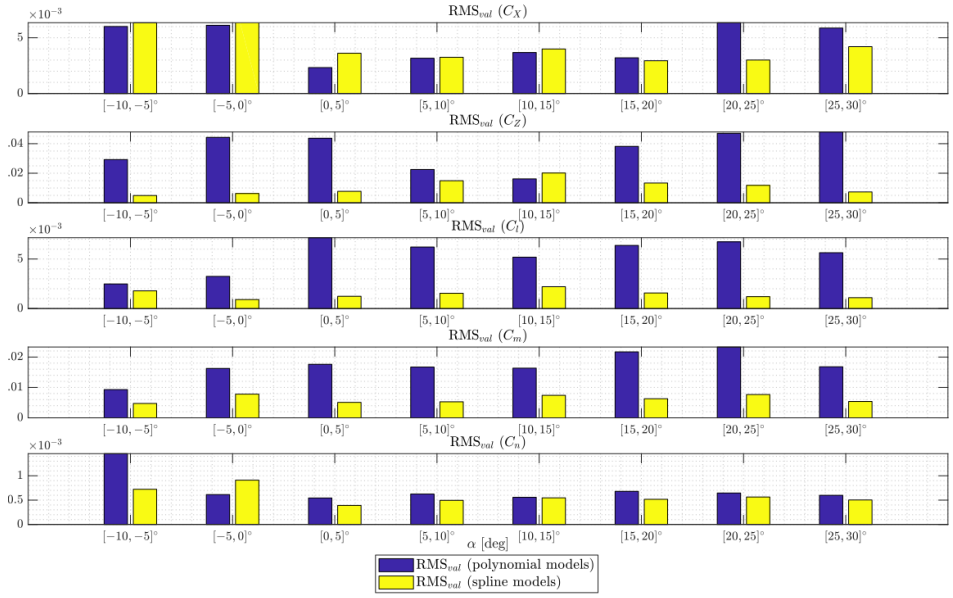

Figure 2.13: RMS of 5 degrees segment in angle of attack. Taken from [50]

At the time of writing, control effectiveness WTE have been conducted, where the control effectiveness was estimated using system identification and sinusoidal control inputs at different frequencies. These new results give further insight of the aerodynamic effects of the Flying V for current and future developments.

Flight Test Experiments

An aerodynamic model of the SSFT was developed with Flight Test Experiments (FTE) with two separate system identification studies [52, 53]. With the insights gathered through the WTE, the SSFT was developed and an initial Maiden flight test was performed successfully. However, there are key differences compared to the WTE model which are as follows:

- Full-wing aircraft instead of a half-wing
- Inclusion of landing gear
- Inclusion of engines
- Inclusion of winglets

Although the initial maiden flight dataset had high uncertainties for the valid system identification, it has provided an understanding of certain aircraft and instrument characteristics, where the unstable Dutch Roll was identified during the flight test. Subsequent flight tests were conducted and have been used to develop an aerodynamic model based on the FTE.

The first study gathered data over eight flight tests [52] and estimated the aerodynamic model using a joint state-parameter estimation method called the Two-Step Method (TSM). With this method, first a state-estimation problem is performed and then the parameter estimation for identifying the aerodynamic coefficients. The state estimation involves the nonlinear equations of motions of the aircraft, where the state is reconstructed using a nonlinear Kalman Filter (KF) such as Extended Kalman Filter (EKF) or Iterated Extended Kalman Filter (IEKF) and aircraft sensor measurements. The Kalman Filter is responsible for removing noise and biases from the measurements by taking the physical relations with the inputs, observations, nonlinear equations of motions and states into account. Using the state estimations, the aircraft measurements can be corrected and using a parameter estimation method to determine or model aircraft parameters, which in this case are the aerodynamic coefficients. An example of the Two-Step Method schematic is shown in Figure 2.14.

The aerodynamic model was developed using a stepwise regression that determined a model structure, where it was determined that compact polynomials with up to second-order terms provided a fit for the aerodynamic model. The model managed to replicate the longitudinal behaviour of the Flying V better

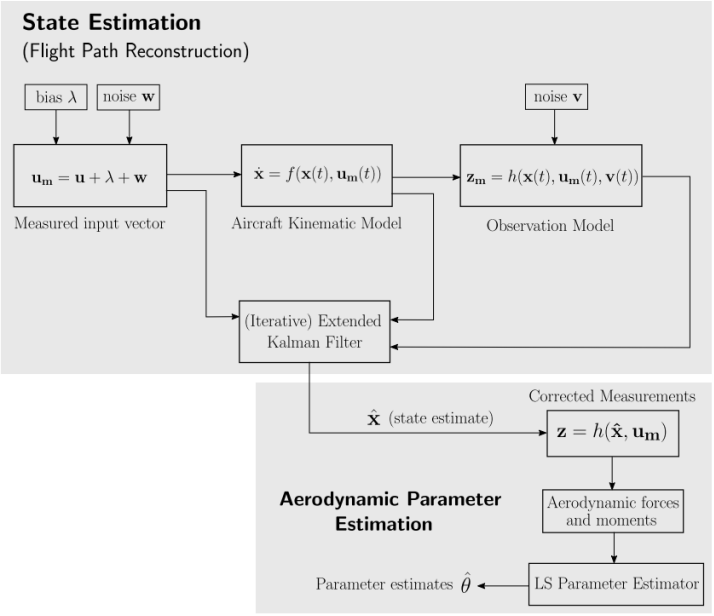

Figure 2.14: Two-Step Method schematic for system identification. Taken from [53]

as the inputs for exciting the lateral dynamics and their respective control inputs, aileron and rudder, were kept conservative to maintain a safe and operable flight [52]. The second study also used the TSM method, but used Ordinary Least Squares for the regression and the model structure was also determined using a stepwise regression technique, resulting in a polynomial model [53].

However, both models described shortcomings when compared to the WTE model as the excitation of the control inputs for system identification is done conservatively to maintain the safe operation of the scaled model and only a limited number of manoeuvres were executed due to the available flight time. Thus, it still needs to be extended with more flights containing different manoeuvres and flight conditions. Moreover, both models have not been scaled against the Full Scale model and further investigation still needs to be performed. Moreover, certain gaps exist in the estimation of the aerodynamic coefficients between the FTE and WTE as the sub-scale wing doesn't model the complete wing aircraft, missing winglets, engine and landing gear also.

Combined Aerodynamic Model

The VLM model was combined with elements of the WTE experiments, to form an aerodynamic model that is able to capture unstable longitudinal effects and lateral effects. The VLM model was used as a baseline, as the control surface layout of the half-wing model is different and the deflections are kept to zero for combining the respective datasets. The elements that are taken from the WTE experiments are the:

- Longitudinal force coefficient (C_X)
- Directional force coefficient (C_Z)
- Pitch moment coefficient (C_m)

The lateral coefficients aren't used as these coefficients from the WTE aren't valid and the VLM model is used instead. The WTE data is scaled according to the Dynamic or Froude scaling method for the approach-and cruise condition (M=0.2 and M=0.85) for angles of attack ranging between -5° and 30°. The scaled WTE data is compared to the VLM data as shown in Figure 2.15, where it can be observed that the scaled WTE data has the same magnitude as the VLM data for the longitudinal and directional force coefficient, but the pitching moment starts higher and the longitudinal instability, pitch break, becomes apparent after an $\alpha = 20^\circ$. To combine the datasets, the pitching moment is vertically translated to match the VLM curve at $\alpha = 15^\circ$ and combined using an interpolating polynomial function *pchip*. After the initial combination it was observed that the aerodynamic model did not contain any zero-lift drag (C_{D_0}) decreasing the fidelity of the model. Due to the limited analysis of the full scale model,

it was then decided to use the zero-lift drag from the Airbus A350-900, which is the reference aircraft for the Flying V. This was added to the aerodynamic model, which results in a combined aerodynamic model as shown in Figure 2.16.

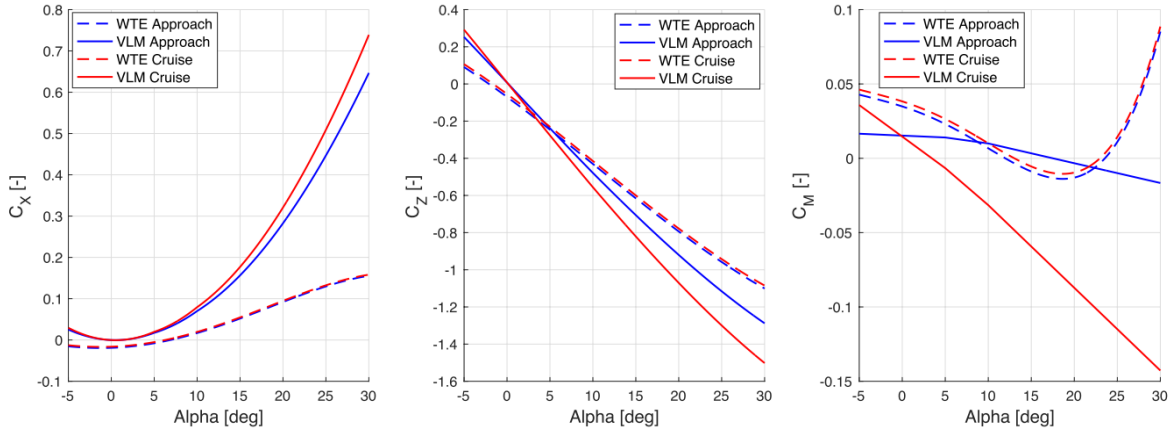

Figure 2.15: Aerodynamic model curves from VLM and scaled WTE for approach and cruise flight conditions [22]

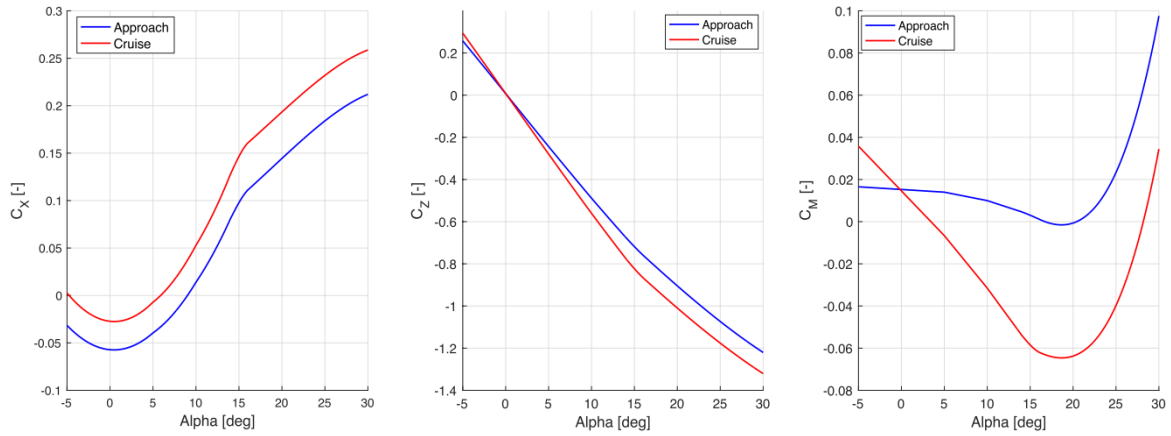

Figure 2.16: Combined Aerodynamic model curves for approach and cruise flight conditions [22]

2.2.3. Conclusion

The following conclusions can be made regarding the use of the aerodynamic model.

- The latest aerodynamic model for the Full-Scale Aircraft is determined by the combination of the VLM model and elements from the WTE, which is able to capture longitudinal instability, pitch break and lateral instability, dutch roll.
- The Flight Test Experiment needs further investigation and validation against the WTE experiments, before it can be scaled to the Full Scale model. Although similar procedure could be applied as with the combined aerodynamic model, the validity of the combination requires additional investigation and with the upcoming new aerodynamic model for the full scale model a new model will be provided, thus not requiring the demand of such an investigation at this moment.

2.3. Flying & Handling Qualities

One important field of study is the analysis of flying & handling qualities, which asses how easy the aircraft is to fly and how well a pilot can operate and perform tasks with the aircraft. Regulatory bodies don't have formal requirements for quantifying the flying & handling qualities, however military standards describe such requirements based on the aircraft's role, which is divided into classification, flight phase, task corresponding to respective flight phase category and the corresponding level of flying quality that is required. Thus, first some theoretical background is described regarding the assessment and analysis of flying & handling qualities (2.3.1). Thereafter, the results of past research activities

for the flying & handling qualities of the Flying V are elaborated (2.3.2). At last, a conclusion is made regarding the latest state of flying and handling qualities research (2.3.3).

2.3.1. Theoretical Background

The flying and handling qualities specification is set by civil authorities and military standards, although civil aviation authorities do not provide quantifiable (analytical) requirements for the compliance of the aircraft's dynamic modes as they're primarily concerned with safety. However, military standards such as *MIL-F-8785C* and its follow-up *MIL-STD-1797A* [54] set up comprehensive and specific requirements and the description of these standards have been comprehensively gathered in *Flight Dynamics Principles by M.V. Cook* [55]. An overview of the aircraft role determination and flying quality levels is described in Table 2.3.

	Aircraft Class
Class I.	Small, light airplanes
Class II.	Medium weight
Class III	Large, heavy
Class IV.	High manoeuvrability
	Flight Phase
Category A	Non-terminal flight phases that require rapid manoeuvring, precision tracking, or precise flight path control
Category B	Non-terminal flight phases that require gradual manoeuvring, less precise tracking and accurate flight path control
Category C	Terminal flight phases that require gradual manoeuvring and precision flight path control
	Flight phase tasks
Category A	Air-to-air combat, Ground attack, Weapon delivery/launch, Reconnaissance, In-flight refuel (receiver), Terrain following, Maritime search, Aerobatics, Close formation flying
Category B	Climb, Cruise, Aerobatics, Loiter, In-flight refuel (tanker), Descent, Aerial delivery
Category C	Takeoff, Approach, Overshoot, Landing
	Flying Level Qualities
Level 1	Flying qualities clearly adequate for the mission flight phase.
Level 2	Flying qualities adequate to accomplish the mission flight phase, but with an increase in pilot workload and, or, degradation in mission effectiveness.
Level 3	Degraded flying qualities, but such that the aeroplane can be controlled, inadequate mission effectiveness and high, or, limiting, pilot workload

Table 2.3: Aircraft classifications, Levels of Flying Qualities [55]

In terms of the MIL-STD convention, the Flying V's requirements are similar to that of an Airbus A350[2], which is Class III aircraft (large, heavy, low/medium manoeuvrability aircraft, see CS-25) in Category B or C phase.

Aircraft Dynamic Modes & MIL Specifications

The aircraft's dynamic modes can be excited from its trimmed equilibrium if it is disturbed by pilot controls, change in power input, airframe configuration changes and by external atmospheric influences such as gust or turbulence. The behaviour of these dynamic modes are inherent to the airframe design and the analysis concerns the stability and handling quality of the aircraft.

The specifications of the MIL-STD requirements for analytical quantification of flying & handling qualities and description of dynamic modes have been gathered in academic and industry textbooks [45, 55, 56]. These specifications describe certain thresholds of the aircraft's dynamic modes through properties such as natural frequency (ω), damping ratio (ζ), period (T), time constant (τ). These properties are derived and gathered through the dynamic equation of motions and the time response of the aircraft and can describe how fast a motion oscillates, how quickly the motion damps out, the time it takes

[2] https://www.tudelft.nl/lr/flying-v

for one oscillation and the time it takes for a motion to decay back to its equilibrium. The threshold for these properties are defined for the three Flying Level Qualities and obtained through empirical research, such that a pilot has good handling qualities. These specifications can then be used for the design of the FCS and combined with handling qualities criterion, which can specifically look the time response and tracking performance or aircraft stability properties and the respective specifications and handling qualities are often described separately for the longitudinal and lateral direction [55].

Longitudinal Dynamic Modes

1. **Short-Period Mode**: The short-period motion is an oscillating pitch rate response. This motion is fast and transient response to an elevator input. To have a sufficient tracking of a reference signal, the short-period must be well damped to reach steady state pitch condition quickly. Table 2.4 summarises the specifications.

Flight Phase	Level 1	Level 2	Level 3
CAT A	$0.34 < \zeta_s < 1.30$	$0.25 < \zeta_s < 2.00$	$0.10 < \zeta_s$
CAT B	$0.30 < \zeta_s < 2.00$	$0.20 < \zeta_s < 2.00$	$0.10 < \zeta_s$
CAT C	$0.50 < \zeta_s < 1.30$	$0.35 < \zeta_s < 2.00$	$0.25 < \zeta_s$

Table 2.4: Short-Period Mode Damping

2. **Phugoid Mode**: The phugoid is commonly described as a lightly damped low-frequency oscillation in speed and coupled into pitch attitude and height, interchanging potential energy with kinetic energy. Table 2.5 summarises the specifications.

Level of Flying Qualities	Damping ratio
Level 1	$\zeta_{ph} > 0.04$
Level 2	$\zeta_{ph} > 0$
Level 3	Unstable, period $T_p > 55$ s

Table 2.5: Phugoid Mode Damping

For evaluating longitudinal handling qualities, criteria such as the CAP, Gibson Criterion, Neald-Smith criteria are used.

Lateral Dynamic Modes

1. **Aperiodic Roll Mode**: The aperiodic roll mode represents a non-oscillatory lateral characteristic response of the roll rate to a roll control input. In case the roll control input is removed, the roll rate should return to zero. Table 2.6 summarises the specifications.

Flight phase	Level 1	Level 2	Level 3
Cat A,C	1.0	1.4	10
Cat B	1.4	3.0	10

Table 2.6: Maximum value for the Aperiodic-Roll mode time constant (τ_r), value in seconds

2. **Spiral Mode**: The spiral mode is a non-oscillatory behaviour and involves a complex coupled motion in roll, yaw and sideslip. Table 2.7 summarises the specifications.

Flight Phase	Level 1	Level 2	Level 3
A,C	$\tau_s > 17.3$	$\tau_s > 11.5$	$\tau_s > 7.2$
B	$\tau_s > 28.9$	$\tau_s > 11.5$	$\tau_s > 7.2$

Table 2.7: Spiral mode time constant, value in seconds

3. **Dutch Roll Mode**: This mode is a damped oscillation in yaw and coupled with roll and to a lesser extent with sideslip. Table 2.7 summarises the specifications.

Flight phase	ζ_d	$\zeta_d\omega_d$	ω_d
Cat A	0.19	0.35	0.5
Cat B	0.08	0.15	0.5
Cat C	0.08	0.10	0.5

Table 2.8: Dutch roll frequency and damping minimum values for level 1 flying qualities

Pilot Opinion

The military specifications primarily focus on providing analytical requirements of flying and handling qualities, however, pilots are the operators of the aircraft and their opinions form an important criterion of handling quality and provide the qualitative assessment of an FCS implementation. Through pilot-in-the-loop simulations and the Cooper-Harper Rating scale, illustrated in Figure 2.17, is a structured rating scale for aircraft handling qualities, quantifies the pilot's experience to a desired performance criteria when performing specific pilot-in-the-loop tasks such as tracking a reference attitude. The Cooper-Harper rating scaler relates the pilot's opinion to the pilot's rating, which can help to further refine the FCS and achieve optimal flying qualities.

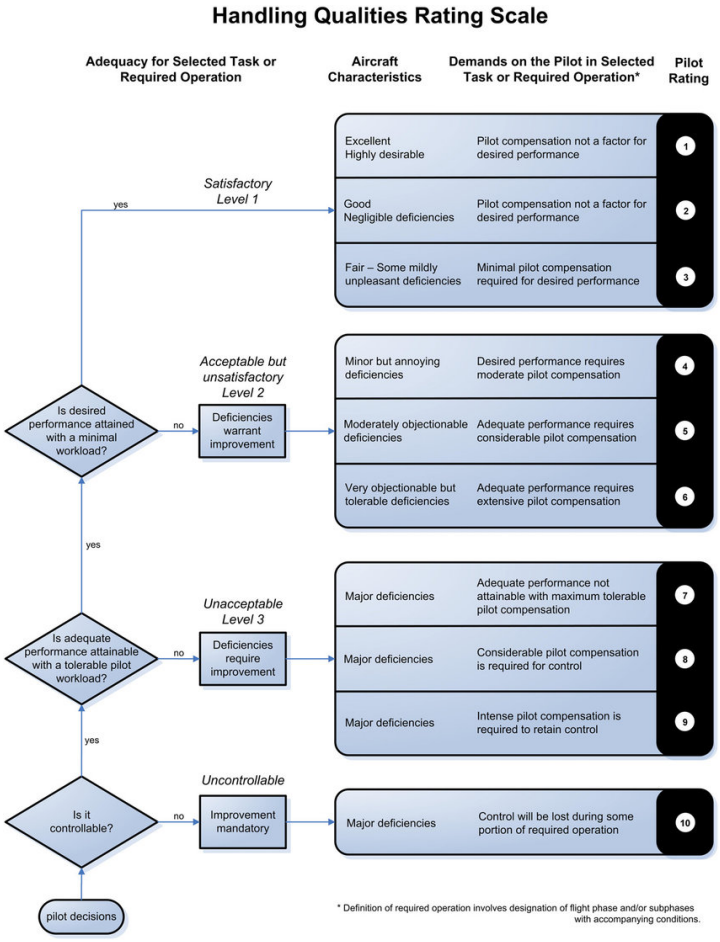

Figure 2.17: Cooper Harper Rating Scale. Taken from [57] that adapted from [58]

2.3.2. Research

The current state of research regarding the analysis and assessment of Flying and Handling qualities for the flying V concerns the following evaluations or sources:

- Handling quality assessment with VLM model [34]
- Wind Tunnel Experiments [48, 50]
- Flight Test experiments [52, 53]

- Three pilot-in-the-loop simulator assessments with direct laws or augmented with a FCS [59–61]
- Nonlinear FCS design and simulation assessment [22, 23]

As the Flying V is different from a conventional aircraft design, certain qualitative assessments and investigations needs to be reviewed critically.

Preliminary Handling Quality Analysis with VLM Model

With the VLM model of the Full-Scale flying, Cappuyns [34] conducted a handling quality analysis regarding the stability and control of the Flying V. Through this study it was established that the Dutch Roll was deemed unstable, limited lateral-directional controllability in case of One Engine Inoperative (OEI) at low speeds. Moreover, at cruise and approach conditions the Phugoid mode were positively damped and stable, for the short period mode the damping ratio was found to be worst at the most forward centre of gravity (CG) position in cruise conditions and better damped at approach conditions with an aft CG position.

Wind Tunnel Test Experiments

Concurrently, before the Flight Test Experiments (FTE) two Wind Tunnel Experiment (WTE) campaigns were conducted where certain flight characteristics were evaluated for approach speed and high angles of attack. According to the WTE research, it was established that the aircraft becomes statically unstable after an angle of attack of $20°$ where the moment coefficient with respect to angle of attack (C_{m_α}) becomes positive as illustrated in Figure 2.18. This phenomena is referred to as pitch break where the aircraft is statically unstable starting from that angle of attack. Moreover, the studies also evaluated the optimum location for center of gravity between 1.345m and 1.425m behind the nose, to trim the aircraft across the range of angle of attack and speed [48]. The optimal center of gravity is at 1.365m. The maiden flight confirmed that the Dutch Roll during approach was unstable [22].

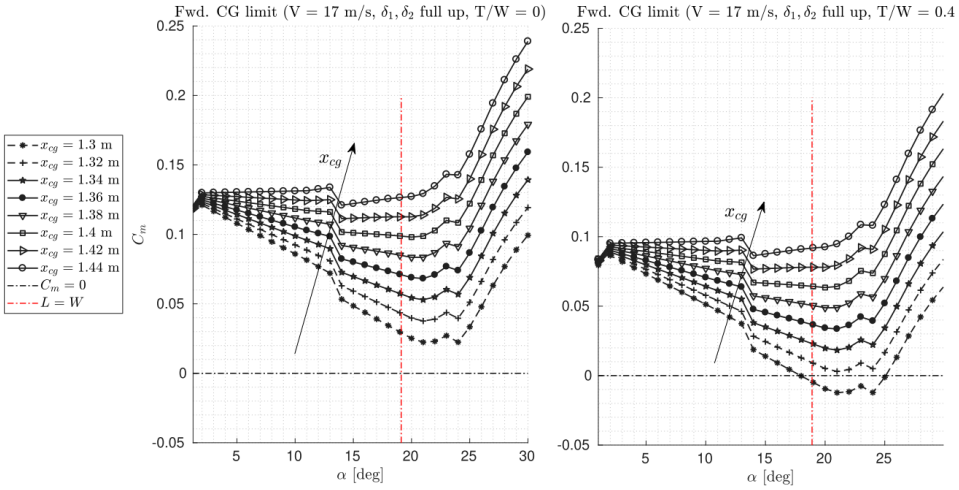

Figure 2.18: Wind Tunnel Experiment result of moment coefficient for the scaled aircraft model with and without thrust effects at different center of gravity locations. Taken from [50]

Piloted Simulator Experiments

Using the obtained VLM model from Cappuyns three piloted simulator experiment studies were conducted, where direct flight control laws were designed to distribute the pilot's control inputs to the respective control surfaces and some studies designed some linear stability augmentation laws to damped unwanted aircraft dynamics.

The first study [36] focused on the evaluation of longitudinal handling qualities, where two Control Allocation (CA) schemes were designed, the first CA is a conventional scheme that considers inboard and outboard deflection in the same direction and second CA considers the deflection in opposite direction, the latter is designed to counter non-minimum phase behaviour in flight path angle response, which has been determined through offline analysis, where the aircraft's longitudinal dynamic modes

through Mode Participation Factor (MPF) are analysed and handling qualities regarding the pitch rate and vertical velocity are analysed. The selected experiments were:

1. Pitch angle tracking task
2. Flight path angle tracking task

The experiments were conducted, and the handling qualities were assessed through Cooper-Harper Rating Scale (CHRS), where it is expected that the handling qualities for Pitch angle control is Level 1 and Level 2 for flight path control. The pilot preferred the first CA scheme due to its higher control authority for both tracking tasks, although the second CA scheme did alleviate the pilot workload in negating the non-minimum phase behaviour on the flight path angle.
The second study [59] concerned investigation of lateral-directional handling qualities by first assessing the handling qualities of the bare-airframe and improve the handling qualities through a prototype FCS, for which a generalized inverse CA scheme with two different stability augmentation systems using linear control laws, SAS-1 & SAS-2. Where For SAS-2 a roll rate feedback loop was included. For the analytical and piloted experiment assessment, the selected handling quality requirements came from military specifications and manoeuvres, which were selected from civil aviation authorities regulatory specifications (CS-25), and the performance of the pilot is taken as criterion. The following tasks were conducted:

- Dutch Roll damping ratio
- Coordinated Turn Capability (CTC): Fly a turn with minimal sideslip while keeping a positive flight path angle
- Time to Bank, Roll Capability (TTB): Fly a turn with at least 30 degree roll angle and positive flight path angle, and next rotate 60 degrees to a 30 degree roll angle in the opposite direction
- One Engine Inoperative Trim (OEI-T): One of the engine is cut in power while in straight, horizontal flight. The pilot is allowed to intervene after 2 seconds and is asked to return the aircraft to the original heading.
- Steady Heading Sideslip (SHS): Use the rudder pedals to attain a constant sideslip angle, while maintaining a constant heading and positive flight path angle

The experiments were conducted with the bare airframe, SAS-1 & -2 for a forward and aft Center of Gravity position and in the Approach, Takeoff, Cruise and making a distinction between All Engines Operative (AOE) and One Engine Inoperative (OEI) in the respective flight condition. From analytical and experimental it was determined that the bare-airframe is insufficient in compliance with the flying handling quality requirements, due to a lack of pitch, roll and yaw control authority in low-speed flight and unstable Dutch Roll. The prototype FCS was able to comply with the Dutch Roll requirement, but the control authority was not sufficient for compliance with the other requirements, with problems of reaching actuator limits and some indications of piloted-induced oscillations (PIO) attributed to the actuator rate limits saturation. The CA scheme yielded adverse axis-coupling when the control surfaces saturated, where in the experiments it was found that as the pitch control surfaces saturated and a roll input was given simultaneously, the CA would trade off pitching moment to obtain a rolling moment, resulting in a nose-down behaviour when rolling.
The third study concerned [60] the analysis of longitudinal handling qualities, similar to the previous studies it also conducted an analytical and experimental assessment of handling qualities through piloted simulations. Moreover, it also designed an FCS using Control Allocation, direct law that scales pilot input by a linear gain to yield proportional elevon deflection, pitch rate command and auto throttle. With the analytic analysis, the following handling quality assessments were performed:

- Phugoid and Short period damping ratio
- Control Anticipation Parameters (CAP)
- Bandwidth criteria
- Gibson dropback criterion

It was determined that Phugoid was at Level 3 in flying qualities, Short Period was found to be Level 1. With the CAP it was determined that with an aft Center of Gravity at Mach 0.2, the flying handling qualities are in the Level 2 boundaries and the faster flight configuration and condition fell within the Level 1 boundaries, however this was determined through a short period approximation model. A slower short period frequency and respective flying quality level corresponds to lower handling qualities

and sluggish control. The bandwidth criteria showed Level 2 handling quality and through the Gibson Dropback criterion it was found that the response of the aircraft ranges from sluggish with an aft CG to abrupt bobbling tendency with a forward CG. The nominal CG was found to be the closest to satisfactory performance. The piloted simulation experiments concerned three tasks:

- Pitch Tracking: follow a pitch reference
- Free Pitch Capturing: Capture a succession of pitch angles
- Go-Around: First the aircraft was initialized in a descent towards the runway and the pilot were instructed to perform a go-around with a target rate as specified by the civil aviation authority standard from EASA.

The experiments showed that the longitudinal handling qualities at lower approach speeds degraded due to sluggish aircraft responsive, limited control authority, insufficient sight angle and tendency to PIO. It was found that higher approach speeds are satisfactory and more aft positions of center of gravity provide better sight angle, better control authority and reduce handling quality minimally. The pitch rate controller was implemented and tuned based on the handling qualities requirements, where the improvement in handling qualities was noticed by all pilots.

Nonlinear FCS design and Simulation Assessment

The piloted experiment studies used the VLM aerodynamic model, which primarily captured the linear aerodynamic behaviour of the Flying V, but from the WTE it was established that on the small-scale model undesired nonlinear behaviour, pitch break, would arises after the angle of attack reaches $20°$. Van Overeem [22] combined the FS VLM model with the results of the WTE model and this resulted in a combined aerodynamic model, which was used to create a simulation model where stability and handling qualities were analysed for Approach and Cruise flight conditions. With this simulation model an FCS was designed using a nonlinear control method, Incremental Dynamic Inversion (INDI).
Before the implementation of the FCS and evaluation of handling qualities, a trim and linearization was designed, with thereafter an evaluation of all longitudinal and lateral dynamic modes as illustrated for approach in Figure 2.19 and cruise in Figure 2.20.

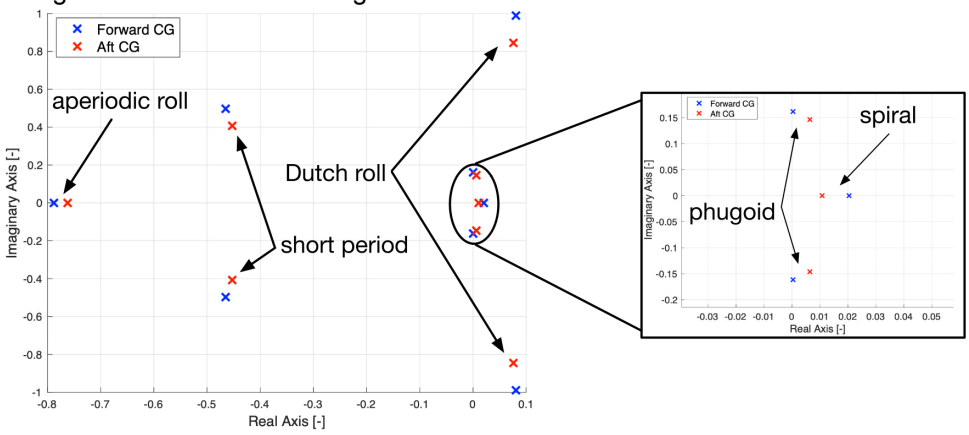

Figure 2.19: Eigenvalues for fwd and aft center of gravity in approach condition [22]

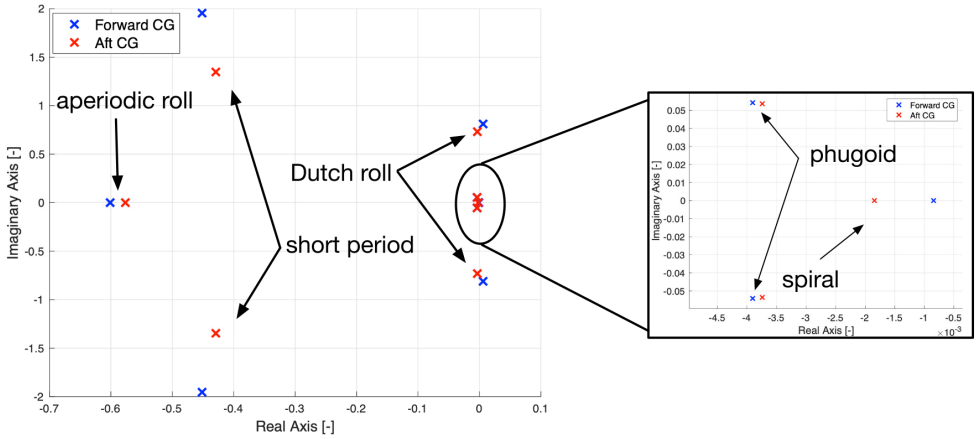

Figure 2.20: Eigenvalues for fwd and aft center of gravity in cruise condition [22]

The short-period of the aircraft was deemed stable and showed Level 1 flying qualities, except for cruise with a forward CG position as that showed Level 2 flying qualities. The phugoid was stable with Level 1 flying qualities, except during the approach where the phugoid is unstable. The dutch roll is unstable during approach and shows Level 3 flying qualities during cruise with an aft CG position. The aperiodic roll mode is stable in approach and cruise with Level 1 flying qualities for Approach (forward and aft CG) and Cruise (forward CG), but Level 2 in Cruise with an aft CG. The spiral mode is unstable during approach, but stable during cruise with Level 1 flying qualities. In addition to evaluation of the dynamic modes, the CAP is also evaluated, where it is determined that during approach Level 1 is obtained with a forward CG and Level 2 with an aft CG. In cruise, the CAP is rated at Level 2 with a forward CG, but Level 1 with an aft CG.
With the bare-airframe dynamic modes assessed, the FCS was designed with INDI as inner control loop and roll, flight path and side slip angles reference control as outer control loop. The evaluation of the bare-airframe showed that the aircraft in Approach condition with a forward CG did not meet the Level 1 flying qualities and through augmentation of the FCS it was determined that all dynamic modes are now stable level 1 flying qualities are met. The CAP was also assesed and it was determined to be at the border of Level 1 handling qualities.

Stougie [23] continued with the efforts of the previous research using a FCS with INDI, but now with Flight Envelope Protection and using linear reference command blocks which are tuned to satisfy the MIL-STD-1797A specifications and gain and phase margin requirements to ensure disturbance rejection capabilities. Moreover, by adding sensor dynamics and making the control system discrete, the effect of time delays can be investigated. This tuning was conducted for the Flying V in cruise condition. The research also specifically focused on cruise and approach conditions with a forward CG as this position was found to be the furthest from reaching Level 1 handling qualities as established in van Overeem's [22] research.
The resulting tuned system provided that all handling qualities are within Level 1 flying qualities, if sensor dynamics are not included, and the overall system is continuous. When adding sensor dynamics, it can be seen that the handling quality requirements are still within Level 1, but the gain and phase margin requirements are not. Thus, adjustments have been made to the sensor dynamics, by adding an angular rate sensor with less time delay and faster sensors and sampling time, which resulted in a system that could be tuned to Level 1 flying qualities. To obtain short period parameters as well as the Control Anticipation Parameter, a Low Order Equivalent System (LOES) fit was conducted on the pitch rate transfer function, this approximates an analytical expression of the short period dynamics through simulating the time response and a fit is obtained when the natural frequency of the phugoid and short-period are separated sufficiently.
In addition to analysing the dynamic modes, the Pitch attitude dropback, Gibson phase rate, Flight-path angle bandwidth and the equivalent time delays for lower order equivalent systems were assessed. The pitch attitude dropback is within the acceptable region and the phase rate criterion was also met, but the flight path bandwidth was on the edge of the requirement and within the Level 1 area.

2.3.3. Conclusions

With all the Flying V research evaluated, the following conclusions regarding the latest state of flying and handling qualities can be described:

- The bare-airframe of the FS Flying V has been assessed through multiple studies, consisting of two offline model simulation assessments, with a focus on an analytical analysis through with the military flying and handling quality requirements, and three pilot-in-loop simulator research studies, which used direct control laws for their FCS that also first performed an analytical analysis and thereafter simulator studies where certain tracking manoeuvres were used and analysed using the Cooper-Hart Rating Scale. These various studies were assessed at either Approach and Cruise condition, or both with different CG positions. The offline simulations focused on assessment of These results identified that the Flying V at its worst condition and CG position had an:
  - The short period had Level 2 flying qualities at cruise with a forward CG [22].
  - Unstable Dutch roll during approach and Level 3 during cruise with an aft CG position [22, 34, 59]
  - One study identified that Phugoid had level 3 flying qualities [60] at low speed conditions and the other identified that phugoid was unstable at Approach [22]
  - Level 2 flying qualities with flight path control [36]
  - Lack of pitch, roll, yaw authority in low-speed flight and saturation control surfaces and some indication of pilot-induced oscillations (PIO) attributed to the saturation of the actuator rate limits [59]
  - Insufficient control authority in lateral-directional in case of OEI at low speeds [34, 59]
  - Within Level 2 boundaries of the CAP with an aft CG at low speeds [60]
  - Bandwidth criterion showed Level 2 handling qualities and from the Gibson Dropback (GB) criterion established sluggish to bobbling tendency with an aft and forward CG respectively [60]
- Through augmentation using a nonlinear FCS the flying and handling qualities of the Flying V were improved, where it was determined that all dynamic modes are now at Level 1 flying qualities at Approach with a forward CG and the CAP at the border of Level 1 flying qualities [22]. When sensor dynamics were added, the Level 1 flying qualities are met, but the gain and phase margin requirements are not. Through adjusting the sensor dynamics and adding an angular rate sensor with less time delay, it resulted in a tunable aircraft for Level 1 flying qualities with a positive gain and phase margin. The flight path bandwidth was on the edge of requirement and within Level 1 area

2.4. Flight Control System Research

This section provides a brief theoretical background on the development of an FCS with a linear flight control law for a linear system (2.4.1), which is a common strategy for FCS design and will thereafter provide an overview of the research that's conducted for the development of Flying V's FCS (2.4.2). At last, a conclusion is made regarding the latest state-of-the-art FCS research (2.4.3).

2.4.1. Theoretical Background: Linear control law design

With the trim data gathered, where the nonlinear model is at a steady-state at the specific flight condition, which can be denoted as the linearization point ($X_0 = (x_{trim}, u_{trim})$. The linearization can be performed through a Taylor series expansion, which for an arbitrary function $g(x)$ about state x_0, is defined as:

$$y = g(x) \tag{2.10}$$

$$y \approx g(x_0) + g'(x_0)(x - x_0) + \frac{g''(x_0)}{2!}(x - x_0)^2 + \frac{g^3(x_0)}{3!}(x - x_0)^3 + ... + \frac{g^n(x_0)}{n!}(x - x_0)^n \tag{2.11}$$

Where g' is the first derivative with respect to x and g^n denotes the nth order derivative. If the function has two states $\mathbf{x} = \{x_1, x_2\}$, the Taylor expansion around states $x_0 = \{x_1|_0, x_2|_0\}$ can be written as:

$$
\begin{aligned}
y \approx g(\mathbf{x_0}) &+ [g_{x_1}(\mathbf{x_0})(x_1 - x_1|_0) + g_{x_2}(\mathbf{x_0})(x_2 - x_2|_0)] \\
&+ \frac{1}{2!}[g_{x_1x_1}(\mathbf{x_0})(x_1 - x_1|_0)^2 + g_{x_1x_2}(\mathbf{x_0})(x_1 - x_1|_0)(x_2 - x_2|_0) + g_{x_2x_2}(\mathbf{x_0})(x_2 - x_2|_0)^2 \\
&+ \frac{1}{3!}[g_{x_1x_1x_1}(\mathbf{x_0})(x_1 - x_1|_0)^3 + 3g_{x_1x_1x_2}(\mathbf{x_0})(x_1 - x_1|_0)^2(x_2 - x_2|_0) \\
&+ 3g_{x_1x_2x_2}(\mathbf{x_0})(x_1 - x_1|_0)(x_2 - x_2|_0)^2 + g_{x_2x_2x_2}(\mathbf{x_0})(x_2 - x_2|_0)^3] + ... \quad (2.12)
\end{aligned}
$$

Where g_{x_1}, g_{x_2} denote the partial derivative of f with respect to x_1 and x_2 and $g_{x_1x_2}$ is the cross-term partial derivative with respect to both states. The Taylor series can grow to expanded expressions and the linearization is done with only taking the first term and first (partial) derivative from the expansion. Thus, disregarding terms which contain higher order (partial) derivatives than 1. The Taylor series around the first order term is then written with a short-hand notation for a set of equations $g(\mathbf{x})$, with n states $\mathbf{x} = \{x_1, x_2, ..., x_n\}$ around $\mathbf{x_0}$ is defined as:

$$
\begin{aligned}
\mathbf{y} &= g(\mathbf{x_0}) + g_{x_1}(\mathbf{x_0})\Delta x_1 + g_{x_2}(\mathbf{x_0})\Delta x_2 + ... + g_{x_n}(\mathbf{x_0})\Delta x_n \\
&= g(\mathbf{x_0}) + \sum_{i=1}^{n} g_{x_i}(\mathbf{x_0})\Delta x_i
\end{aligned} \quad (2.13)
$$

With the lineraization routine described the LTI system, in state-space format, is defined as:

$$\Delta\dot{\mathbf{x}} = \mathbf{A}\Delta x + \mathbf{B}\Delta u \quad (2.14)$$

$$\Delta\mathbf{y} = \mathbf{C}\Delta x + \mathbf{D}\Delta u \quad (2.15)$$

Where $\mathbf{A}, \mathbf{B}$ are the state matrix and input matrix respectively for the state equation $f(\mathbf{x}, \mathbf{u})$ and $\mathbf{C}, \mathbf{D}$ are the output matrix and input matrix respectively for the output equation $h(\mathbf{x}, \mathbf{u})$. The $\Delta\dot{x}, \Delta x, \Delta u$ describe the change of system state due to input changes from the linearization point. These matrices in the state space equation are defined as following:

$$
A = \frac{\partial \mathbf{f}}{\partial \mathbf{x}}|_{X_0} = \left\{ \begin{bmatrix} \frac{\partial f_1}{x_1} & \frac{\partial f_1}{x_2} & \cdots & \frac{\partial f_1}{x_n} \\ \frac{\partial f_2}{x_1} & \frac{\partial f_2}{x_2} & \cdots & \frac{\partial f_2}{x_n} \\ \vdots & \vdots & \ddots & \vdots \\ \frac{\partial f_n}{x_1} & \frac{\partial f_n}{x_2} & \cdots & \frac{\partial f_n}{x_n} \end{bmatrix} \right|_{X_0} \quad B = \frac{\partial \mathbf{f}}{\partial \mathbf{u}}|_{X_0} = \left\{ \begin{bmatrix} \frac{\partial f_1}{u_1} & \frac{\partial f_1}{u_2} & \cdots & \frac{\partial f_1}{u_m} \\ \frac{\partial f_2}{u_1} & \frac{\partial f_2}{u_2} & \cdots & \frac{\partial f_2}{u_m} \\ \vdots & \vdots & \ddots & \vdots \\ \frac{\partial f_n}{u_1} & \frac{\partial f_n}{u_2} & \cdots & \frac{\partial f_n}{u_m} \end{bmatrix} \right|_{X_0} \quad (2.16)
$$

$$
C = \frac{\partial \mathbf{h}}{\partial \mathbf{x}}|_{X_0} = \left\{ \begin{bmatrix} \frac{\partial f_1}{x_1} & \frac{\partial f_1}{x_2} & \cdots & \frac{\partial f_1}{x_n} \\ \frac{\partial f_2}{x_1} & \frac{\partial f_2}{x_2} & \cdots & \frac{\partial f_2}{x_n} \\ \vdots & \vdots & \ddots & \vdots \\ \frac{\partial f_k}{x_1} & \frac{\partial f_k}{x_2} & \cdots & \frac{\partial f_k}{x_n} \end{bmatrix} \right|_{X_0} \quad D = \frac{\partial \mathbf{h}}{\partial \mathbf{u}}|_{X_0} = \left\{ \begin{bmatrix} \frac{\partial f_1}{u_1} & \frac{\partial f_1}{u_2} & \cdots & \frac{\partial f_1}{u_m} \\ \frac{\partial f_2}{u_1} & \frac{\partial f_2}{u_2} & \cdots & \frac{\partial f_2}{u_m} \\ \vdots & \vdots & \ddots & \vdots \\ \frac{\partial f_k}{u_1} & \frac{\partial f_k}{u_2} & \cdots & \frac{\partial f_k}{u_m} \end{bmatrix} \right|_{X_0} \quad (2.17)
$$

One classic control technique that can be applied to design the flight control laws is Proportional-Integral-Derivative control, which is a linear control method that a proportional, integral and derivative gain term to decrease an error $e(t)$, which can be the difference between the feedback response of the plant (aircraft) ($y(t)$) and reference command ($r(t)$), thus resulting in *control* error $e(t) = r(t) - y(t)$ [62, 63]. The resulting control input is then defined as:

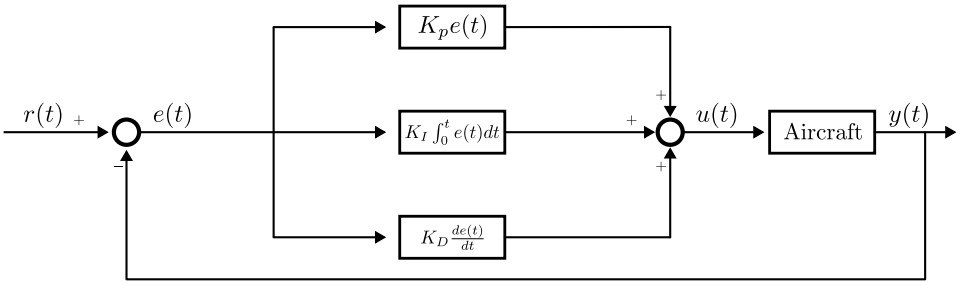

Figure 2.21: Proportional Integral Derivative (PID) Control

$$u(t) = K_P e(t) + K_I \int_0^t e(t)dt + K_D \frac{de(t)}{dt} \tag{2.18}$$

The proportional gain (K_P) compensates the control output proportional to the size of the error $e(t)$, the integral gain (K_I) provides a control output concerning the cumulative error to ensure that the system reaches the desired reference with no steady-state error and the derivative gain (K_D) provides a control output relates the rate of change of the error and suppress oscillatory system response. The block diagram of this control method is shown in Figure 2.21.

2.4.2. Research

The FCS has to ensure that the Flying V complies with the Flying and Handling qualities established by civil aviation authorities. Two key research activities have contributed to the design of Flying V FCS.

- Flying V - FCS1: Incremental Nonlinear Dynamic Inversion control FCS [22]
- Flying V - FCS2: FEP with INDI FCS [23]

The first research used the investigations towards the handling qualities to design an FCS using an inner loop stabilisation with the Incremental Dynamic Inversion (INDI) method and an outer loop with roll angle (ϕ), sideslip angle (β) and flight path angle (γ) controllers were designed using the Nonlinear Dynamic Inversion method. The designed FCS improved the stability and handling qualities [22] and the assessment was conducted with the Flying V at approach condition with a forward CG.
The robustness of the FCS was assessed with aerodynamic model uncertainties, where a standard deviation is applied between 0% and 25 % from its true value by a scaling factor ranging from 0.0 to 0.25. A 3211 manoeuvre was applied for the flight path angle and roll angle trajectory to assess the tracking performance and effect of uncertainty.
It was determined that the INDI controller is able to cope with uncertainties in the aerodynamic coefficients with respect to angle of attack (α), sideslip (β) and pitch rates ($\hat{p}, \hat{q}, \hat{r}$) and still provide good tracking experience. However, when the control effectiveness, which is obtained from the aerodynamic model and are the coefficients related to the contribution of aerodynamic forces and moments due to control surface deflection, has uncertainty and decreases in magnitude, the control surfaces saturate as higher deflections are required to maintain good tracking performance. For future FCS development, it was suggested to research the following items:

- Perform additional research on the magnitude of the aerodynamic uncertainty
- Analyse the effect of FCS on CAP
- Include sensor dynamics and analyse measurement time delay, sampling frequency, inertia uncertainty and center of gravity mismatch.
- Due to low roll angle that can be achieved without saturating the control surfaces, incorporate the inboard elevon for roll control

The FCS, developed by van Overeem [22], was further developed with the addition of Flight Envelope Protection (FEP) [23]. Compared to the previous research, the following additions and modifications were made:

- Flight Envelope Protection system ensures safe operation and control within the flight envelope and limits by integrating the protection laws for the Angle of Attack (AoA), load factor and roll angle
- The outer loop controllers were changed to use a C-star control law and pitch, roll reference and sideslip compensation reference controller blocks, which receive commaned pilot stick inputs. These reference controller blocks are tuned using an optimisation algorithm that takes the MIL-STD-1797A requirements for longitudinal and lateral direction, control surface activity, settling time, overshoot, gain and phase margin and attitude bandwidth into account as constraints or limits
- Control Allocation was implemented that uses a cascading algorithm taking the actuator limits and maximum control deflections into account
- Added sensor dynamics, actuator synchronisation and Pseudo-Control Hedging (PCH). The sensor dynamics resulted in a discrete-time FCS, but the actuator and aircraft dynamics were kept as continuous-time systems
- Gain scheduling for the FEP controller gains depending on airspeed and linearly interpolated between cruise condition tuning and tuning done at a airspeed of 100 m/s at 1 km altitude and for the lateral gain an additional tuning point was added at 70 m/s at 1 km altitude

The effects of sensor dynamics resulted that the sensors specifications had to be adjusted to ensure Level 1 Flying Qualities with the tuning routine, moreover through simulating a tracking task, it was observed that the control activity increased as sampling time increased, and the tracking error also increased.
The robustness of the FCS was analysed through aerodynamic uncertainty and sampling time, where a simulation is conducted with a step roll rate input and this also has an influence in the C* input as it is coupled with the roll angle. The tracking of the C* and roll rate are evaluated as a Root Mean Squared (RMS) error.
It was concluded that a sampling time above 0.1s causes the system to become unstable. The FCS was shown to be robust against aerodynamic uncertainty, with difference of aerodynamic coefficient up to 20 %. The uncertainty in the aerodynamic coefficients for the longitudinal coefficients and lateral coefficients are shown in the first two box plots in Figure 2.22. However, when uncertainty is applied to the control effectiveness, there is a higher variance of the aircraft response

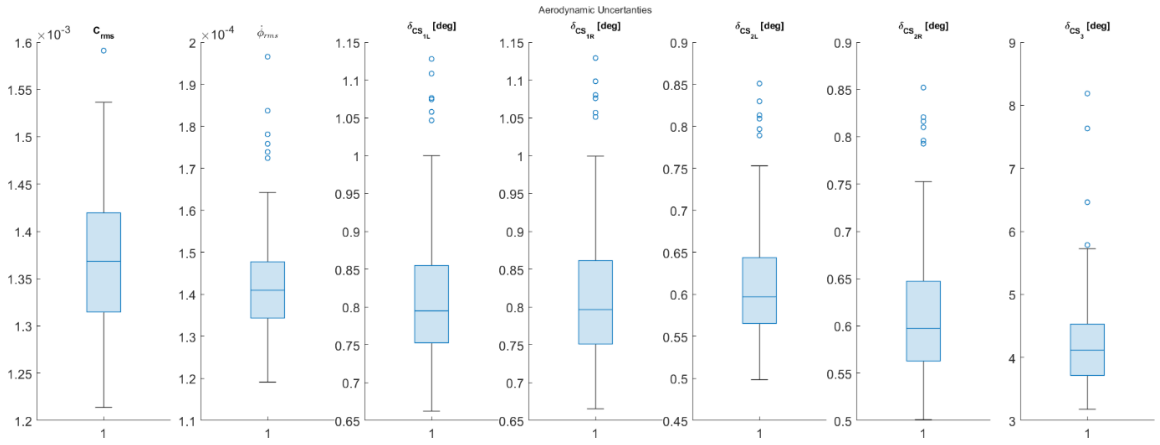

Figure 2.22: Boxplots showing the variance in tracking error and control surface activity, with varying aerodynamic uncertainty [23]

Moreover, the control surface activity ($\delta_{CS_{activity}}$) was also evaluated, which is defined as following:

$$\delta_{CS_{activity}} = \frac{\int_0^T |\delta_{CS_i^{L/R}}| dt}{T} \tag{2.19}$$

Where T is the total timespan of the simulation and the average control deflection that is required to perform the tracking task, increases due to higher uncertainty. This is problematic especially for the rudder (δ_{CS3}), which exhibits oscillatory behaviour and saturates due to the uncertainty.

At last the FEP was evaluated though two different simulations with first a simulation that has a step $C*$ step input and no thrust and the second simulation has a block input $C*$ within a certain interval and a roll rate ($\dot{\phi}$) command. These simulations were performed at two different altitudes, 13 km as cruise height and 1 km, resulting in two different simulation scenarios.
It was determined that with FEP, the aircraft can reach angles of attack near the (safety) limit and return to a lower angle of attack. The roll angle is close to the limit and the load factor did not exceed the limits. However, during the manoeuvres, oscillations of the rudder in all simulation scenarios. With the first simulation scenario at cruise altitude, the amplitude of the oscillations remained small, but in the second simulation scenario it oscillated from maximum to minimum deflections. At 1 km in the second simulation scenario, the rudder, and elevons are hitting their saturation limits, indicating that the aircraft is at its limits for this manoeuvre. This was attributed to the tuning of the controller being done in a limited envelope and as the airspeed dips below that. However, despite these limits the sideslip angle does not become too large, and the aircraft stays within the limits set by the FEP.
The research suggests additional investigations towards the following items:

- Investigate multiple points of CG as well as CG location mismatch
- Improve FEP by adding more safety measures, such as $V_{min/max}$ protection or minimum AoA and load factor protection or including more aircraft states, such as AoA rate for AoA protection.
- Include the influence of aero-elasticity effects and time delay due to computation time by the FCS
- Improve the gain scheduling, by making it dependent on air density
- Investigate whether the required sensors are feasible for the Flying V or change control laws, that can cope with time delays

2.4.3. Conclusions

The latest Flying V FCS research result developed a simulation model and system, where through the FEP the aircraft is able to provide protection against pilot control inputs that may exceed the flight envelope of the aircraft. Moreover, through adding sensor dynamics and creating a discretized system, the aircraft can be simulated to identify the effects of time delays and sampling time. The implemented nonlinear INDI control algorithm also provides robustness against aerodynamic uncertainties up to a 20 % deviation.

2.5. Aircraft Simulation Model

The aircraft simulation model concerns the simulation model that forms the baseline setup for this research. This simulation model is gathered from the latest Flying V FCS [23] research and the overall high-level layout is illustrated in Figure 2.23. The FCS also illustrates the various sampling times used for the respective blocks. The aerodynamic model that's implemented in the simulation model is the combined aerodynamic model as described in Section 2.2.2.

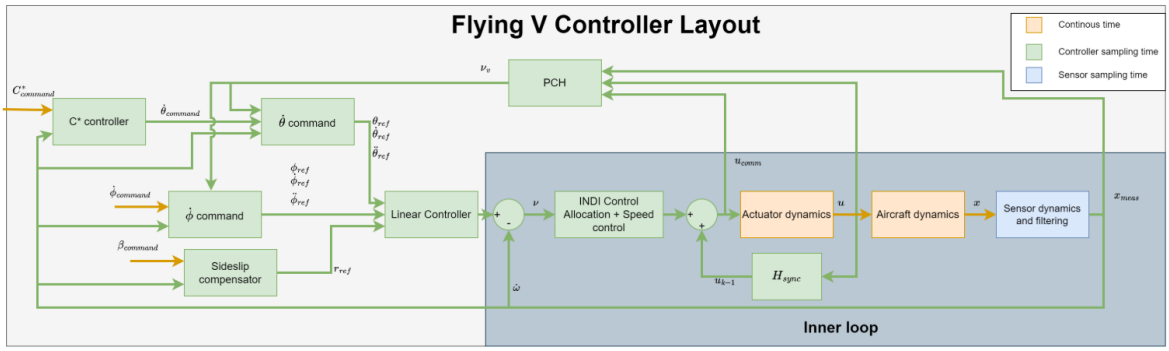

Figure 2.23: Current Flying V simulation model and FCS [23]

This diagram illustrates the complete Flying V FCS layout, and these blocks will be elaborated separately. At first the aircraft dynamics can be elaborated, where the reference frames in which the aircraft exists are described first (2.5.1) and thereafter the Equations of Motions (EOM) can be described (Sec-

tion 2.5.2). The actuator dynamics concern the control surface actuator servo's and the throttle servo for the aircraft engine (2.5.3).

2.5.1. Reference Frames

A reference frame defines a coordinate system or set of axes within where the position, orientation, and other properties of objects (e.g., aircraft and spacecraft) are described and measured in [45]. The reference frames used for the simulation model are the Vehicle-carried normal Earth reference frame (E-frame), the Body-fixed reference frame (B-frame) and the aerodynamic reference frame. These reference frames will be described briefly. At last, the transformation matrices to go from one reference frame to another are described.

Vehicle-carried Normal Earth Reference Frame

The Vehicle-carried Reference, as shown in Figure 2.24, describes a spherical Earth with the $X_E Y_E$ tangential to the surface of the Earth. The X_E-axis is directed to the north and the Y_E-axis is directed 90 degrees to the right of the X_E-axis. The Earth is approximated as a sphere, which means that the gravitational attraction vector and the Z_E is pointed towards the center of the Earth.

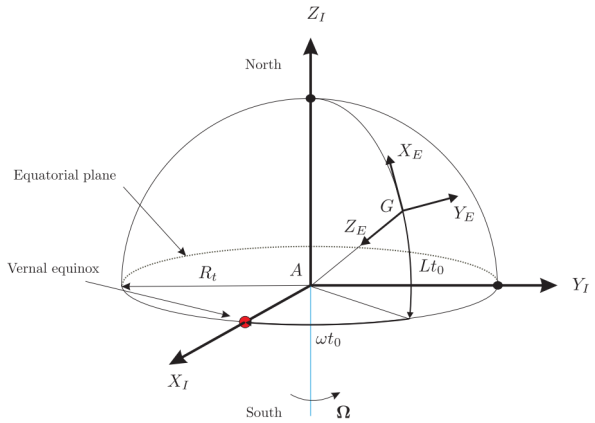

Figure 2.24: Vehicle-carried normal Earth Reference frame [45]

Body-Fixed Reference Frame

The Body-fixed reference frame, as shown in Figure 2.25, is a right-handed coordinate system, with its origin located at the centre of mass of a vehicle (e.g. aircraft). The X_B-axis is located in the plane of symmetry and points forward. The Z_B-axis is also located in the symmetry plane and points downwards. The Y_B-axis points perpendicular to both X_B and Z_B-axis. In the Body-fixed reference frame the body velocities (u, v, w), rotational rates (p, q, r) and positive forces (F_X^B, F_Y^B, F_Z^B) and moments (M_X, M_Y, M_Z) for each axis are also indicated.

Aerodynamic Reference Frame

The aerodynamic reference frame origin is the same as the Body-fixed reference frame. The X_a-axis is in the direction of the aerodynamic velocity V_a, which is defined as the velocity of the center of mass G relative to the undisturbed air. The Z_a-axis is in the symmetry plane of the aircraft and the Y_a-axis is perpendicular to the $X_b Z_b$ plane to complete the axis system. The angles α and β are the aerodynamic angle of attack and aerodynamic sideslip respectively and denote the orientation of the aerodynamic reference frame with respect to the body-fixed reference frame.

Transformation Matrices

The reference frames are used to express the motion of the aircraft by differential equations, however the derivation for the differential equation can be described separately for each respective reference frame. To couple the motions in each reference frame and get an overall set of equations that describe the aircraft motion through time, in one particular reference frame, a transformation between reference frames is necessary. A transformation is expressed as a matrix, which is composed of a translation

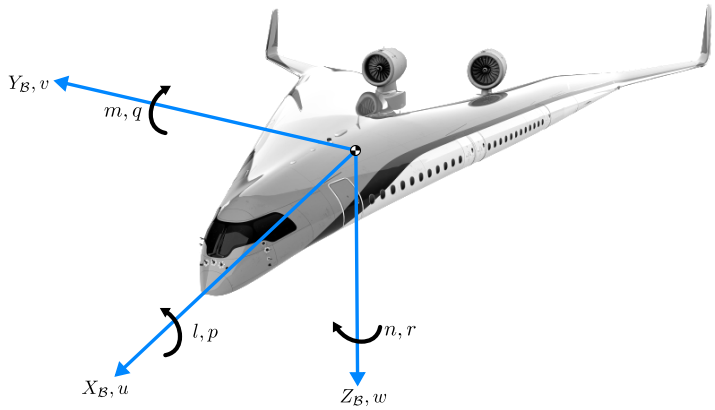

Figure 2.25: Body-fixed reference frame [22, 45]

from the origin of a reference frame towards a target frame. There are two transformations of relevance for this simulation, which is the body-reference Euler frame with the Euler angles described as following for an aircraft:

- ϕ: roll angle
- θ: pitch angle
- ψ: yaw angle

This transformation describes the transition from the orientation of an inertial reference frame to the orientation of the body-fixed reference frame. One common matrix of this reference frame is the 3-2-1 euler-sequence, described as a rotation ψ around the Z-axis first, rotation θ around the Y-axis and at last a rotation ϕ around the X-axis. This results in the following matrix:

$$[T_{BE}] = \mathbf{C}_{\psi}(\psi)\mathbf{C}_{\theta}(\theta)\mathbf{C}_{\phi}(\phi) \tag{2.20}$$

$$= \begin{bmatrix} \cos\psi & \sin\psi & 0 \\ -\sin\psi & \cos\psi & 0 \\ 0 & 0 & 1 \end{bmatrix} \begin{bmatrix} \cos\theta & 0 & \sin\theta \\ 0 & 1 & 0 \\ \sin\theta & 0 & \cos\theta \end{bmatrix} \begin{bmatrix} 1 & 0 & 0 \\ 0 & \cos\phi & \sin\phi \\ 0 & -\sin\phi & \cos\phi \end{bmatrix} \tag{2.21}$$

$$= \begin{bmatrix} \cos\theta\cos\psi & \sin\psi\cos\theta & -\sin\theta \\ \sin\phi\sin\theta\cos\psi - \sin\psi\cos\phi & \sin\phi\sin\theta\sin\psi + \cos\phi\cos\psi & \sin\phi\cos\theta \\ \sin\phi\sin\psi + \sin\theta\cos\phi\cos\psi & -\sin\phi\cos\psi + \sin\theta\sin\psi\cos\phi & \cos\phi\cos\theta \end{bmatrix} \tag{2.22}$$

The second transformation of relevance is the transformation from body-fixed reference frame to aerodynamic reference frame, which consist of two consecutive rotations, where first a rotation α about the Y_B-axis and then a rotation β around the Z_B-axis. Resulting in the following transformation matrix:

$$[T_{aB}] = \begin{bmatrix} \cos\beta & \sin\beta & 0 \\ -\sin\beta & \cos\beta & 0 \\ 0 & 0 & 1 \end{bmatrix} \begin{bmatrix} \cos\alpha & 0 & \sin\alpha \\ 0 & 1 & 0 \\ -sin\alpha & 0 & \cos\alpha \end{bmatrix} \tag{2.23}$$

$$= \begin{bmatrix} \cos\beta\cos\alpha & \sin\beta & \cos\beta\sin\alpha \\ -\sin\beta\cos\alpha & \cos\beta & -\sin\beta\sin\alpha \\ -sin\alpha & 0 & \cos\alpha \end{bmatrix} \tag{2.24}$$

Several useful relations are defined to relate the aerodynamic velocity vector V_a in the aerodynamic reference frame to the aerodynamic angle of attack α and sideslip β angles. The aerodynamic velocity vector magnitude, α and β are defined as:

$$V_a = \sqrt{u^2 + v^2 + w^2} \tag{2.25}$$

$$\alpha = \arctan \frac{w}{u} \tag{2.26}$$

$$\beta = \arcsin \frac{v}{V_a} \tag{2.27}$$

Where u, v, w are the body velocity of the aircraft. If wind is included, the aerodynamic velocity and body-fixed velocity need to be transformed using the transformation matrix T_{aB}.

2.5.2. Equations of Motion

The following assumptions are made to describe the equations of motion of the aircraft [22, 34]:

- The aircraft is a rigid body and has constant mass
- The Earth is flat and non-rotating and inertial reference frame
- There is zero wind and a perfect atmosphere
- The resultant thrust lies in the symmetry plane
- The gravitational acceleration is constant

The forces acting on the aircraft consist of gravity, propulsion forces and aerodynamic forces. It is assumed that the distributed forces can be replaced with point forces that generate moments around the center of gravity. With the flat and non-rotating Earth assumption, the vehicle-carried normal Earth reference frame is similar to an inertial reference frame [45].

The equation of motion for the simulation model describes a 6-Degree of Freedom (DOF) dynamic system and are formed by the translational dynamics, rotational dynamics and the kinematics.

Translational dynamics

The translational dynamics express the change of velocity of the aircraft. The dynamics are derived through Newton's second law:

$$\dot{\mathbf{v}}^E = \frac{\mathbf{F_{ext}}^B}{m} \tag{2.28}$$

Where $\dot{\mathbf{v}}_E$ is the acceleration of the aircraft in E-frame and equal to the external forces (F_{ext}) over the mass (m). To transform the equation to body-fixed reference frame, the transport theorem is used:

$$\dot{\mathbf{v}}^E = \dot{\mathbf{v}}^B + \omega^B_{B/E} \times \mathbf{v}^B \tag{2.29}$$

Where $\mathbf{v}_B$ is the velocity of the aircraft expressed in B-frame components ($\begin{bmatrix} u & v & w \end{bmatrix}$) and $\omega_{B/E}$ is the angular velocity of the B-frame with respect to the E-frame ($\begin{bmatrix} p & q & r \end{bmatrix}$). The F_{ext} consist of the gravitational force onto the aircraft, aerodynamic forces and propulsion forces are need to be expressed in the B-frame. The gravitational force is defined in the E-frame as:

$$F^B_g = [T_{BE}]F^E_g = \begin{bmatrix} \sin\theta \\ \sin\phi\cos\theta \\ \cos\phi\cos\theta \end{bmatrix} mg \tag{2.30}$$

The aerodynamic forces are calculated through the aerodynamic coefficients obtained from the aerodynamic model, which is the combined aerodynamic model as explained in 2.2.2. This results in the final expression of the aircraft's translational dynamics:

$$\dot{\mathbf{v}}^B = -\mathbf{\Omega_{B/E}}^B \mathbf{v}^B + \frac{F^B_g}{m} + \frac{F^B_{aero}}{m} + \frac{F^B_{thrust}}{m} \tag{2.31}$$

Where $\Omega^B_{B/E}$ is the angular velocity matrix defined as:

$$\Omega_{B/E}^{B} = \begin{bmatrix} 0 & -r & q \\ r & 0 & -p \\ -q & p & 0 \end{bmatrix} \tag{2.32}$$

After integration of the body-fixed velocity vector, it is possible to obtain the velocity in the E-frame, through applying the transformation $[T_{EB}]$, which results into the following expression:

$$\mathbf{v}^{E} = [T_{EB}]\mathbf{v}^{B} \tag{2.33}$$

$$\begin{bmatrix} V_N \\ V_E \\ V_D \end{bmatrix} = [T_{EB}] \begin{bmatrix} u \\ v \\ w \end{bmatrix}^{B} = \begin{bmatrix} V_N \\ V_E \\ V_D \end{bmatrix} \tag{2.34}$$

Integrating the Earth-fixed velocity, obtains the position of the aircraft in the E-frame, as described below:

$$\mathbf{x}^{E} = \int_{0}^{T} \begin{bmatrix} V_N \\ V_E \\ V_D \end{bmatrix} = \begin{bmatrix} x_E \\ y_E \\ z_E \end{bmatrix} \tag{2.35}$$

Rotational Dynamics

The rotational dynamics are derived through the change in angular momentum in E-frame components, with $\mathbf{M}$ as the moment acting on the aircraft.

$$\dot{\mathbf{H}}^{E} = \mathbf{M} \tag{2.36}$$

Using the transport theorem, the change in angular momentum is derived with respect to the B-frame, which results in the following expression:

$$\dot{\mathbf{H}}^{B} + \omega_{B/E} \times \mathbf{H}^{B} = \mathbf{M} \tag{2.37}$$

The angular momentum in the body frame is described as:

$$\mathbf{H}^{B} = \mathbf{I}^{B}\omega_{B/E} \tag{2.38}$$

Where $\mathbf{I}$ represent the inertia matrix defined as:

$$\mathbf{I} = \begin{bmatrix} I_{xx} & -I_{xy} & -I_{xz} \\ -I_{yx} & I_{yy} & -I_{yz} \\ -I_{zx} & -I_{zy} & I_{zz} \end{bmatrix} \tag{2.39}$$

The rigid body is assumed to be constant in mass, which results in the time derivative of angular moment in the B-frame described as:

$$\dot{H}^{B} = \mathbf{I}^{B}\dot{\omega}_{B/E} \tag{2.40}$$

Substituting the above expressions in the angular momentum equation Equation (2.36) and rewriting to get the change in angular rate results in the final expression:

$$\dot{\omega}_{B/E} = \mathbf{I^{-1}}^{B}\mathbf{M} - \mathbf{I^{-1}}^{B}\Omega_{B/E}^{B}\mathbf{I}^{B}\omega_{B/E} \tag{2.41}$$

With the expressions determined for the angular velocity, it is possible to determine the change in attitude represented as the euler angles, through the euler kinematic matrix defined as following:

$$\begin{bmatrix} \dot{\phi} \\ \dot{\theta} \\ \dot{\psi} \end{bmatrix} = \begin{bmatrix} 1 & \sin\phi\tan\theta & \cos\phi\tan\theta \\ 0 & \cos\phi & -\sin\phi \\ 0 & \frac{\sin\phi}{\cos\theta} & \frac{\cos\phi}{\cos\theta} \end{bmatrix} \begin{bmatrix} p \\ q \\ r \end{bmatrix} \tag{2.42}$$

In matrix form this equation will be written as:

$$\dot{\theta}^B = \mathbf{N}(\theta)^B \omega_{B/E}^B \tag{2.43}$$

Complete set of Equations of Motion

With all the dynamics and equations derives, the complete set of equations of motion for 6-DOF simulation is shown in Equation (2.44).

$$\begin{bmatrix} \dot{\mathbf{x}}^E \\ \dot{\mathbf{v}}^B \\ \dot{\omega}_{B/E}^B \\ \dot{\theta}^B \end{bmatrix} = \begin{bmatrix} [T_{EB}] & 0 \\ -\mathbf{\Omega_{B/E}}^B & 0 \\ 0 & -\mathbf{I^{-1}}^B \Omega_{B/E}^B \mathbf{I}^B \\ 0 & \mathbf{N}(\theta)^B \end{bmatrix} \begin{bmatrix} \mathbf{v}^B \\ \omega_{B/E}^B \end{bmatrix} + \begin{bmatrix} 0 \\ \frac{\mathbf{F}^B}{m} \\ \mathbf{I^{-1}}^B \mathbf{M} \\ 0 \end{bmatrix} \tag{2.44}$$

With the complete set of states and force and moment vector defined as:

- Aircraft position: x_E, y_E, z_E
- Aircraft (body) velocity: u, v, w
- Aircraft angular (body) rates: p, q, r
- Aircraft attitude: ϕ, θ, ψ
- Forces: F_X, F_Y, F_Z
- Moments: M_X, M_Y, M_Z

Writing out the matrix vector multiplications results in the following complete expressions for the aircraft states in Earth frame for the aircraft position and body frame:

$$\begin{aligned}
\dot{x_E} &= (u\cos(\theta) + (v\sin(\phi) + w\cos(\phi))\sin(\theta))\cos(\psi) - (v\cos(\phi) - w\sin(\phi))\sin(\psi) \\
\dot{y_E} &= (u\cos(\theta) + (v\sin(\phi) + w\cos(\phi))\sin(\theta))\sin(\psi) + (v\cos(\phi) - w\sin(\phi))\cos(\psi) \\
\dot{z_E} &= -u\sin(\theta) + (v\sin(\phi) + w\cos(\phi))\cos(\theta) \\
\dot{u} &= vr - wq - g\sin(\theta) + \frac{F_X}{m} \\
\dot{v} &= wp - ur + g\sin(\phi)\cos(\theta) + \frac{F_Y}{m} \\
\dot{w} &= uq - vp + g\cos(\phi)\cos(\theta) + \frac{F_Z}{m} \\
\dot{p} &= \frac{I_{zz}}{I^*}M_X + \frac{I_{xz}}{I^*}M_Z + \frac{(I_{xx} - I_{yy} + I_{zz})I_{xz}}{I^*}pq + \frac{((I_{yy} - I_{zz})I_{zz} - I_{xz}^2)}{I^*}qr \\
\dot{q} &= \frac{M_Y}{I_{yy}} + \frac{(r^2 - p^2)I_{xz}}{I_{yy}} + \frac{(I_{zz} - I_{xx})}{I_{yy}}pr \\
\dot{r} &= \frac{I_{xz}}{I^*}M_X + \frac{I_{xx}}{I^*}M_Z + \frac{((I_{xx} - I_{yy})I_{xx} + I_{xz}^2)}{I^*}pq + \frac{(-I_{xx} + I_{yy} - I_{zz})I_{xz}}{I^*}qr \\
\dot{\phi} &= p + \sin(\phi)\tan(\theta)q + \cos(\phi)\tan(\theta)r \\
\dot{\theta} &= \cos(\phi)q - \sin(\phi)r \\
\dot{\psi} &= \frac{\sin(\phi)}{\cos(\theta)}q + \frac{\cos(\phi)}{\cos(\theta)}r
\end{aligned} \tag{2.45}$$

With I^* defined as following:

$$I^* = I_{xx} * I_{yy} - I_{xx}^2 \tag{2.46}$$

The forces and moments are defined as following:

$$\begin{aligned} F_X &= F^B_{X_{\text{aero}}} + F^B_{grav_X} + T_1 + T_2 \\ F_Y &= F^B_{Y_{\text{aero}}} + F^B_{grav_Y} \\ F_Z &= F^B_{Z_{\text{aero}}} + F^B_{grav_Z} \\ M_X &= M^B_{X_{\text{aero}}} \\ M_Y &= M^B_{Y_{\text{aero}}} - (T_1 + T_2)T_{dz} \\ M_Z &= M^B_{Z_{\text{aero}}} + (T_1 - T_2)T_{dy} \end{aligned} \tag{2.47}$$

With T_1, T_2 the thrust force produced by the left and right engine and T_{dy}, T_{dz} are the respective moment arm lengths. The CG and reference position at which the aerodynamic forces act are described with x_{cg} and x_{ref} respectively.

2.5.3. Actuator Dynamics

The actuator model for the control surfaces are modelled as a second-order transfer function, shown in Equation (2.48) where the values are obtained from Matamoros [64].

$$H_{act} = \frac{\omega_{act}^2}{s^2 + 2\zeta_{act}\omega_{act}s + \omega_{act}^2} = \frac{4000}{s^2 + 140s + 4000} \tag{2.48}$$

The position and rate limit of the actuators are shown in the Table 6.4:

	Inboard and outboard elevons ($\delta_{CS1}^{L/R}$ & $\delta_{CS2}^{L/R}$) min,max	Rudder ($\delta_{CS3}^{L/R}$) min, max
Position limits ($\dot{u}$) [deg]	-25,25	-30,30
Rate limits (u) [deg/s]	-80,80	-120,120

Table 2.9: Control Surface actuator limits

The thrust is modelled as a first order lag as shown by Equation (2.49), with the maximum thrust based on the reference value of $3.79 \cdot 10^5$ N based on the Trent XWB-84 engine.

$$H_{thrust} = \frac{1}{\tau_{eng}s + 1} = \frac{1}{0.2s + 1} \tag{2.49}$$

2.5.4. Inner loop & Control Allocation

The inner loop INDI control law is extended with a control allocation algorithm to ensure efficient use of control surfaces, where it is responsible for the stabilization of the angular rate. The control input by the INDI control law is defined as following:

$$\mathbf{u} = \mathbf{u}_0 + \underbrace{\mathbf{P}(\mathbf{v} - \dot{\mathbf{x}}_\mathbf{0})}_{\Delta u} \tag{2.50}$$

Where:

- $\mathbf{u}$ is the computed control input sent to the actuators for the respective control surface to reach the desired deflection angle
- $\mathbf{u0}$ is previous control input, which is the current control surface deflection angle
- $\mathbf{\Delta u}$ is the incremental control input command, which is formed by the INDI control method
- $\mathbf{P}$ is the pseudo-inverse of the control effectiveness matrix $\mathbf{G}(\mathbf{x})$ as shown in Equation (2.51)), which contains non-dimensional aerodynamic control surface moment derivatives

- $\mathbf{v}$ is the desired reference, which is the roll moment $\dot{p}_r$, pitch moment $\dot{q}_r$ and yaw moment $\dot{r}_r$ rates. These reference inputs are generated by the outer loop
- $\dot{\mathbf{x}}_\mathbf{0}$ is the measured state derivative, which is the roll moment $\dot{p}$, pitch moment $\dot{q}$ and yaw moment $\dot{r}$ rates.

$$G(\mathbf{x}) = \frac{\rho V^2 Sc}{2}\mathbf{I}^{-1}\begin{bmatrix} C_{l^L_{\delta_{CS1}}} & C_{l^R_{\delta_{CS1}}} & C_{l^L_{\delta_{CS2}}} & C_{l^R_{\delta_{CS2}}} & C_{l_{\delta_{CS3}}} \\ C_{m^L_{\delta_{CS1}}} & C_{m^R_{\delta_{CS1}}} & C_{m^L_{\delta_{CS2}}} & C_{m^R_{\delta_{CS2}}} & C_{m_{\delta_{CS3}}} \\ C_{n^L_{\delta_{CS1}}} & C_{n^R_{\delta_{CS1}}} & C_{n^L_{\delta_{CS2}}} & C_{n^R_{\delta_{CS2}}} & C_{n_{\delta_{CS3}}} \end{bmatrix} \tag{2.51}$$

As observed, the control effectiveness is not squared and can not be inverted. Moreover, because there are more control surface for generating a specific moment for the aircraft, a control allocation algorithm is used that makes the most effective choice on which control surface is used.
The control allocation algorithm is a cascading algorithm with the first step of computing the Moore-Penrose pseudo-inverse of the control effectiveness matrix ($\mathbf{G}(\mathbf{x})$) computed as expressed in Equation (2.52).

$$\mathbf{P} = \mathbf{G}^T(\mathbf{G}\mathbf{G}^T)^{-1} \tag{2.52}$$

The second step is an algorithm that makes the most effective choice on which control surface with respect to the control input for the moment.

CA algorithm [23]
The algorithm takes actuator limits, such as actuator rate ($\dot{u}_{max}, \dot{u}_{min}$) and control surface limits into account, expressed by Equation (2.53) [65].

$$\begin{aligned} \Delta\mathbf{u}_{max} &= \min(\dot{\mathbf{u}}_{max}\frac{\omega_{act}}{2\zeta_{act}}, \mathbf{u}_{max} - \mathbf{u}) \\ \Delta\mathbf{u}_{min} &= \max(\dot{\mathbf{u}}_{min}\frac{\omega_{act}}{2\zeta_{act}}, \mathbf{u}_{min} - \mathbf{u}) \end{aligned} \tag{2.53}$$

The required control deflections $\mathbf{u}$ are calculated by Equation (2.54) and the control effectiveness matrix is noted as $\mathbf{B}$.

$$\mathbf{u} = \mathbf{P}\mathbf{m}^*_{des} \tag{2.54}$$

$$\mathbf{m}^*_{des} = \frac{2\mathbf{I}}{\rho V^2 S}(\mathbf{v} - \dot{\mathbf{x}}_\mathbf{0}) \tag{2.55}$$

If the demanded control deflections limits as computed by Equation (2.53) are not exceeded, then they will be used for the control deflections.

If any control surface deflection limits are reached then the control surface deflection will be computed as per the following three scenarios, in this order:

1. **Scenario 1**: If the rudder ($\delta^{L/R}_{CS3}$) has reached its limit
   - The control surface will be set to either its limit or to the required yaw moment divided by $C_{l^{L/R}_{\delta_{CS3}}}$
   - The column related to the control surface, and the row related to the yaw moment, removed from the control effectiveness matrix. The desired yaw moment is removed from the $\mathbf{m}^*_{des}$
   - The new $\mathbf{m}^*_{des}$ is calculated by subtracting the generated moment by the control surface from $\mathbf{m}^*_{des}$
2. **Scenario 2**: If either the outboard elevons ($\delta^{L/R}_{CS2}$) or both have reached their limits
   - Find which of these two control surfaces is the most over its limit, and calculate $a = u/u_{lim}$. Scale the other control surface with a, so that direction is preserved between these two control surfaces.
   - Calculate the new $\mathbf{m}^*_{des}$ by subtracting the generated moments from $\mathbf{m}^*_{des}$
   - Remove the rows related to $\delta^{L/R}_{CS2}$ from the control effectiveness matrix

3. **Scenario 3**: If either the inboard elevons ($\delta_{CS1}^{L/R}$) or both have reached their limits
   - Find which of these two control surfaces is the most over its limit, and calculate $a = u/u_{lim}$. Scale the other control surface with a, so that direction is preserved between these two control surfaces.
   - Calculate the new $\mathbf{m}_{des}^*$ by subtracting the generated moments from $\mathbf{m}_{des}^*$
   - Remove the rows related to $\delta_{CS1}^{L/R}$ from the control effectiveness matrix

If one of the inboard or outboard control surfaces is at its deflection limits, the other control surfaces will no longer be scaled to prevent the control surfaces from staying locked at their deflection limit. Thus, the direction, the ratio between moments, is temporarily not guaranteed until the control surface is no longer at its limit.
After this, there are four cases:

1. $\mathbf{B}$ has more columns than rows: in this case, the Moore-Penrose pseudo-inverse is used to invert the $\mathbf{B}$.
2. $\mathbf{B}$ has the same amount of rows as columns: it can be inverted normally.
3. $\mathbf{B}$ has fewer columns than rows: The problem is now over-determined, and the result will not fully meet the desired moment. To minimize the error, the following pseudo-inverse is used [66]: $\mathbf{P} = (\mathbf{B}_{red}^T \mathbf{B}_{red})^{-1} \mathbf{B}_{red}^T$
4. $\mathbf{B}$ is empty, meaning there are no control surfaces left to allocate. In this case, the control allocation does not completely meet the desired moment.

With the new inverted $\mathbf{B}$ matrix and $\mathbf{m}_{des}^*$, the other control surfaces can be allocated. If some control surfaces reach their limit, the algorithm starts again, until no surfaces are over the limit, or there are no control surfaces left to allocate.

2.5.5. Outer Loop and Flight Envelope Protection

The design and selection of outer loop control blocks with Flight Envelope Protection (FEP) was based on the FCS proposed by Lombaerts [67] with some changes [23] for the Flying V implementation. This resulted in an outer loop control structure with four major blocks, namely the:

1. C^* controller block with pitch reference model for longitudinal channel control
2. A roll reference model for the roll channel control
3. Sideslip compensator for the yaw channel control
4. Linear Controller that converts the outputs of the three aforementioned control blocks into a virtual control signal $\mathbf{v}$

The Flight Envelope Protection (FEP) feature is incorporated with the C^* control block and roll, pitch and sideslip reference model and is discussed with the respective control blocks themselves. The tuning of the gains in the blocks is done through a optimisation routine.

1. C^* controller and pitch reference model

For longitudinal control, a C^*, also referred as *C-star*, control block was combined with a pitch reference model. C^* is based on the C^* criterion [68], shown in Equation (2.56), which is a control law that mix both pitch rate (q) and load factor ($n_{z_{pilot}}$) at the pilot-station, where for the lower speed regimes the pitch rate is more dominant and for the higher speed the load factor is dominant. The application of the C^* control law has been used in various aircraft, for example in Airbus A320 [69]. The control law was selected to increase the familiarity that pilots have when flying with the Flying V for the first time.

$$C^* = \frac{V}{g} q + n_{z_{pilot}} \tag{2.56}$$

The C^* control block is illustrated in Figure 2.26, receives a C^* command from the pilot that is multiplied by $\frac{\cos(\theta)}{\cos(\phi)}$ to include turn compensation and lower the commanded load factor at high pitch angles [23, 67]. By subtracting the pitch rate from the command control input, a commanded load factor can be determined. However, before this is done, it can also been observed that the C^* control block is guarded to not exceed a maximum or minimum Angle of attack (α) and load factor.

Angle of attack Protection

The angle of attack protection is implemented to ensure that the Flying V stays in its flight envelope at all times and to prevent it from reaching the pitch-break up effect, which already start at angle of attack above 20 degrees and the aircraft at an angle of attack higher than 34 ends up in an unrecoverable state even with maximum control deflections. In practice, the maximal recoverable angle of attack can be lower, as in an ideal scenario you could deflect from maximum to minimum deflection.
The maximum angle of attack (α_{max}) protection only becomes active for angles higher than 15 degrees, and the minimum (α_{min}) for angles of attack below 0 degrees, these values are chosen to make sure that the protection does not limit the Flying V's manoeuvrability in normal flight. The angle of attack protection is computed as the maximum load factor ($n_{z_{\alpha_{max}}}$) and minimum ($n_{z_{\alpha_{min}}}$) as shown in Equation (2.57). $K_{\alpha_{max}}$ and $K_{\alpha_{min}}$ are gain values which are tuned to satisfy the desired performance and flying and handling quality.

$$\begin{aligned} n_{z_{\alpha_{max}}} &= n_z + K_{\alpha_{max}}(\alpha_{max} - \alpha) \\ n_{z_{\alpha_{min}}} &= n_z + K_{\alpha_{min}}(\alpha_{min} - \alpha) \end{aligned} \tag{2.57}$$

Load factor Protection

The load factor is defined as the ratio of lift L over weight W, $n_z = \frac{L}{W}$, the maximum load factor is calculated using the equation of motions, resulting in the following Equation (2.58) [67]. Where $C_{L_{max}}$ is the maximum lift coefficient at an angle of attack of 25 degrees and $\Delta C_{L_{max}}$ is set to 0.01. The maximum $n_{z_{max}}$ is set as 2.5 and $n_{z_{min}}$ is equal to -1.

$$n_{z_{\text{max}}} = \max\left(-1, \min\left(2.5, 1 + \frac{(C_{L_{\text{max}}} - \Delta C_{L_{\text{max}}})\, qS}{W}\cos(\phi) - n_y \sin(\phi) - \cos(\gamma) + \frac{T}{W}\sin(\alpha)\cos(\phi)\right)\right) \tag{2.58}$$

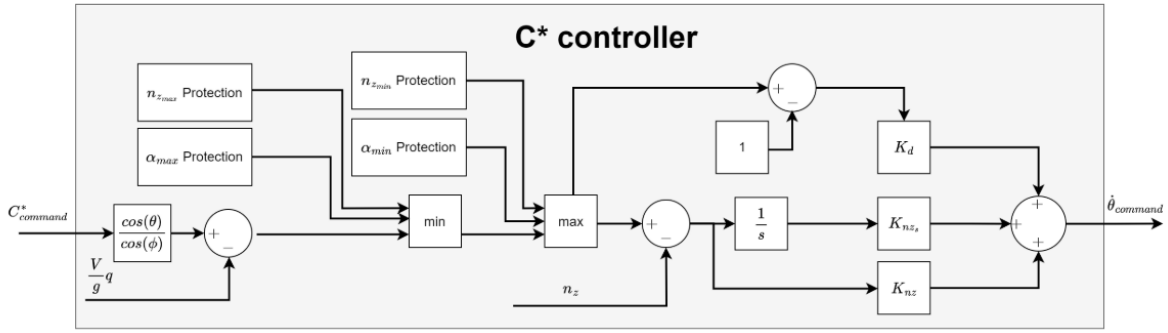

Figure 2.26: Block diagram of the C^* controller [23]

The computed protected load factor is used to get a $\dot{\theta}_{command}$ for the pitch reference model. This is determined using a PI-control with a feedforward path, which uses the real load factor as its reference with three gain values (K_d, K_{nz_s}, K_{nz}).
The pitch reference model acts as second-order filters as illustrated in Figure 2.27, with the relations between gains and damping ratio defined as:

$$\begin{aligned} K_1 &= 2\zeta\omega \\ K_2 &= \frac{\omega}{2\zeta} \end{aligned} \tag{2.59}$$

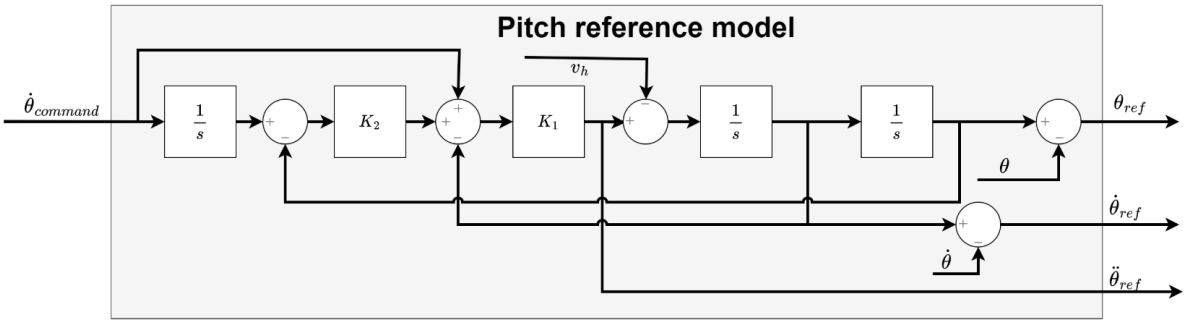

Figure 2.27: Block diagram of the pitch reference model [23]

2. Roll reference model

The roll reference model is identical to the pitch reference model, but it also has roll protection in the reference model, as illustrated in Figure 2.28. The input is the roll rate command from the pilot, and the reference model acts as a Rate Control Attitude Hold controller [23, 67].

Roll angle Protection

The roll angle protection is calculated through the equations of motion relations and expressed by Equation (2.60), which limits the roll angle and roll rate. To not limit the manoeuvrability in normal flight, the roll angle protection is only active when the roll angle is within two degrees of the limit.

$$\begin{aligned} \phi_{\text{max}} &= \min\left(66, \arccos\left(\frac{mg\cos(\gamma)}{T\sin\alpha + (C_{L_{\text{max}}} - \Delta C_{L_{\text{max}}})\, qS}\right)\right) \\ \dot{\phi}_{\text{max}} &= K_{\phi_{\text{protect}}}(\phi_{\text{max}} - \phi) \\ \dot{\phi}_{\text{min}} &= K_{\phi_{\text{protect}}}(-\phi_{\text{max}} - \phi) \end{aligned} \tag{2.60}$$

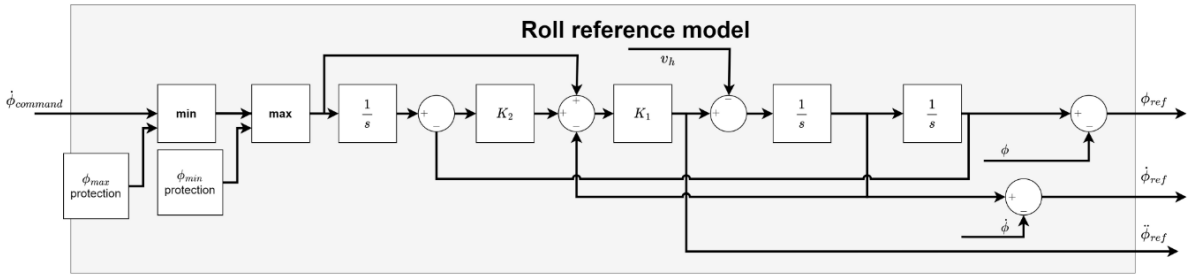

Figure 2.28: Block diagram of the roll reference model [23]

3. Sideslip compensator

The sideslip compensator provides sideslip control and not yaw rate control, illustrated in Figure 2.29. The vertical velocity (w) is approximated by Equation (2.61) and the use of this control law requires sideslip angle measurements [23].

$$w \approx V\sin(\alpha) \tag{2.61}$$

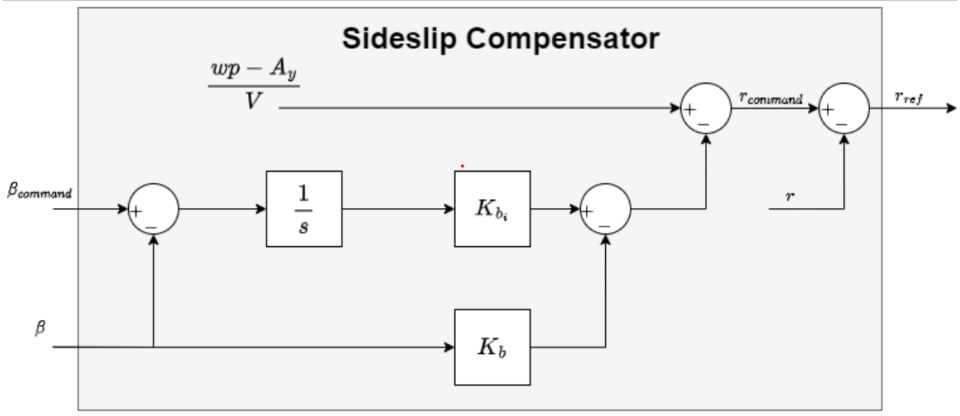

Figure 2.29: Block diagram of the sideslip compensator reference model [23]

4. Linear controller

The linear controller converts the outputs of the reference models and sideslip compensator to virtual signal v. This linear controller is a PI controller with the control law Equation (2.62) obtained from [67].

$$\begin{aligned} v_p &= \left(K_\phi + \frac{K_{\phi I}}{s}\right) \cdot \phi_{ref} + K_{\dot{\phi}} \cdot \dot{\phi}_{\text{ref}} + K_{\ddot{\phi}} \cdot \ddot{\phi}_{ref} \\ v_q &= K_\theta \cdot \theta_{ref} + K_{\dot{\theta}} \cdot \dot{\theta}_{ref} + K_{\ddot{\theta}} \cdot \ddot{\theta}_{ref} \\ v_r &= K_r \cdot r_{ref} \end{aligned} \tag{2.62}$$

2.5.6. Tuning

The tuning of the gains in the outer loop control blocks are done through a multi-objective optimisation, extensively described by Stougie [23]. The optimisation is performed separately for the longitudinal and lateral design parameters, and the optimisation is done according to a scoring for the objectives:

- The MIL-STD-179A flying and handling quality requirements
- Gain and Phases Margins
- Low Order Equivalent System (LOES) fit
- Attitude bandwidth

2.5.7. Pseudo-Control Hedging

Pseudo Control Hedging (PCH) is a way to prevent actuator wind up, which can happen due to a high deviation in commanded input signal that is drives the actuator to its saturation limits, which continuously accumulates to a high error. Through PCH, the virtual control signal to the inner loop is lowered by calculating the difference between the demanded moment and estimated moment, which then computes commanded signals, which are achievable by the actuator to reach the desired control surface deflections. This virtual control hedge is expressed by Equation (2.63) [70].

$$\mathbf{v_h} = \mathbf{G}(\mathbf{x})(\mathbf{u}_{comm} - \mathbf{u}_{actual}) \tag{2.63}$$

For the Flying V FCS, the virtual control hedge is subtracted for the pitch and roll reference model, but not the yaw moment.

2.5.8. Sensor Dynamics & Filtering

The sensor parameters for the FCS sensor dynamics are based on values from Grondman [70] for the sensors of the Cessna Citation II PH-Lab laboratory aircraft with an overview of these sensor parameters provided in Table 2.10. The noise and bias are modelled by white noise that's added to the signal. The sampling of the signals are done through zero-order hold blocks available in Matlab and integrators

in the controllers will be replaced by discrete integrators using Tustins approximation [23] as expressed by Equation (2.64). MATLAB automatically converts discrete signals to continuous time signals.

$$\frac{1}{s} \approx \frac{T_s(z+1)}{2(z-1)} \tag{2.64}$$

To obtain level 1 flying qualities, these baseline sensor parameters, the time delay for the sensors and control blocks have been adjusted for the Flying V FCS [23]. A high level overview of the sensor dynamics are shown in Figure 2.30.

Sensor	Sampling rate [Hz]	Time delay [s]	Noise	Bias	Filter time constant
p, q, r [rad/s]	50	0.1	$1 \cdot 10^{-9}$	$3 \cdot 10^{-5}$	0.05
ϕ, θ [rad]	50	0.1	$1 \cdot 10^{-9}$	$4 \cdot 10^{-3}$	0.05
V [m/s]	1/0.065	0.325	$1 \cdot 10^{-4}$	2.5	0.05
α, β [rad]	50	0.1	$7.5 \cdot 10^{-8}$	$3 \cdot 10^{-5}$	0.05
$A_x.A_yA_z$	50	0.1	$1 \cdot 10^{-5}$	$2.5 \cdot 10^{-3}$	0.05

Table 2.10: Baseline Sensor parameters [70]

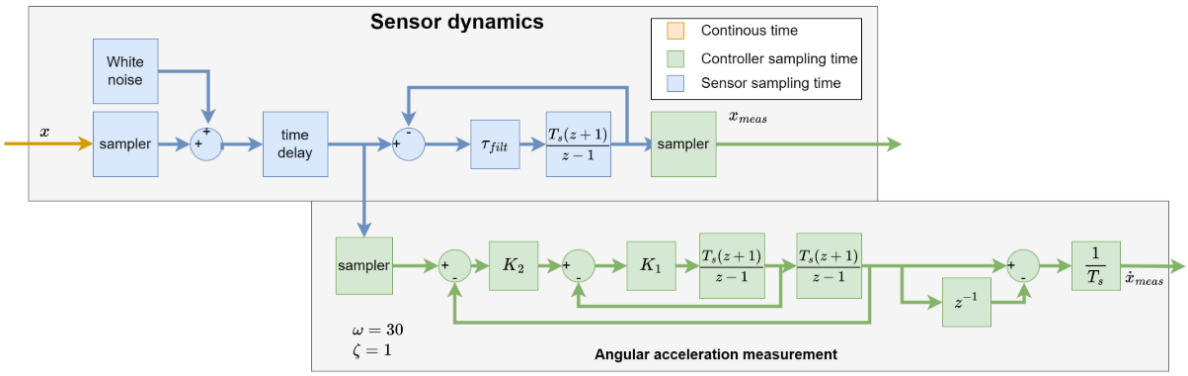

Figure 2.30: Sensor dynamics model [23]

To obtain the angular accelerations, the output of the body rate filters is first filtered by a second order filter and then differentiated through Matlab's discrete control blocks.The instantaneous change of pitch angle θ and change of roll angle ϕ are calculated using the gyroscopes. It is assumed that the air density and actuator positions are known without any time delay, bias, or noise.

The inner loop control signal is also discretised as following:

$$\mathbf{u}_k = \mathbf{u}_{k-1} + \mathbf{G}^{-1}(\mathbf{x}_{k-1})(\mathbf{v}_k - \frac{\mathbf{x}_{k-1} - \mathbf{x}_{k-2}}{T_s}) \tag{2.65}$$

A synchronisation filter is applied to ensure that u_{k-1} is in sync with the angular acceleration measurements, as time delays originating from for example sensors causing a time difference could degrade the performance of the FCS. This synchronisation filter consists of the same second-order filter that is applied to obtain the angular acceleration. The time delay was set to be $2ms$ higher to cope with unaccounted time delays [23].

There is no filtering present to eliminate the noise and biases in the system and estimate the aircraft's signals and states.

2.6. Adaptive FCS Requirements

Based on the existing research for the Flying V FCS, it has been observed that when the control effectiveness estimations are deviated, the aircraft has a higher variance in its response and the control surfaces exhibit oscillatory behaviour. In addition, when the aircraft is flying in a condition at which it

has not been tuned, there is a relation regarding air density and dynamic pressure, which causes the control surfaces to exhibit oscillatory behaviour and reach its control surface deflection limits. This has been attributed to the gain scheduling being done at an insufficient set of points.
The existing FCS has been evaluated through several handling quality criterion and tracking reference simulations, where it was established that the augmentation through a nonlinear FCS control method provided Level 1 flying qualities.

When looking at the development and research opportunity for the implementation of adaptive control methods into the FCS, it can be determined that the existing INDI could be modified or replace with a nonlinear and adaptive control method. Moreover, the FCS has not been investigated in a fault-tolerant scenario, and thus it is unknown if the designed FCS is able to cope in a fault-tolerant scenario, which also provides the research opportunity for an adaptive FCS.
Depending on the adaptive FCS method, it may not be necessary to re-evaluate the FCS as in-depth as the previous researches, however it may be interesting to observe what level of flying quality the aircraft can achieve when it's under a fault-tolerant scenario, which allows the investigation on how an adaptive FCS is able to perform in such a scenario. Moreover, several tracking experiments observed saturation in control deflections, and these experiments can be re-enacted to observe the improvements that an adaptive FCS can provide.

2.7. Conclusion

This chapter provided a literature review regarding the state-of-the-art research focused on the development of the FCS for the Flying V. With the literature review conducted, some research sub-questions can be answered:

1. What are the results and lessons from previous research on developing the FCS for the Flying V?
   (a) What is the current state of handling qualities of the Flying V?
      - There have been separate assessment for the bare-airframe of the Flying V and the augmented Flying V with an FCS or CA algorithm
      - Bare-airframe: Level 1 & Level 2 with respect to its longitudinal dynamic modes. Level 3 to unstable with respect to the Dutch roll. Experimental simulations reveal unstable behaviour and control saturation.
      - Augmented airframe with FCS: Several FCS using linear control laws and different CA schemes. Simulator experiments and offline experiments with linear flight control laws reveal that the Dutch Roll is still stable and control surfaces saturate. The nonlinear FCS from [23] was shown to stabilise the dynamic modes and provide Level 1 Flying qualities.

   (b) What are the latest development in aerodynamic modelling for the Flying V?
      - The latest aerodynamic model for the Full-Scale Aircraft is determined by the combination of the VLM model and elements from the WTE, which is able to capture longitudinal instability, pitch break and lateral instability, dutch roll. At the time of writing, a new Full-Scale Flying V model has been developed for use with the FCS. The Flight Test Experiment needs further investigation and validation against the WTE experiments, before it can be scaled to the Full Scale model.

   (c) What is the current state of the Flying V simulation model?
      - The current Flying V simulation model is developed using the combined aerodynamic model. The FCS for the Flying V is developed with the nonlinear Incremental Dynamic Inversion (INDI) method with Flight Envelope Protection, white noise, sensor dynamics, time delays and discretisation.

   (d) What assumptions and uncertainty are present in the simulation model of the Flying V?
      - The implemented aerodynamic model is estimated at a limited set of flight conditions and developed from a combination of linear aerodynamic data for the full scale aircraft and nonlinear data of a half-wing subscale wind tunnel experiment, which has limited validity to investigate and observe the aircraft's dynamics across different flight condition
      - Due to the combined aerodynamic model there is an uncertainty in the aerodynamic model and future iteration would require updates of the FCS to cope with this

- There is no engine simulation model that provides the thrust at the various flight condition, but it is computed to achieve the necessary trim at the flight condition
- The sensors have been adjusted to conform to Level 1 flying qualities, and it is unknown if these sensors are available in the industrial market
- The mass, weight and moment of Inertia of the aircraft remains the constant during the simulation
- Zero wind and perfect atmosphere

(e) What are the specifications and requirements for that apply to an FCS with an adaptive control method?

- Achieve Level 1 flying qualities
- Achieve satisfactory performance with uncertainties as good or better than the existing simulation model
- Achieve satisfactory tracking performance with fault-tolerant scenarios

2. What evaluation metrics are suitable to assess the adaptive control method for the FCS?
   (a) What are the flying & handling qualities criteria, which have been evaluated with the FCS?
   - Several simulator experiments with linear FCS and offline simulations with nonlinear FCS.
   - CAP, Gibson Tracking, Gibson phase.
   - Different longitudinal and lateral manoeuvres and tracking experiments were conducted.

   (b) What assessment for evaluating uncertainties/delays have been performed?
   - Aerodynamic uncertainty
   - Influence of time delays

3

Nonlinear & Adaptive Control Methods

This chapter concerns an overview of all relevant state-of-the-art nonlinear & control methods. For each method, the description of the method and their respective state-of-the-art application. The following research questions:

- What advancements have there been in the applications of nonlinear & adaptive methods?
    1. What methods have been implemented for fault tolerant control?
    2. What method is the most suitable for fulfilling the requirements for the Flying V?

3.1. Backstepping Approaches

This section concerns the backstepping-based approach, which are a class of methods based upon Lypaunov stability theorem and has had various applications and research for nonlinear control. First, the Backstepping (BS) will be elaborated (3.1.1), which presents the theoretical foundations of this method with a description on the application in flight control. Secondly, a description of the Incremental Backstepping (IBS) will be described (3.1.2), which replaces the feedback of system dynamics in the control law by sensor measurements/estimations. At last, the adaptive schemes or frameworks applied with (I)BS are further elaborated (3.1.3).

3.1.1. Backstepping

Backstepping (BS) control is a recursive, Lyapunov-based, nonlinear control method. The application of the method starts with a scalar equation that is separated by the largest number of integrations from the control input and 'step back' towards the (physical) control input. At each step, a 'virtual' control law is calculated, where the state variables are considered in the design of the control method. The 'virtual' control law is designed as per Lyapunov's theory and stability concepts, thus guaranteeing global asymptotic stability and tracking. The last step is where the 'real' control law is found. Several works of literature provide a comprehensive description of the method and its design [15, 71–73].

First theorems and definitions regarding Lyapunov stability theory are described as it forms the basis of the BS method, and then a general procedure for recursive BS is described. To overcome the high design effort required for applying this technique, Command Filtered Backstepping (CFBS) was developed. At last, state-of-the-art applications in flight control are described.

Lyapunov Stability, Theory and Control Design

The description and outline of BS applications has been comprehensively gathered in [73]. For the description of Lyapunov's Stability, Theory and application to control design the following nonlinear dynamic system is considered:

$$\dot{\mathbf{x}} = \mathbf{f}(\mathbf{x}), \qquad \mathbf{x}(t_0) = \mathbf{x}_0 \tag{3.1}$$

where $\mathbf{x} \in \mathbb{R}^n$ is the state and $\mathbf{f}$ satisfies Lipschitz condition locally, which is defined as:

Definition 3.1 **Lipschitz condition**

A function $f(\mathbf{x}, t)$ satisfies a Lipschitz condition on $\mathbb{D}$ with Lipschitz constant L if [1]*:*

$$|\mathbf{f}(\mathbf{x}, \mathbf{t}) - \mathbf{f}(\mathbf{x}, \mathbf{y}) \leq L|\mathbf{x} - \mathbf{y}| \tag{3.2}$$

for all points $(\mathbf{x}, t)$ and $(\mathbf{y}, t)$ in $\mathbb{D}^2$

The equilibrium point $\mathbf{x}_0 \in \mathbb{R}^n$ satisfies the relation $\mathbf{f}(\mathbf{x}_0) = \mathbf{0}$ where it can be assumed that without loss of generality, that the system has an equilibrium point $\mathbf{x}_0 = 0$. The concept of stability is concerned with the investigation and characterisation of the behaviour of dynamic systems. For control systems, the concern of stability is regarding changing the properties of dynamic systems such that they exhibit acceptable behaviour when perturbed from their operating point by external forces [20]. Fundamental concepts of stability were introduced by Alexandr Lyapunov who describes the stability of a nonlinear system around equilibrium point [14, 15] as:

Definition 3.2 **Stability in the sense of Lyapunov**

The equilibrium point $\mathbf{x}_0$ of the nonlinear system (Equation (3.1)*) is:*

- ***stable*** *if for each $\epsilon > 0$ and any $t_0 > 0$, there exists a $\delta(\epsilon, t_0) > 0$ such that:*

$$|\mathbf{x}(t_0)| < \delta(\epsilon, t_0) \Rightarrow |\mathbf{x}(t)| < \epsilon \qquad \in t \geq t_0$$

- ***uniformly stable*** *if for each $\epsilon > 0$ and any $t_0 > 0$, there exists a $\delta(\epsilon) > 0$ such that:*

$$|\mathbf{x}(t_0)| < \delta(\epsilon) \Rightarrow |\mathbf{x}(t)| < \epsilon \qquad \forall t \geq t_0$$

- ***unstable***

Figure 3.1 illustrates the concept of stable, uniformly stable and unstable in $\mathbb{R}^2$

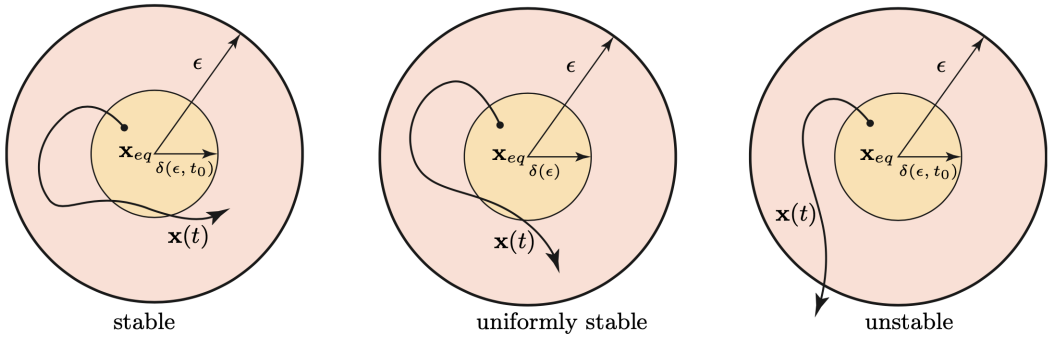

Figure 3.1: Lyapunov stability illustrated in $\mathbb{R}^2$. Taken from [20]

If the equilibrium point $\mathbf{x}_0 = 0$ is stable, the time to return to stability after it has been perturbed, can be described as:

- ***asymptotically stable*** *if it is stable, and for any $t_0 > 0$, there exists a $\eta(t_0) > 0$ such that:*

$$|\mathbf{x}(t_0)| < \eta(t_0) \Rightarrow |\mathbf{x}(t)| \to 0 \qquad t \to \infty$$

- ***uniformly asymptotically stable*** *if it is uniformly stable, and there exists an $\delta > 0$ independent of t such that $\forall \epsilon > 0$ there exists a $T(\epsilon) > 0$ such that:*

$$|\mathbf{x}(t_0)| < \delta \Rightarrow |\mathbf{x}(t)| < \epsilon \qquad \forall t \geq t_0 + T(\epsilon)$$

- ***exponentially stable*** *If for any $\epsilon > 0$ there exists a $\delta(\epsilon) > 0$ such that:*

$$|\mathbf{x}(t_0)| < \delta \Rightarrow |\mathbf{x}(t)| < \epsilon e^{-\alpha(t-t_0)} \qquad \forall t > t_0 \geq 0$$

  for some $\alpha > 0$
- ***globally exponentially stable*** *if exponential stability is satisfied for any initial state $\mathbf{x}(t_0)$*
- ***marginally stable*** *if it is stable (in the sense of Lyapunov) but not asymptotically stable*

To determine the stability without explicitly solving the differential equation, Lyapunov's direct method can be applied. The method concerns finding a suitable function $V(x)$ with the following definition:

Definition 3.3 -

A continuously differentiable scalar function $V(x)$ is:

- ***positive definitive** if $V(0) = 0$ and $V(x) > 0$ for $x \neq 0$*
- ***positive semi-definitive** if $V(0) = 0$ and $V(x) \geq 0$ for $x \neq 0$*
- ***negative (semi-)definitive** if $-V(0) = 0$ is positive (semi-) definite*

The Lyapunov function can be defined as:

Definition 3.4 **Lyapunov function**

*A continuously differentiable scalar function $V(x)$ is said to be a **Lyapunov function** for the system (Equation (3.1)), if its time derivative along the system's trajectories is negative semi-definite:*

$$\dot{V}|_{\dot{x}=f(x,t)} = \frac{\partial V}{\partial t} + \frac{\partial V}{\partial x} f(x,t) \leq 0, \qquad \forall t \geq 0, \forall x \in \mathbb{R}^n$$

The stability of the system around equilibrium point $\mathbf{x}_0$ can now be determined with the Lyapunov's Direct Method theorem to describe the asymptotic stability and this results in the theorem by LaSalle and Yoshizawa [15]:

Definition 3.5 **LaSalle-Yoshizawa**

Let $x_0 = 0$ be an equilibrium point and suppose that f is locally Lipschitz in x and uniformly in t. Let V be a continuously differentiable function such that:

- $\gamma_1(x) \leq V(x,t) \leq \gamma_2(x)$
- $\dot{V}|_{\dot{x}=f(x,t)} = \frac{\partial V}{\partial t} + \frac{\partial V}{\partial x} f(x,t) \leq -W(x) \leq 0$

$\forall t \geq 0, \forall x \in \mathbb{R}^n$, where γ_1 and γ_2 are continuous positive definitive functions and where W is a continuous function. Then all solutions of the nonlinear system satisfy:

$$\lim_{t \to \infty} W(x(t)) = 0$$

In addition, if W(x(t)) is positive definite, then the equilibrium $x_0 = 0$ is globally uniformly asymptotically stable

Now consider the system to be controlled:

$$\dot{\mathbf{x}} = \mathbf{f}(\mathbf{x}, \mathbf{u}), \qquad (\mathbf{x_0}, t_0) = (\mathbf{0}, 0), \qquad f(\mathbf{x_0}, t_0) = 0 \tag{3.3}$$

where $\mathbf{x} \in \mathbb{R}^n$ is the system state and $\mathbf{u} \in \mathbb{R}$ the control input. The control objective is to design a stabilising feedback control law $\alpha(\mathbf{x})$ for the control input such that the equilibrium point $x_0 = 0$ is globally asymptotically stable. To prove the stability, a function $V(\mathbf{x})$ can be chosen as a Lyapunov candidate and requires that the derivative with the stabilising feedback control law satisfies $\dot{V}(\mathbf{x}) \leq -W(\mathbf{x})$, where $W(\mathbf{x})$ is a positive definite function. [71].

This is a challenging task as a stabilising control law for the system may exist, but satisfying the condition may fail because of a poor choice of $V(x)$ and $W(x)$. If it exists, then the corresponding system possesses a Control Lyapunov Function (CLF), which is defined as [15, 71]:

Definition 3.6 **Control Lyapunov Function**

A smooth positive definite and radially unbounded function V, with $V(\mathbf{0}) = 0$ and $V(\mathbf{x}) > 0$ for $\mathbf{x} \neq \mathbf{0}$, is called a CLF if there exists a $u \in \mathbb{R}$ that satisfies:

$$\inf_{u \in \mathbb{R}} \left\{ \frac{\partial V}{\partial \mathbf{x}} f(\mathbf{x}, u) \right\} < 0, \qquad \forall x \neq 0$$

Determining an appropriate CLF can be as complex as designing the stabilising feedback law. With the backstepping procedure these problems can be tackled where you determine $V(x)$ and $\alpha(x)$ for scalar systems. In most works of literature the following CLF is commonly applied [15, 71, 73]:

$$V(x) = \frac{1}{2}x^2 \tag{3.4}$$

Recursive backstepping

The concept of recursive backstepping is to design a controller in a recursive way and consider state variables (x_i) as "virtual controls" and design intermediate "virtual" control laws. Starting with the scalar equation that is separated by the largest numbers of integrations from the control input u. In other words, the backstepping approach determines how to stabilise the subsystem using the state and how to make the next state stabilise the subsystem, and this process is recursively done until the final control law u is designed. Each control law is designed with Lyapunov's theory and stability principles, thus resulting in asymptotic stability and boundness for the cascaded subsystems.
The recursive backstepping approach, outlined by Sonneveld [15], allows for the design of a controller applicable to a wide range of nonlinear systems in a structured, recursive manner. The following assumptions are made for the application [15]:

- The nonlinear system is in strict-feedback form
- The nonlinear system is control-affine
- The nonlinear system dynamics are available and known

Starting from the state that is the 'furthest' from the actual control input u, three steps are taken to apply the backstepping technique:

1. Introduce a virtual control and error state, and rewrite the current state equation in terms of these
2. Choose a CLF for the system, treating it as a final stage
3. Choose a stabilising feedback term for the virtual control that makes the CLF stabilisable.

The CLF is augmented at the subsequent steps to reflect the presence of new virtual states, but the same three stages are followed at each step. The recursive backstepping procedure is illustrated in Figure 3.2

Consider the application of this procedure for a strict feedback nonlinear system for a tracking task:

$$\begin{aligned} \dot{x}_1 &= f_1(x_1) + g_1(x_1)x_2 \\ \dot{x}_2 &= f_2(x_1, x_2) + g_2(x_1, x_2)x_3 \\ &\vdots \\ \dot{x}_n &= f_n(x_1, x_2, ..., x_n) + g_n(x_1, x_2, ..., x_n)u \end{aligned} \tag{3.5}$$

where $x_i \in \mathbb{R}, u \in \mathbb{R}$ and $g_i \neq 0$. The control objective is to force output $y = x_1$ to asymptotically track the reference signal y_r whose first n derivative are assumed to be known and bounded.
The backstepping procedure starts by defining the tracking errors as:

$$\begin{aligned} z_1 &= x_1 - y_r \\ z_i &= x_i - \alpha_{i-1}, \qquad i = 2, ..., n \end{aligned} \tag{3.6}$$

The nonlinear system can be rewritten in terms of these new variables as:

$$\begin{aligned}\dot{z}_1 &= f_1(x_1) + g_1(x_1)x_2 - \dot{y}_r \\ \dot{z}_2 &= f_2(x_1, x_2) + g_2(x_1, x_2)x_3 - \dot{\alpha}_1 \\ &\vdots \\ \dot{z}_n &= f_n(x_1, x_2, ..., x_n) + g_2(x_1, x_2, ..., x_n)u - \dot{\alpha}_{n-1}\end{aligned} \tag{3.7}$$

The Control Lyapunov Functions (CLFs) are selected as:

$$V_i = V_{i-1} + \frac{1}{2}z_i^2, \qquad i = 1, ..., n \tag{3.8}$$

and the (virtual) feedback controls as:

$$\begin{aligned}\alpha_1 &= \frac{1}{g_1}[-c_1 z_1 - f_1 + \dot{y}_r] \\ \alpha_i &= \frac{1}{g_n}[-g_{i-1}z_{i-1} - c_i z_i - f_i + \dot{\alpha}_{i-1}], \qquad i = 2, ..., n \\ u &= \alpha_n\end{aligned} \tag{3.9}$$

with gains $c_i > 0$.

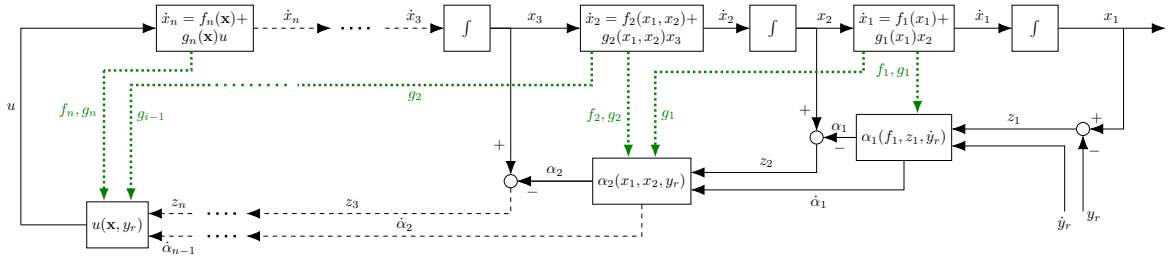

Figure 3.2: Recursive backstepping procedure. The green lines represent information required for control design. Adapted from [20] and [15]

Command Filtered Backstepping

For the design of a control law with BS, it can be observed that time derivatives of the reference command y_r and virtual control, $\dot{\alpha}_i$ must be known, however, it can be challenging to determine analytical expressions for the derivative as they can contain part of the system dynamics and cumbersome to determine. The use of command filtering as described in [74] furthers the practical application of BS, due to the simplification of determining the command derivatives, where the raw intermediate commanded reference signals are passed through a filter before it is used as a final reference. The benefits of using this approach as described by [74] are:

1. Decoupling of the design of the controllers for the backstepping iterations
2. Avoiding the tedious algebra related to computing the command signal derivatives. This computation becomes especially burdensome for scalar backstepping with $n > 3$ or vector backstepping

Moreover, command filters can be used to incorporate magnitude and rate constraints on the control input and intermediate states as ilustrated in Figure 3.3 & 3.4 [73–75].

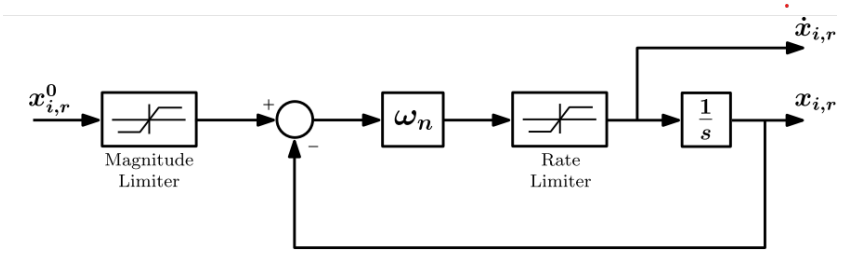

Figure 3.3: First order filter while enforcing magnitude, bandwidth and rate limits constraints. Taken from [73]

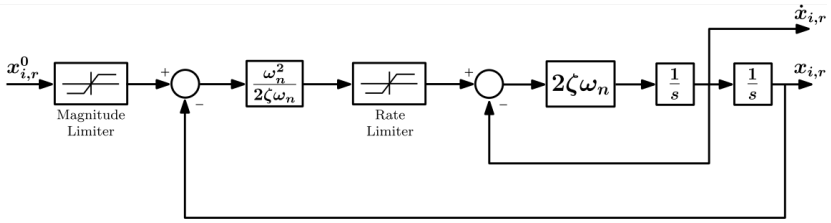

Figure 3.4: Second order filter while enforcing magnitude, bandwidth and rate limits constraints. Taken from [73]

The design approach for Command-Filtered Backstepping (CFBS) is outlined in [73, 76] and is described as the following for a second-order system in strict-feedback form:

$$\dot{x}_1 = f_1(x_1) + g_1(x_1)x_2$$
$$\dot{x}_2 = f_2(x_1, x_2) + g_2(x_1, x_2)u$$

It is assumed that f_i, g_i and their first partial derivatives are continuous and bounded. For the system, x_1 is the output command variable. The tracking errors can be defined as:

$$z_1 = x_1 - x_{1,r}$$
$$z_2 = x_1 - x_{2,r}$$

The reference command and its derivative are defined as $x_{i,r}, \dot{x}_{i,r}$ and are obtained using the raw, unfiltered commands denoted as $x^0_{i,r}$ with the command filter. With the application of command filtering the modified tracking errors are defined as:

$$\bar{z}_1 = z_1 - \mathcal{X}_1$$
$$\bar{z}_2 = z_2 - \mathcal{X}_2$$

The variables $\mathcal{X}_1, \mathcal{X}_2$ are an estimation of the effect that the command filter has on the tracking error. The dynamics of these variables are defined as stable linear filters, which can be a first or second-order, low-pass filter with unity low-frequency (DC) gain [73]:

$$\dot{\mathcal{X}}_1 = -c_1\mathcal{X}_1 + g_1(x_{2,r} - x^0_{2,r})$$
$$\dot{\mathcal{X}}_2 = -c_2\mathcal{X}_2 + g_2(u - u^0)$$

By design of the filter, the signal $(x_{i,r} - x^0_{i,r})$ and its derivative $\dot{x}_{i,r}$ is bounded and small. Therefore, as long as g_i is bounded, then $\mathcal{X}_i$ is bounded. The Control Lyapunov Functions (CLFs) are set up for the modified tracking errors. Where for the first CLF the following expression and derivative are defined:

$$V_1 = \frac{1}{2}\bar{z}_1^2$$
$$\dot{V}_1 = \bar{z}_1\dot{\bar{z}}_1$$
$$= \bar{z}_1[f_1 + g_1x_2 - \dot{x}_{1,r} - \dot{\mathcal{X}}_1]$$

As with the standard (recursive) BS procedure, the stabilising control law must render the time derivative to be negative (semi-) definite:

$$\alpha_1 \triangleq x_{2,r} = \frac{1}{g_1}[-c_1z_1 - f_1 + \dot{x}_{1,r}]$$

However, instead of directly applying this control law, the raw unfiltered $x^0_{2,r}$ control law is designed. Rewriting $x_2 = z_2 + x^0_{2,r}$ and inserting $\dot{\mathcal{X}}_1$ and simplifying results in the following expression:

$$\dot{V}_1 = [f_1 + g_1z_2 - \dot{x}_{1,r} + c_1\mathcal{X}_1 + g_1x^0_{2,r}]$$

A possible choice for $x^0_{2,r}$ is:

$$\alpha_i \triangleq x^0_{2,r} = \frac{1}{g_1}[-c_1z_1 - f_1 + \dot{x}_{1,r}] - \mathcal{X}_2$$

Inserting this choice yields:

$$\begin{aligned}\dot{V}_1 &= \bar{z}_1[f_1 + g_1 z_2 - \dot{x}_{1,r} + c_1\mathcal{X}_1 + (-c_1 z_1 - f_1 + \dot{x}_{1,r}) - g_1\mathcal{X}_2] \\ &= \bar{z}_1[-c_1(z_1 - \mathcal{X}_1) + g_1(z_2 - \mathcal{X}_2)] \\ &= \bar{z}_1[-c_1\bar{z}_1 + g_1\bar{z}_2] \\ &= -c_1\bar{z}_1^2 + \bar{z}_1 g_1 \bar{z}_2\end{aligned}$$

The cross term $\bar{z}_1 g_1 \bar{z}_2$ is removed in the second design step, where CLF V_2 is defined as following:

$$V_2 = V_1 + \frac{1}{2}\bar{z}_2^2$$

Its time derivative should be rendered negative (semi-) definite:

$$\begin{aligned}\dot{V}_2 &= \dot{V}_1 + \bar{z}_2\dot{\bar{z}}_2 \\ &= \dot{V}_1 + \bar{z}_2[f_2 + g_2 u - \dot{x}_{2,r} - \dot{\mathcal{X}}_2]\end{aligned}$$

Inserting the expressions for $\dot{V}_1$ and $\dot{\mathcal{X}}_2$ and simplifying results in the following time derivative:

$$\dot{V}_2 = -c_1\bar{z}_1^2 + \bar{z}_1 g_1 \bar{z}_2 + \bar{z}_2[f_2 - \dot{x}_{2,r} + c_2\mathcal{X}_2 + g_2 u^0]$$

A possible choice for u^0 is:

$$u = \frac{1}{g_2}(-c_2 z_2 - f_2 + \dot{x}_{2,r} - g_1 z_1)$$

This yields:

$$\dot{V}_2 = -c_1\bar{z}_1^1 - c_2\bar{z}_2^2$$

The derivation, properties, and proof are presented by Farrell [74] states that the compensated tracking errors of the command filtered backstepping approach have the same stability properties as the standard backstepping approach.

State-of-the-art Applications

Recursive Backstepping and Command Filtered Backstepping has been applied on 2nd order nonlinear flight control system [15, 75] and succesful application for a fixed-wing UAV [77]. These applications will be described further in detail.

BS has been applied to develop longitudinal control for a second-order nonlinear model, as presented in [15]. The system as set up in Equation (3.10) consists of longitudinal force (f_1) and moment equation (f_2) with aerodynamic coefficients represented as third-order polynomials.

$$\begin{aligned}\dot{x}_1 &= x_2 + f_1 + g_1 u \\ \dot{x}_2 &= f_2 + g_2 u \\ \text{with states} \\ x_1 &= \alpha, \quad x_2 = q\end{aligned} \tag{3.10}$$

To bring the system in strict-feedback form (or lower-triangular form) it was assumed that the control surface was a pure moment generator, thus removing the contribution of the control surface in the longitudinal force direction ($g_1 = 0$) and to compensate for the neglected control term an integrator term ($\lambda = \int_0^t z_1 dt$) was added in its control design. Resulting in the backstepping control law as expressed by 3.11.

$$\begin{aligned}u &= \frac{1}{g_2}[-c_2 z_2 - z_2 - f_2 + \dot{\alpha}_1] \\ \text{with} \\ z_1 &= x_1 - y_r \quad z_2 = x_2 - \alpha_1 \\ V_1(z_1) &= \frac{1}{2}[z_1^2 + k_1\lambda_1^2] \quad V_2(z_1, z_2) = V_1 + \frac{1}{2}z_2^2 \\ \alpha_1 &= -c_1 z_1 - k_1\lambda_1 - f_1 + \dot{y}_r, \quad c_1 > 0\end{aligned} \tag{3.11}$$

The numerical simulation shows that the controller can track the reference signal for different sets of gain values. However, when the full model is used the autopilot without the integrator term ($k_1 = 0$) can only achieve bounded tracking, these results are shown in Figure 3.5 & 3.6.

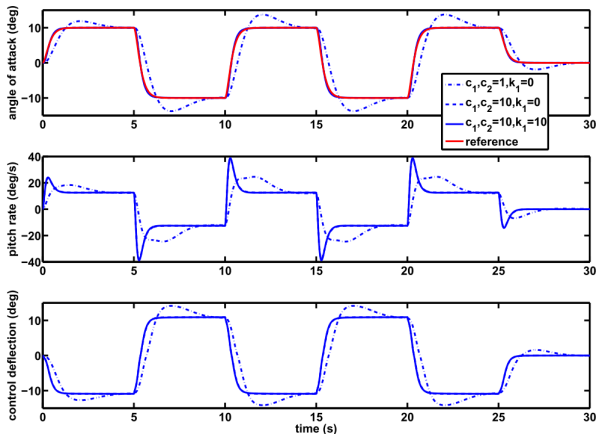

Figure 3.5: The tracking response, pitch rate response and control deflection with an backstepping implementation designed with three sets of gain values for an idealized 2nd order nonlinear system example. Taken from [15]

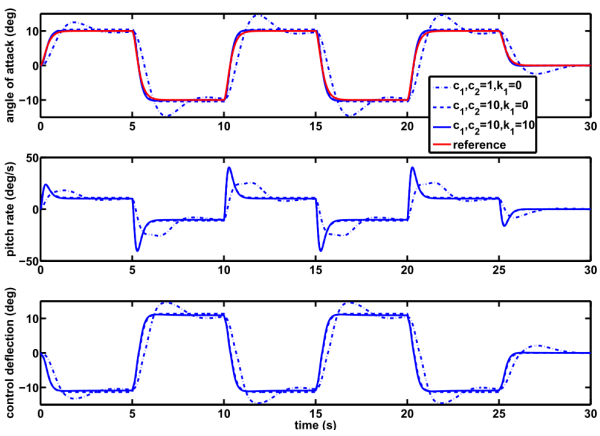

Figure 3.6: The tracking response, pitch rate response and control deflection with an backstepping implementation designed with three sets of gain values for the full 2nd order nonlinear system example. Taken from [15]

Backstepping in the presence of uncertain nonlinearities or unknown parameters has been analysed by [75], where *nonlinear damping* was used to counteract the uncertainty. The application of this nonlinear damping term can be illustrated through a scalar system with uncertainty as shown in Figure 3.7.

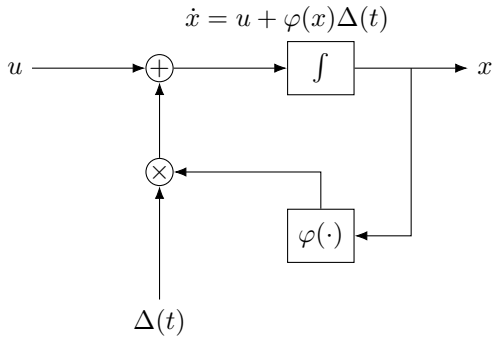

Figure 3.7: A system with "matched" uncertainty. Taken from [71]

Where $\varphi(x)$ is a known smooth nonlinearity described as x^2 with $\Delta(t)$ as an uncertainty that represents an exponentially decaying function in time described as $\Delta(0)e^{kt}$. It can be observed that for a chosen combination of initial conditions of $x(0)$ and $\Delta(0)$ will escape in finite time and to overcome this, a nonlinear damping term ($s(x)$) is added to the backstepping control law as shown by Equation (3.12).

$$u = -cx - s(x)x \tag{3.12}$$

The design of $s(x)$ is done accordingly to the CFL $V(x) = \frac{1}{2}x^2$, yielding to the control law shown in Equation (3.13), which can guarantee global uniform boundness of x and convergence, regardless of how small gains κ and c are chosen [71, 75].

$$\begin{aligned} s(x) &= \kappa\varphi^2(x), \quad \kappa > 0 \\ u &= -cx - \kappa\varphi^2(x) \end{aligned} \tag{3.13}$$

With this nonlinear damping term, a robust recursive backstepping procedure is designed and applied to the 2nd order nonlinear system, which was previously investigated, but now with uncertainty [75] as

expressed in Equation (3.14).

$$\begin{aligned} \dot{x}_1 &= x_2 + f_1(x_1) + w^T(x_1)\Delta_1(u) \\ \dot{x}_2 &= f_2(x_1) + g_2(x_1)u \end{aligned} \tag{3.14}$$

Where $w(x_1) = g_1$ and $\Delta_1(u) = u$. The numerical simulation results as shown in Figure 3.8 show that the designed robust control law is able to track the reference signal with less error compared to the standard backstepping implementation.

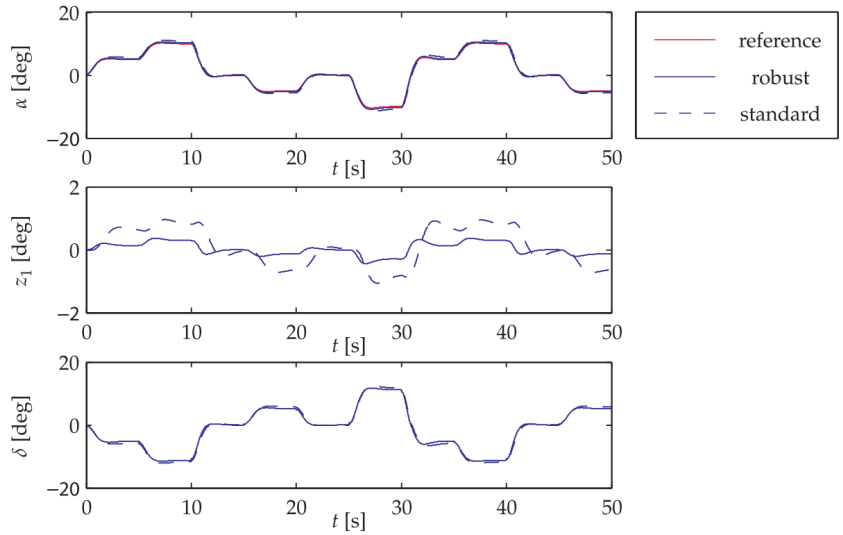

Figure 3.8: Tracking response, error and commanded control input with a comparison of the standard and robust backstepping design. Taken from [75]

The application of Command-Filtered Backstepping (CFBS) for the 2nd order nonlinear systems is applied by van Oort [75]. With this approach, second order filters are used instead of the analytical derivative to produce the reference (control) commands and the final control output is constrained to show the effect of constraining the input on the filters and closed-loop response. The numerical simulation output is shown in Figure 3.9 with no integrator term ($k_1 = 0$), where it can be observed that the designed control law is able to track the reference signal.

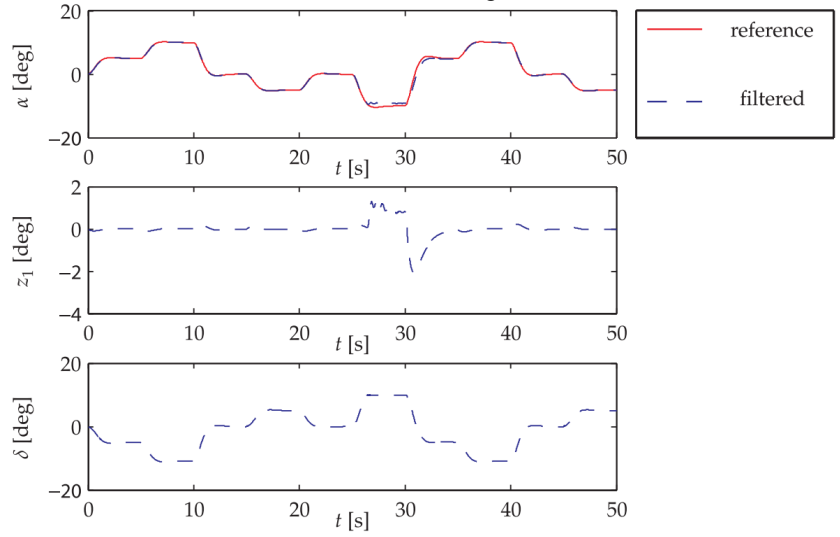

Figure 3.9: Tracking response, error and commanded control input with a comparison of the command-filtered backstepping design. Taken from [75]

However, the control design was applied to a system with known dynamics and relatively small uncertainties were considered. Thus, if these uncertainties become larger, the closed-loop performance will degrade and possibly result in an unstable closed-loop system. Moreover, robust control design tend to yield to a conservative control law, especially when uncertainties are large and the application of

nonlinear damping terms or switching control functions may result in undesirable high gain control or chattering in control signal [15, 75].

The application of CFBS applied as a robust path following control of a fixed-wing UAV [77] with the goal to track a reference path under wind disturbance. Its performance has been validated via hardware-in-the-loop simulations and flight tests. The CFBS is applied to generate a robust scheme for a roll command to steer the fixed-wing UAV. The hardware-in-the-loop simulations compare CFBS and traditional BS, where it is shown that the CFBS scheme can cope with wind disturbance and follow the circular reference path. It is also shown that the roll command designed with CFBS is less noisy compared to BS, where numerical differentiation is used to compute the derivative of the desired course angle. The flight tests showed CFBS enables the aircraft to achieve the necessary tracking performance for roll guidance.

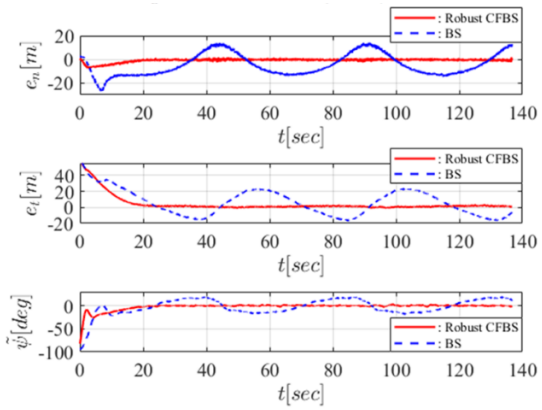

Figure 3.10: Error of the path tracking states: cross-track, along-track and course angle error. Taken from [77]

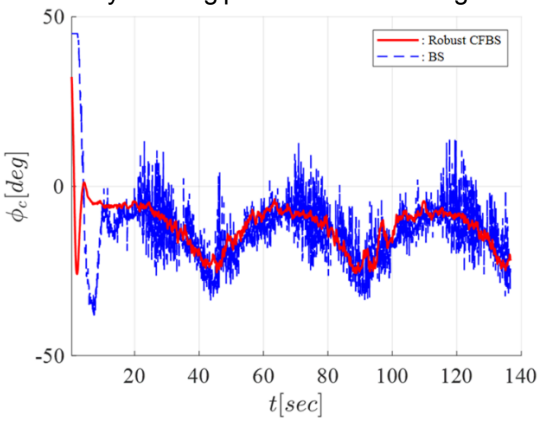

Figure 3.11: Roll angle command comparison between Robust CFB and BS. Taken from [77]

Advantages/Disadvantages
The following advantages of Backstepping can include:

Advantages

- Lyapunov-based nonlinear control method, which guarantee global asymptotic stability/tracking
- Control designer has freedom in selecting what dynamics to use in the control law design to achieve desired properties

The following disadvantages of Backstepping can include:

Disadvantages

- The formulation of recursive backstepping is defined for a system in strict-feedback form
- Requires accurate knowledge of nonlinear system dynamics (model-based information) for control law design and parametric uncertainties can result in an unstable closed loop system
- BS requires analytical derivations, which can be solved by applying command filters
- Increased complexity when applied to high order systems with the recursive procedure, which resolves into designing multiple loops and tuning of gains

3.1.2. Incremental Backstepping

The developments of Incremental Backstepping (IBS) has found its foundation through the application and research developments of Incremental Nonlinear Dynamic Inversion [18, 20, 21, 78, 79]. IBS proposes a reformulation of the recursive backstepping design that relies on feedback of sensor measurements that provides estimates of the nonlinear system states and control/actuator state, and uses this to send new control commands in increments. This is also described as incremental control.

The formulation of IBS is elaborated in [20, 21] for spacecraft control and [73, 76] for the flight control. The design procedure follows similar steps as recursive backstepping and for the description of the design procedure of incremental backstepping, certain steps will not be expressed in great detail.

Considering the following cascaded second order nonlinear systems as illustrated in Figure 3.12 and expressed by Equation (3.15).

$$\begin{aligned}\dot{\xi} &= \mathbf{h}(\xi) + \mathbf{k}(\xi)\mathbf{x} \\ \dot{\mathbf{x}} &= \mathbf{f}(\xi, \mathbf{x}) + \mathbf{G}(\xi, \mathbf{x})\mathbf{u}\end{aligned} \tag{3.15}$$

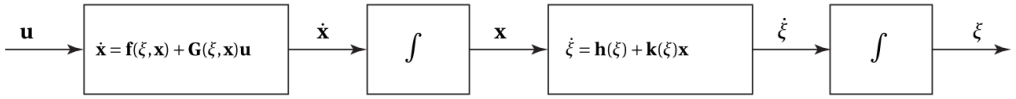

Figure 3.12: Cascaded structure of second order nonlinear system Equation (3.15). Taken from [20]

The first state equation can represent a system's kinematics and the second system the dynamic. The control input u represents a control surface and $\mathbf{G}(\xi, \mathbf{x})$ represents a control input matrix.
Similar to the recursive backstepping procedure, the subsystem that's the furthest away from the input is considered first. The tracking error is defined for the cascaded system:

$$\mathbf{z} = \mathbf{x} - \mathbf{x}_{des} = \mathbf{x} - \alpha(\xi) \tag{3.16}$$

with $\alpha(\xi)$ as the virtual control law that will be designed. The second step is to construct a CLF for the first subsystem, which can be chosen as:

$$V_1(\xi) = \frac{1}{2}\xi^T\xi \tag{3.17}$$

Thereafter, the virtual control law, the stabilising function, ($\alpha(\xi)$) can be designed such that the derivative of the CLF (V_1) is negative definite.
With the control law of the first subsystem defined, the final control law ($\mathbf{u}$) can be defined. The 2nd subsystem is written in terms of the error state:

$$\dot{\mathbf{z}} = \dot{\mathbf{x}} - \dot{\alpha}(\xi, \mathbf{x}) = \mathbf{f}(\xi, \mathbf{x}) + \mathbf{G}(\xi, \mathbf{x})\mathbf{u} - \dot{\alpha}(\xi, \mathbf{x}) \tag{3.18}$$

The CLF for the 2nd subsystem can be defined as:

$$V_2(\xi, \mathbf{x}) = V_1 + \frac{1}{2}\mathbf{z}^T\mathbf{z} \tag{3.19}$$

The selection of the final control law u needs to make the derivative of V_2 negative definite, however compared to recursive backstepping, the control law for $\mathbf{u}$ will be determined in incremental form, which is obtained through the following steps:

Step 1: First-order Taylor series expansion
Consider the 2nd subsystem:

$$\dot{\mathbf{x}} = \mathbf{f}(\xi, \mathbf{x}) + \mathbf{G}(\xi, \mathbf{x})\mathbf{u}$$

Taking the first-order Taylor series expansion around the current state $\mathbf{y}_0 = [\xi_0, \mathbf{x}_0]$ and input $[\mathbf{u}_0]$ results in the following expression:

$$\dot{\mathbf{x}} \approx \mathbf{f}(\mathbf{y}_0) + \mathbf{G}(\mathbf{y}_0)\mathbf{u_0} + \frac{\partial}{\partial \mathbf{y}}\left[\mathbf{f}(\mathbf{y}) + \mathbf{G}(\mathbf{y})\mathbf{u}\right]\Big|_{x=x_0, u=u_0}(\mathbf{y} - \mathbf{y_0}) + \frac{\partial}{\partial \mathbf{u}}\left[\mathbf{G}(\mathbf{y})\mathbf{u}\right]\Big|_{x=x_0, u=u_0}(\mathbf{u} - \mathbf{u}_0) + \mathrm{H.O.T} \tag{3.20}$$

Here $\mathrm{H.O.T}$ are higher order terms that are neglected for the first-order approximation of $\dot{\mathbf{x}}$.

Step 2: Time-Scale Separation
When the sampling rate of the sensors measuring the state derivative is sufficiently high, the linearization error is small and can be written as:

$$\dot{\mathbf{x}} \approx \dot{\mathbf{x}}_0 + A_0\Delta\mathbf{y} + B_0\Delta\mathbf{u} \tag{3.21}$$

where

$$\begin{aligned} \Delta\mathbf{y} &= \mathbf{y} - \mathbf{y_0}, \qquad \Delta\mathbf{u} = \mathbf{u} - \mathbf{u_0} \\ A_0 &= \frac{\partial}{\partial \mathbf{y}} \left[\mathbf{f}(\mathbf{y}) + \mathbf{G}(\mathbf{y})\mathbf{u}\right]\Big|_{x=x_0, u=u_0} \\ B_0 &= \frac{\partial}{\partial \mathbf{u}} \left[\mathbf{G}(\mathbf{y})\mathbf{u}\right]\Big|_{x=x_0, u=u_0} = \mathbf{G}(\mathbf{y}_0) \end{aligned} \tag{3.22}$$

The variables $\Delta\mathbf{y}$ and $\Delta\mathbf{u}$ are expressed as the incremental state vector and incremental control input respectively.
Assuming a sufficiently time-scale separated system, where the increment in state $\Delta\mathbf{y}$ is much smaller than the increment in both state derivative $\Delta\dot{\mathbf{y}}$ and input $\Delta\mathbf{u}$, the former term can be neglected [20, 21]. This results in a simplified linearised expression for the 2nd subsystem:

$$\dot{\mathbf{x}} \approx \dot{\mathbf{x}}_0 + B_0 \Delta\mathbf{u} \tag{3.23}$$

Step 3: Incremental Backstepping Control Law Design
With the subsystem written in incremental form, the backstepping procedure is continued, where the tracking error is now expressed as:

$$\dot{\mathbf{z}} = \dot{\mathbf{x}} - \dot{\alpha}(\xi, \mathbf{x}) \approx \dot{\mathbf{x}}_0 + B_0\Delta\mathbf{u} - \dot{\alpha}(\xi, \mathbf{x}) \tag{3.24}$$

The control law is now expressed in incremental form $\boldsymbol{\Delta}\mathbf{u}$ and needs to be designed to yield CLF V_2 negative definite. One choice for incremental control vector is:

$$\Delta\mathbf{u} = B_0^{-1}[-c_2\mathbf{z} - \dot{\mathbf{x}}_0 + \dot{\alpha} - \frac{\partial V_1}{\partial \xi}\mathbf{k}(\xi)] \tag{3.25}$$

To obtain the total control input $\mathbf{u}$, the current control input $\mathbf{u}_0$ needs to be added to the incremental control input $\Delta\mathbf{u}$ as following:

$$\mathbf{u} = \mathbf{u_0} + \Delta\mathbf{u} \tag{3.26}$$

A schematic overview of the incremental backstepping approach is illustrated in Figure 3.13.

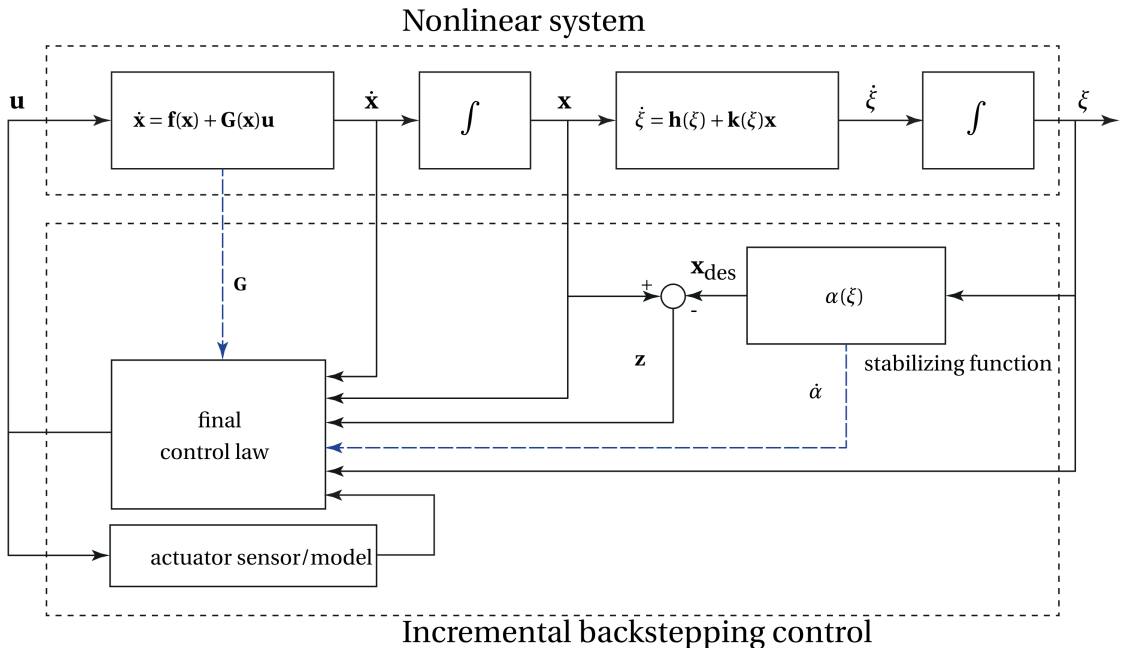

Figure 3.13: Incremental Backstepping control diagram. Blue lines represent information required for control design. Taken from [21]

For the application of incremental backstepping the following assumptions are implicitly made [20, 21]:

1. Complete and accurate knowledge of states is available
2. Sensors to measure the acceleration $\dot{\mathbf{x}}$ with sufficiently high sampling rate need to exist and be available
3. Sensor to measure the current control input (actuator) need to be available or estimated on the basis of a high-fidelity model of the actuator dynamics
4. Time-scale seperation where it is assumed that the state derivatives evolve faster than the state upon fast control action, which directly influences the dynamics of the rigid body
5. Fast control action is assumed, where the dynamics of the actuator (and control surface) evolve much faster than the states

State-of-the-art Applications

Incremental Backstepping has various applications in spacecraft control [20, 21] for attitude and rate control. IBS in flight control has been applied for a numerical simulation F-16 model and augmented with command filters comparing it with conventional recursive BS [73], where the robustness against aerodynamic uncertainties was assessed. Application on a fixed-wing unmanned aerial vehicle (UAV) with command filtering showed robustness against model uncertainties and disturbances [76].

A study that applies IBS with the same second order nonlinear system used for the recursive backstepping approach is discussed in [21]. Under nominal situations, the performance of the IBS had relatively the same tracking performance and closed-loop response as BS. When aerodynamic uncertainties were applied to the system's dynamics, the conventional backstepping was not able to cope with large uncertainties and the nominal performance is lost and/or degraded as shown in Figure 3.14. However, IBS is able to maintain tracking performance without significant loss or degradation, as shown in Figure 3.15 [21].

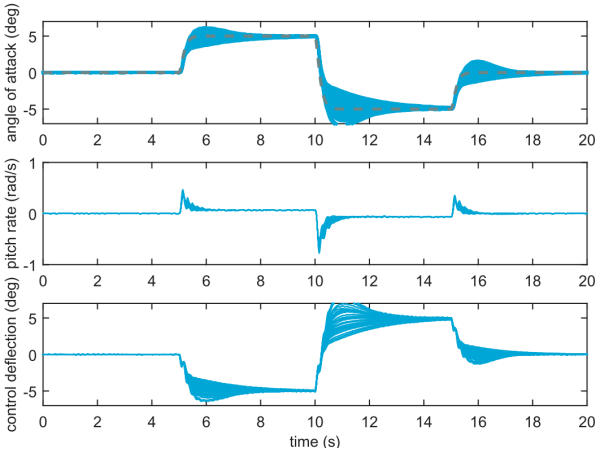

Figure 3.14: Backstepping control law tracking performance for a nonlinear system with aerodynamic uncertainties. Taken from [21]

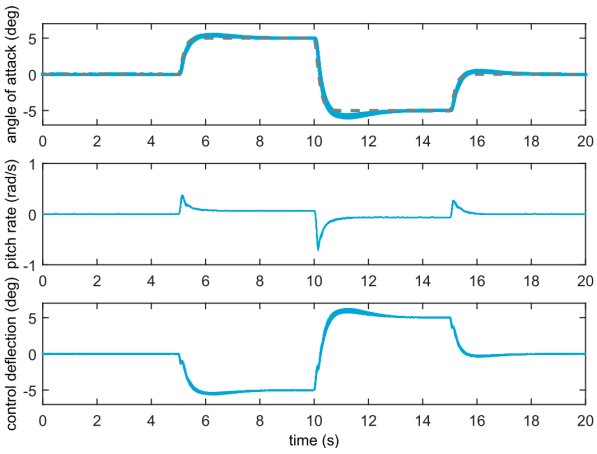

Figure 3.15: Incremental Backstepping control law tracking performance for a nonlinear system with aerodynamic uncertainties. Taken from [21]

The robustness and tuning of IBS with respect to uncertainties in its control effectiveness in terms with and without actuator dynamics has been analysed by [80]. The study also asserts the assumption regarding fast actuator dynamics. This analysis was done using two different simulation models, one of which is the same nonlinear second order system used in the previous study described previously, the other is an F-16 simulation model. The study started with the incorporation of the uncertainty γ, without actuator dynamics, described for a strict-feedback cascaded system. IBS has robustness against uncertainties in the plant dynamics, but it has not been assessed on whether uncertainties in $g_{2,0}$, the control effectiveness term in the IBS control law, will influence the performance of the IBS. To investigate this, an uncertainty parameter γ is defined as:

$$\gamma = \frac{g_{2,0}}{g_u} = \frac{g_{2,0}}{g_{2,0} + \Delta g} \tag{3.27}$$

Incorporating the uncertainty into the control law results in the expression described by Equation (3.28). When $\gamma = 1$, there are no uncertainties in the system, when $\gamma \neq 1$ there are uncertainties in the system. The study only considers $\gamma > 0$.

$$\dot{x}_2 = \gamma(-g_1^T z_1 - c_2 z_2 + \dot{\alpha}) + (1-\gamma)\dot{x}_{2,0} \tag{3.28}$$

The inclusion of actuator dynamics is represented by the following equation:

$$\dot{u} = -\tau u + \tau u_e \tag{3.29}$$

where $u_e = u_0 + \Delta u$ and $1/\tau$ is the time constant of the actuator. The incremental input from the IBS control law passes through the actuator before it enters the system, and the complete closed-loop cascaded system is described by the block diagram Figure 3.16.

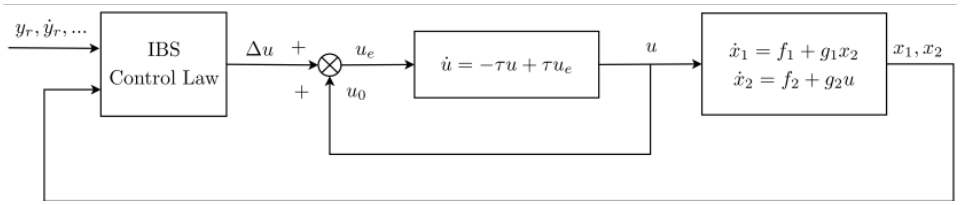

Figure 3.16: Block diagram of closed-loop system including actuator dynamics. Taken from [80]

An unstable uncertainty condition was chosen and analysed using two tuning methods, γ rule, where a compensation factor is used to stabilise the system, and actuator compensation, where the actuator dynamics can be approximated as a first-order low pass filter and a compensator based on desired actuator dynamics is designed with a desired time constant ($1/\tau_d$).
The tracking performance of the system with actuator dynamics is shown in Figure 3.17, where it can be established that IBS has an oscillatory response in the presence of unstable uncertainty, but with the tuning methods the system's performance can be recovered. This analysis has been repeated for the F-16 simulation model, where IBS also suffered from performance degradation and both tuning methods recover the tracking performance.
The study showed how IBS performs in the presence of control effectiveness uncertainties and developed two tuning methods, which could be applied to recover the system's performance. Moreover, it was concluded that the tuning methods could be extended to Fault Tolerant Control (FTC), because it can potentially cope with larger model uncertainties caused by faults [80].

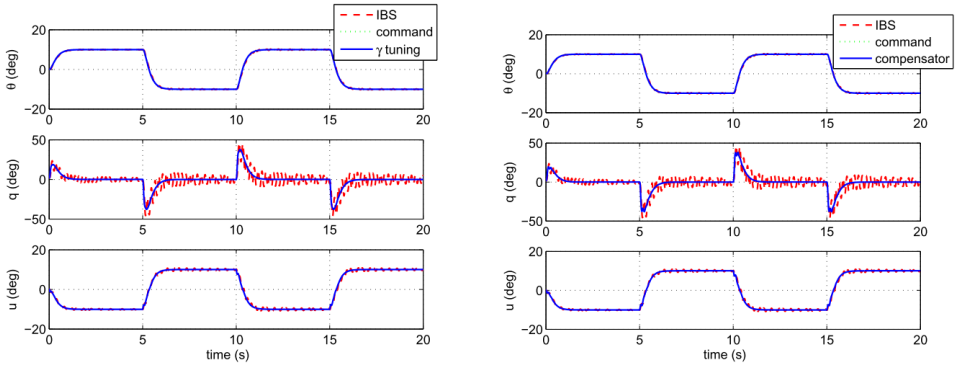

Figure 3.17: System tracking performance in the presence of unstable uncertainty (Left) with γ tuning. (Right) with actuator compensation. Taken from [80]

The design of an FTC system has been proposed by [81], where an Active Fault-Tolerant Control System (AFTCS) was developed consisting of a sensor Fault Detection and Diagnosis (FDD) system and a controller designed with IBS. The developed system is able to cope with Intertial Measurement Unit (IMU) sensor and Air Data Sensors (ADS) faults, actuator faults and process faults. The FDD system uses two variants of Extended Kalman Filters (EKF) to detect and diagnose IMU and ADS faults, but also estimate filtered state for the controllers. The FTC system is designed with an IBS control law to cope with actuator and process faults and receives the information from the FDD system. In addition, second-order command filters are implemented with position limits for the control surface

actuators. The complete overview of the AFTCS applied to a Cessna Citation II aircraft simulation model is shown in Figure 3.18.

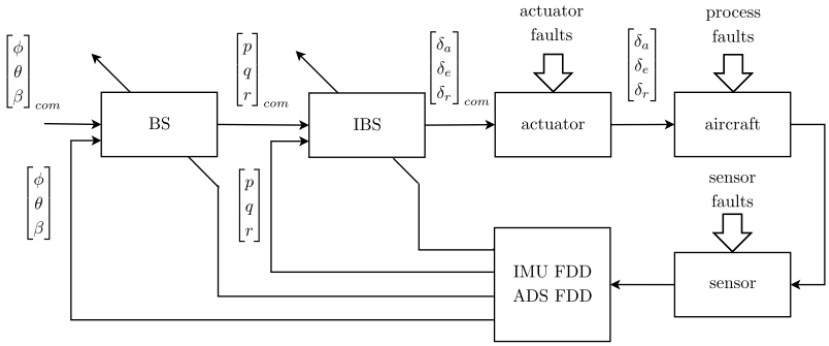

Figure 3.18: AFTCS block diagram. Taken from [81]

The simulation of the system was first performed without IMU FDD system with only IMU faults, thereafter it was examined with FDD and various fault scenarios. The first analysis showed the performance of IBS degraded in the presence of IMU sensor, where the sideslip showed oscillations and non-zero even when there are no manoeuvres. If the fault magnitude increased, a larger influence would display, and this showed that the IBS would maintain satisfactory performance only when an IMU FDD is implemented. The second analysis first showed that the AFTCS is able to work well when there are no faults, indicating that there are no false alarms. After that, the AFTCS was tested in the presence of sensor faults for the IMU and ADS first and the actuator fails consecutively where after $t > 70s$ all the actuators fail. The results of the simulation are shown in Figure 3.19, where it can be observed that the system has consecutive faults, but still can estimate the aircraft state and cope with the actuator faults to provide satisfactory performance. One aspect that has not been taken into account is the time delays due to the FDD system, which may affect the performance of the controller.

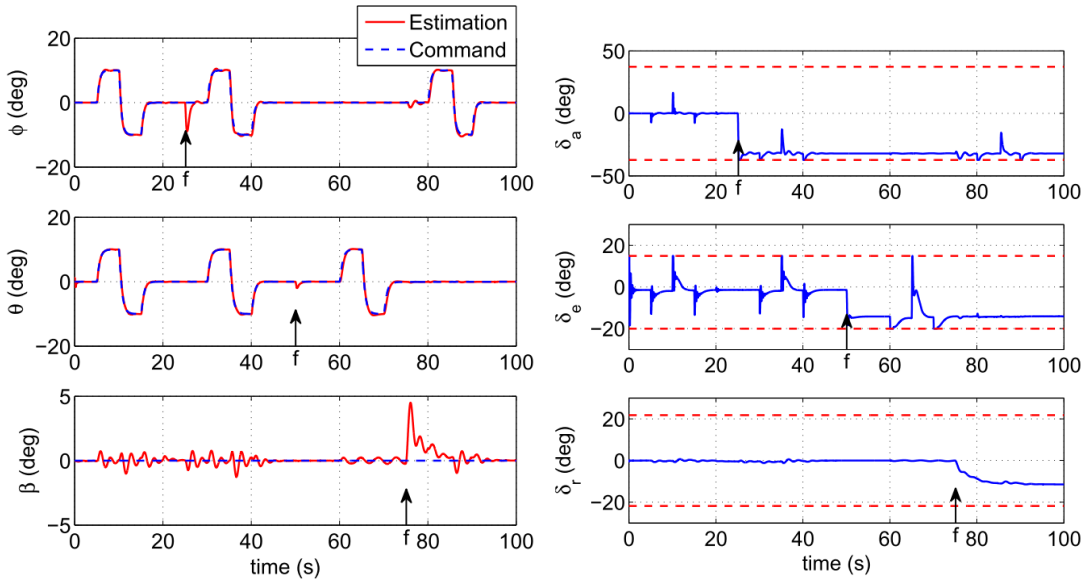

(a) Command for aircraft attitude and their estimated state under faults

(b) Control surface deflections and their limits in the presence of faults

Figure 3.19: Simulation results of the AFTCS in the presence of sensor and actuator faults. Taken from [81]

Command Filtered IBS (CFIBS) has been applied for a fixed-wing UAV in [76]. The IBS control laws were designed for aerodynamic attitude and trajectory control, where first numerical simulations experiments were conducted to analyse the robustness of the designed IBS control law in the presence of control effectiveness uncertainties, where it was found that the IBS was able to maintain its tracking performance. Thereafter, multiple flight tests were conducted and verified IBS application in real

world flight with parameter uncertainties, delayed measurements and turbulence disturbances. It was shown that the designed system with IBS could accurately track a reference signal while requiring little knowledge of the model parameters.

IBS has also been demonstrated by real-world flight tests on a Cessna Citation II aircraft with angular accelerometer (AA) feedback in [82]. Previous studies used estimations of angular accelerations for the feedback into the IBS control law, however using AA sensors it is expected that the performance of the controller improves due to lower sensor delay. Under nominal manoeuvres, the IBS controller provided satisfactory performance without AA feedback and with AA feedback the improvement was negligible. Through simulation studies, it was determined that AA does substantially increase the robustness in the presence of model mismatch and improved the fault tolerance.

IBS was reformulated and combined with Sliding Mode Control (SMC) in [18]. SMC is a nonlinear control method where the system's dynamics is brought and controlled along a sliding surface which constrains and stabilises the system while also providing robustness against uncertainties. The research resulted in the development of an Incremental Backstepping Sliding Mode Control (IBSMC) framework, where numerical simulations verified that it has better robustness than backstepping in the presence of model uncertainties, sudden actuator faults and structural damages.

Advantages/Disadvantages

The following advantages of Incremental Backstepping are described as:

Advantages

- Asymptotic Stability properties of BS
- Less model knowledge required compared to BS
- Better robustness in the presence of uncertainties compared to BS
- Numerical simulations verify that it is able to maintain performance in fault scenarios
- Real world applications with IBS have proven satisfactory results

The following disadvantages of Incremental Backstepping are described as:

Disadvantages

- Time delays can degrade performance and sensors need to provide accurate measurements
- Large uncertainties or model mismatches in the control effectiveness can introduce degraded performance
- Design and tuning for higher order system still involves the complexity of multiple loops

3.1.3. Adaptive Schemes for (Incremental) Backstepping Control

This section concerns the discussions of adaptive schemes used for BS and IBS. As established in the previous sections, BS and IBS can degrade in performance in the presence of uncertainties. Thus, adaptive schemes with BS and IBS, allow for a more sophisticated way to deal with these large uncertainties, whereby the model parameters of the system are estimated and adapted during flight. Moreover, it allows for control design that is able to reconfigure and adapt when faults appear with the aircraft and reduce the efforts required by the pilot to maintain safe operation [15, 73, 75]. Due to the extensive range of theory, the results, and findings of the applied techniques are primarily elaborated.

Adaptive Backstepping

Adaptive backstepping (ABS) has been extensively research and applied in [15], where Constrained Adaptive Backstepping (CABS), Inverse Optimal Adaptive Backstepping and Immersion and Invariance (I&I) Adaptive Backstepping were examined and three Adaptive flight control frameworks were designed:

1. Integrated ABS
2. Modular ABS with Least Squares (LS)
3. ABS with Immersion and Invariance (I & I)

These frameworks were applied on an F-16 simulation model with fault scenarios such as sudden actuator faults and large aerodynamic uncertainties.
It was shown that the standard adaptive approach with tuning functions, which involved dynamic parameter laws driven by tracking errors. The control law design with ABS involved tuning functions where the system's dynamics were parameterised with regressor functions involving the real system parameters and the CLF was augmented with the parameter estimation error and updated accordingly through a designed adaptation gain. The virtual control laws were also selected to satisfy CLF and therefore a Lyapunov-based adaptation law is developed. However, the design of the tuning based functions involved tedious calculation of analytical functions, determining update gains and is sensitive to input saturation. Large tracking errors could cause unlearning of the approximated parameters in the design of the control laws, and thus convergence to the true parameters is not guaranteed.
CABS involves the use of command filters and enforces input or state constraints, to overcome these shortcomings. Inverse Optimal ABS involves the use of a cost functional that simplifies tuning and design of CABS, but due to the complexity of this approach it wasn't deemed suitable for further application.
CABS is implemented for an integrated ABS framework, as shown in Figure 3.20 and has been compared to a traditional modular ABS with Least Squares (LS) parameter estimation, shown in Figure 3.21. The difference is that modular ABS uses the states instead of the tracking error for the parameter update and decouples the identifier from the controller.

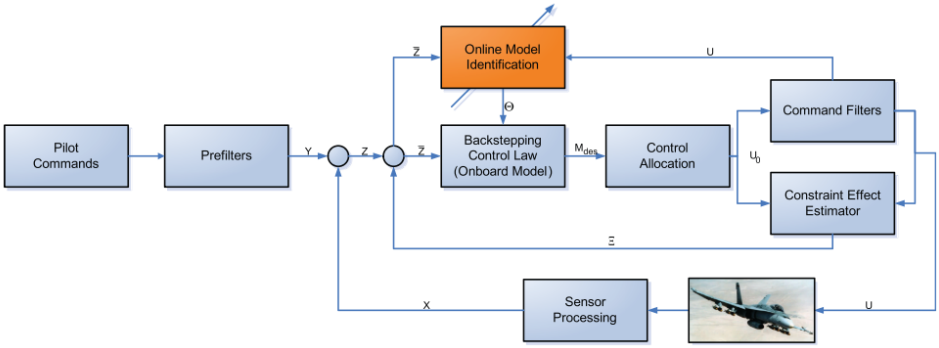

Figure 3.20: Integrated Adaptive Backstepping control framework. Taken from [15]

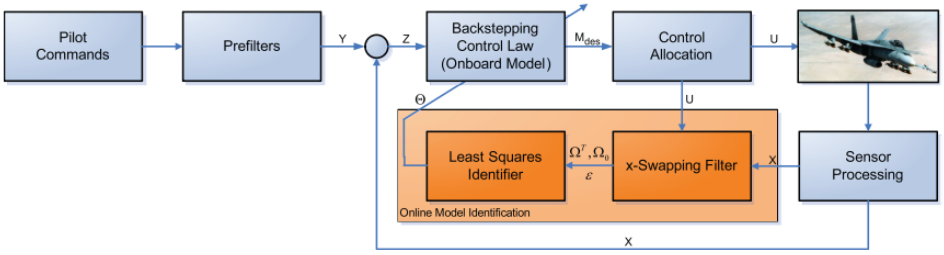

Figure 3.21: Modular Adaptive Backstepping control framework. Taken from [15]

The research study applied the ABS frameworks and evaluated with an F-16 simulation model. The aerodynamic model is partitioned and identified with a B-spline network to allow for linear in the parameter localised partitions with smooth transitions, and new parameter estimates are continuously adapted with the B-spline network. A Stability and Control Augmentation (SCAS) system has been designed, which satisfies the handling qualities requirements across the entire flight envelope of the model. Numerical simulation is performed where several types of sudden changes in dynamic behaviour are observed. The results of this simulation showed that the modular adaptive design provided the best estimates of aerodynamic coefficients, tuning required less effort, but nonlinear damping gains need to be tuned with care to avoid high gain feedback signals. The modular ABS also had a higher computational load due to the requirement of higher dynamical order (more states) compared to integrated ABS identifier, which uses the tracking errors. The study also develops a nonlinear estimator, which combines the CABS to form a modular adaptive control scheme, as illustrated in Figure 3.22. This is referred to as the immersion and Invariance control framework.

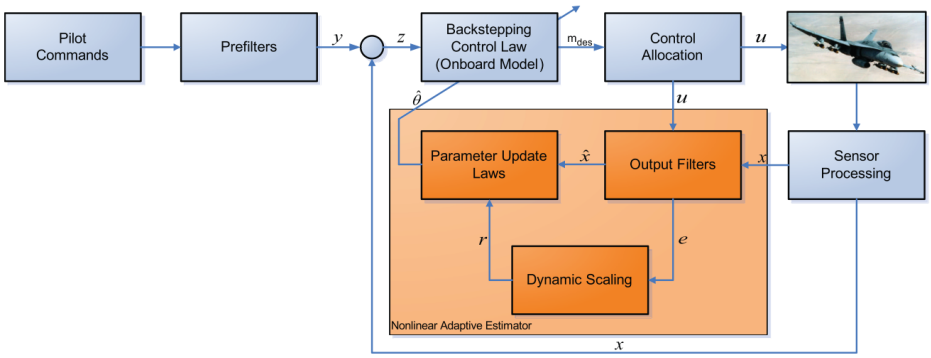

Figure 3.22: Immersion & Invariance Adaptive Backstepping control framework. Taken from [15]

The numerical simulations using this framework demonstrate a higher level of tracking performance with stronger provable stability and convergence properties, while also achieving modularity in its design. However, the estimator employs overparametrization, which results in higher computational load, while also increasing design complexity.
Adaptive ABS as presented in [75], applied the integrated and modular ABS frameworks to achieve desired performance characteristics over the whole flight envelope and maintain that in the presence of faults and failures. The developed control was verified with numerical simulations and in the presence of faults and failures the system provided stability, enhanced performance and survivability of the aircraft in post-failure conditions.

The importance of reference signals for these adaptive methods should also be highlighted, where it should be persistently exciting to guarantee that the parameter estimators converge to the true values.

Adaptive Incremental Backstepping

ABS update the parameters of the system dynamics used in the design of the BS control law. Adaptive schemes with IBS require less model information in its design, where only the control effectiveness is modelled and adapted with parameter estimation. The first notable development and application of adaptive IBS has been developed in [73], where IBS with Command-Filtering was designed and evaluated with three parameter estimators methods: Tuning Functions (TF), Recursive Least-Squares (RLS) and Immersion & Invariance (I&I) for a numerical simulation model of an F-16 aircraft. Compared to modular ABS with RLS, there are no nonlinear damping terms included.
With the reduction of model-based information, the design of the control laws and parameter update laws were significantly simplified compared to ABS. The robustness of the designed adaptive controllers were evaluated and compared to non-adaptive BS and IBS through introducing uncertainties in the aerodynamic damping coefficients and introducing a time-varying magnitude uncertainty in the control effectiveness parameter used in the IBS control law.
It was shown that IBS has better robustness against uncertainties compared to BS, but with the time varying control effectiveness parameter, it has not been able to provide satisfactory tracking performance. The three designed adaptive controllers were all able to provide satisfactory performance as shown in Figure 3.23. The accuracy of the parameter estimation using a constant function approximate, where the control effectiveness is a constant value over time, is shown in 3.24.

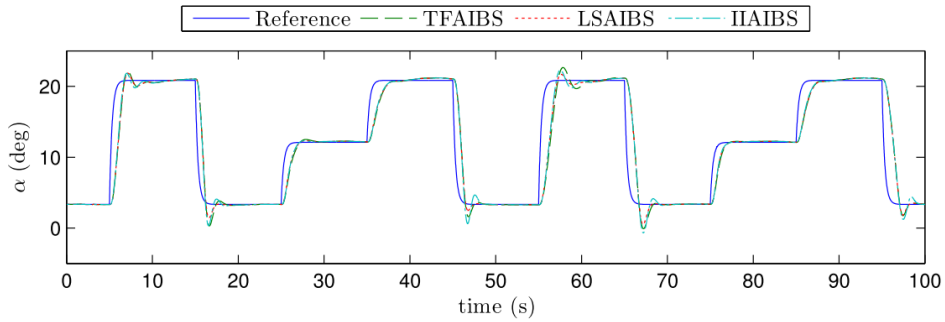

Figure 3.23: Tracking performance of adaptive IBS with three different parameter estimation methods. Taken from [73]

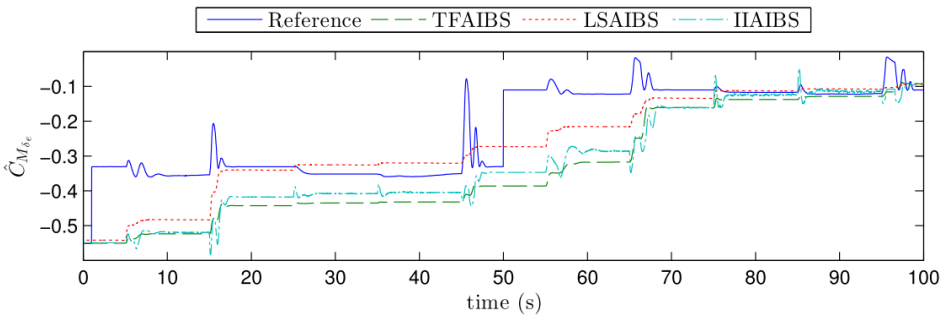

Figure 3.24: Parameter estimation results. Taken from [73]

The RLS estimator had very low design complexity and from visual inspection the accuracy of the parameter estimation seem closer, but the closed-loop stability in case of uncertainties could not be proven and converging to the true values is essential. The design of the I&I estimator was the highest, but compared to the Tuning-Functions, its analytical expressions can be easily derived and the dynamics of the estimator error simplified the tuning process of the controller compared to TF and RLS. Moreover, it was determined in all simulations the reference signal could be improved for obtaining richer information that would converge to the true parameter.

IBS has been combined with a Gaussian Process (GP) online identification framework in [83]. GP considers the parameter estimation as a statistical problem, where the uncertainty of a system is distributed over functions that follow a Gaussian distribution. The framework updates the control effectiveness estimates, but also incorporating the functional relationship between the inner and outer control loop. Thus resulting in an indirect adaptation for the control effectiveness in the IBS control law. The framework has been simulated with a nonlinear model of the Boeing 747 in failure scenarios and loss of effectiveness, but also when unmodeled first or second order actuator dynamics appear due to failure. The numerical simulation was compared to IBS and adaptive IBS with TF and RLS. In the failure scenario, it was determined that GP parameter estimation was similar to RLS and online GP showed satisfactory tracking performance. In the latter two scenarios RLS worked well, but GP's superior adaptation resulted in the best tracking response as it "switched off" the harmful interaction of the failed and non-failed elevator. Thus showcasing its capabilities as an adaptation algorithm for IBS.

3.2. Dynamic Inversion Approaches

This section discusses the nonlinear and adaptive control approaches, based upon the principle of dynamic inversion. First the conventional nonlinear dynamic inversion approach is discussed (3.2.1) with thereafter an explanation of the incremental dynamic inversion approach (3.2.2). At last, the adaptive schemes used for NDI and INDI are elaborated (3.2.3).

3.2.1. Nonlinear Dynamic Inversion

Nonlinear Dynamic Inversion (NDI) is a nonlinear control method that aims to linearize a nonlinear system through the cancellation of nonlinear system dynamics via state feedback, also referred to as Feedback Linearization [14]. For the application of NDI, the following conditions need to be fulfilled:

- Number of inputs and outputs are the same
- The system is affine in input
- Full knowledge of the system model and states

The derivations of the NDI are elaborated in detail in [14, 18]. A multi-input and output (MIMO) system with a $n \times m$ control input matrix $G(x)$ and is defined as follows:

$$\dot{\mathbf{x}} = \mathbf{f}(\mathbf{x}) + \mathbf{G}(\mathbf{x})\mathbf{u} \tag{3.30}$$

$$\mathbf{y} = \mathbf{h}(\mathbf{x}) \tag{3.31}$$

The control input is defined as following:

$$\mathbf{u} = A^{-1}(\mathbf{x})[\mathbf{v}(\mathbf{x}) - \mathbf{b}(\mathbf{x})] \tag{3.32}$$

Whereby, $A(x)$ and $\mathbf{b(x)}$, as shown in Equation (3.34), are constructed by determining the input-output relationship using Lie-derivatives, which is defined as following:

Definition 3.7 **Lie derivative**

Let $h : \mathbb{R}^n \to \mathbb{R}$ be a smooth scalar function and $\mathbf{f} : \mathbb{R}^n \to \mathbb{R}^n$ be a smooth vector field on $\mathbb{R}^\times$, then the Lie derivative of h with respect to f is a scalar function defined by $L_f h = (\nabla h)\mathbf{f}$.

The application of Lie derivative can be defined recursively as following:

$$\begin{aligned} L^0_{\mathbf{f}} h &= h \\ L^i_{\mathbf{f}} h &= L^i_{\mathbf{f}}(L^{i-1}_{\mathbf{f}} h) = \nabla(L^{i-1}_{\mathbf{f}} h)\mathbf{f}, \qquad \text{for } i = 1, 2, 3, ... \end{aligned} \tag{3.33}$$

The virtual tracking input ($\mathbf{v(x)}$), represents the desired state derivative and can be generated by a linear control law and the tracking error dynamics. This linear control law can be designed and tuned to desired handling qualities.

$$A(x) = \begin{bmatrix} L_{g_1} L_f^{r_1-1} h_1(x) & L_{g_2} L_f^{r_1-1} h_1(x) & . & L_{g_m} L_f^{r_1-1} h_1(x) \\ L_{g_1} L_f^{r_2-1} h_2(x) & L_{g_2} L_f^{r_2-1} h_2(x) & . & L_{g_m} L_f^{r_2-1} h_2(x) \\ . & . & . & . \\ . & . & . & . \\ L_{g_1} L_f^{r_m-1} h_m(x) & L_{g_2} L_f^{r_m-1} h_m(x) & . & L_{g_m} L_f^{r_m-1} h_m(x) \end{bmatrix} \tag{3.34a}$$

$$\mathbf{b(x)} = \begin{bmatrix} L_f^{r_1} h_1 \\ L_f^{r_2} h_2 \\ . \\ . \\ L_f^{r_m} h_m \end{bmatrix} \tag{3.34b}$$

$$\mathbf{v} = -k_1 \mathbf{e} - k_2 \frac{\mathbf{de}}{\mathbf{dt}} - k_2 \frac{\mathbf{d^2 e}}{\mathbf{dt^2}} - k_{n-1} \frac{\mathbf{d^{n-1} e}}{\mathbf{dt^{n-1}}} + \frac{\mathbf{d^n x_d}}{\mathbf{dt^n}} \tag{3.34c}$$

A block diagram of the NDI control law is shown in Figure 3.25

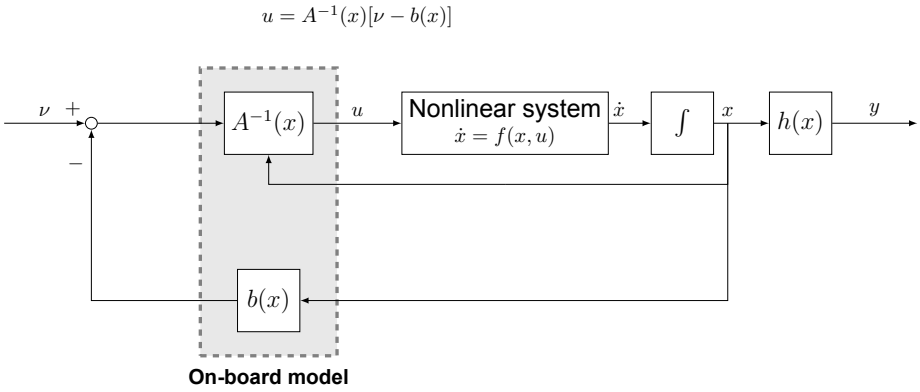

Figure 3.25: Block diagram of Nonlinear Dynamic Version. $A(x), b(x)$ contain nonlinear dynamics of the system [14]

State-of-the-art Applications

NDI control has seen extensive research [84], descried as model-based NDI, and has most notably been implemented in the Lockheed F-35 Lightning II [16, 17]. Advantages of the applications concern the absence of any need in gain scheduling over the flight envelope and decoupling between input-output relations, resulting in an inner loop that linearizes the aircraft dynamics and an outer loop that can be designed to achieve desired flying qualities [18, 85].

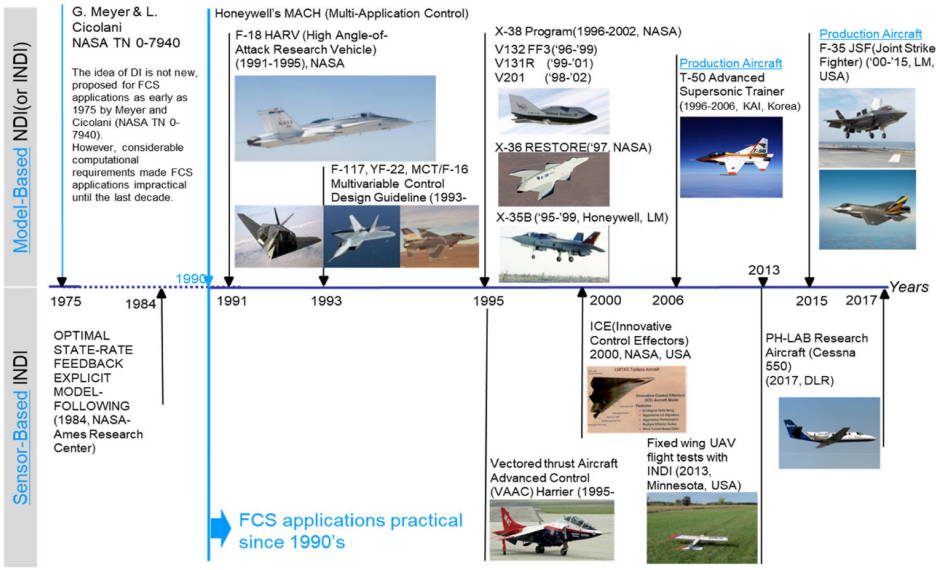

Figure 3.26: NDI timeline and applications. Taken from [84]

The NDI control architecture for the F-35 is designed with augmented control loops where the aircraft dynamics dependent portions $(A(x), \mathbf{b}(\mathbf{x}))$ are incorporated in the On-Board Model (OBM) and the Effector Blender (EB) respectively. The requirement of the additional augmentation control is due to the precise knowledge of the aerodynamics model and perfect sensor and actuators. Moreover, it is difficult to accurately model high-order nonlinear effects due to airframe, mass properties and propulsion characteristics of the aircraft. Therefore, NDI control does not completely cancel out the aircraft dynamics and this results in mismatches leading to adverse closed-loop dynamics effects, which degrade the performance and flying qualities of the aircraft.
For the development of the control architecture, the OBM is developed in a sophisticated manner, where 3 million data points were gathered using wind tunnel test data, that would maximize NDI control performance throughout the whole flight envelope. The EB is an iterative solver, which determines the optimal control surface commands taking control surface rate and position limits into account. Special augmentation and control algorithms were designed, which used the error signal between measured angular acceleration from the sensor and estimated angular acceleration from a mathematical model as feedback variable to compensate for modelling errors and challenges encountered in the effectiveness of an NDI-only control law. The outer linear control loop consist of pilot inputs, which are translated to desired aircraft movements and compared against the aircraft state. This is then inserted into the regulator, which are designed according to desired flying handling qualities. A complete overview of the implemented control architecture is shown in Figure 3.27.

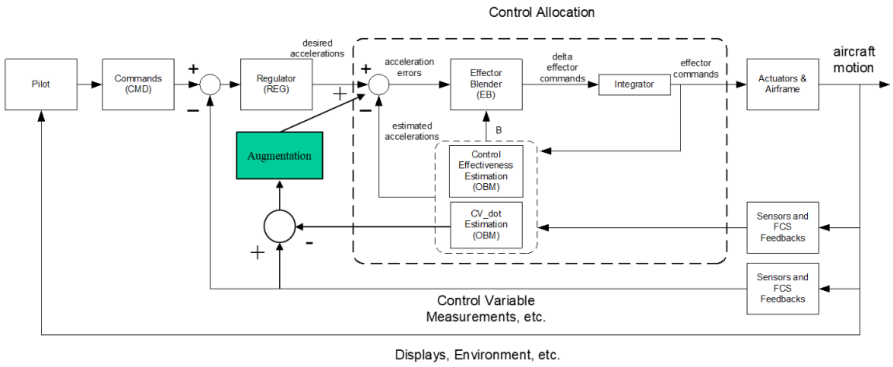

Figure 3.27: NDI control architecture including additional augmentation control for F-35. Taken from [84]

The main drawback of NDI is the required accurate knowledge of the nonlinear system dynamics, which is very difficult to meet in reality due to model simplifications, computational errors, external disturbances, sensor noise, failures. Robust control techniques have been applied in the outer loop control

to overcome this main drawback, but the resulting control laws result in closed-loop systems can be marginally or overly conservative in performance and stability robustness [18, 85]. Thus, recent state-of-the-art applications focus on adaptive (I)NDI or Incremental NDI.

Advantages/Disadvantages
The following advantages of Nonlinear Dynamic Inversion are described as:

Advantages

- Design procedure easily applicable to MIMO systems
- Simple inner and outer loop structure, where the inner loop is responsible for linearization (stabilisation) and outer loop can be designed and tuned with various types of controllers, such as linear control methods
- Extensive research history with real-world implementation

The following disadvantages of Incremental Backstepping are described as:

Disadvantages

- Closed-loop stability is not ensured
- Requires accurate model knowledge throughout the flight envelope
- Inversion is not always achieved or possible
- Uncertainties can significantly degrade flying qualities and performance

3.2.2. Incremental Nonlinear Dynamic Inversion

One disadvantage of NDI is that a complete system model is required for designing the control system, to overcome this drawback INDI uses control effectiveness and sensor estimates for its control law design, thus requiring less model knowledge and replacing the system dynamics, by sensor estimates [18, 24, 27]. For this approach the control input can be derived for an even more general system:

$$\dot{\mathbf{x}} = \mathbf{f}(\mathbf{x}, \mathbf{u}) \tag{3.35}$$

Taking the Taylor series expansion, the system can be linearized at the current time point (x_0, u_0):

$$\dot{x} \approx f(x_0, u_0) + \frac{\partial f(x,u)}{\partial x}|_{x=x_0, u=u_0}(x - x_0) + \frac{\partial f(x,u)}{\partial u}|_{x=x_0, u=u_0}(u - u_0) \tag{3.36a}$$

$$\approx \dot{x}_0 + F((x_0, u_0))(x - x_0) + G(x_0, u_0)(u - u_0) \tag{3.36b}$$

$$\approx \dot{x}_0 + F((x_0, u_0))\Delta x + G(x_0, u_0)\Delta u \tag{3.36c}$$

Using the time-scale separation principle, the linearisation can be simplified and from which the control input can be derived:

$$\dot{x} \approx \dot{x}_0 + G(x_0, u_0)\Delta u \tag{3.37}$$

$$\Delta u = G^{-1}(x_0, u_0)(v - \dot{x}_0) \tag{3.38}$$

Whereby $G(x_0, u_0)$ is the control effectiveness matrix.
For the application of incremental INDI the following assumptions are implicitly made [20, 21, 24]:

1. Complete and accurate knowledge of states is available
2. Sensors to measure the acceleration $\dot{\mathbf{x}}$ with sufficiently high sampling rate need to exist and be available
3. Sensor to measure the current control input (actuator) need to be available or estimated on the basis of a high-fidelity model of the actuator dynamics
4. Time-scale seperation where it is assumed that the state derivatives evolve faster than the state upon fast control action, which directly influences the dynamics of the rigid body
5. Fast control action is assumed, where the dynamics of the actuator (and control surface) evolve much faster than the states
6. Control effectiveness matrix is invertible

A block diagram of the INDI control law is shown in Figure 3.28.

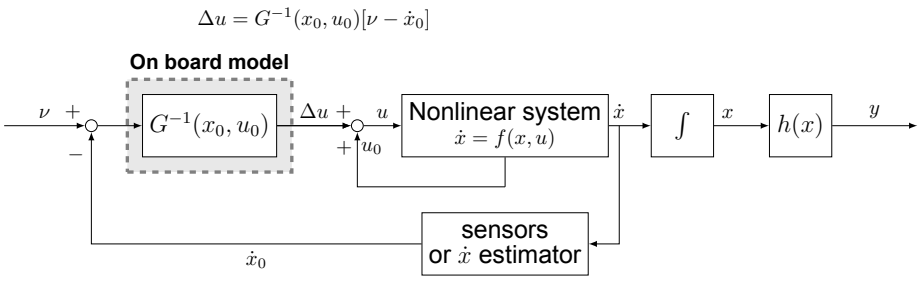

Figure 3.28: Block diagram of Nonlinear Dynamic Version. $G(x_0, u_0)$ contain nonlinear dynamics of the system [18, 19]

State-of-the-art Applications

Early conceptualisation of INDI is referred to as ”simplified” or ”modified”- NDI, with one of the first applications being on a VAAC Harrier aicraft [86], as shown in the timeline of NDI-based approaches in Figure 3.26. INDI has then seen multiple space and flight control applications [21, 24, 25, 70, 76, 87, 88].

One of the first notable applications was for applied in [27] for attitude control of a drone, which proved INDI's capabilities in real-world scenarios under the presences of disturbances, sensor noise, actuator dynamics. However, drones are smaller vehicles whose sensitivities and dynamics are at different scales compared to a real-world aircraft. Thus, the application of INDI on a commercial aircraft was first explored in [24], where it was implemented as attitiude controller with a simulation model of the Cessna Citation II. Two controllers were designed, one of which is a continuous-time INDI implementation and discrete-time INDI implementation to simulate the effect of real-time delays. Moreover, Psuedo Control Hedging (PCH) was implemented to alleviate performance degradation issues due to control saturation. A schematic of the controller architecture is shown in Figure 3.29. Analytical results showed the margins of closed-loop stability as measurement sampling time delay and control effectiveness uncertainties. Real-world phenomena were also analysed, through adding random noise, bias, model mismatches, discretization, and time delays with numerical simulation. These results provided further insights on the improvements for INDI.

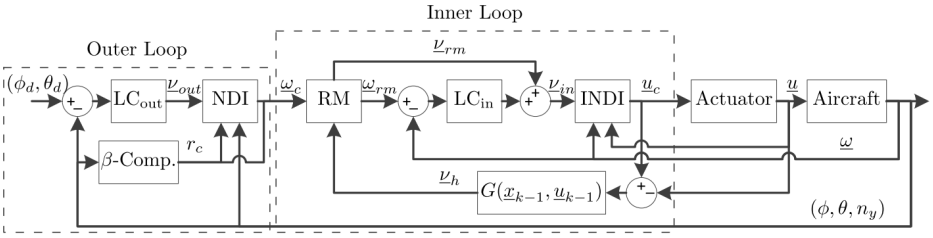

Figure 3.29: Attitude control architecture with INDI in the inner loop and a linear controller in the outer loop. Taken from [24]

INDI has been demonstrated for fault-tolerant control in the presence of actuator faults in [88] for trajectory control of the Cessna Citation II where it obtained comparable performance when there are no faults or model uncertainties. Although, slight differences were still observed and showed some performance degradation where there is still deviation from the desired reference inputs. However, control authority was still present as INDI would compensate for the actuator faults. INDI was implemented on a fixed-wing aircraft was shown with an UAV [76] and further validating its real world applicability through repeated flight tests.

The robustness and stability in the presence of external disturbances with INDI were studied in [18], where a reformulation of INDI was described such that it can be applied without the time-scale separation assumption and its improved robustness was verified compared to NDI. Moreover, similar to IBS it was combined with SMC to result in a newer and robust control variant. The stability and robustness properties of INDI when regular, which singular perturbations such as transportation lags, elastic airframe effects or other types of unknown or unmodeled dynamics were investigated in [26]. It was recommended that the use of additional model information as a form of complementary augmentation can further improve the design and application of INDI. Further research presented in [89] presented

an analysis of discrete-time domain analysis of INDI with SMC for fault-tolerant flight control, where the stability and robustness against faults such as actuator faults, control reversal, sensing errors are demonstrated.
A new approach of INDI, namely Hybrid INDI, was developed in [25], where it was augmented with a complementary filter that supplies angular acceleration estimation based on sensor measurement and on-board model output. The application was verified by designing an attitude controller for the F-16 aircraft simulation model as shown in Figure 3.30. Simulations with aerodynamic uncertainties (in magnitude) and measurement delays showed the improved capabilities of Hybrid INDI compared to INDI, but the limitations in noise filtering capabilities were encountered where a trade-off between noise filtering and response time has to be made to obtain good performance.

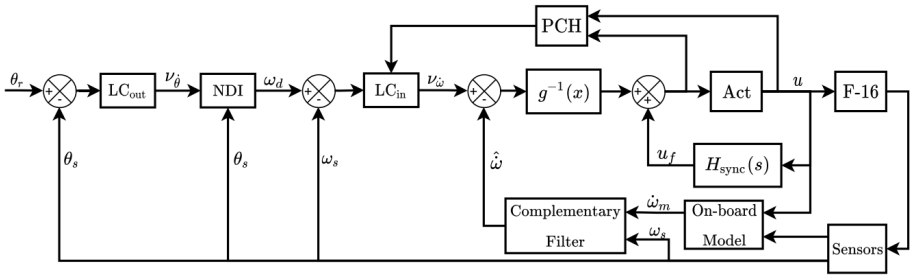

Figure 3.30: Block diagram of attitude control with Hybrid INDI. Taken from [25]

Advantages/Disadvantages

The following advantages of Nonlinear Dynamic Inversion are described as:

Advantages

- Design procedure easily applicable to MIMO systems
- Simple inner and outer loop structure, where the inner loop is responsible for linearization (stabilisation) and outer loop can be designed and tuned with various types of controllers, such as linear control methods
- Less model knowledge required compared to NDI
- Better robustness against uncertainties compared to NDI

The following disadvantages of Incremental Backstepping are described as:

Disadvantages

- Closed-loop stability is not ensured
- Inversion is not always achieved or possible
- Uncertainties can significantly degrade flying qualities and performance
- Measurement time delays can have significant impact on performance

3.2.3. Adaptive (Incremental) Nonlinear Dynamic Inversion

This section concerns the discussions of adaptive schemes used for NDI and INDI. As previously established in the presence of uncertainties, NDI and INDI can degrade in performance in the presence of uncertainties and the uncertainty can be incorporated into the control design to improve the robustness of these techniques. However, when these uncertainties are large the performance can significantly degrade, where unknown parameters can disturb the stability of the system. Thus, adaptive schemes applied on NDI and INDI allows for a more sophisticated way to deal with these large uncertainties and the model parameters of the system are estimated and adapted during flight. Due to the extensive range of theory, the results, and findings of the applied techniques are primarily elaborated.

Adaptive NDI

Early explorations of Adaptive NDI concerned combinations with black box approaches such as neural networks or Model Reference Adaptive Control (MRAC), where either a black-box or gray box reference models are created of the aircraft dynamics. Notable advancement of ANDI has been extensively researched in [85], where it was applied for the purpose to design a fault tolerance flight control system

(FTFC). The aerodynamic model is set up with a first order Taylor Series expansion with respect to the aircraft states, and these model parameters will be adapted online using RLS in the inner loop. The inner loop stabilises the body angular rates, and new estimates were provided in the second and third outer loop for aerodynamic angle tracking. This adaptive control law was tested through numerical simulations with a B747 model and tested with pilot in the loop simulations. Moreover, an Adaptive Recursive Orthogonal Least Squares (AROLS) was applied to (re-)identify the aerodynamic model.
The adaptation is implemented in the inner loop for NDI rate control as shown in Figure 3.31, here the Two-Step Method (TSM) is applied where the aircraft state is measured and estimated with IEKF and then an Aerodynamic Model Identification (AMI) is performed, where the aerodynamic coefficients in the NDI control law are estimated and updated with RLS. The second outer loop and third outer loop, as shown in Figure 3.32, has a *Local Gradient Determination* (LGD), where the force coefficient derivatives are computed on-line, eventually resolving to aircraft roll angle and aerodynamic angle virtual control inputs for the inner rate control loop. The LC, represent the linear controllers, which are proportional and integral control gains to be tuned using a Multi-Objective Parameter Synthesis, that takes various constraints, such as overshoot, control activity into account. In addition, Psuedo Control Hedging (PCH) and Control Allocation (CA) were implemented to round off the complete FTFC.

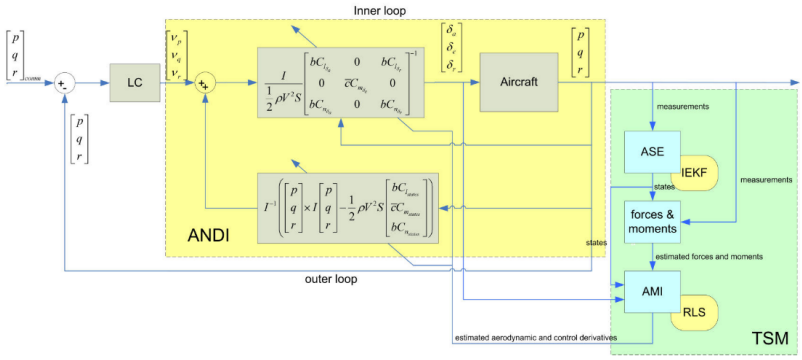

Figure 3.31: NDI rate control loop. Taken from [85]

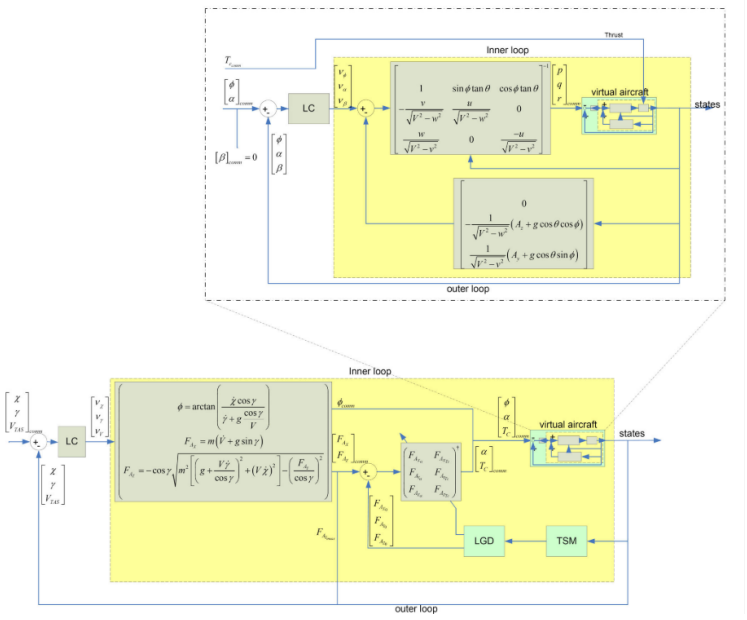

Figure 3.32: NDI autpilot with bottom block diagram being the third NDI loop for navigitional tracking and the second loop for zero sideslip roll and angle of attack control. Taken from [85]

The designed control system has been evaluated through piloted simulations in fault scenarios such as stabilizer runaway, rudder loss and engine separation. The experiment resulted that the controller is successful in recovering the ability to control the damaged aircraft and reduces physical workload as FTFC compensates, providing cooperative effort with the pilot for safe and operable flight. This

resulted in valuable insight and improvement on the real-world application of ANDI.
Recent application of ANDI concerned the use of a Recursive tensor-product (TP) simplex B-splines aerodynamic model in [29] with NDI as shown in Figure 3.33. The approach was compared to standard Multivariable Simplex B-spline model structure, where it yielded a comparative approximation accuracy, while requiring less model parameters.

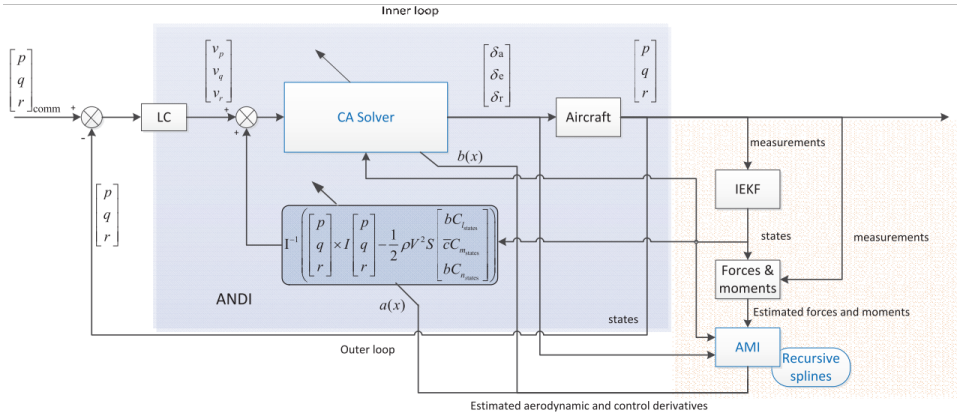

Figure 3.33: ANDI with recursive spline method. Taken from [29]

Adaptive INDI

INDI has seen various successful real world applications, and adaptive INDI has made continuous advancements in the applications for drones [27], Vertical Take-off and Landing (VTOL) drones [90] and various adaptive IDNI approaches for consistent handling qualities have been applied with an F-16 simulation model in [91].
The first real-world application presented in [27] used the Least Mean Squares (LMS) adaptive filter to update the parameter estimation of the drone's actuator effectiveness used in the INDI control law for angular acceleration. The LMS adaptive filter calculates the difference between expected acceleration based upon the inputs and measured acceleration, where $\mathbf{G}$ models the control effectiveness and μ_1, μ_2 are adaptation constants that adjust the rate of adaptation. A block scheme of the INDI control scheme is shown in Figure 3.34.

$$\begin{aligned} \mathbf{G}(k) &= \mathbf{G}(k-1) - \mu_2 \left(\mathbf{G}(k-1) \begin{bmatrix} \Delta\omega_f \\ \Delta\dot{\omega}_f \end{bmatrix} - \Delta\dot{\Omega}_f \right) \begin{bmatrix} \Delta\omega_f \\ \Delta\dot{\omega}_f \end{bmatrix}^T \mu_1 \\ \mathbf{G} &= \begin{bmatrix} \mathbf{G_1} & \mathbf{G_2} \end{bmatrix} \end{aligned} \tag{3.39}$$

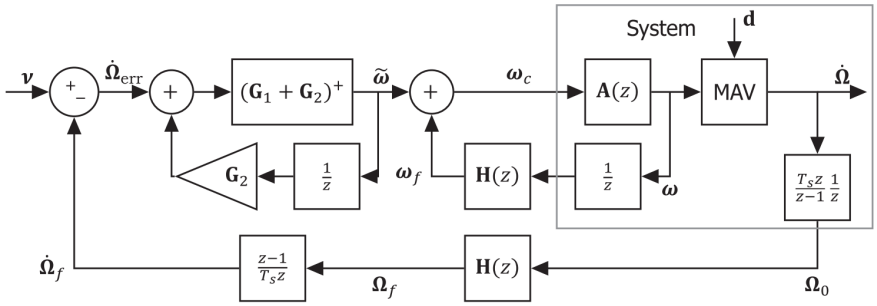

Figure 3.34: INDI control scheme, where $A(z)$ is the actuator dynamics and $H(z)$ is the second order filter. Taken from [27]

An attitude outer loop control is responsible for steering the drone. Several experiments were performed to analyse the performance, disturbance rejection and adaptation of the adaptive INDI controller. From these experiments, it was observed that when the drone's configuration was changed a mismatch occurred in the control effectiveness and that without adaptation the drone's performance would degrade, whereas with adaptation the drone was able to maintain its tracking performance.

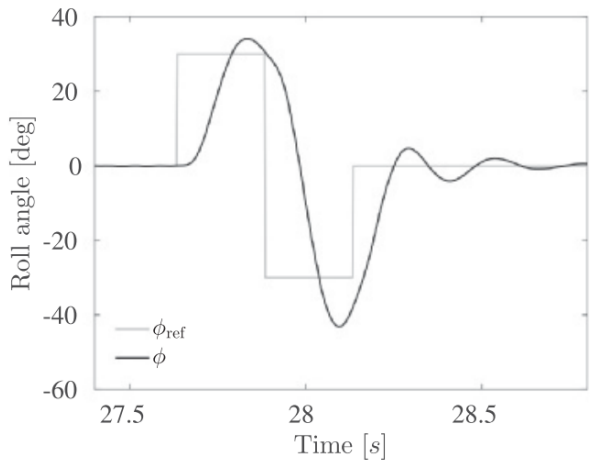

Figure 3.35: INDI CE underestimation results in slow response [27]

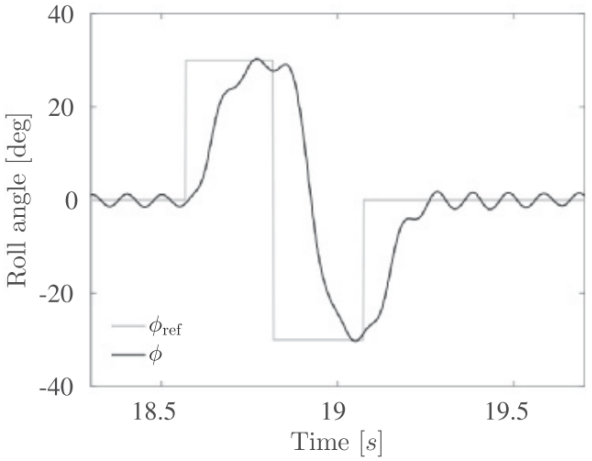

Figure 3.36: INDI CE overestimation results in oscillatory response [27]

Adaptive INDI has been combined with multivariate B-splines for the application of a VTOL drone, which can adapt the controller effectively and store previous adaptations with a multivariate B-spline during real-time flights [90]. The selection for B-splines were made on its applicability in creating a smooth global model, which is able to retain and store its estimation, but also allow for local updates during adaptation. Moreover, it is able to flexibly model non-linear dynamics over the flight envelope. The block diagram of the INDI control loop is shown in Figure 3.37. The adaptation rule used in the research is a Kernel Based - Recursive Least Squares (KB-RLS), which only differs in initialization from standard RLS as it takes the *null* space of the smoothness matrix, which consists of constraints on the global spline model to preserve continuity, for the multivariate B-spline model into account.

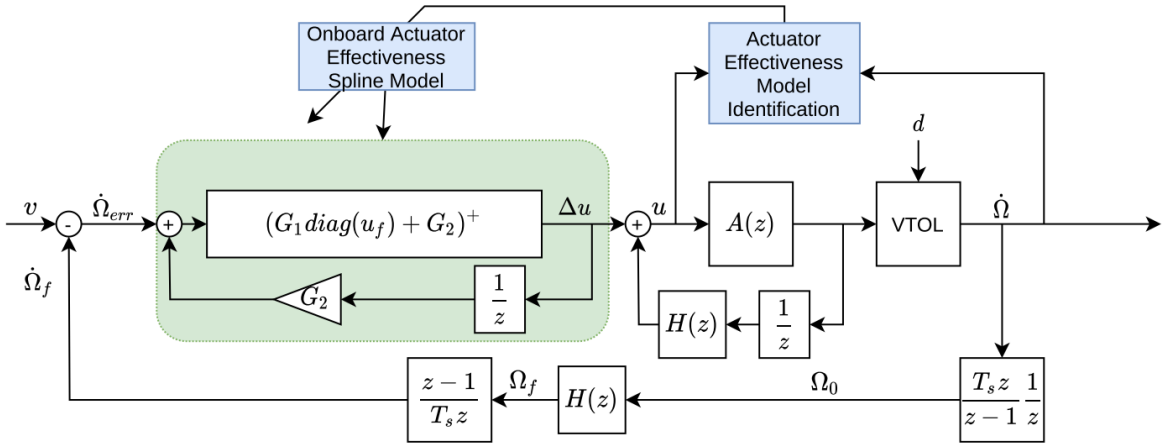

Figure 3.37: Spline based adaptive INDI block diagram. [90]

The resulting research findings showed the capabilities of adaptive INDI with a parametric model such as multivariate B-spline for storing and modelling the control effectiveness throughout its flight envelope.

The research towards various adaptive INDI schemes for consistent handling qualities in [91] analysed whether online correction of on-board control effectiveness would decrease sensitivity of handling qualities and control performance. The research specifically focused on the application of adaptive INDI for pitch rate dynamics with adaptation using the Least Mean Squares (LMS) parameter estimation method and the sensitivity of the handling quality would be assesed for several flight conditions, CG position, inertia changes, aerodynamic mismatches and elevator effectiveness deviations from $\pm 15\%$ of the nominal value. The results revealed that it was able to decrease the handling quality variations, but in the presence of large CG shifts the time-scale separation assumption was impaired. Consequently, the true estimation of the control effectiveness was not obtained with the implemented method.

In [92] an adaptive INDI-SMC control architecture, as shown in Figure 3.38 was proposed with the goal for fault-tolerant flight control. Several fault scenarios were introduced, such as actuator faults, control reversal, sensing imperfections, and it was shown through numerical simulation that A-INDI-SMC was able to actively resist and adapt to the fault scenarios.

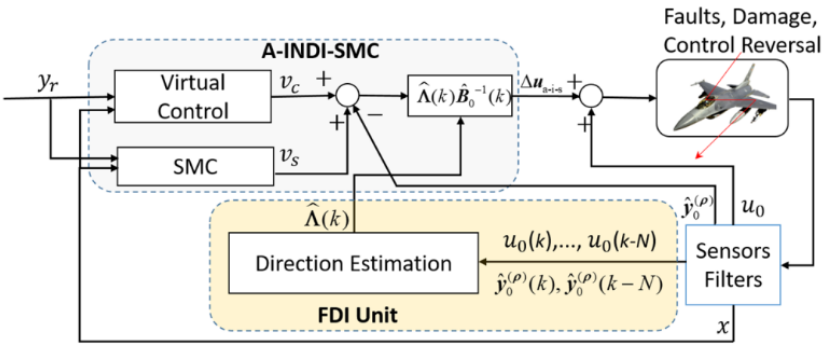

Figure 3.38: A-INDI-SMC block diagram [92]

3.3. Control Method Selection and Motivation

This section elaborates on the selection of control method to be used, where advantages and disadvantages were elaborated for the respective methods and a motivation is made for the selected method.

State-of-the art applications with Backstepping (BS) and Nonlinear Dynamic Inversion (NDI) have shown various capabilities when nonlinear control methods are used instead of traditional classical control techniques. BS has the advantage that due to its Lyapunov based design approaches, asymptotic stability can be ensured. Moreover, BS also allows control designers to select which dynamics to include into the control law design, but due to its recursive and strict-feedback requirement its practical applications have been limited. Whereas NDI has shown real-world application with its relatively simple design procedure, where tuning is primarily necessary in its outer control loop, whereas BS has to be tuned and selected such that its CLF is satisfied. Both of these nonlinear control methods require accurate model knowledge, which in the case of the Flying V isn't certain.
This leads to favouring the incremental control version of these respective methods, Incremental Backstepping and Incremental Nonlinear Dynamic Inversion, where they both show greater robustness against uncertainties. Both of these methods have seen various real-world applications and verified its capabilities for fault-tolerant flight control system design. Incremental Backstepping, while more simplified, is still a complex design procedure compared to INDI. Moreover, both of these methods still degrade in performance when large uncertainties are encountered.

Adaptive schemes for (I)BS (I)NDI, where for adaptive BS various frameworks have been developed with differing success, these developed framework show verified results in the design of fault-tolerant flight control systems. Adaptive IBS has seen real world applications, where its Lyapunov based stability properties allow for asymptotic control stability, whereas adaptive INDI's stability hasn't been proved yet. However, the simplification of (I)NDI control design compared to adaptive (I)BS and recent applications have shown its capabilities to store and adapt control effectiveness parameters throughout its flight envelope deem it to be more suitable for application. Various applications of adaptive BS and ABS show its significant effort required where multiple control loops and gains have to be tuned, whereas for adaptive NDI and INDI, the tuning primarily concerns linear controller in the outer loop control, which could result in less effort required for the implementation in the Flying V FCS. Thus, an overall preference can be made for adaptive NDI and INDI.
The state-of-the-art applications of adaptive NDI have validated its use for fault-tolerant control, whereas adaptive INDI has seen real world applications on drones and VTOLs and simulation models, which leads into a potential application for adaptive INDI for fault-tolerant control on the Flying V.

This leads into the selection for the appropriate adaptive control method for the Flying V FCS. Adaptive BS and NDI would require extensive model knowledge and identification of all system dynamics, which for a developing project such as the Flying V may not be completely feasible at the moment. Therefore, adaptive IBS and INDI are more applicable, as they both require less knowledge of the complete model.

Moreover, the inner loop of the Flying V as described in Section 2.5.4, implemented an INDI control implemented for its rate control. Thus, an evolvement to adaptive INDI for fault-tolerant control allows preserving the current control architecture as much as possible and doesn't require a reduces the complexity in tuning compared to adaptive IBS.

3.3.1. Parameter Estimation

The purpose of parameter estimation is to converge to an estimation of the true model parameter with a certain model structure and optimization criterion. This optimization criterion can operate in single update steps or multiple iterations, where continuous adaptation is desired. Moreover, the model structure defines the characteristics (e.g. constant, linear, quadratic, non-linear) of the parameters and their relationships and various model structures were identified in this literature research. Such as:

- Constant
- Polynomials
- B-spline
- Multivariate B-spline
- Neural Networks

In addition different parameter estimation methods were presented, such as LMS, RLS, dynamic scaling laws.

The existing Flying V aerodynamic model has been modelled by polynomial models and spline models, which doesn't present a need towards highly parametric models such as Multivariate B-spline, Neural Networks. Moreover, from the various state-of-the art applications, recursive least squares has seen success given its ability to accurately estimate the true parameters.

3.4. Conclusion

From the literature research towards nonlinear & adaptive control methods, the following research (sub)-questions are answered:

- What advancements have there been in the applications of nonlinear & adaptive methods?
  - Nonlinear control methods such as Backstepping and Nonlinear Dynamic Inversion have been applied in various simulation studies, whereas the latter has real world application on a high performance fighter jet. However, notable drawbacks from its requirement of accurate model knowledge is not always feasible due to significant effort required in flight testing and real-world phenomena such as noise, external disturbances influence the system dynamics. The development of Incremental Nonlinear Dynamic Inversion and Incremental Backstepping thereafter, resulted in nonlinear control techniques, which required less model knowledge as only control effectiveness is required and the feedback of system dynamics is replaced by sensor dynamics. Moreover, it has better robustness against uncertainties and disturbances compared to its non-incremental versions. This has been verified and validates through multiple simulation studies and real world applications on CS-25 class aircraft, drones, VTOL. Some drawbacks are encountered as noise and measurement time delays increase, where INDI specifically has been augmented with filters to result in a Hybrid INDI technique. When model uncertainties and especially control effectiveness uncertainties are significantly large, it can lead to degradation in performance. Thus, adaptive schemes for these nonlinear control methods allow for sophisticated way to deal with these uncertainties and various reconfigurable controllers have been developed for fault-tolerant control.

1. What methods have been implemented for fault-tolerant control?
   - Incremental Backstepping and Incremental Nonlinear Dynamic Inversion have shown to passively reject actuator faults and compensate for these faults. Adaptive BS and NDI have seen various successive applications to maintain safe flight in the presence of sensor, actuator, and engine faults.
2. What method is the most suitable for fulfilling the requirements for the Flying V?
   - As identified from the literature research, adaptive INDI is suitable as it preserves the current control architecture design while advancing it to fault-tolerant control.

4

Preliminary Analysis

This chapter presents a preliminary analysis where a pitch rate control law is designed with PI control, Incremental Dynamic Inversion (IDI) and adaptive IDI (AIDI) for a pitch reference tracking task. These control laws are applied to a longitudinal linear, time-invariant (LTI) model, obtained from an F-16 simulation mode, which has been used in many research studies with the aforementioned studies in the literature research.
In the preliminary analysis a robustness analysis will be conducted to observe how PI and IDI compare in the presence of uncertainties and thereafter several fault scenarios will be analysed, comparing IDI and AIDI.
The goal is to gain insight on the robustness of these methods and asses how these controllers compare to faults. The following sub-research question can thus be partially answered:

- How does the adaptive FCS cope with faults compared to the non-adaptive FCS?

4.1. Simulation setup

A linear, time-invariant (LTI) models longitudinal model is derived based on the F-16 simulation model from the University of Minnesota. This simulation model has been used and modifified in various state-of-the-art applications of (I)BS and (I)NDI [15, 25, 26, 75, 80, 91].
The longitudinal model forms the bare-airframe dynamics (4.1.1). A control system is designed for pitch rate control, which adds actuator dynamics, sensor dynamics and three separate control systems with different control laws will be designed with the PI, IDI and adaptive IDI control law (4.2). The pitch rate tracking experiment (4.2.6) and the tuning procedure (4.2.7) for these control laws are elaborated as last.

4.1.1. Bare-airframe dynamics

The simulation model provides a trim and linearization with two different aerodynamic models, hi-fi and low-fi, valid for up to a Mach speed of 0.6. The lo-fi model is a subset hi-fi aerodynamic model and does not include an leading-edge flap control surface and the subsequent models are described in literature [63, 93]. The lo-fi is used for the analysis.
With the trim function provided in the simulation model, which defines a steady-state trim when a cost of $1e{-}29$ has been achieved for the respective flight condition. From the trim state, an LTI model is derived for longitudinal motion of the aircraft. The flight condition and aircraft parameters are defined in Table 4.1 and the trim state results are defined in Table 4.2. It was determined that the system is stable and the dynamic longitudinal modes achieve level 1 flying qualities as per the mil-spec requirements as described in 2.3.1.

The longitudinal model has the following form and involves the respective states:

$$\dot{x} = A_0\mathbf{x} + B_0\mathbf{u} \tag{4.1}$$
$$x = \begin{bmatrix} h & V_T & \alpha & \theta & q \end{bmatrix} \tag{4.2}$$
$$u = \begin{bmatrix} \delta_e \end{bmatrix} \tag{4.3}$$

The A_0 matrix has the aerodynamic stability derivatives and B_0 matrix has the linearized control stability derivatives linearized around the trim point. The complete LTI system is expressed by Equation (4.4).

The following assumptions are made for the LTI model:

- Constant mass and moment of inertia and center of gravity position
- Constant Thrust
- Simulation valid around the linearized condition

Parameter	Unit	Value
Flight Condition		
Altitude (h)	km	6.1
Velocity (V_T)	m/s	153.31
Dynamic pressure ($\bar{q}$)	Pa	7688.83
Aircraft properties		
mass (m)	kg	9295
CG position (x_{cg})	m	0.35$\bar{c}$
I_{xx}	kg $\cdot$ m^2	12871.2
I_{yy}	kg $\cdot$ m^2	75667.9
I_{zz}	kg $\cdot$ m^2	85532.2
I_{xz}	kg $\cdot$ m^2	1331.5
Airframe geometry		
b	m	9.14
S	m^2	27.87
$\bar{c}$	m	3.45

Table 4.1: Simulation Parameters

Parameter	Unit	Value
Cost Function	-	$2.25\text{e}{-29}$
Thrust	N	9646.36
Elevator Deflection	deg	-2.74
Angle of Attack	deg	5.45
Dynamic modes		
Short Period	[-]	-0.6545 $\pm$ 1.318i (Level 1)
Phugoid	[-]	-0.00494 $\pm$ 0.088i (Level 1)

Table 4.2: Trim cost & states and dynamic modes

$$\begin{bmatrix} \dot{h} \\ \dot{V}_T \\ \dot{\alpha} \\ \dot{\theta} \\ \dot{q} \end{bmatrix} = \begin{bmatrix} 0 & 7.05e-13 & -503 & 503 & 0 \\ 1.15\text{e}{-4} & -1.35\text{e}{-2} & 5.34 & -32.17 & -1.34 \\ 2.14\text{e}{-6} & -2.52\text{e}{-4} & -0.55 & -1.86\text{e}{-13} & 0.95 \\ 0 & 0 & 0 & 0 & 1 \\ 2.64\text{e}{-20} & -3.1\text{e}{-18} & -1.85 & 0 & -0.76 \end{bmatrix} \begin{bmatrix} h \\ V_T \\ \alpha \\ \theta \\ q \end{bmatrix} + \begin{bmatrix} 0 \\ 5.15\text{e}{-2} \\ -1.16\text{e}{-2} \\ 0 \\ -9.74\text{e}{-2} \end{bmatrix} \begin{bmatrix} \delta_e \end{bmatrix} \tag{4.4}$$

4.2. Control System Design

The design of the control system has been inspired by the various studies concerning stability, robustness of adaptive nonlinear control methods. Two studies from [91, 94] have primarily formed the design of the control system for pitch rate control and the actuator and sensor dynamics used for this system have been extensively been elaborated there.

The LTI system with actuator (4.2.1) and sensor models (4.2.2) form the aircraft dynamics. Moreover, the F-16 simulation model also supplies an International Standard Atmosphere (ISA) model, which calculates the dynamic pressure ($\bar{q}$) throughout the simulation and this is also added to the aircraft dynamics. With the aircraft dynamics described, the control system using Proportional-Integral (PI) control (4.2.3), IDI control (4.2.4) and adaptive IDI control (4.2.5) is elaborated. At last, the tuning procedure (4.2.7) for these controllers is outlined.

4.2.1. Actuator Dynamics

The F-16 simulation model includes actuator dynamics using first-order low-pass dynamics, as shown by Equation (4.5).

$$A(s) = \frac{\omega_{\text{act}}}{s + \omega_{\text{act}}} \tag{4.5}$$

Here ω_{act} is the actuator bandwidth, which is set to 20.2 rad/s, but is increased to a higher bandwidth as elaborated in [91], where it is set to 60 rad/s. A higher bandwidth is beneficial for fast changing commands or rejecting disturbances, moreover the actuator dynamics also include deflection saturation and rate saturation, where the maximum & minimum deflection and rate of deflection are limited, which is $\pm$ 25 deg and $\pm$ 60 $^\circ/s$ respectively. The block diagram of the actuator dynamics are shown in Figure 4.1.

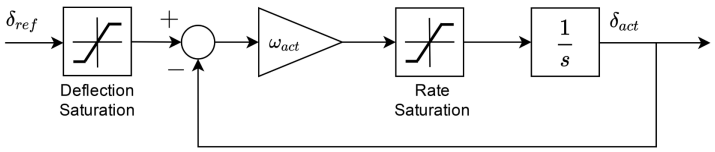

Figure 4.1: Block diagram of the actuator dynamics, including deflection and rate saturation limits. Taken from [91]

4.2.2. Sensor Models

For this preliminary analysis, the sensor models to measure the pitch acceleration and pitch rate are implemented to make the system closer to real-world system. Sensor delays, compute delays and noise are not included in this analysis. The sensor model for pitch rate is a rate and linear acceleration sensor with notch filter, and modeled by second order dynamics as shown in Equation (4.6) and elaborated in [25, 91].

$$H_{RN}(s) = \frac{0.0001903s^2 - 0.005346s + 1}{0.0004942s^2 + 0.03082s + 1} \tag{4.6}$$

The pitch acceleration is measured using an angular accelerometer with second-order dynamics of the structure as shown in Equation (4.7) [91].

$$H_{AA}(s) = \frac{\omega_{\text{AA}}^2}{s^2 + 2\zeta_{\text{AA}}\omega_{\text{AA}} + \omega_{\text{AA}}^2} \tag{4.7}$$

The filter parameters are set to $\omega_{\text{AA}} = 30rad/s$ and $\zeta_{\text{AA}} = 1$. The aircraft dynamics with the sensor measurement is shown in Figure 4.2.

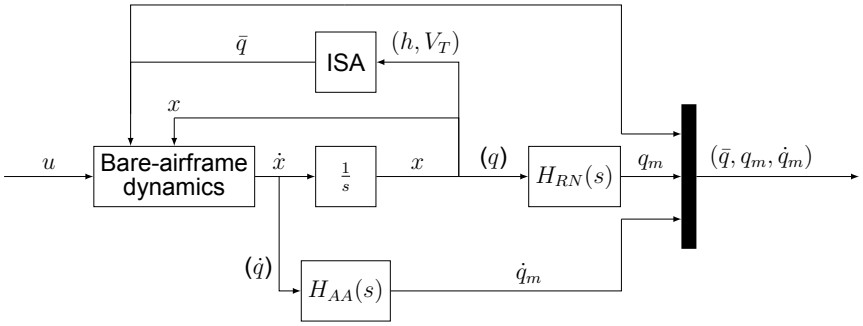

Figure 4.2: Aircraft Dynamics

4.2.3. Linear Controller

A proportional integral (PI) controller is implemented as the linear Control method with the following description for the inner and outer loop respectively:

$$u_{\text{cmd}} = K_{p1}(\dot{q}_{\text{des}} - \dot{q}_m) + \frac{K_{I1}}{s}(\dot{q}_{\text{des}} - \dot{q}_m) \tag{4.8}$$

$$\dot{q}_{\text{des}} = K_{p2}(q_{\text{ref}} - q_m) + \frac{K_{I2}}{s}(q_{\text{ref}} - q_m) \tag{4.9}$$

The block diagram of the control system is shown in Figure 4.3.

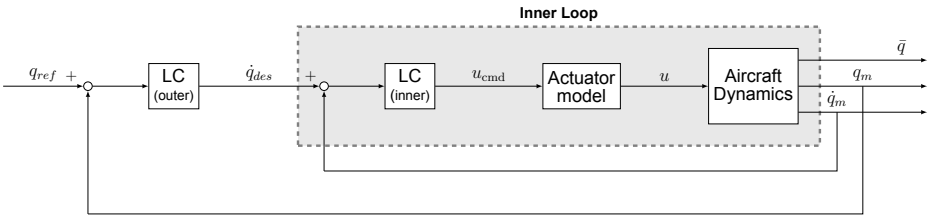

Figure 4.3: PI pitch rate control system

4.2.4. Incremental Dynamic Inversion Controller

The derivation of this control law is based on INDI, but now the controller is applied to a linear system and is defined as IDI. It starts with the equation of motion for the pitch dynamics:

$$\dot{q} = \frac{I_{zz} - I_{xx}}{I_{yy}}pr + \frac{I_{xz}}{I_{yy}}(r^2 - p^2) + \frac{1}{I_{yy}}M \tag{4.10}$$

The moment M is defined as following:

$$M = \bar{q}S\bar{c}C_{m,T} \tag{4.11}$$

$$C_{m,T} = f(\alpha, \beta, q, \delta e) = C_m(\alpha, \delta e) + C_z(\alpha, \beta, q, \delta_e)[x_{cgr} - x_{cg}] + C_{m_q}(\alpha) \tag{4.12}$$

$$C_{z,T} = C_z(\alpha, \beta, \delta e) + C_{z_q}(\alpha)\frac{\bar{c}q}{2V} \tag{4.13}$$

Where $C_{m,T}$ is the total pitch moment coefficient and $C_{z,T}$ is the vertical force coefficient acting on the aircraft. The reference point x_{cgr} is set at 0.35$\bar{c}$ and C_{m_q}, C_{z_q} are the damping coefficients. These coefficients are acquired from the low-fi aerodynamic dataset.
To derive the IDI control law, the equation of motion is linearized with the first order Taylor series around the trim point, as expressed by Equation (4.14).

$$\dot{q} = \frac{\bar{q_0}S\bar{c}}{I_{yy}}\left(\frac{\partial C_{m,T}(x_0, u_0)}{\partial x}\Delta x + \frac{\partial C_{m,T}(x_0, u_0)}{\partial \delta_e}\Delta\delta_e\right) \tag{4.14}$$

$$= \frac{\bar{q_0}S\bar{c}}{I_{yy}}C_{m_x}\Delta x + \frac{\bar{q_0}S\bar{c}}{I_{yy}}C_{m_{\delta_e}}\Delta\delta_e \tag{4.15}$$

It is assumed that the rolling (p) and yawing moment (r) are very small and from observing the pitching dynamics and respective aerodynamic dataset, it is determined that it only depends on the angle of attack (α), pitch rate (q) and elevator deflection (δ_e), which results in the following expression:

$$\dot{q} = M_\alpha\Delta\alpha + M_q\Delta q + M_{\delta_e}\Delta\delta_e \tag{4.16}$$

Here $M_\alpha, M_q, M_{\delta_e}$ are the state and control derivatives as included in the longitudinal LTI model in Equation (4.4).
For IDI it is assumed that the sampling time is sufficiently high, and the state dynamics are sampled by sensors, which results in the following expression:

$$\dot{q} = \dot{q}_0 + M_{\delta_e}\Delta\delta_e \tag{4.17}$$

$$M_{\delta_e} = \frac{\bar{q_0}S\bar{c}}{I_{yy}}C_{m_{\delta_e}} \tag{4.18}$$

Setting $\dot{q}_0$ as the desired pitch acceleration $\dot{q}_{des}$, applying time-scale separation and solving for $\Delta\delta_e$ results in the IDI control law [91]:

$$\Delta\delta_e = \left[\frac{\bar{q}_0 S\bar{c}}{I_{yy}} C_{m_{\delta_e}}(x_0, u_0)\right]^{-1} (\dot{q}_{des} - \dot{q}_0) = G^{-1}(x_0, u_0)(\dot{q}_{des} - \dot{q}_0) \tag{4.19}$$

$$\delta_e = \delta_{e_0} + \Delta\delta_e \tag{4.20}$$

Here $G(x_0, u_0)$ is the Control Effectiveness (CE) term, also referred as on-board model, obtained through the linearization of the equation of motions. The longitudinal LTI model has the control derivatives for the pitch dynamics, and for the preliminary analysis it will be used as the CE term. Moreover, as the IDI control law computes an increment of control deflection, the previous control deflection is obtained from the previous timestep and synchronized with the measurement of pitch acceleration by applying the same delay from the H_{AA} filter [91].

$$G_{OBM} = \frac{\bar{q}_0 S\bar{c}}{I_{yy}} C_{m_{\delta_e}} = -9.74\text{e}{-2} \qquad \left[\frac{1}{\text{deg} \cdot s^2}\right] \tag{4.21}$$

$$C_{m_{\delta_e}} = -1\text{e}{-2} \qquad \left[\frac{1}{\text{deg}}\right] \tag{4.22}$$

The outer loop controller is a linear control block, which computes the desired pitch acceleration (q_{des}) and the complete block diagram is shown in Figure 4.4.

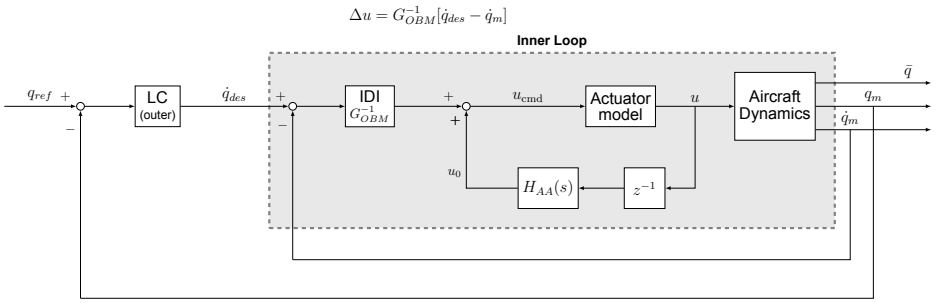

Figure 4.4: IDI pitch rate control system

4.2.5. Adaptive IDI Controller

As mentioned in the previous section, the CE term G is directly acquired from the LTI model, however in the real world there could be multiple uncertainties in the derivation of this term due to physical influences (e.g. uncertainty in mass and moment of inertia or aerodynamic data) or time-varying as dynamic pressure influences the effectiveness of the control surface. Moreover, in cases of fault scenarios regarding actuator and the control surface, CE will change and cause a model-mismatch and this could lead to performance degradation or unstable scenarios. The study [91] has extensively researched various adaptive methods for pitch rate control and one of them is the use of Recursive Least Squares (RLS), which is the parameter estimation method of interest and is applied in this preliminary analysis. The RLS - IDI, now defined as the Adaptive IDI (AIDI), controller is formulated from the linearized pitch dynamics, where $\tilde{G}_{OBM}$ is now an uncertain parameter:

$$\dot{q} = \dot{q}_0 + \tilde{G}_{OBM}\Delta\delta_e \tag{4.23}$$

This uncertain parameter can be estimated or as done in the research of [91] adjusted through a correction factor that will be estimated. The factor is estimated by formulating a prediction model, that determines the increment of pitch acceleration between timesteps. This increment is defined as following:

$$\Delta q_0 = \dot{q}_0 - \dot{q}_{-1} = \theta \cdot \phi \tag{4.24}$$

$$\phi = G_{OBM}\Delta\delta_{e,0} \tag{4.25}$$

$$\theta = \hat{c} \tag{4.26}$$

$$\tag{4.27}$$

Here ϕ is the basis function and θ is the parameter to be estimated and the current and previous timestep for the estimation. The RLS algorithm is formulated as the following [85, 91]:

$$K_{k+1} = P_k \phi_{k+1} \left(\lambda + \phi_{k+1}^T P_k \phi_{k+1} \right)^{-1} \tag{4.28}$$

$$\hat{\theta}_{k+1} = \hat{\theta}_k + K_{k+1} \left(z_{k+1} - \phi_{k+1}^T \hat{\theta}_k \right) \tag{4.29}$$

$$P_{k+1} = \frac{1}{\lambda} \left(I - K_{k+1} \phi_{k+1}^T \right) P_k \tag{4.30}$$

Here P_k is the parameter covariance, which sets the confidence in the initial estimation of θ, where a low value of P_k is set when the initial estimation of θ_0 is accurate and high when the initial estimation is uncertain, which leads to high initial adaptation. The forgetting factor, λ sets how much of previous datasets should be used in the parameter estimation and is set between 0 and 1, but most commonly a value between 0.98 and 1 is used as a lower value can lead to oscillatory adaptation. K_{k+1} calculates the gain to update the parameter θ based on the error between the prediction model and real output (z_{k+1}), which is the incremental pitch acceleration. This results in an adaptive IDI control law as following and the block diagram of the control system is shown in Figure 4.5

$$\Delta\delta_e = \left(\hat{c} \cdot G_{OBM} \right)^{-1} \left(q_{des} - \dot{q}_0 \right) \tag{4.31}$$

The initial covariance (P_0) is set to 100 as there is high uncertainty expected in the initial CE. The forgetting factor (λ) is set to 0.9998 and the initial estimation for the scaling factor (θ_0) is set to 1.0. During the analysis, these values will be adjusted accordingly if necessary.

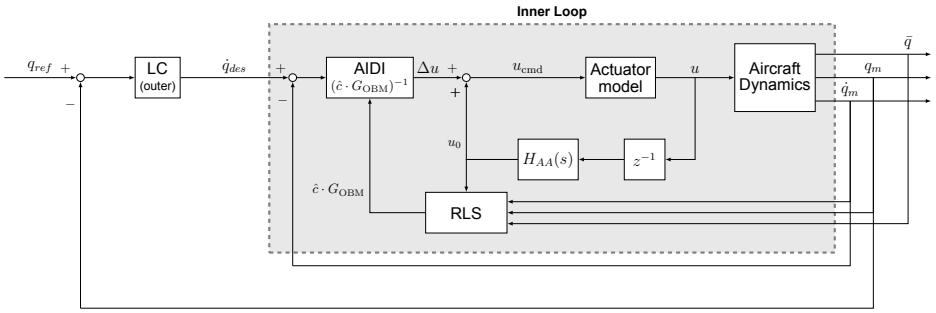

Figure 4.5: AIDI pitch rate control system

4.2.6. Pitch Tracking Experiment

Control system is synthesized to track a reference pitch rate (q_{ref}) reference, which can be generated by control stick deflections from the pilot. This pitch rate reference has been designed to keep the aircraft within the linearized flight condition and is shown in Figure 4.6.

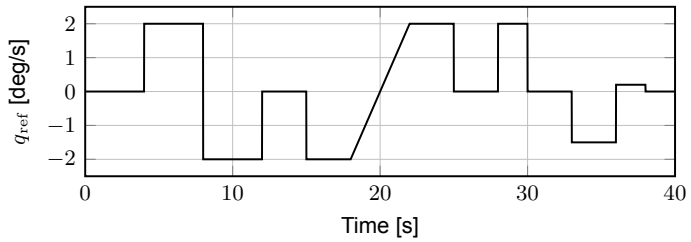

Figure 4.6: Pitch rate reference input

4.2.7. Tuning Procedure

The gains in the control system have to be tuned and this will be done similarly to the Flying V tuning algorithm, which takes multiple objectives and constrains concerning various handling qualities and

performance of tracking reference into account for determining the optimal gains.
The performance of tracking the pitch rate reference is evaluated through the Root Mean Square Error (RMS), the maximum error and control activity. These metrics are formulated as following:

$$RMS = \sqrt{\frac{1}{N}\sum_{i=1}^{N}(q_{ref} - q)^2} \tag{4.32}$$

$$\max(e) = \max(q_{ref} - q) \tag{4.33}$$

$$\delta_{e_{\text{activity}}} = \int_0^T \dot{\delta}_e^2 dt \tag{4.34}$$

Here N is the total timesteps and T is the total simulation time.

The Gibson Dropback criterion is used as the handling quality constraint. The development of this criterion has stemmed from the investigation and criteria for Pilot Induced Oscillation (PIO) on highly augmented flight control systems on maneuverable aircraft [95]. The Gibson dropback criterion is analyzed in the time domain, where the aircraft receives and pitch rate command reference through a stick deflection from the pilot and is then released. The following parameters are computed to form the criterion:

- The ratio between maximum and steady state pitch rate q_{ss}, q_{max}: $\frac{q_{max}}{q_{ss}}$
- The Difference between the steady-state pitch attitude (θ_{ss}) at stick release, and after it has been released (θ_{release}). This difference is referred to as Dropback (DB) if positive or Overshoot (OS) if negative, which is then divided by the steady-state pitch rate to form the parameter used by the criterion: $\frac{DB(OS)}{q_{ss}}$

These parameters are prescribed to a region, where it relates the criterion parameters to response abruptness, sluggishness, bobbling or satisfactory as shown by the example presented in Figure 4.7.

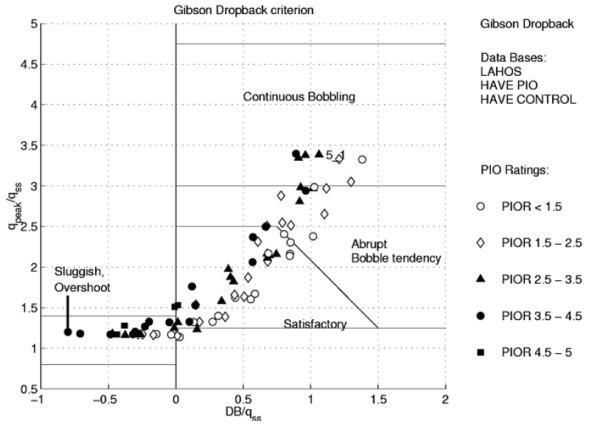

Figure 4.7: Gibson dropback criterion regions with results from three landing databases studies. Taken from [95]

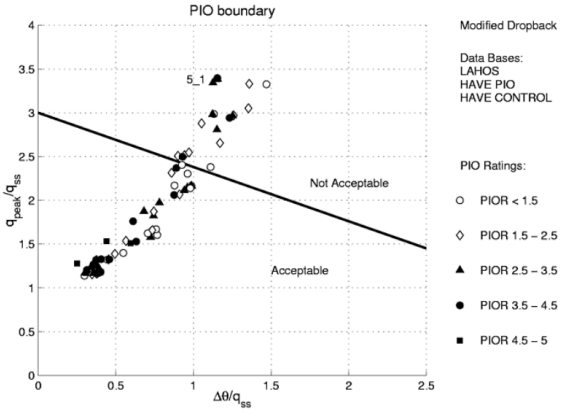

Figure 4.8: Updated Gibson dropback criterion regions with results from three landing databases studies. Taken from [95]

An updated version of the criterion was defined, which improves some shortcomings of the Gibson dropback as the criterion as defined by Gibson is influenced by time delay. Thus, the parameter for the pitch attitude is changed to the pitch attitude dropback, which is the difference between the peak pitch attitude (θ_{peak}) and steady state (θ_{ss}) after the stick has been released. This eliminated the time delay in the dropback parameter and as per the newly defined criterion it cannot be negative anymore, where a region between acceptable dropback and unacceptable dropback is now defined as shown by the example in Figure 4.8. Assessments with the Gibson criterion favor a system with zero DB or OS, meaning that the pitch rate response accurately follows the pitch attitude, which is also important for controlling the flight path of the aircraft [95].
With the Gibson Dropback criterion, the gains are constrained such that they provided desired closed-loop dynamics

The optimal gains will be determined through using the Matlab *fminsearch* optimisation function, where

the evaluation metrics are weighted such that they have the same relative magnitude and importance, and the handling quality constraints will be used as penalization boundaries, which penalizes the determined gains if they go over satisfactory and acceptable dropback boundaries.
This results in a score for a set of gains, where a lower score means that the set of gains satisfy the performance and handling quality criteria optimally. Moreover, the RMS and max error for the gibson dropback criterion is used as evaluation, which leads to faster convergence to an optimal set of gains. This results in the following scoring:

$$\mathrm{SCORE1} = 100 * \mathrm{RMS}(e_{\mathrm{tracking}}) + 10 * \max(e_{tracking}) + 5\mathrm{e}{-3} * \delta_{e_{activity}} \tag{4.35}$$

$$\mathrm{SCORE2} = 100 * \mathrm{RMS}(e_{\mathrm{gibson}}) + 10 * \max(e_{gibson}) + 1\mathrm{e}3 * q_{overshoot_{\mathrm{penalty}}} + 1\mathrm{e}3 * \mathrm{DB}_{\mathrm{penalty}} \tag{4.36}$$

$$\mathrm{SCORE} = \mathrm{SCORE1} + \mathrm{SCORE2} \tag{4.37}$$

$$\tag{4.38}$$

The selection of weights in these scoring functions have been chosen based upon trial and error to result in optimal and fair scoring for all controllers. The optimal gains for the IDI controller will also be used for the AIDI controller. This resulted in the following sets of gains:

Controller	Gains	Score
PI	K_P^{inner} = -4.01 K_I^{inner} = -9.94 K_P^{outer} = 22.88 K_I^{outer} = 13.9	93.1
IDI	K_P = 10.28 K_I = 3.23	91.3

Table 4.3: Optimal gains

4.3. Simulation Results

This section concerns all simulation results for the preliminairy analysis. First the nominal results are observed, where the PI & IDI controllers are compared (4.3.1). Secondly the robustness analysis will be conducted, where PI & IDI controllers are compared and the worst case result will be analysed with the AIDI controller (4.3.2). At last the IDI and AIDI controllers are assesed in various fault scenarios (4.3.3.).

4.3.1. Nominal System Results

The nominal pitch tracking results and results for the Gibson criterion are shown in Table 4.4 and from closer inspection through the pitch tracking error as shown in Figure 4.9, it can be observed that at certain step changes the PI controller error is larger, but they're within order of error as determined by the RMS.

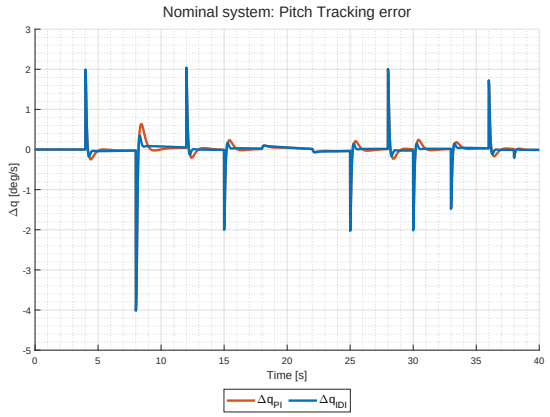

Figure 4.9: PI & IDI: Pitch tracking error

The remaining aircraft states are shown in Figure 4.10, where it can be observed that the pitch tracking reference starts and ends approximately at the same altitude and velocity, moreover as shown in [91], the CE of the elevator on the pitch dynamics changes due to variation in velocity and dynamic pressure as shown in Figure 4.11. Although in the nominal simulation results and robustness analysis, the CE remains constant in the bare-airframe, the variation in CE can be used to simulate a time varying CE to approximate the change as it would appear in non-linear simulation.

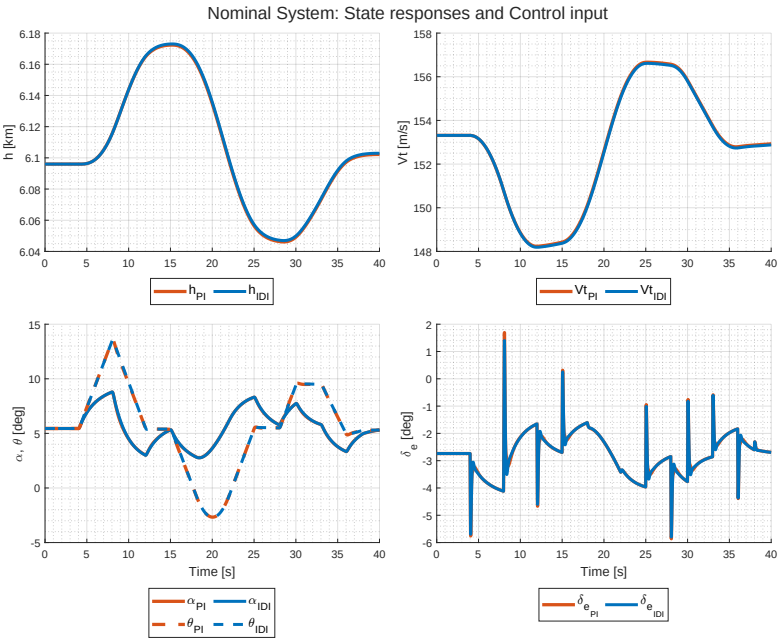

Figure 4.10: PI & IDI: All system states error

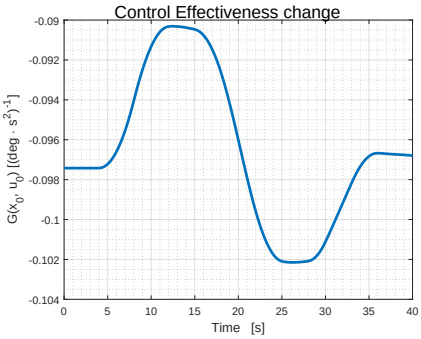

Figure 4.11: IDI: Control effectiveness change

Controller	RMS$(e)_{\text{tracking}}$	$\frac{\mathbf{q_{max}}}{\mathbf{q_{ss}}}$	$\frac{\mathbf{DB(OS)}}{\mathbf{q_{ss}}}$
PI	2.95e−1	1.09	−1.23e−5
IDI	2.88e−1	1.06	3.86e−5

Table 4.4: PI & IDI: Pitch tracking and gibson criterion result

The Gibson dropback criterion results as shown in Figure 4.12 & 4.13 show that both controllers were tuned to be within the satisfactory region.

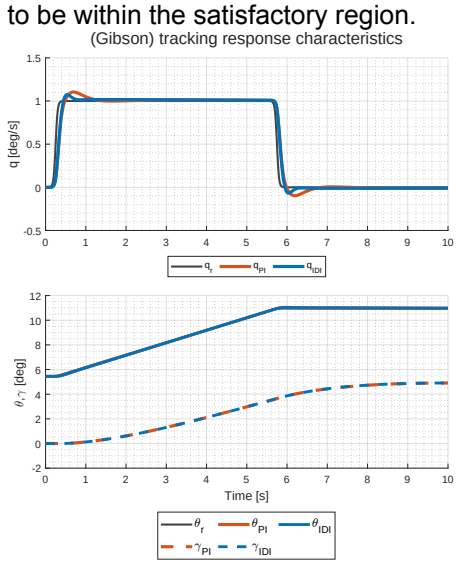

Figure 4.12: PI & IDI: Gibson dropback tracking result

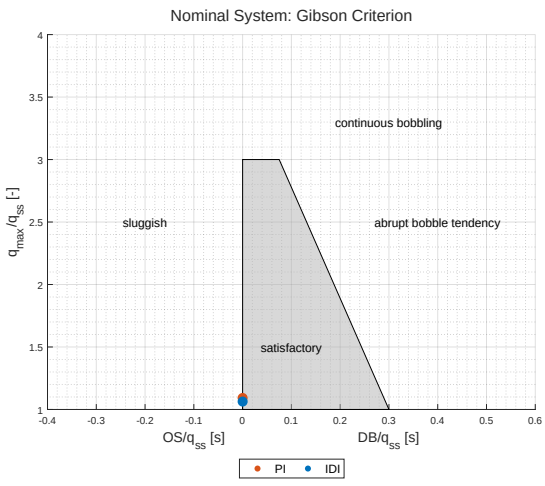

Figure 4.13: PI & IDI: Gibson Criterion result

4.3.2. Robustness Analysis

Robustness is described as the system capabilities to maintain performance when subjected with disturbances or uncertainties. The robustness analysis will be conducted through applying a deviation in the nominal value of state and control derivatives for the pitch dynamics, as expressed in 4.16. This deviation is applied using the *ureal* function in MATLAB to create an uncertain parameter with a $\pm\%$ deviation of the nominal value in magnitude only. Three uncertainty cases are set-up:

- **Uncertain Case (UC) 1**: M_α, M_q may deviate up to $\pm 75\%$
- **Uncertain Case (UC) 2**: M_{δ_e} may deviate up to ± 30 %
- **Uncertain Case (UC) 3**: Combines both UC1 and UC2

These uncertain parameters are sampled using the *usample* function in MATLAB, which randomly samples the uncertain parameter in a uniform distribution. The robustness analysis will thus concern a Monte Carlo simulation where 500 samples are randomly taken. At last, the worst UC case is analyzed using AIDI.

The RMS for all cases are normalized against the nominal RMS performance and the influence of uncertainty is shown in Figure 4.14. It can be observed in all cases, that the PI controller is affected the most from the uncertainty compared to IDI. A higher value of M_q results in a lower RMS compared to the nominal performance due to the control surface having higher effectiveness, but a lower value results in degraded performance, is shown in the second and third case as a wider spread of RMSE is obtained.
For IDI a model mismatch in CE can lead to performance degradation. This is also observed in the tracking response and control surface deflection as shown in Figure 4.15 & 4.16, where higher control surface deflections are required, which could lead to further wear on the actuators.

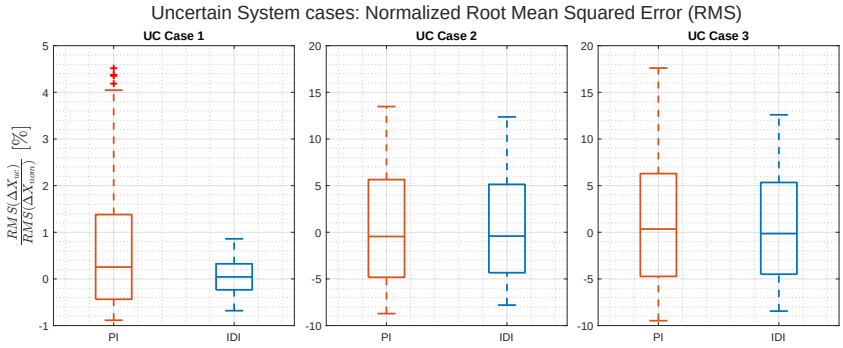

Figure 4.14: PI & IDI: Normalized RMS

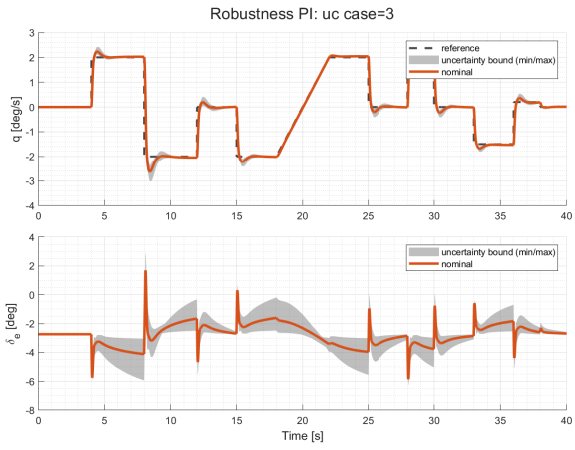

Figure 4.15: PI: UC case 3 tracking response and control surface deflection

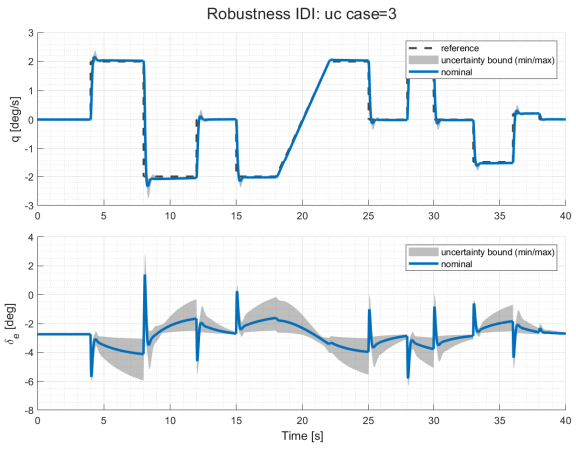

Figure 4.16: IDI: UC case 3 tracking response and control surface deflection

The effect of uncertainty in the Gibson criterion for the three cases is shown in Figure 4.17 & 4.18, where for each case the axes limits are adjusted to observe the spread and effect of uncertainty on the criterion. Here it can be observed that the uncertainty in the state dynamics, as shown in the first case,

leads to OS and outside the satisfactory region of the Gibson criterion. The second case has a linear effect on the criterion, where the IDI controller has the highest change in maximum pitch rate overshoot, which shows how significant the influence of model mismatch has for IDI, whereas PI spreads to more OS or DB. The third case leads to a wider spread. In all cases, it can be observed that the PI controller is the most affected from uncertainty.

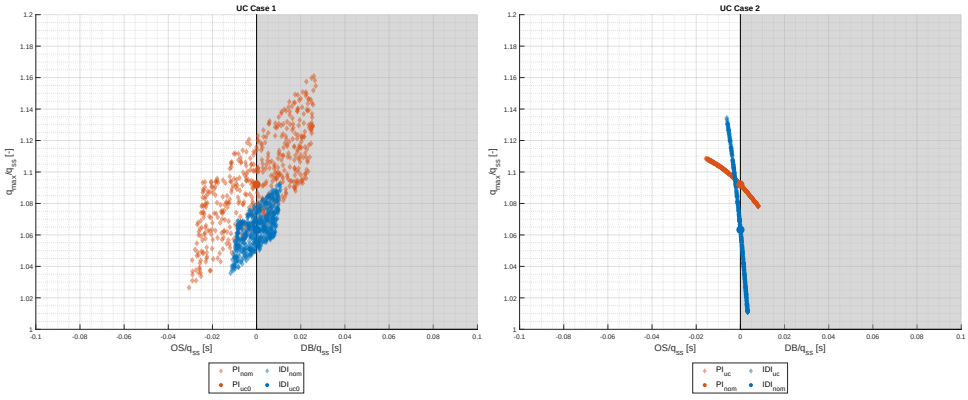

Figure 4.17: PI & IDI: Uncertainty Case 1 & 2 for Gibston Criterion

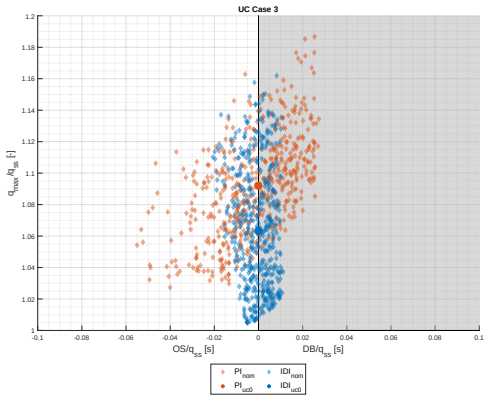

Figure 4.18: PI & IDI: Uncertainty Case 3 for Gibston Criterion

UC 3 is repeated with the AIDI controller and the RMS for the tracking experiment is shown in Figure 4.19, where it can be determined that AIDI has a smaller deviation of RMS, moreover the mean of the RMS is lower compared to the nominal RMS, which shows that the AIDI controller improves the performance. The CE estimation error is shown in Figure 4.20, where RLS is able to adapt and estimate the true CE term.

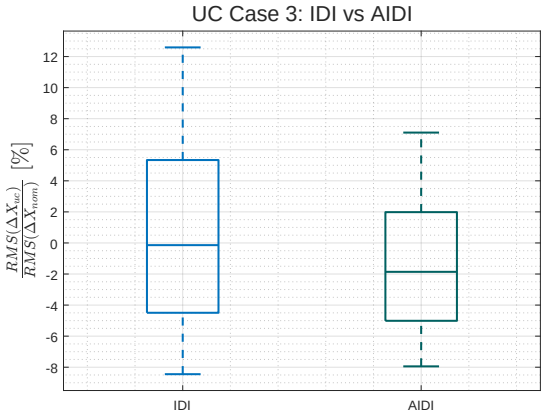

Figure 4.19: IDI & AIDI: RMS for uncertainty case 3

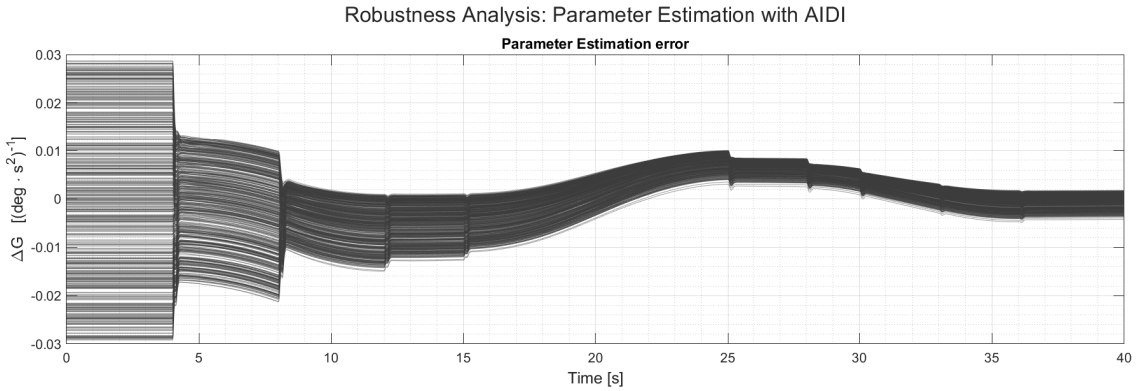

Figure 4.20: IDI & AIDI: Parameter estimation for UC3

4.3.3. Fault-tolerant Analysis (IDI/AIDI)

This section presents several Fault Scenario (FC), where the IDI and AIDI controllers are compared and asses for their fault-tolerance. Several studies have assessed faults with various Moreover, as described in the previous section, the CE for the pitch dynamics in the bare-airframe, the last entry of the B_0 matrix, will now also change during the simulation as this term varies throughout the simulation to more closely approximate the non-linear simulation as presented in [91]. It is shown that the AIDI is able to approximate the true CE of the aircraft as shown in Figure 4.21.
To assess the fault-tolerance of these controllers, three FC are evaluated:

- **Fault Scenario 1**: At $t = 20$ during the tracking experiment, the effectiveness of the control surface is halved, where $B_{fault} = \frac{1}{2}B_0$
- **Fault Scenario 2**: FC1 now also has a disturbance acting on the control surface and measured by the actuator, this signal is shown in Figure 4.22
- **Fault Scenario 3**: At $t = 20$ during the tracking experiment, the control surface will have control reversal and a fault, where now $B_{fault} = -\frac{1}{2}B_0$. The noise as experienced in the previous scenario will also be added

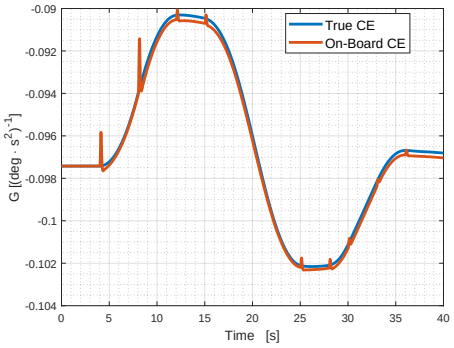

Figure 4.21: True CE v.s. estimated CE

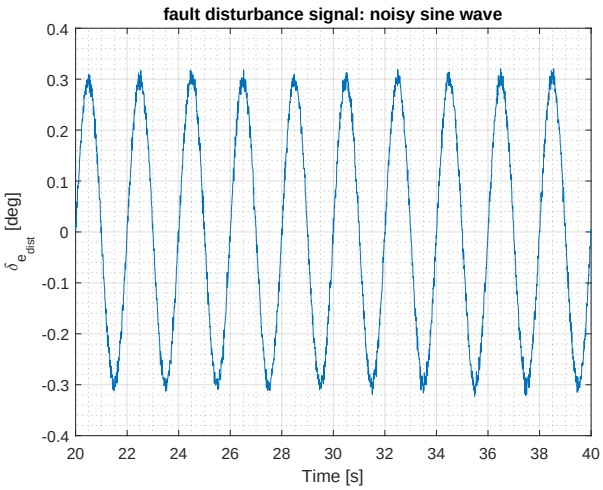

Figure 4.22: Disturbance signal acting on the control surface starting from $t \geq 20$ during the tracking experiment. Noisy sine wave with $u_{\text{dist}}\ 0.3 * \sin(2\pi f t) + 0.01 * \mathcal{N}(0,1)$ with $f = \frac{1}{2}$ Hz

Fault Scenario 1:

The pitch rate tracking comparison is shown for FC1 is shown in Figure 4.23, where it can be observed that both controllers are able to cope with the introduced fault starting and the performance between both controllers are relatively close. However, looking at the parameter estimation as shown in Figure 4.24, the adaptation to the true CE happens at a slow rate. This could be because of the control excitation not being sufficient, as shown in the tracking result, where the signal and control surface isn't

richly supplied with excitation and only upon the step changes the controller adapts.

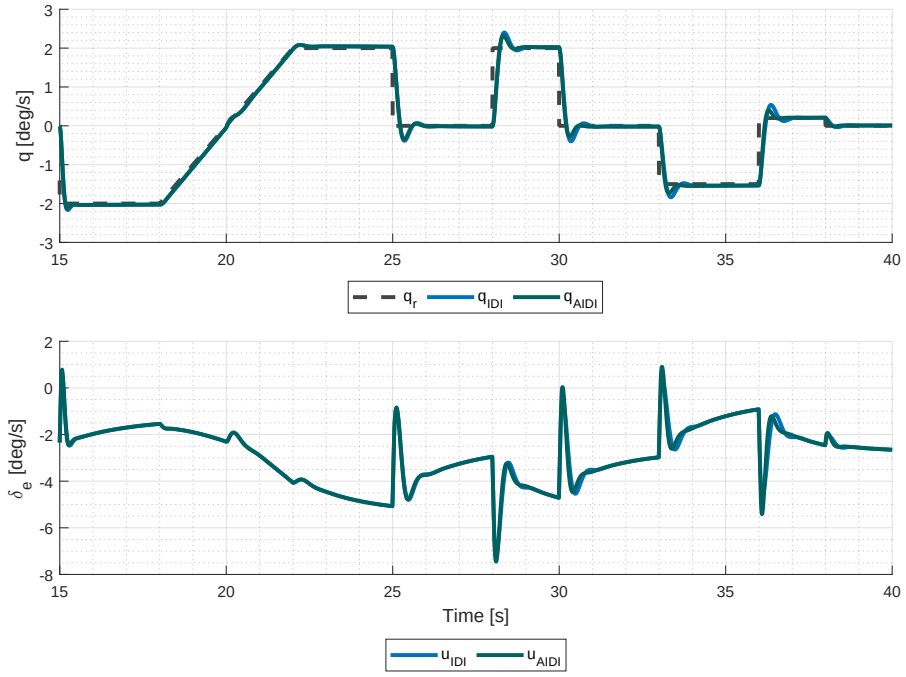

Figure 4.23: FC1: tracking performance $\lambda = 0.9998, P_0 = 100$

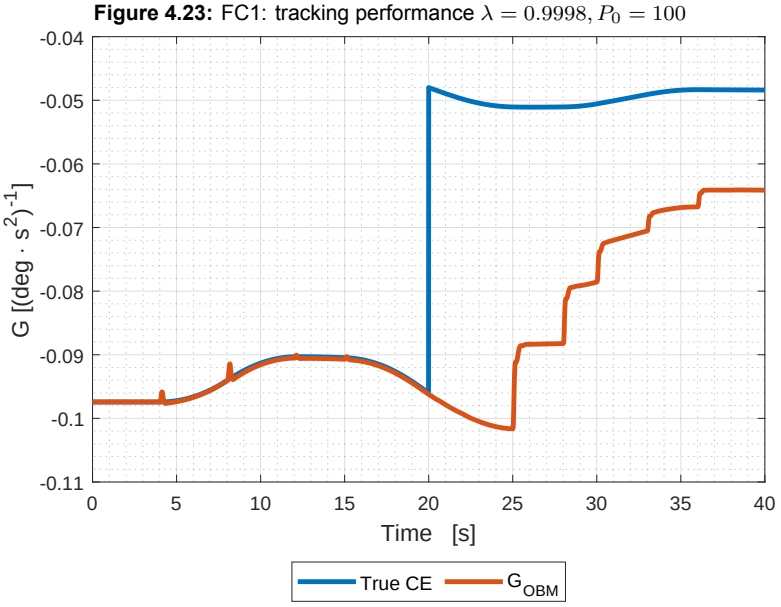

Figure 4.24: FC1: CE parameter estimation with $\lambda = 0.9998, P_0 = 100$

Through trial-and-error it was observed that changing the forgetting factor to $\lambda = 0.995$, results in faster adaptation as shown in Figure 4.25, but going lower than that would lead to oscillation. For the remainder of the fault scenarios, this forgetting factor will be used.

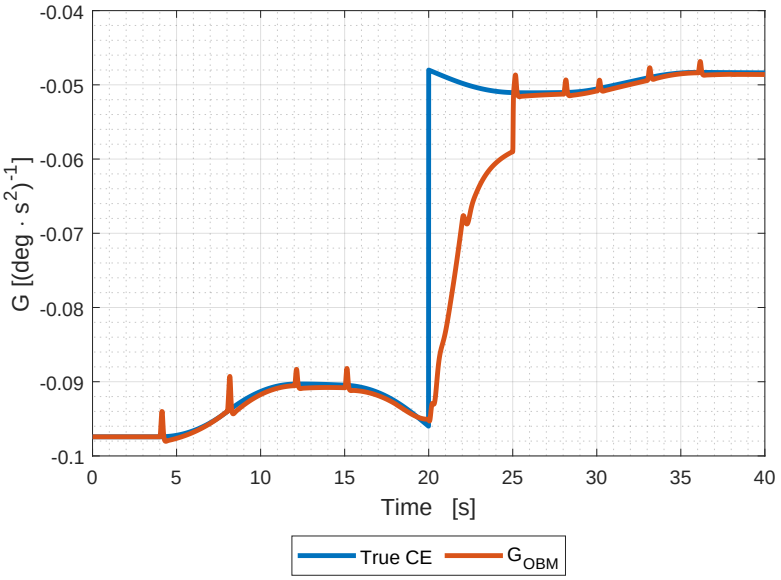

Figure 4.25: FC1: CE estimation $\lambda = 0.995, P_0 = 100$

Fault Scenario 2:
The pitch rate tracking comparison is shown for FC2 is shown in Figure 4.26, where it can be observed that the IDI controller is oscillating more than the AIDI, which is able to reject the disturbance more appropriately. Moreover, the effect of the disturbance and noise doesn't have much influence on the parameter estimation, as shown in Figure 4.27.

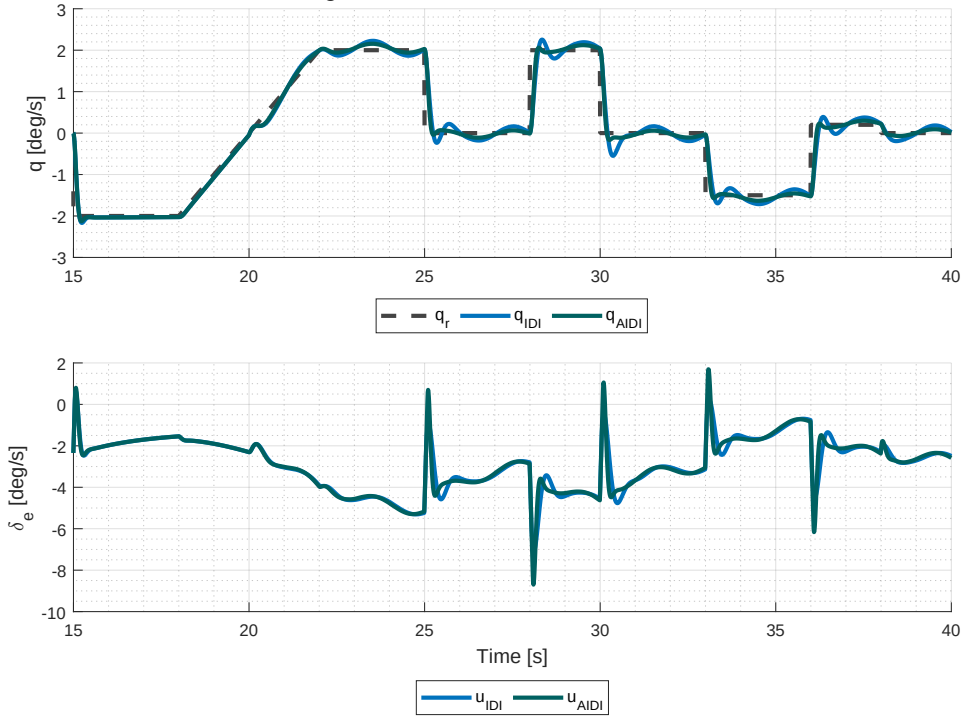

Figure 4.26: FC2: tracking performance $\lambda = 0.995, P_0 = 100$

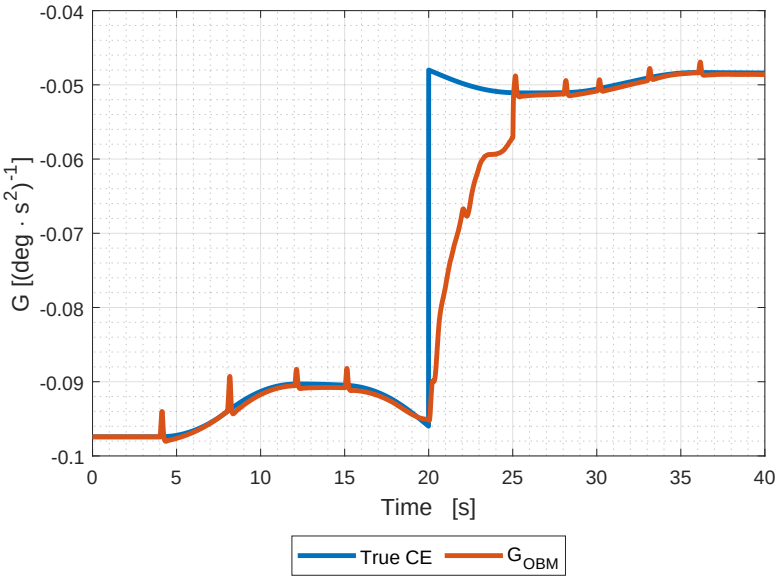

Figure 4.27: FC2: CE parameter estimation with $\lambda = 0.995, P_0 = 100$

Fault Scenario 3:

The pitch rate tracking comparison is shown for FC3 is shown in Figure 4.28, where it can be observed that the IDI controller is now unstable, but the AIDI is able to adapt and keep tracking the reference, while also rejecting the disturbance on the control surface. Moreover, as shown in the CE estimation Figure 4.29, the RLS estimator immediately flips towards the new true CE with the opposite sign and half in value. This is primarily caused, by the instantaneous change and therefore excitation on the control surface as shown in the tracking plot, thus further highlighting the important that the control surfaces needs to be excited sufficiently for the parameter estimation.

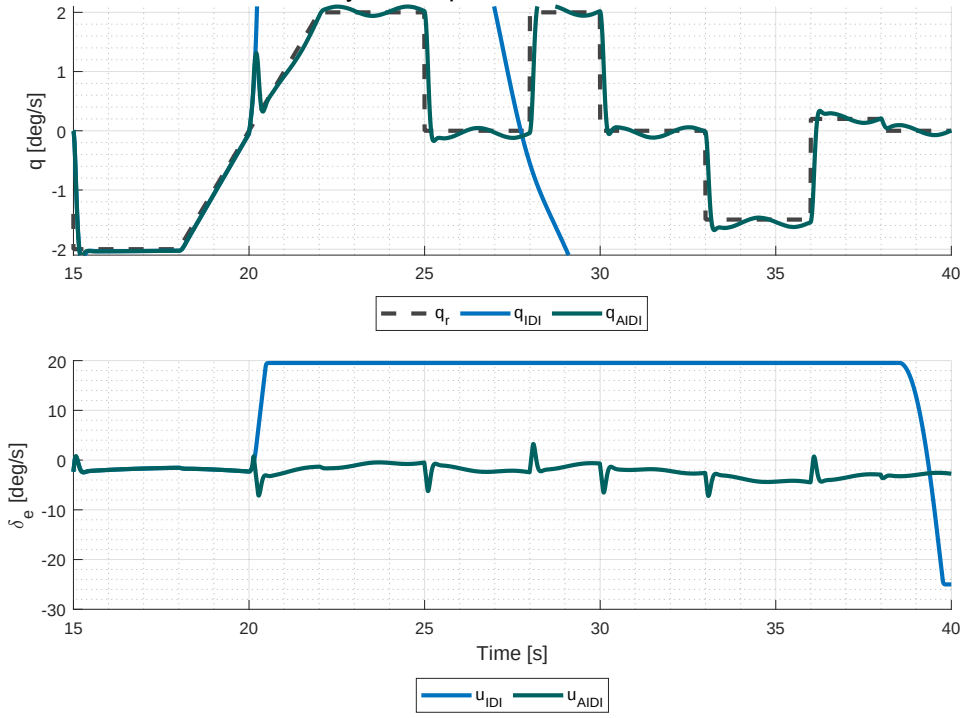

Figure 4.28: FC3: tracking performance $\lambda = 0.995, P_0 = 100$

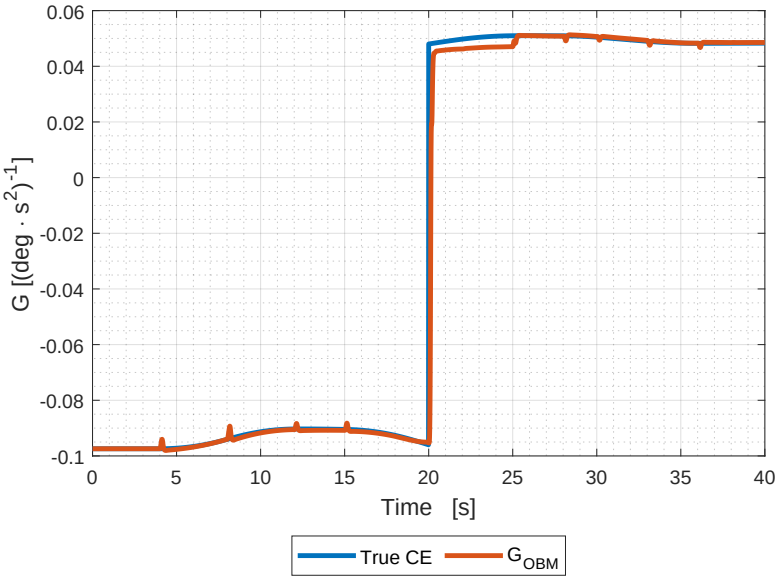

Figure 4.29: FC3: CE parameter estimation with $\lambda = 0.995, P_0 = 100$

4.4. Conclusion

This preliminary analysis has analysed the robustness of an linear control method, PI against a linear version of the INDI control method. It was observed that IDI had higher robustness against parametric uncertainties in the bare-airframe model concerning the states and control input for the pitch dynamics. Moreover, with the use of an adaptive IDI with RLS implementation, the performance degradation was lowered and even improved compared to IDI.
Several fault scenarios have been analysed, where a preliminary answer can be given to this sub research question:

- How does the adaptive FCS cope with faults compared to the non-adaptive FCS?
  - It is observed that when faults are introduced on the control effectiveness, where it is reduced by 50 % control surface, IDI and AIDI are able to keep tracking the reference. Moreover, the control surface also needs to be sufficiently excited to estimate the true CE, which was adjusted by lowering the forgetting factor. Upon the addition of noise and control reversal, it was observed that the IDI controller had degraded in tracking performance and became unstable in the latter situation. Whereas the AIDI was able to keep tracking the pitch rate reference.

5

Literature Research Conclusion

This chapter concerns the discussion and conclusion with the insights gained through the literature study, describing state-of-the-art applications and the preliminary research. Firstly, the main findings and answers for the research questions will be described, thereafter an outline for the application of adaptive incremental Dynamic Inversion (INDI) with RLS for the Flying V is defined, concerning future research steps.

Firstly, the existing literature and research of the Flying V was described, where the following research and sub research questions were answered:

1. What are the results and lessons from previous research on developing the FCS for the Flying V?
   (a) What is the current state of handling qualities of the Flying V?
      - There have been separate assessment for the bare-airframe of the Flying V and the augmented Flying V with an FCS or CA algorithm
      - Bare-airframe: Level 1 & Level 2 with respect to its longitudinal dynamic modes. Level 3 to unstable with respect to the Dutch roll. Experimental simulations reveal unstable behaviour and control saturation.
      - Augmented airframe with FCS: Several FCS using linear control laws and different CA schemes. Simulator experiments and offline experiments with linear flight control laws reveal that the Dutch Roll is still stable and control surfaces saturate. The nonlinear FCS from [23] was shown to stabilise the dynamic modes and provide Level 1 Flying qualities.

   (b) What are the latest developments in aerodynamic modelling for the Flying V?
      - The latest aerodynamic model for the Full-Scale Aircraft is determined by the combination of the VLM model and elements from the WTE, which is able to capture longitudinal instability, pitch break and lateral instability, Dutch roll. At the time of writing, a new Full-Scale Flying V model has been developed for use with the FCS. The Flight Test Experiment needs further investigation and validation against the WTE experiments, before it can be scaled to the Full Scale model.

   (c) What is the current state of the Flying V simulation model?
      - The current Flying V simulation model is developed using the combined aerodynamic model. The FCS for the Flying V is developed with the Nonlinear Incremental Dynamic Inversion (INDI) method with Flight Envelope Protection, white noise, sensor dynamics, time delays and discretisation.

   (d) What assumptions and uncertainty are present in the simulation model of the Flying V?
      - The implemented aerodynamic model is estimated at a limited set of flight conditions and developed from a combination of linear aerodynamic data for the full scale aircraft and nonlinear data of a half-wing subscale wind tunnel experiment, which has limited validity to investigate and observe the aircraft's dynamics across different flight conditions

- Due to the combined aerodynamic model there is an uncertainty in the aerodynamic model and future iteration would require updates of the FCS to cope with this
- There is no engine simulation model that provides the thrust at the various flight condition, but it is computed to achieve the necessary trim at the flight condition
- The sensors have been adjusted to conform to Level 1 flying qualities, and it is unknown if these sensors are available in the industrial market
- The mass, weight and moment of inertia of the aircraft remains the constant during the simulation
- Zero wind and perfect atmosphere

(e) What are the specifications and requirements for that apply to an FCS with an adaptive control method?
- Achieve Level 1 flying qualities
- Achieve satisfactory performance with uncertainties as good or better than the existing simulation model
- Achieve satisfactory tracking performance with fault-tolerant scenarios

2. What evaluation metrics are suitable to assess the adaptive control method for the FCS?
   (a) What are the flying & handling qualities criteria, which have been evaluated with the FCS?
   - Several simulator experiments with linear FCS and offline simulations with nonlinear FCS.
   - CAP, Gibson Tracking, Gibson phase.
   - Different longitudinal and lateral manoeuvres and tracking experiments were conducted.

   (b) What assessment for evaluating uncertainties/delays have been performed?
   - Aerodynamic uncertainty
   - Influence of time delays

From the literature study towards nonlinear & adaptive control methods, it was determined that the chosen method is adaptive INDI with Recursive Least Squares (RLS), the following research (sub)-questions are answered:

- What advancements have there been in the applications of nonlinear & adaptive methods?
  - Nonlinear control methods such as Backstepping and Nonlinear Dynamic Inversion have been applied in various simulation studies, whereas the latter has real world application on a high performance fighter jet. However, notable drawbacks from its requirement of accurate model knowledge is not always feasible due to significant effort required in flight testing and real-world phenomena such as noise, external disturbances influence the system dynamics. The development of Incremental Nonlinear Dynamic Inversion and Incremental Backstepping thereafter, resulted in nonlinear control techniques, which required less model knowledge as only control effectiveness is required and the feedback of system dynamics is replaced by sensor dynamics. Moreover, it has better robustness against uncertainties and disturbances compared to its non-incremental versions. This has been verified and validates through multiple simulation studies and real world applications on CS-25 class aircraft, drones, VTOL. Some drawbacks are encountered as noise and measurement time delays increase, where INDI specifically has been augmented with filters to result in a Hybrid INDI technique. When model uncertainties and especially control effectiveness uncertainties are significantly large, it can lead to degradation in performance. Thus, adaptive schemes for these nonlinear control methods allow for sophisticated way to deal with these uncertainties and various reconfigurable controllers have been developed for fault-tolerant control.

  1. What methods have been implemented for fault-tolerant control?
     - Incremental Backstepping and Incremental Nonlinear Dynamic Inversion have shown to passively reject actuator faults and compensate for these faults. Adaptive BS and NDI have seen various successive applications to maintain safe flight in the presence of sensor, actuator, and engine faults.
  2. What method is the most suitable for fulfilling the requirements for the Flying V?
     - As identified from the literature research, adaptive INDI is suitable as it preserves the current control architecture design while advancing it to fault-tolerant control.

In the preliminary analysis, the following three different controllers were designed for pitch rate control:

1. Linear control: Proportional-Integral
2. Linear version of INDI, called IDI
3. Adaptive IDI with RLS

With these controllers an robustness analysis was performed, where parametric uncertainties in the pitch dynamics were introduced, after that fault scenarios, where the control effectiveness of the control surface was reduced, were analysed. It was determined that in all cases the adaptive IDI was able to have less performance degradation and cope with the faults. The following answer could be partially answered based on the insights gained during this analysis:

- How does the adaptive FCS cope with faults compared to the non-adaptive FCS?
  - It is observed that when faults are introduced on the control effectiveness, where it is reduced by 50 % control surface, IDI and AIDI are able to keep tracking the reference. Moreover, the control surface also needs to be sufficiently excited to estimate the true CE, which was adjusted by lowering the forgetting factor. Upon the addition of noise and control reversal, it was observed that the IDI controller had degraded in tracking performance and became unstable in the latter situation. Whereas, the AIDI was able to keep tracking the pitch rate reference.

With the literature research completed, an outline of steps is defined towards the applications of adaptive INDI for the Flying V, where certain activities are described. The FCS used for the future research is the current FCS with FEP as defined by the study of Stougie et al.

Step 0 - Preparation At the time of writing a new aerodynamic model has been provided as mentioned in the literature study of the Flying V research. This new model will give new aerodynamic estimates and characteristics. The existing FCS used for the Flying V needs to be updated This step concerns the work in preparation for the next step, which represents the main work of the research. The follow activities are conducted:

1. The *new* (RANS) aerodyanmic model is implemented into the simulation model
2. (lower-level priority) Linearize the aircraft dynamics and observe the aircraft dynamics with the newer aerodynamic model to observe the changes in dynamic modes
3. Update the trim routine to work with the new aerodynamic model
4. Update control gains using the existing tuning procedure

Certain activities can be done concurrently with the other steps

Step 1 - Adaptive INDI (inner loop) The current FCS has an inner loop where INDI has been applied for rate control. The chosen implementation concerns adaptive INDI ith RLS, which is applied in the inner loop where the principal elements will reside for the adaptive control:

1. On board model
   - The control effectiveness ($\frac{C_i}{\delta_j}$) can be modelled through a polynomial model with fixed regressors, whose selection are based upon the existing knowledge of the aerodynamic model
   - The selection of a polynomial model was determined on the basis of current understanding of the aerodynamic data of the Flying V, which have been effectively modelled through polynomial models
2. Adaptation mechanism
   - The adaptation mechanism is done through parameter estimation of the control effectiveness, whereby Recursive Least Squares (RLS) is chosen given its successful applications in online adaptive flight control and fault tolerance control design. The identification of the control effectiveness is done using the jacobian of the aircraft dynamics w.r.t. control surfaces ($\frac{\Delta \dot{p}}{\Delta \delta_j}, \frac{\Delta \dot{q}}{\Delta \delta_j}, \frac{\Delta \dot{r}}{\Delta \delta_j}$)
3. Design for control surface excitation and rich signals for reference tracking and identifying the CE terms

The following activities are conducted:

1. Adaptive INDI is implemented
2. The selection of excitation for the identification of control effectiveness parameter

3. The assessment of adaptation is done through flying the aircraft at various flight conditions and observing if the adaptation identifies the appropriate value
4. The tracking performance of the implemented adaptation loop is assessed
    - Inspired from existing literature and previous research activities of the Flying V
5. Fault scenarios are conducted to observe how the adaptive INDI is able to cope with these faults

The polynomial model that's determined within this step is stored and used for the implementation in the adaptive FCS

Step 2 - Extension to outer loop Evaluate the adaptive FCS, which include the flight controller blocks, FEP and sensor dynamics, through the following activities

1. See how the adaptive control algorithm copes with sensor dynamics (noise, bias)
2. Tracking performance tasks, which have been conducted in previous studies, are used to observe the improvements
3. Assessment of select handling qualities of interest, some of which may not have been conducted in previous FCS studies (e.g. Dropback Criterion)
4. Fault scenarios are conducted to observe how the adaptive FCS is able to cope with these faults and how it compares to the non-adaptive FCS

Part III

Additional Results

6

Additional Results

This chapter describes the results generated to obtain the main research contribution as described in the paper, in addition to additional results to further give insight on the research conducted in the thesis. Firstly the description of the new simulation model is defined (6.1), which formed around a new aerodynamic model used in this research, this newer model demanded an updated trim procedure and tuning routine the control gains with the handling quality results at last. At last additional simulation results (6.2) are given

6.1. New Simulation Model

The simulation model used for this research is based upon the latest development of FCS for the Flying V as described in [23, 96]. The aircraft parametric design and aerodynamic model has since then received multiple revisions [9, 44, 97, 98], and will be used to form the basis of a new simulation model that's used in this research. The decision to develop a new simulation model is made due to many aspects of the previous code requiring significant overhaul for the use of this research. Moreover, certain errors have also been identified and corrected in previous research using this model [99].

The aircraft parameters concerning mass and CG are established in [9], with a family optimised Flying V, FV-1000 aircraft, which defines a Maximum Take-off Weight (MTOW) of 266 tonnes and a Maximum Landing Weight 76% of its MTOW. The family optimised FV has also been further researched with the study regarding stability and control [97] and the optimisation of fuel-burn and control authority. A safe range of CG positions was determined to guarantee stability and control during flight. The most forward (longitudinal) position of CG with MLW is at approximately 28.5m, distanced from the nose, and 29.1m at MTOW, the most aft position is 30.1m, as illustrated in Figure 6.1. The approach speed for the FV-1000 is established at 76 $\frac{m}{s}$, which was set at 68.62 $\frac{m}{s}$) in the previous research [100].
The moment of inertia was determined through a lumped mass method as established in [34], which is a source of uncertainty, as it has not been updated in the research with the newer geometry. The mean aerodynamic chord ($\bar{c}$) is 18m, the surface (S) is 898 m^2 and the span (b) is 65 m.

6.1.1. Updated Aerodynamic Model

The aerodynamic model is from an early iteration of the study in [98], and is derived from a combination of RANS and VLM simulations at various flight envelope points from Mach (M) 0.2 to 0.7 with height (h) 0m to 9750m, as shown in Figure 6.2, at various CG positions. The flight envelope now defines more points with the aim to capture the necessary datapoints to describe a step-climb from takeoff to cruise and at last approach. Thus with a more readily available dataset the approach and cruise condition can be interpolated or extrapolated respectively. It was also identified that the pitch-break up is present at a lower α of 11 deg, and decreases at higher altitude and Mach numbers. The model is delivered look-up table for force and moments in the body frame and consists of the dependencies as shown in Table 6.1.

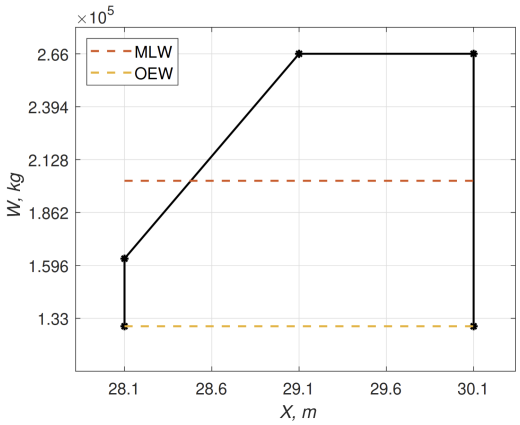

Figure 6.1: Dimensional Center of Gravity (CG) and aircraft weight loading. Taken from [98]

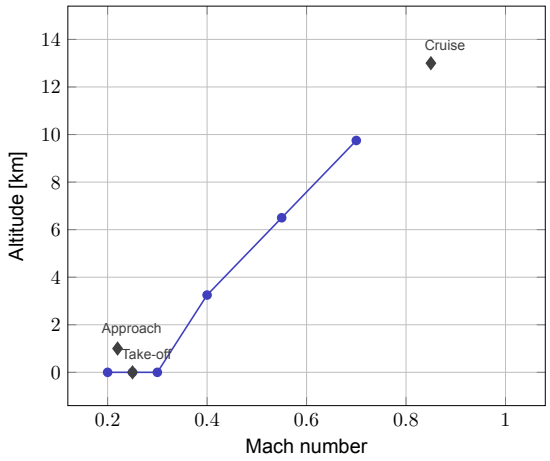

Figure 6.2: Aerodynamic model, flight envelope points. The Diamond points indicate the approach and cruise flight condition, which will be interpolated/extrapolated respectively

at: M & h	α	β	$\hat{p}$	$\hat{q}$	$\hat{r}$	$\delta_{e_{i/o}}$	$\delta_{a_{i/o}}$	δ_r
C_X	r					r	r	r
C_Y		r			v		r	r
C_Y	r			v		r		
C_l		r	v		v		r	r
C_m	r			v		r		
C_n		r	v		v		r	r

Table 6.1: Force and moment aerodynamic coefficients, r and v denotes RANS and VLM simulations respectively, and *i* denotes inner elevon and *o* outer elevon. Adapted from [98]

The aerodynamic coefficients for the control surfaces, are modeled as ganged control surfaces as elevator deflection (δ_e), aileron deflection (δ_a) for the inner and outboard elevons. These respective aerodynamic coefficients will be split seperately for each control surface with the assumption is made that the deflection of a single elevon will account for 50 % of the performance brought by the deflection of either both, as elevator, or asymetrically, as aileron. The rudders on each winglet will still be defined as a single control input in the model.

6.1.2. Trim Procedure

As the newer aerodynamic model describes a larger envelope of flight conditions a new trim routine has been developed, due to the older trim routine not able to provide a steady-state trim as described in [99]. Acquiring a trim is of high importance for the linearisation of the non-linear dynamics, upon

which the tuning and handling qualities are determined upon.
In the trim routine, The aircraft is considered to be in a nominal condition with all engines functioning, no crosswind or gust. The trim function accepts the following inputs:

$$\text{Trim input} = \begin{bmatrix} u_b & \alpha & \delta_a & \delta_e & \delta_r & T1 & T2 \end{bmatrix}^T \tag{6.1}$$

The cost function is defined as following:

$$\begin{aligned} \text{Cost} = W_{\dot{h}}\dot{h}^2 + W_{\dot{u}}\dot{u}^2 + W_{\dot{v}}\dot{v}^2 + W_{\dot{w}}\dot{w}^2 + W_{\dot{p}}\dot{p}^2 + W_{\dot{q}}\dot{q}^2 + W_{\dot{r}}\dot{r}^2 \\ + W_{\dot{\phi}}\dot{\phi}^2 + W_{\dot{\theta}}\dot{\theta}^2 + W_{\dot{\psi}}\dot{\psi}^2 \\ + W_V(V_{ac} - V_{ref})^2 + + W_T(T1 - T2)^2 + W_\gamma(\gamma_{ac} - \gamma_{ref})^2 \end{aligned} \tag{6.2}$$

The aircraft is trimmed for straight-and-level flight and is trimmed until all state derivatives are as small as possible. The trim analysis results are shown in Table 6.2 is conducted with the following conditions:

- Bare-airframe
- $V = V_0$
- $h = h_0$
- $\phi = \psi = \beta = 0$
- $p = q = r = 0$
- Each trimmed steady-state is simulated for 300 seconds (5 minutes) to observe its trimmed state behaviour
- Center of gravity in forward position or aft position
- A MLW of 202160 kg is used for the approach flight condition and a MTOW of 266000 kg is used for all other flight points
- Maximum α of 25 deg.

Flight condition	Mach	Cost	V_{trim} [m/s]	α [deg]	δ_{CS} [deg]	T [kN]
	Forward CG					
Takeoff	0.20	2.41e-13	68.06	21.98	-0.69	525.08
	0.25	3.14e-11	85.07	14.04	-2.64	210.33
	0.30	5.49e-13	102.08	9.56	-6.25	83.79
Approach	0.23	5.14e-13	77.37	14.76	-4.16	168.02
	0.30	2.42e-13	100.93	8.37	-7.05	53.68
Cruise	0.85	4.52e-11	250.80	6.32	-3.60	107.34
	Aft CG					
Takeoff	0.20	1.04e-11	68.06	20.75	5.19	501.59
	0.25	3.49e-13	85.07	13.17	0	202.02
	0.30	4.04e-14	102.08	8.91	-3.63	94.18
Approach	0.23	1.94e-12	77.39	13.76	-4.16	156.14
	0.30	2.61e-13	100.93	7.49	-3.44	71.31
Cruise	0.85	8.21e-13	250.80	5.89	-1.94	104.94

Table 6.2: Trim results for all conditions

The trim results given an overview of the steady-state trim for level wing flight, the overall trend is that at forward center of gravity the required angle of attack and control surface deflection is higher, however at the takeoff condition with an aft center of gravity a pitch down moment is induced, which requires a positive (downwards) deflection to counteract, whereas at other flight conditions the aircraft exhibits a pitch-up, which requires a negative (upwards) deflection to counteract.
With the trim a linearised state space can be derived, whereby a steady-state simulation is performed up to 300s. Here it can be observed that as the aircraft is flying slower and is near the pitch break, which acts earlier at lower velocity at the respective flight conditions, dynamic instability occurs as as shown in Figure 6.3, thus requiring further stability augmentation systems for safe and operable flight at this flight condition. At higher velocities, the steady state trim is stable, below the pitch-break up, and only a small numerical perturbation is observed Figure 6.4.

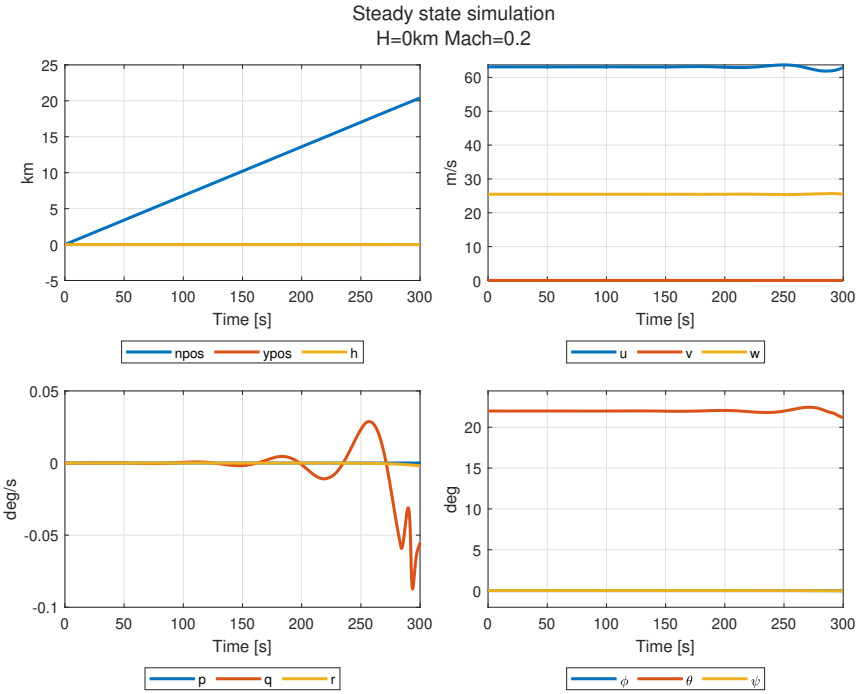

Figure 6.3: Steady state trim of takeoff at Mach=0.2 with fwd CG

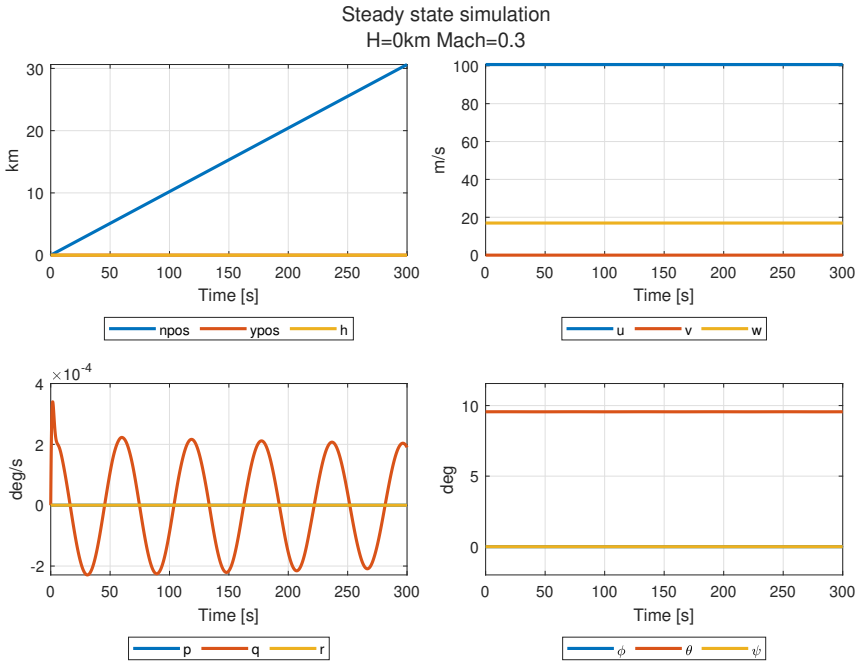

Figure 6.4: Steady state trim of cruise at Mach=0.3 with fwd CG

Linearization Verification & Bare-airframe Dynamic Modes

With the trim obtained, a linearization of the aircraft dynamics is conducted, whereby the dynamics are decoupled into longitudinal and lateral dynamics to analyse the eigenvalues, which are plotted in Figure 6.5 & 6.6.

With respect to Approach and Cruise condition, it can be determined that the phugoid mode is stable, but near the origin and the right half pole plane, whereas the short period is stable. For takeoff the dynamic mode for phugoid is unstable. This is valid for forward and aft center of gravity. The lateral modes, reveal that the Dutch Roll is also very near the origin and right half pole plane, with an unstable

spiral.

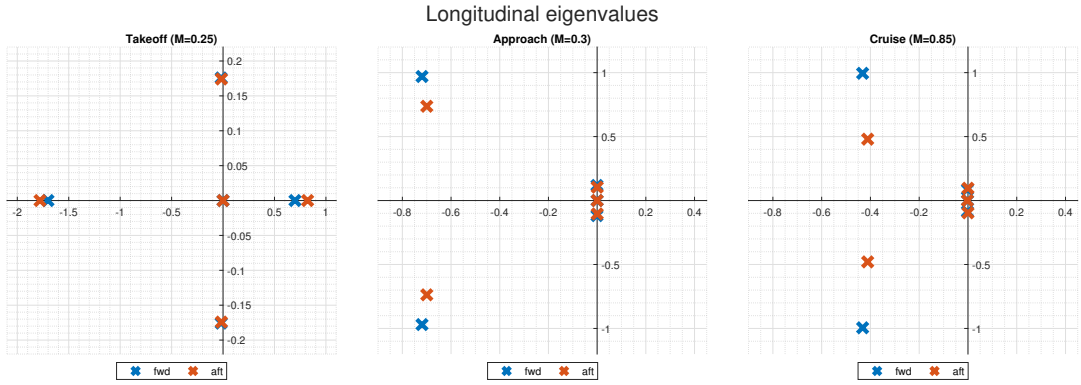

Figure 6.5: Longtiudinal eigenvalues at forward and aft centre of gravity for three flight conditions

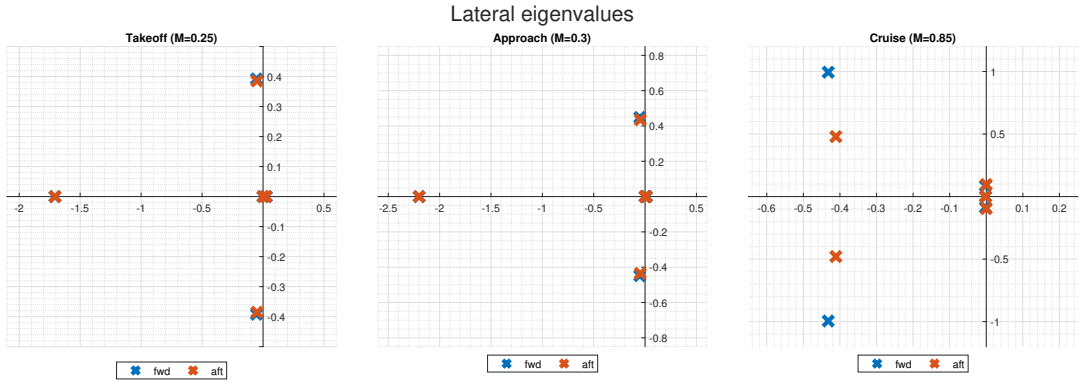

Figure 6.6: Lateral eigenvalues at forward and aft centre of gravity for three flight conditions

To get a sense of the characteristic of the dynamic mode, an excitation can be introduced. This is done by a step input on the inboard elevons ($CS1_L$ & $CS1_R$) for the longitudinal dynamics, and an asymmetric elevon block input and rudder input for the lateral. The excitation also serves as a linearization verification to observe how closely the linearized state space and decoupled state space match the dynamics of the nonlinear system. This analysis for the approach and cruise condition respectively with a forward center of gravity and the nonlinear, linearized state space and decoupled state dynamics are simulated respectively shown in Figure 6.11 & 6.12 for Longitudinal dynamics and

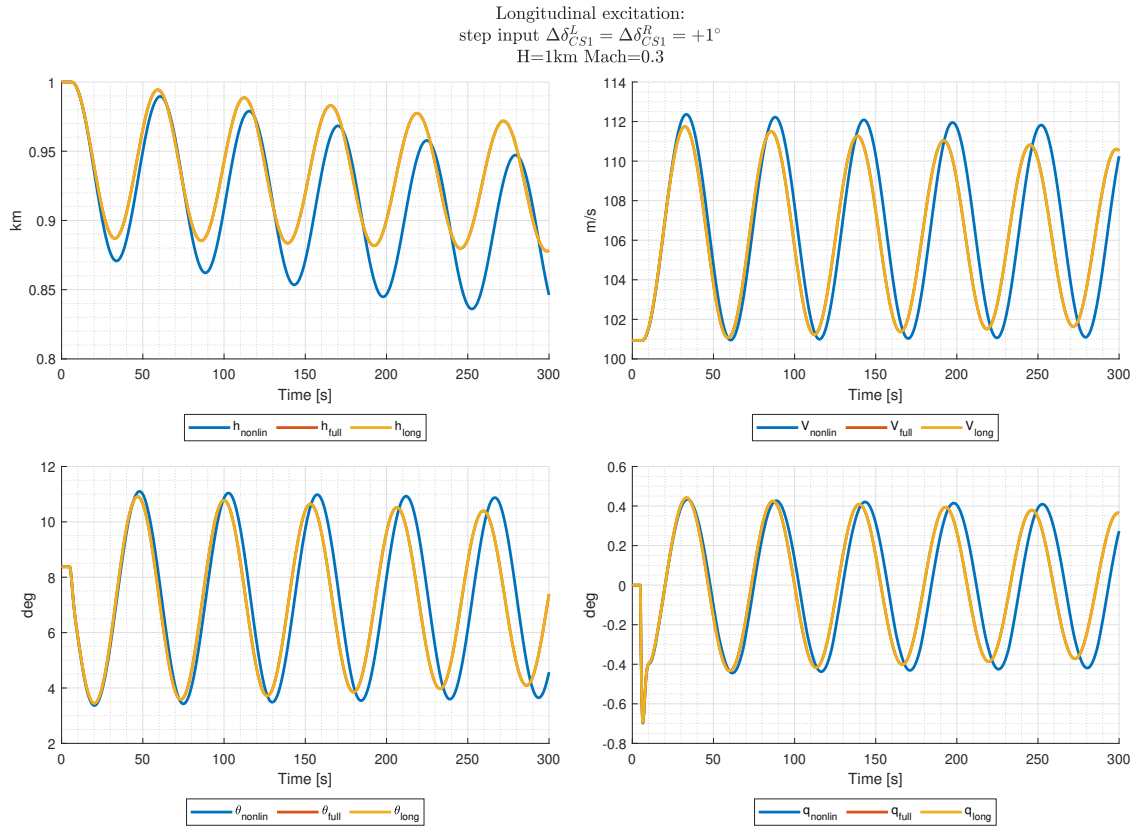

Figure 6.7: Longtiudinal excitation at forward CG for approach

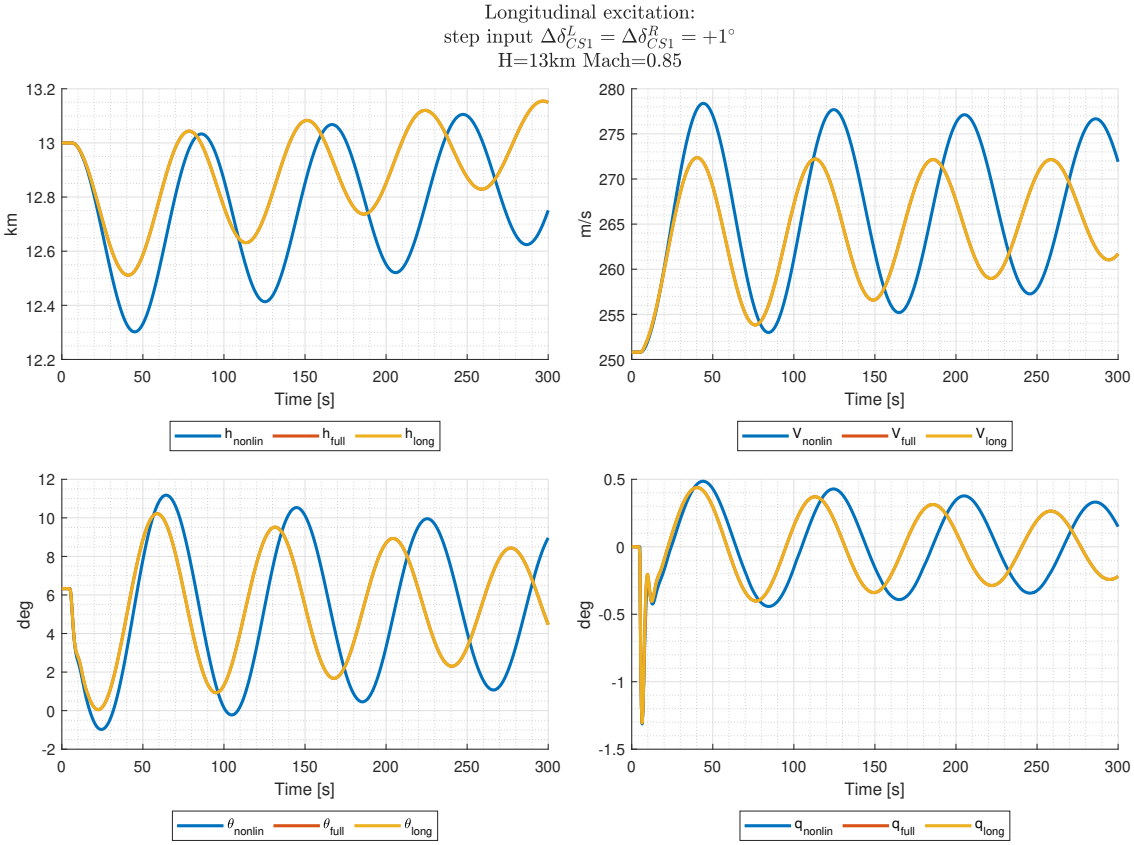

Figure 6.8: Longtiudinal excitation at forward CG for cruise

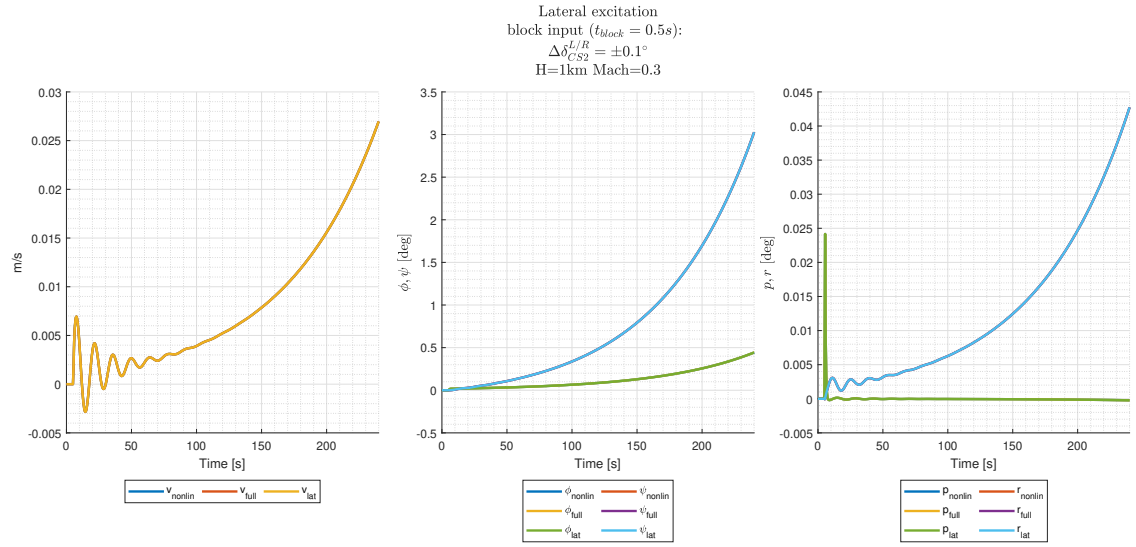

Figure 6.9: Lateral Excitation at forward CG for approach with asymmetric elevon input

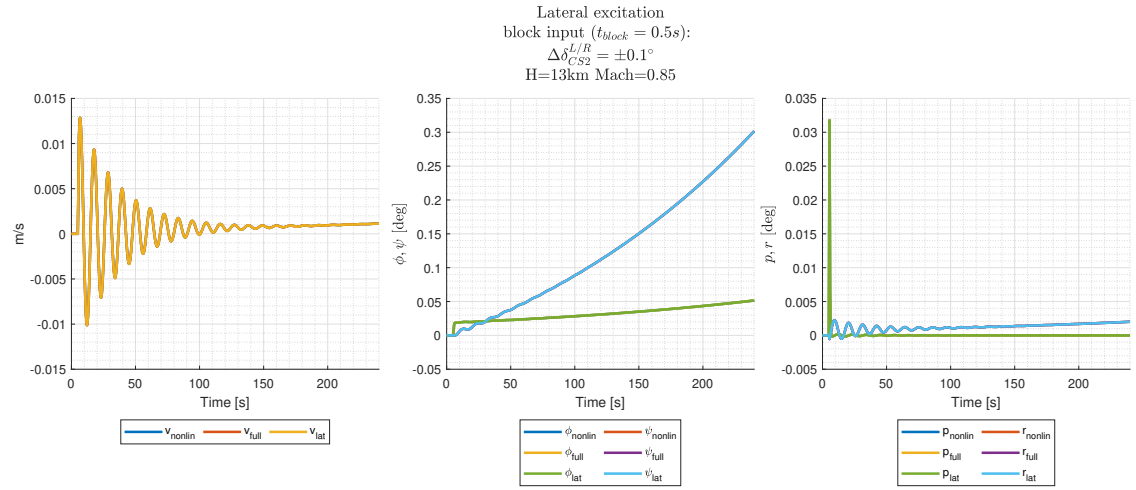

Figure 6.10: Lateral excitation at forward CG for cruise with asymmetric elevon input

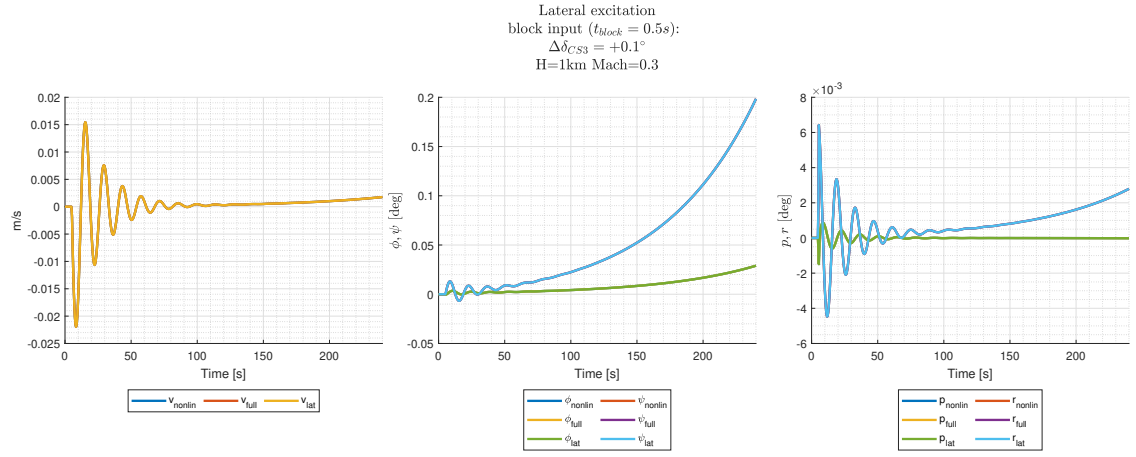

Figure 6.11: Lateral Excitation at forward CG for approach with rudder input

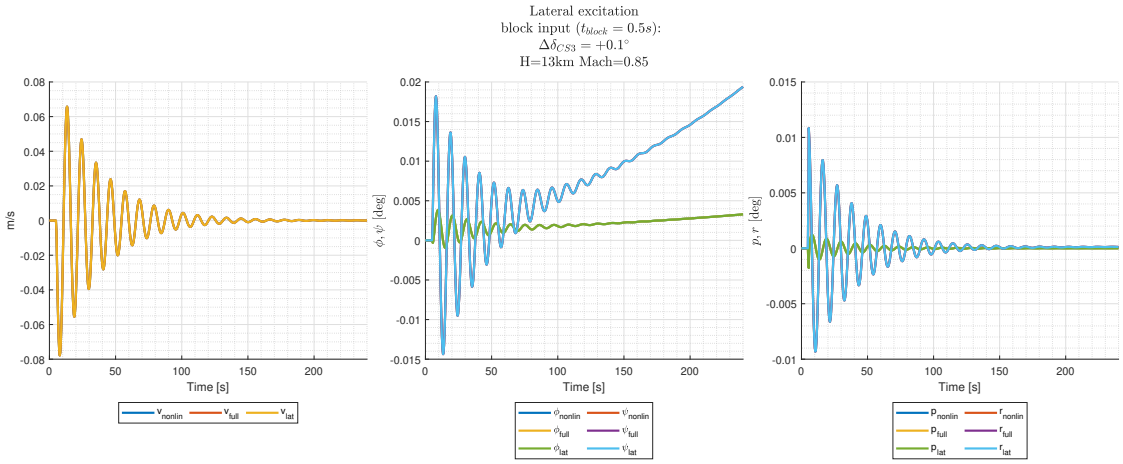

Figure 6.12: Lateral excitation at forward CG for cruise with rudder input

For the longitudinal excitation, it can be observed that the short period quickly damps, but the phugoid is underdamped and remains oscillatory, the lateral excitation reveals a Dutch roll that's stable, but the dynamics diverge due to the unstable spiral.

6.1.3. Sensor Dynamics

The sensors used in the Flying V simulation model are based upon the description provided in [96, 101], which based its sensor parameters on the specifications used in [70]. As the baseline sensor parameter specifications wouldn't obtain level 1 handling qualities for the Flying V, some adjustments were made to obtain that and it is assumed that such sensors characteristics are obtainable. The sensor characteristics used for this research are shown in Table 6.3. Additionally noise and bias is also added to the control surface output, and these are assumed to be available from the actuators.

State	Noise (σ)	Bias	Delay [ms]	Sampling rate [Hz]	Filter time constant
p, q, r [rad/s]	1.5×10^{-9}	3.0×10^{-5}	50	100	0.04
ϕ, θ, ψ [rad]	$1.0 \times 10{-}9$	4.0×10^{-3}	50	50	0.05
f_x, f_y, f_z [rad]	1.5×10^{-5}	2.5×10^{-3}	100	50	0.05
α, β [rad]	7.5×10^{-8}	3.0×10^{-3}	100	100	0.05
h [m]	4.5×10^{-3}	8.0×10^{-3}	150	20	0.05
V [m/s]	8.5×10^{-4}	2.5	150	20	0.05
δ_{CSi} [rad]	1.5×10^{-9}	2.5×10^{-5}	-	100	-

Table 6.3: Sensor parameters, based on [70]

6.1.4. Actuators

The elevon and rudder actuator dynamics in the previous simulation model used actuator parameters were derived from more agile aircraft's [101], and it is desired to use actuator parameters that match a passenger aircraft more closely. Thus actuator parameters of an B747 simulation model, which are derived from the parameters in [102, 103] and are defined in Table 6.4. The limits of the control surfaces were not changed.

The control surface actuators are modelled as a 2nd order system:

$$H_{act} = \frac{\omega_0^2}{s^2 + 2\zeta\omega_0 s + \omega_0^2} \tag{6.3}$$

The engine is modelled as a first order system with a maximum thrust of 379 kN [101]:

$$H_{eng}(s) = \frac{1}{0.2s + 1} \tag{6.4}$$

	Inboard and outboard elevons ($\delta_{CS1}^{L/R}$ & $\delta_{CS2}^{L/R}$) min,max	Rudder ($\delta_{CS3}^{L/R}$) min, max
Position limits ($\dot{u}$) [deg]	-25,25	-30,30
Rate limits (u) [deg/s]	-40,40	-45,45
Natural frequency (ω_0) [rad/s]	35	35
Damping coefficient (ζ) [-]	0.8	0.8

Table 6.4: Control Surface actuator limits and actuator parameters

6.1.5. Gain Tuning Results

The tuning of the gains in the outer loop control blocks are done through a multi-objective optimisation, extensively described by Stougie [23]. However, tuning was done through trial-and-error with random sampling of gains until various objectives were minimized and constraints were satisfied.
The tuning routine has been modified to use *PatternSearch* in MATLAB™and longitudinal and lateral gains have been tuned for the new aerodynamic model for the Takeoff, Approach, and Cruise conditions at a forward and aft CG as outlined in Table 6.5. The details of the handling criterions were elaborated in Section 2.3.1 and in summary are taken from:

- The MIL-STD-179A flying and handling quality requirements [54, 55, 95]
  - Dynamic modes
  - Control Anticipation Parameter (CAP) [104, 105]
  - Gibson dropback [104]
- Stability margins [106] computed at the broken loop location just before the INDI control law input as done by [23]
- Low Order Equivalent System (LOES) fit [54, 107]
- Attitude bandwidth for longitudinal control [105, 108]
- Tracking performance with block inputs

Flight Condition	Mach speed [-]	Height [km]
Takeoff	0.25	0.0
Approach	0.30	1.0
Takeoff	0.85	13.0

Table 6.5: Tuned flight conditions

An example of the PatternSearch algorithm output is presented in Figure 6.5, where several iterations are presented of the objective score value for several iterations, where at each iterations an population of 16 sets of gain parameters are evaluated, which thereafter converges to the optimal set of gains. To limit the wide exploration of gain values a limit of the maximum and minimum gains are set, which is [-20,20] respectively. The output of the gain values and minimization of the handling and tracking quality objectives is shown in Figure 6.14 to 6.16. An handling quality objective is completely satisfied when its Score reaches 0 (or set as a very small value for the logarithmic scale), but it has been observed during the optimisation that not all objectives can fully be satisfied.

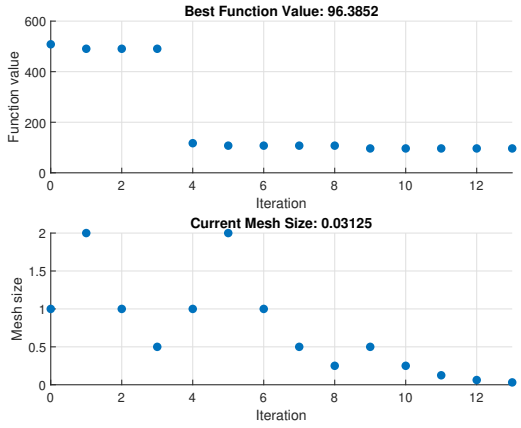

Figure 6.13: Patternsearch training result example

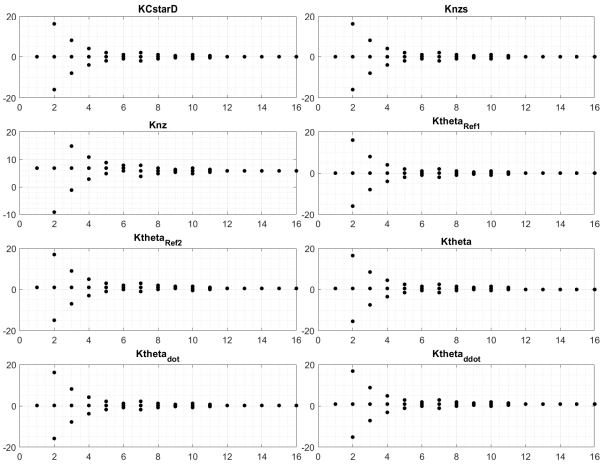

Figure 6.14: Gain Score training

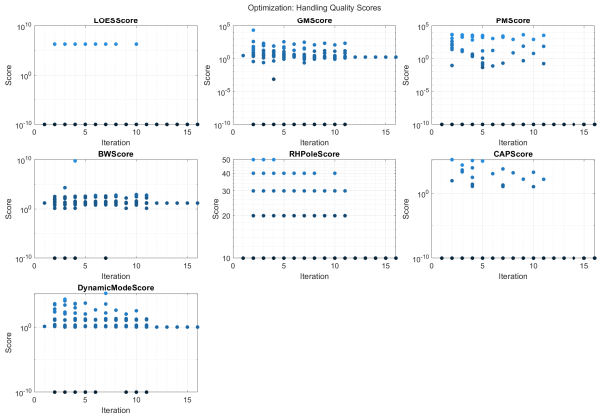

Figure 6.15: Tracking Quality score result

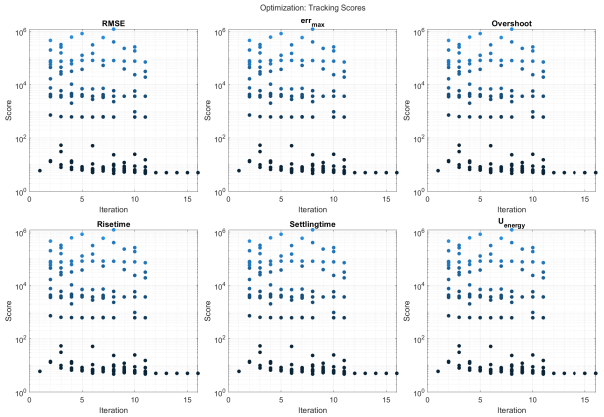

Figure 6.16: Tracking Quality score result

Flying & Handling Quality Results

The LOES fit for the longitudinal and lateral dynamics is performed for the pitch rate, vertical load factor transfer function and roll rate, sideslip angle respectively. This LOES fit is then used for the handling criterion regarding dynamic modes, CAP, and bandwidth criterion for the longitudinal dynamics. The LOES fit cost is determined through an objective function whereby the Low Order transfer function dynamics are evaluated against the higher order dynamics as outlined by [23]. The threshold at which a fit is deemed sufficient is set at 15 in this research and the result for each flight condition at forward and aft CG is shown in Figure 6.17 where it can be observed that it is satisfied.

With the LOES fit obtained, the dynamic modes for the augmented aircraft with FCS are determined, however the phugoid dynamic mode isn't taken into account with this research as it is assumed that the short period transfer function fit can be directly obtained with the approximated short-period transfer function. The results are shown in Table 6.6 to 6.8 with the ideal flying quality requirements for all conditions defined in Table 6.9 based on the most constraining thresholds defined in the MIL-SPEC 1797A requirements.

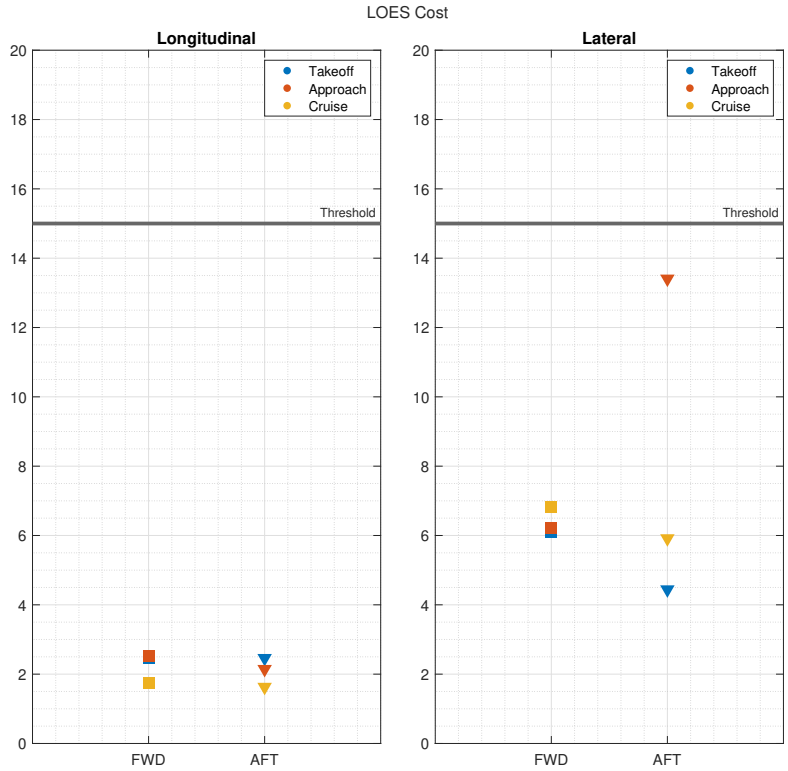

Figure 6.17: LOES Score results

Dynamic mode	Takeoff					
	Forward			Aft		
	ζ	ω	T_s	ζ	ω	T_s
Short Period	0.545	2.298	0.796s	0.699	1.739	0.821s
Dutch Roll	2.798	44.549	0.008s	0.443	2.254	0.999s
Aperiodic Roll	-	-	0.036s	-	-	0.114s
Spiral	-	-	0.150s	-	-	90.224s

Table 6.6: Damping ratio and natural frequency for dynamics of the Flying-V for Takeoff condition.

Dynamic mode	Approach					
	Forward			Aft		
	ζ	ω	T_s	ζ	ω	T_s
Short Period	0.650	1.396	1.100s	0.650	1.456	1.056s
Dutch Roll	2.483	7.266	0.055s	3.079	5.680	0.057s
Aperiodic Roll	-	-	0.166s	-	-	0.890s
Spiral	-	-	20.900s	-	-	0.890s

Table 6.7: Damping ratio and natural frequency for dynamics of the Flying-V for Approach condition.

It can be determined that the Short Period and Dutch Roll are at level 1 flying qualities, however the Spiral mode isn't satisfied and the LOES fit approximates a similar time constant for the Aperiodic Roll and Spiral at Approach and Cruise flight conditions, highlighting a deficiency in the LOES fit.

The CAP results is shown in Figure 6.18, where it is determined that the CAP criterion falls within Level 1 flying quality, however the CAP criterion also defines thresholds for the time delay of the pitch rate transfer function, which is acquired from the LOES fit, and it can be determined that the Level 1 threshold isn't met for all conditions.

Dynamic mode	Cruise					
	Forward			Aft		
	ζ	ω	T_s	ζ	ω	T_s
Short Period	0.691	1.454	0.994s	0.840	1.466	0.811s
Dutch Roll	1.037	9.957	0.096s	0.404	11.062	0.223s
Aperiodic Roll	-	-	1.148s	-	-	0.225s
Spiral	-	-	1.148s	-	-	0.225s

Table 6.8: Damping ratio and natural frequency for dynamics of the Flying-V for Cruise condition.

Dynamic mode	Ideal flying qualities requirements
Short Period	Level 1: $0.5 < \zeta_{sp} < 1.3$ Level 2: $0.35 < \zeta_{sp} < 2.0$ Level 3: $\zeta_{sp} > 0.25$
Dutch roll	Level 1: $\zeta_{dr} > 0.08$, $\omega_{dr} > 0.5$, $\zeta_{dr}\omega_{dr} > 0.15$ Level 2: $\zeta_{dr} > 0.02$, $\omega_{dr} > 0.5$, $\zeta_{dr}\omega_{dr} > 0.05$ Level 3: $\zeta_{dr} > 0.0$, $\omega_{dr} > 0.4$
Aperiodic roll	Level 1: $T_r < 1.4$ s Level 2: $T_r < 3.0$ s Level 3: $T_r < 10.0$ s
Spiral	Level 1: $T_s > 28.9$ s Level 2: $T_r > 11.5$ s Level 3: $T_r > 7.2$ s

Table 6.9: Dynamic mode requirements for tuning, based on [109]

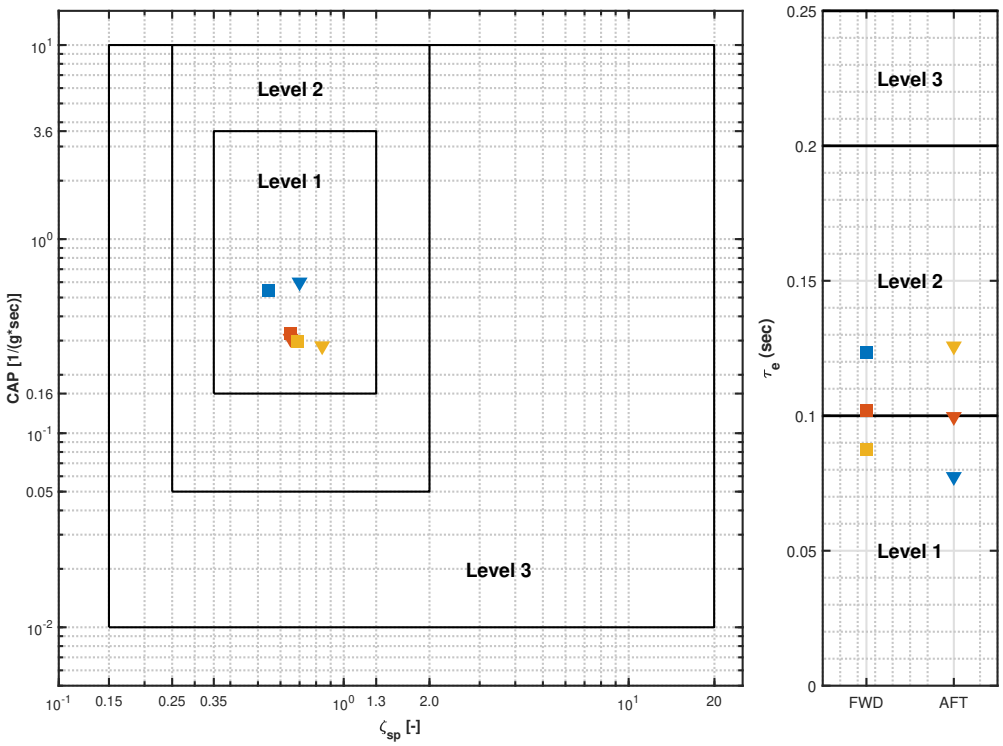

Figure 6.18: CAP results, thresholds found in [105]

The bandwidth criterion results are shown in Figure 6.19 with pitch transfer function obtained through linearization of the higher order dynamics and the bandwidth criterion limits taken from [108] for all flight conditions. It can be determined that the phase delay meets the desired threshold, however the Bandwidth isn't resolved appropriately.

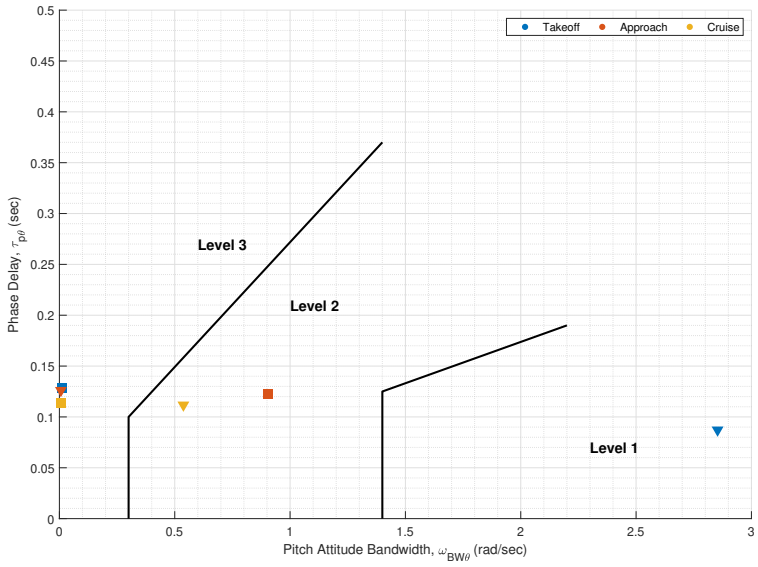

Figure 6.19: Bandwidth results, figure based on [108]

The Gibson dropback result for a commanded C* command with respect to the pitch rate is shown in Figure 6.20, where it is determined that the Approach condition satisfies the criterion, however Takeoff and Cruise need further improvement.

The stability margin with the lowest margin as provided by the function *allmargin* from 10^{-4} to 10^{-4} are determined with the results shown in Figure 6.21. The thresholds are defined to achieve at least ($\pm$) 6 dB of gain margin and 45° of phase margin. From the tuning, it can be determined that Approach and Cruise are meeting or near to the minimum margin thresholds, however the Takeoff condition has the least margin.

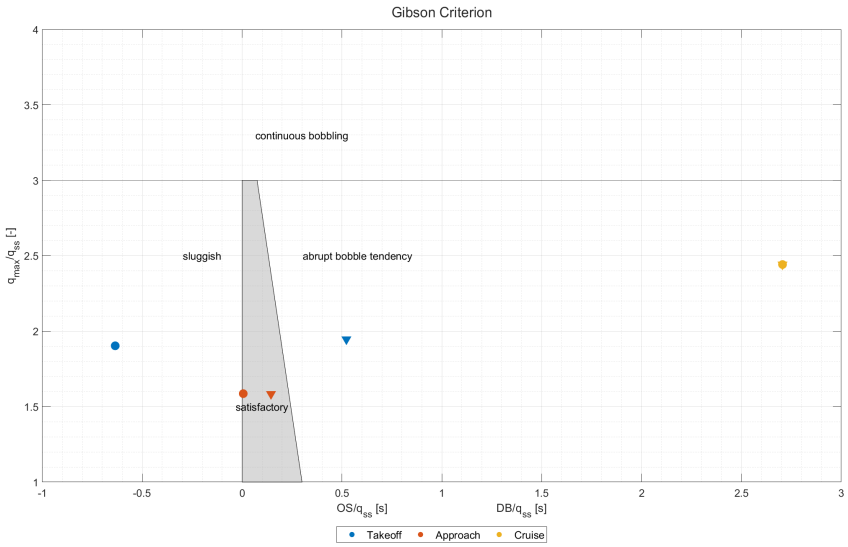

Figure 6.20: Gibson dropback results

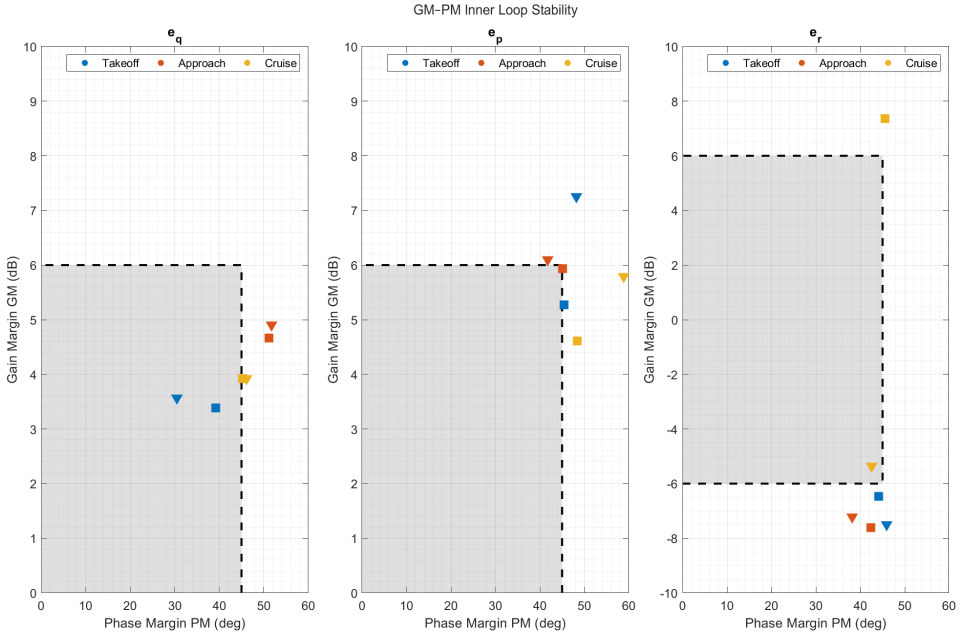

Figure 6.21: Stability results

Tracking Results

The tuning of the reference tracking is done for the longitudinal and lateral dynamics respectively and done with the handling qualities. The results of the tuning are shown in Table 6.10 with the tracking response for all conditions shown in Figure 6.22 and 6.23. For the tuning at the Takeoff condition, the tracking reference was reduced as the original reference would lead to destabilized scenario. At AFT CG the tracking performance degrades for the lateral dynamics increase and more control effort is required.

Tracking State	Metric	Takeoff		Approach		Cruise	
		FWD CG	*AFT CG*	*FWD CG*	*AFT CG*	*FWD CG*	*AFT CG*
C^*	RMSE	0.057	0.067	0.058	0.0559	0.055	0.0533
	Peak (g)	0.69	0.74	0.603	0.06	0.64	0.61
	OS (%)	13.00	16.57	6.88	9.50	7.40	5.20
	RiseTime (s)	0.27	0.28	0.48	0.48	0.29	0.46
	SettlingTime (s)	2.64	3.52	3.04	3.54	2.78	2.77
	δ energy	18.36	26.20	4.54	4.77	2.80	2.96
ϕ	RMSE	0.30	0.30	0.327	0.363	0.310	0.350
	Peak ($\circ/s$)	2.62	3.00	3.55	3.91	3.27	3.94
	OS (%)	31.97	50.46	18.59	30.36	8.99	31.60
	RiseTime (s)	0.30	0.48	0.29	0.33	0.24	0.37
	SettlingTime (s)	4.53	5.94	4.94	2.87	8.47	5.17
	δ energy	19.19	17.86	22.78	27.92	15.13	17.97
β	RMSE	0.310	0.272	0.337	0.321	0.338	0.300
	Peak ($\circ$)	1.33	1.34	2.24	2.45	2.28	2.39
	OS (%)	0.29	0.89	12.32	22.74	14.30	19.71
	RiseTime (s)	0.94	2.78	1.19	0.96	1.30	0.88
	SettlingTime (s)	6.28	6.16	4.34	6.16	6.17	6.64

Table 6.10: Tuning Summary for tracking at FWD and AFT CG Positions

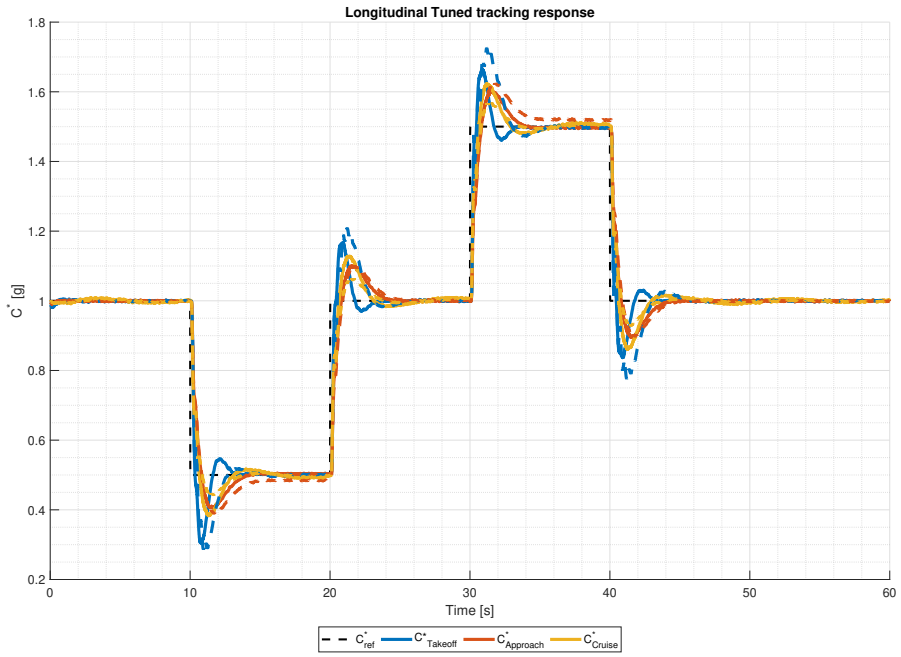

Figure 6.22: Longitudinal Tracking response summary

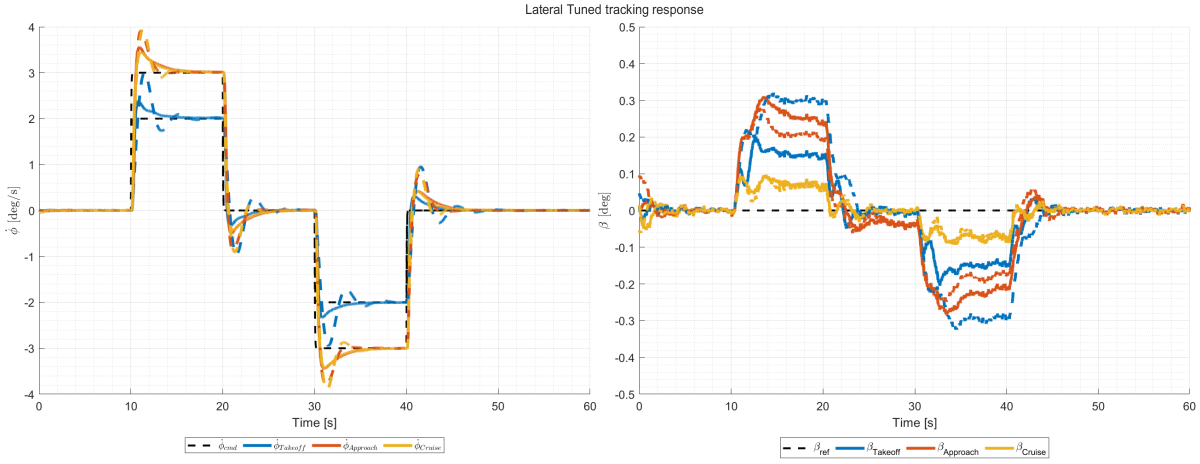

Figure 6.23: Lateral Tracking response summary

6.2. Simulation Results

This section provides additional simulation results concerning the combined longitudinal and tracking task as shown in Figure 6.24. This control tasking task is designed to keep the aircraft level and at steady state at the end of the simulation and the nominal results at Approach condition (FWD CG) is shown in Figure 6.26 and 6.30.

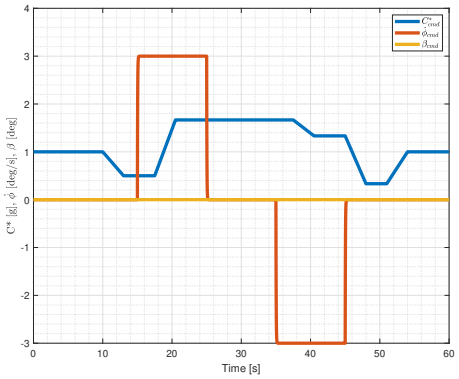

Figure 6.24: Control Tracking task

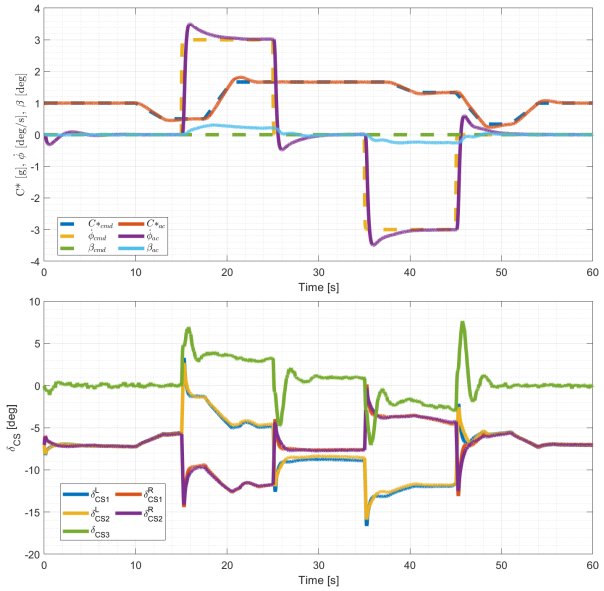

Figure 6.25: Nominal result at Approach (FWD CG): tracking response and control surface deflections

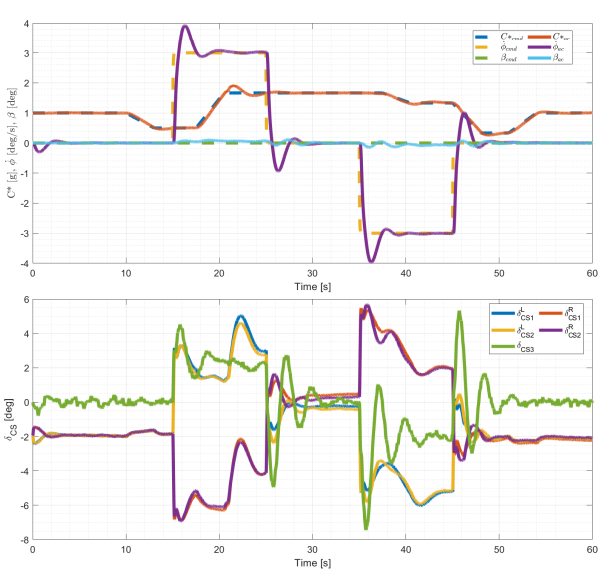

Figure 6.26: Nominal result at Cruise (AFT CG): tracking response and control surface deflections

From the simulation, it can be observed that the variation of dynamic pressure has a proportional effect on the control effectiveness and the initial control effectiveness initialised varies as shown in Figure 6.27 and 6.28.

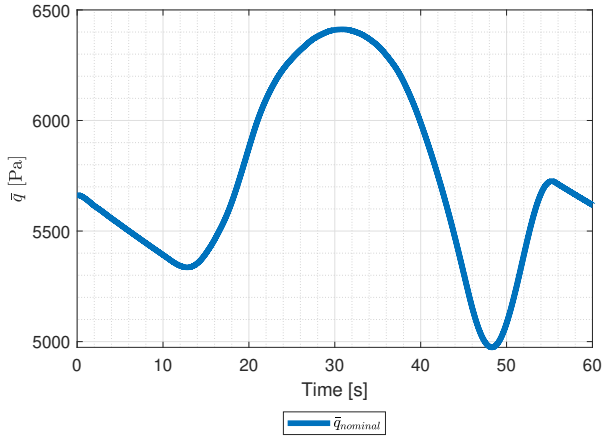

Figure 6.27: Approach (FWD CG): Change in dynamic pressure

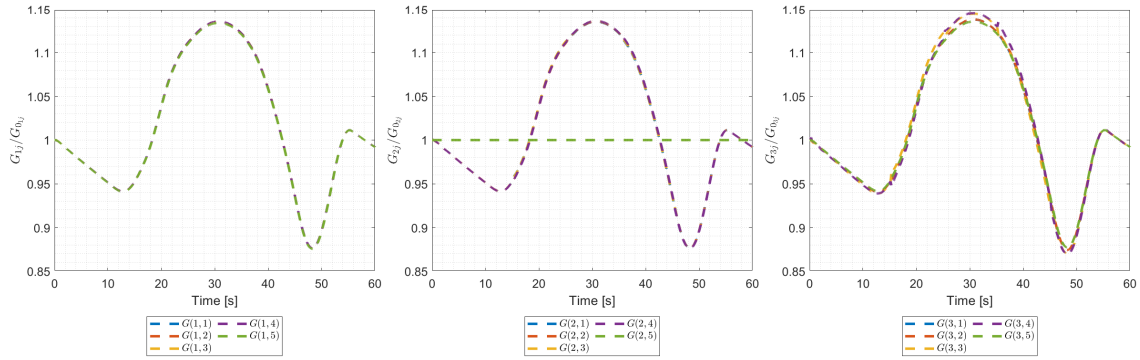

Figure 6.28: Approach (FWD CG): Change in Control Effectiveness

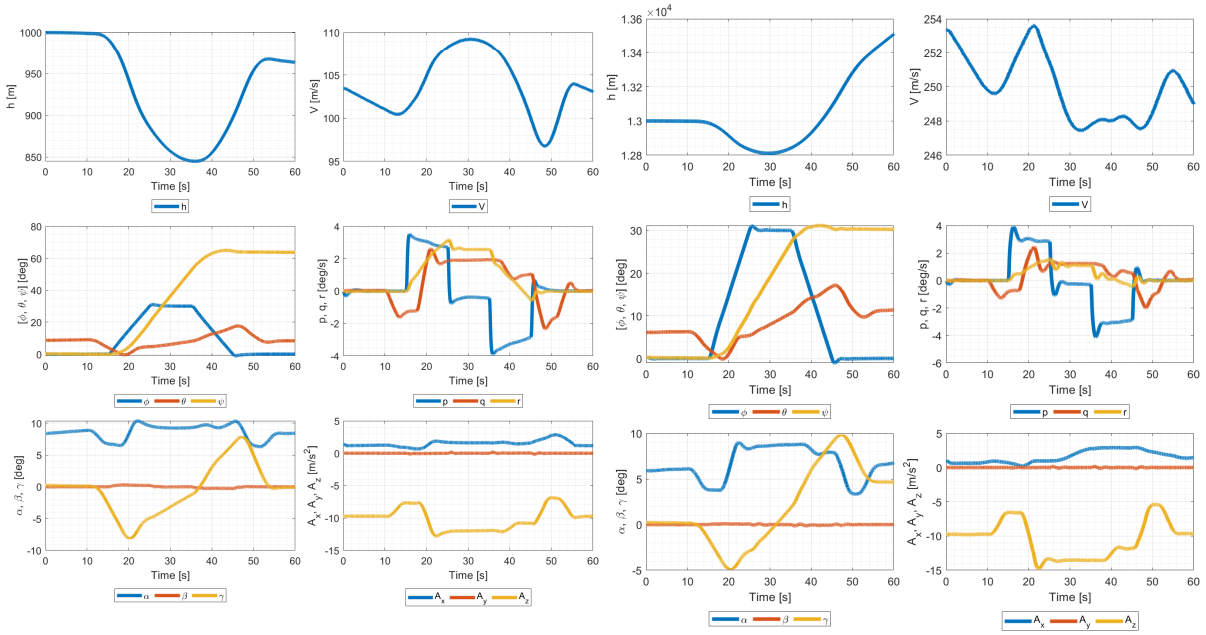

Figure 6.29: Approach (FWD CG): nominal case states

Figure 6.30: Cruise (AFT CG): nominal case states

The following additional results at Approach with a FWD CG and Cruise with an AFT CG are analysed

1. On-board model mismatch
2. Asymmetric structural fault

The Recursive Least Squares (RLS) filter and Variable Forgetting Factor has the following configuration for the simulation:

$$P_0 = 100\mathbf{I}^{5x5}$$
$$\lambda_{max} = 1 \qquad \lambda_{min} = 0.995$$
$$\Sigma_0 = 0.01$$

The adaptation with RLS incorporates the residual, or described as innovation, based on the measured rotational acceleration demand and the rotational acceleration by the control surfaces at time step $k-1$. This residual is formulated as:

$$\epsilon_k = \Delta\dot{\omega}_{k-1} - \hat{G}\Delta U_{k-1} \tag{6.5}$$

On-board Model Mismatch

The INDI control law in the inner loop has a dependency on its On-Board Model (OBM), which is initialised at linearisation and contains the control effectiveness of the control surfaces. A model mismatch between the OBM and the real control effectiveness dynamics could lead to degraded performance, and adaptation to correct for this mismatch could be beneficial. An analysis was performed, where the OBM has 25% less control effectiveness, and this is compared against the nominal tracking response, where the OBM matches the real dynamics. The results are shown in Table 6.11 with and without adaptation with the relative difference of INDI without adaptation. For this set of results, no control excitation was used for the identification.

State [RMSE]	Method	Case	Approach	Cruise
			FWD CG	*AFT CG*
C^* [g]	INDI	Nominal	0.0322	0.0348
		-25 % OBM	0.0302 (-6.21%)	0.0300 (-13.79%)
	AINDI	Nominal	0.0314 (-2.48%)	0.0298 (-14.36%)
		-25 % OBM	0.0311 (-3.41%)	0.0295 (-15.22%)
$\dot{\phi}$ [deg/s]	INDI	Nominal	0.3233	0.3417
		-25 % OBM	0.3196 (-1.14%)	0.3284 (-3.89%)
	AINDI	Nominal	0.3217 (-0.49%)	0.3349 (-1.99%)
		-25 % OBM	0.3211 (-0.68%)	0.3319 (-2.86%)
β [deg]	INDI	Nominal	0.1093	0.0371
		-25 % OBM	0.1094 (+0.09%)	0.0344 (-7.27%)
	AINDI	Nominal	0.1095 (+0.18%)	0.0408 (+9.97%)
		-25 % OBM	0.1096 (+0.27%)	0.0342 (-7.81%)
Metric				
$\delta_{CS_{activity}}$ [deg/s^2]	INDI	Nominal	24.240	13.415
		-25 % OBM	34.978 (+44.3%)	19.846 (+47.9%)
	AINDI	Nominal	28.494 (+17.54%)	22.100 (+64.7%)
		-25 % OBM	31.621 (+30.44%)	21.855 (+62.9%)

Table 6.11: RMSE and Control surface activity results at Approach and Cruise for tracking at FWD and AFT CG Position respectively

In the approach condition, the OBM model mismatch has marginal influence on the tracking performance and the increase with control activity corresponds to higher maximum deflections, where with adaptation the increase isn't as high. In the cruise condition, the decrease of the OBM effectiveness improves the tracking performance, and the control surface activity also increases.

In the nominal case, with adaptation this can be elaborated with the innovation as shown in Figure 6.31, where each axis residual is shown and at last the residual norm. It can be observed that the highest residual occurs as the aircraft has to follow the lateral tracking reference, and this subsides as the tracking reference is met. These residual errors lead to the Variable Forgetting Factor (VFF) adjusting itself as shown in Figure 6.32 and lead to the control effectiveness factor adapting, as shown in Figure 6.33, where it can be observed in the first column that the control effectiveness with respect to the angular acceleration are adapted proportionally.

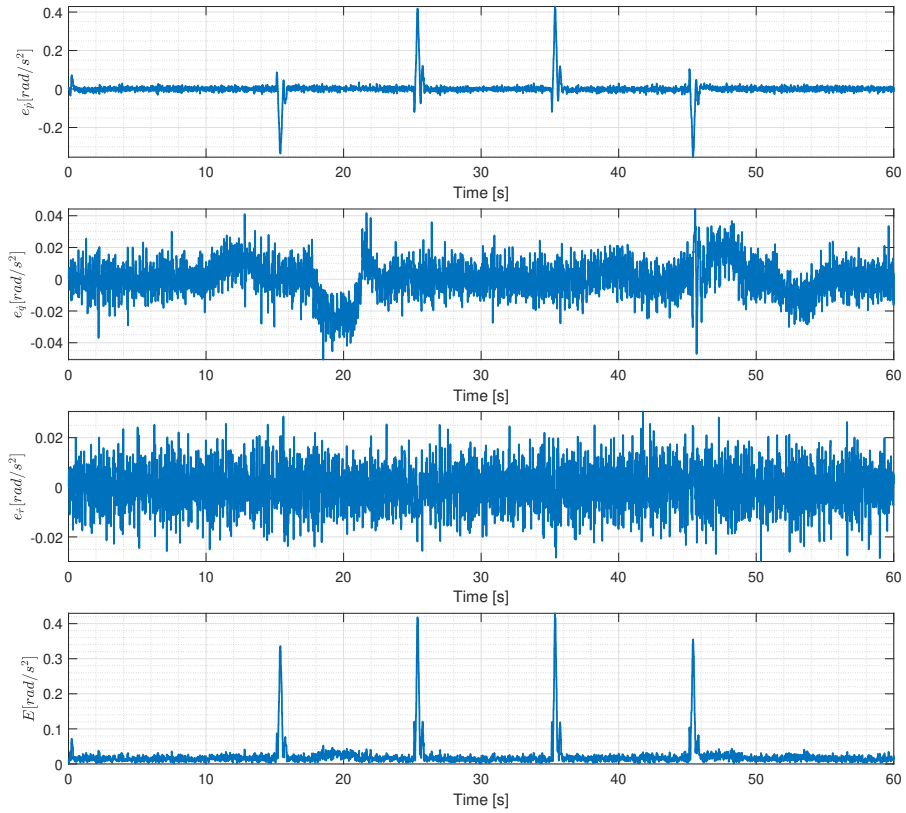

Figure 6.31: Approach (FWD CG), adaptive INDI: Innovation in nominal case

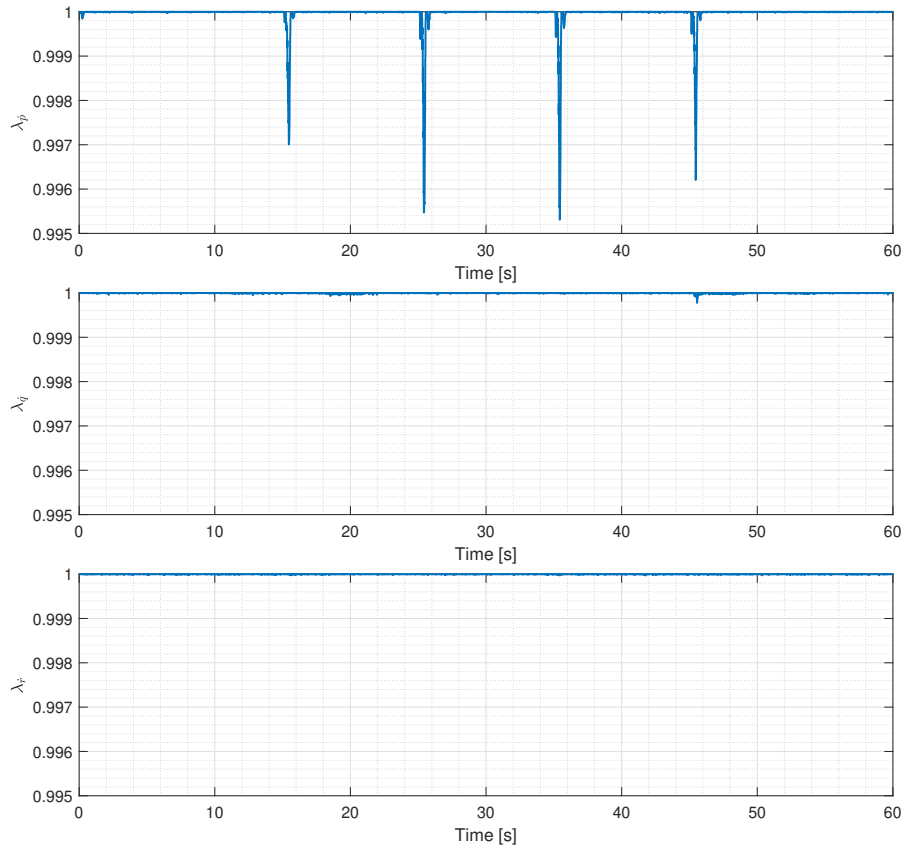

Figure 6.32: Approach (FWD CG), adaptive INDI: Variable Forgetting Factor in the nominal case

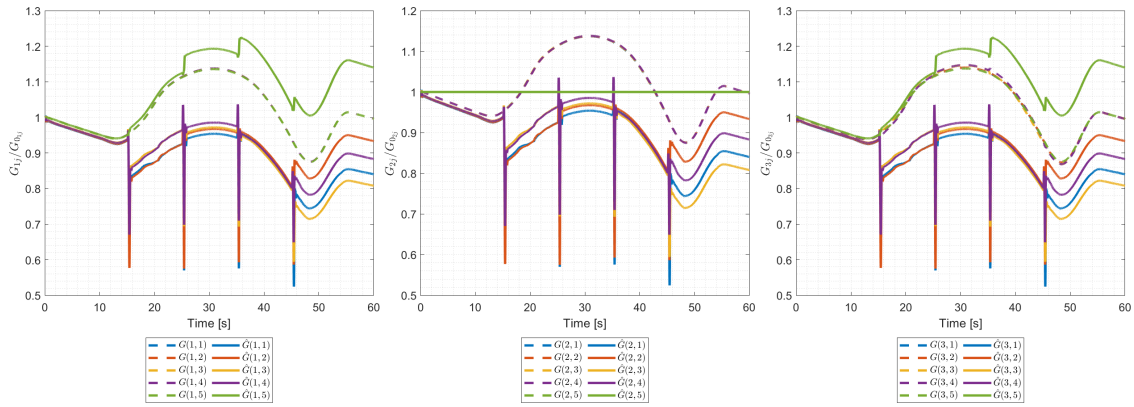

Figure 6.33: Approach (FWD CG), adaptive INDI: Control effectiveness in the nominal case

With adaptation in the OBM mismatch case, the mismatch of the CE is adjusted and corrected for as shown in Figure 6.34 and it's characteristic to slightly underestimate the CE occurs.

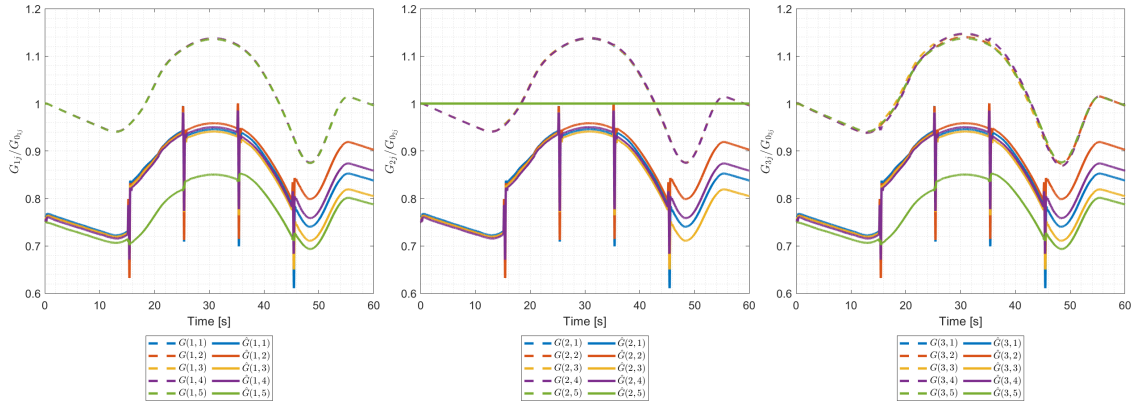

Figure 6.34: Approach (FWD CG), adaptive INDI: Control effectiveness in the OBM mismatch case

Examining a higher underestimation case for the Approach condition, where there is a 40% OBM mismatch with the results shown in Table 6.12 reveals that there is a limit at which INDI can cope with OBM mismatch. It is evaluated that the high underestimation leads to an oscillatory control surface deflections, which affect the tracking of the C* command as shown in Figure 6.35 & 6.36.

State [RMSE]	Method	Approach
C^* [g]	INDI	0.0765 (+ 137.10%)
	AINDI	0.0308 (-4.33%)
$\dot{\phi}$ [deg/s]	INDI	0.3192 (-1.27%)
	AINDI	0.3208 (-0.79%)
β [deg]	INDI	0.1096 (+0.24%)
	AINDI	0.1096 (+0.32%)
Metric		
$\delta_{CS_{activity}}$ [deg/s^2]	INDI	164.0714 (+576%)
	AINDI	37.5893 (+55.0%)

Table 6.12: RMSE and Control surface activity results at Approach and Cruise for tracking at FWD and AFT CG Position respectively

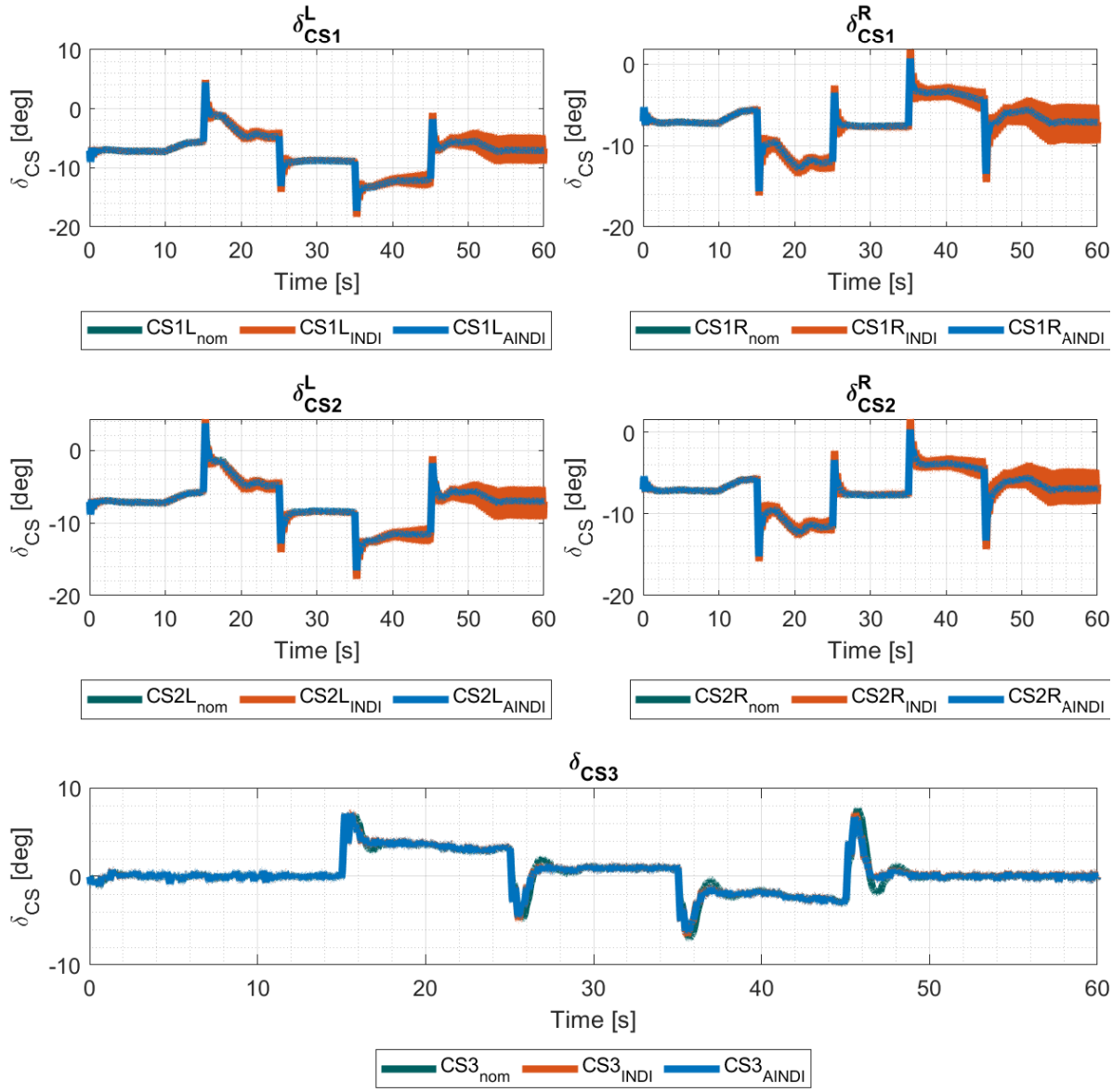

Figure 6.35: Approach (FWD CG), adaptive INDI: Control surface deflection with -40% OBM mismatch case

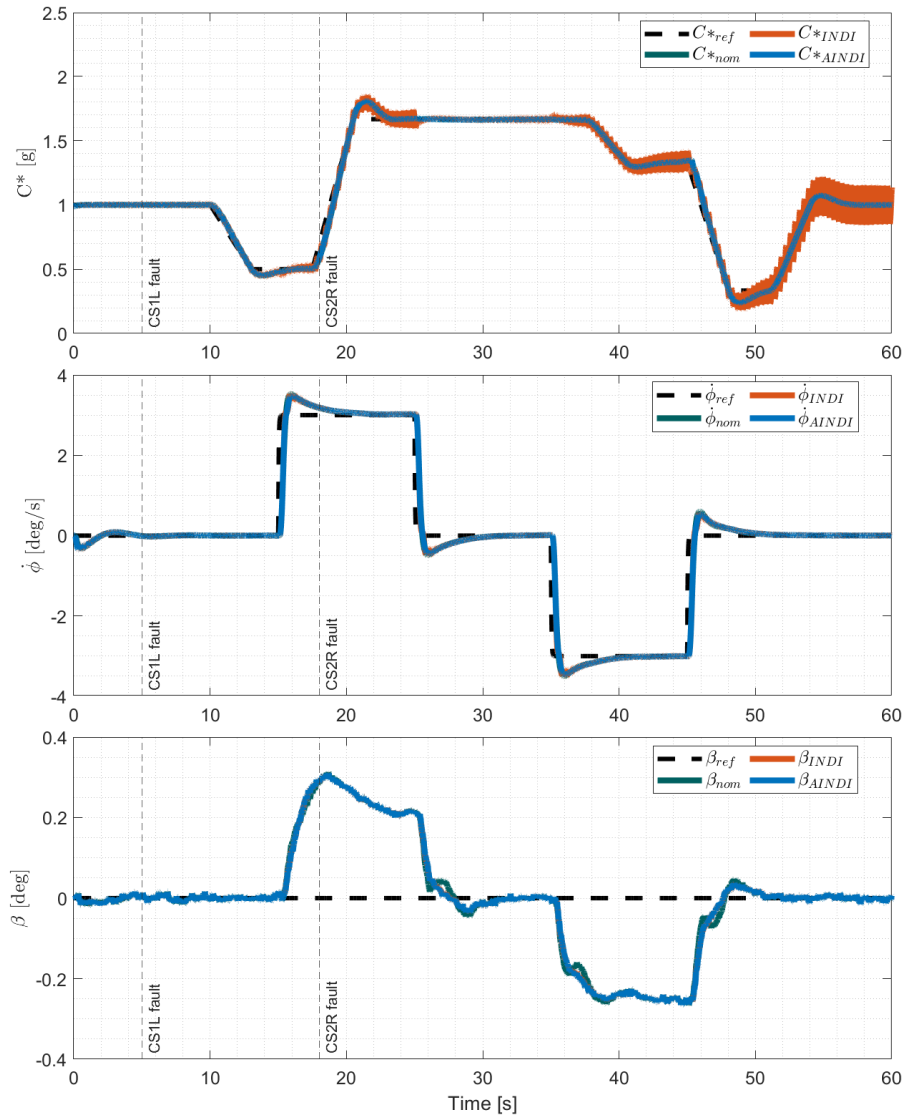

Figure 6.36: Approach (FWD CG), adaptive INDI: Tracking with -40% OBM mismatch case

Although the adaptation doesn't estimate the true parameter, its adaptation is able to correct for the mismatch and track the reference accurately.

Asymmetric Structural Fault

An asymmetric structural fault, where the inboard elevon on the left hand side, and outboard elevon on the right-hand side lose their effectiveness completely. This is only analysed for the Cruise condition at AFT CG and the Approach condition has been analysed in the Scientific Paper (Part 1). The relative change against the nominal condition is also provided, and it can be observed that adaptation leads to significantly better tracking, as shown in Figure 6.37. Without adaptation INDI oscillates as it has difficulty in tracking the C* command and near its pitch break, due to the severe reduction of control authority with the faulted control surfaces, this is also evident with the control surface deflection comparison as shown in Figure 6.38 and aircraft state in Figure 6.39.
The adaptation of the CE is shown in Figure 6.42 where it is observed that the adaptation also underestimates the control effectiveness of the healthy surfaces and this reconfiguration leads to the control deflection to achieve the desired tracking performance.

State [RMSE]	Method	Cruise
		AFT CG
C^*	INDI AINDI	0.16704 (+380 %) 0.04415 (+26.8%)
$\dot{\phi}$	INDI AINDI	0.42078 (+23.1 %) 0.37695 (+10.3 %)
β	INDI AINDI	0.04060 (+9.43%) 0.04010 (+8.08 %)
Metric		
$\delta_{CS_{activity}}$	INDI AINDI	31.7433 (+136 %) 33.6425 (+150 %)

Table 6.13: RMSE and Control Surface Activity at Cruise for tracking at FWD and AFT CG Position respectively

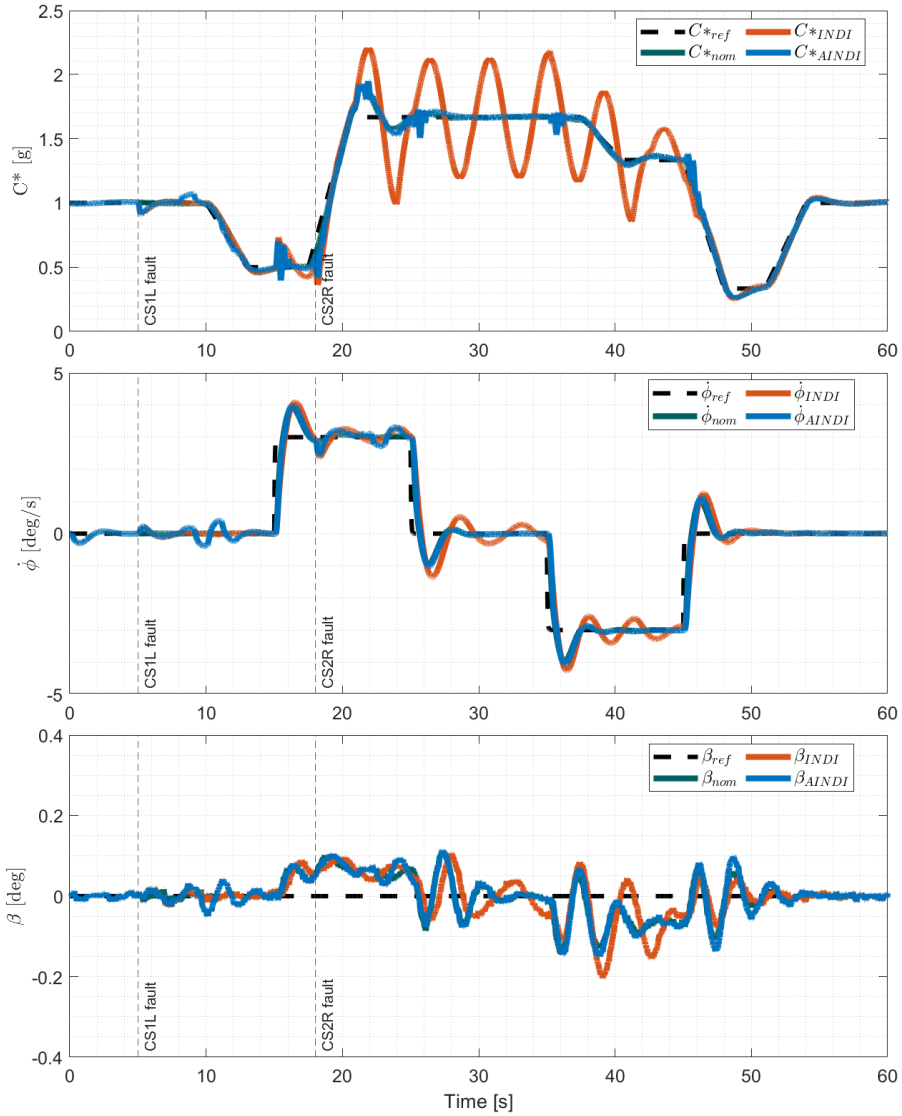

Figure 6.37: Cruise (AFT CG): Reference Tracking comparison

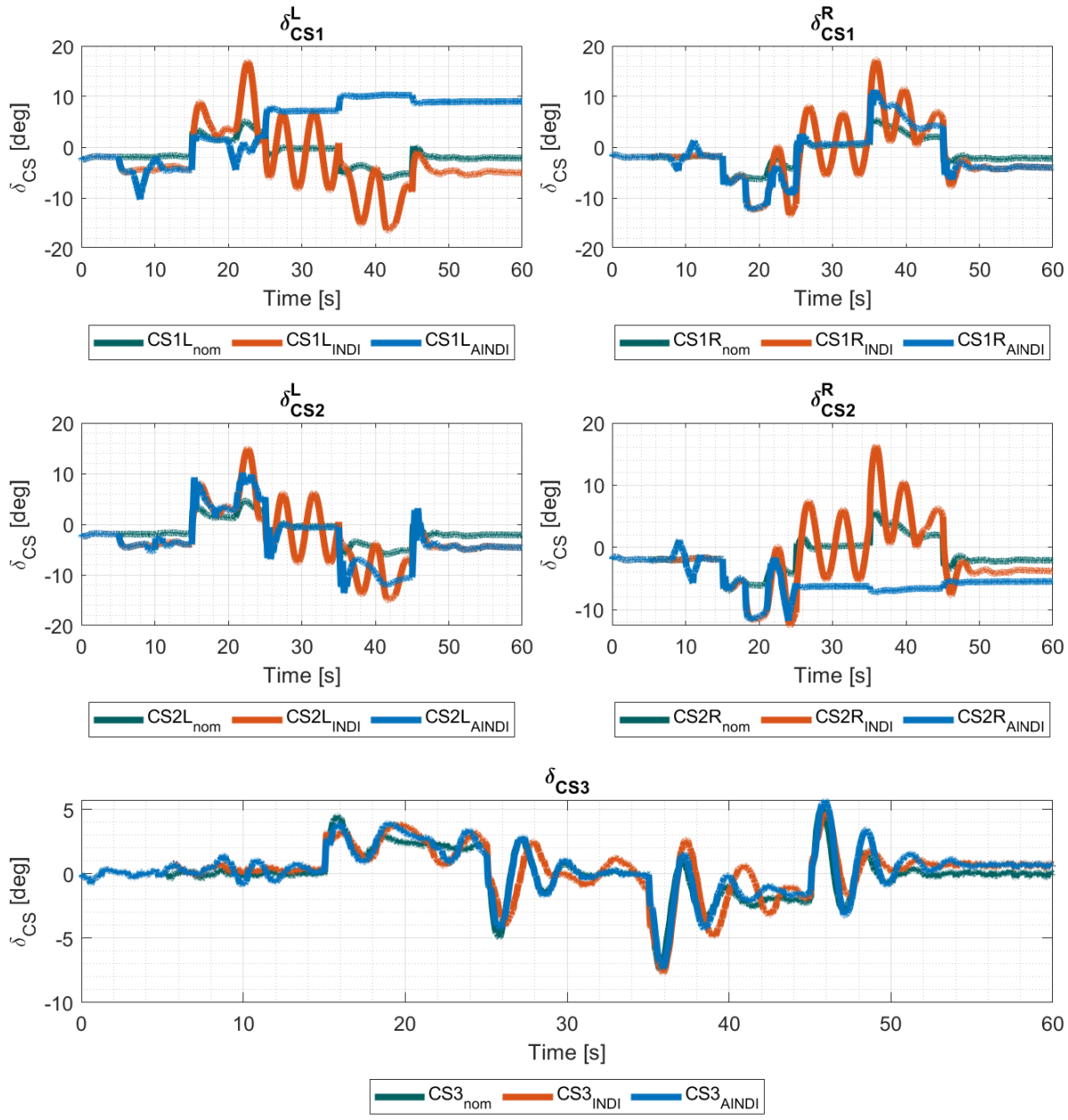

Figure 6.38: Cruise (AFT CG): Control surface deflection comparison

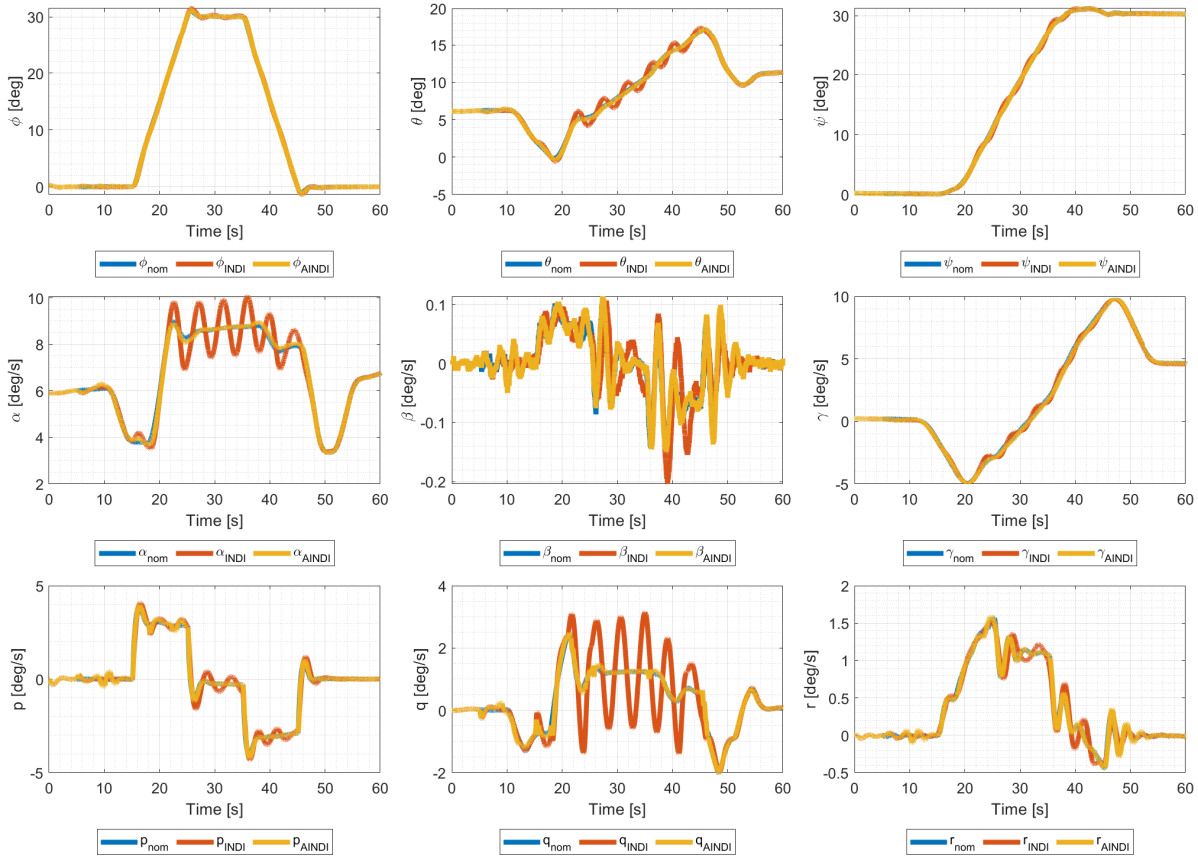

Figure 6.39: Cruise (AFT CG): Aircraft State comparison

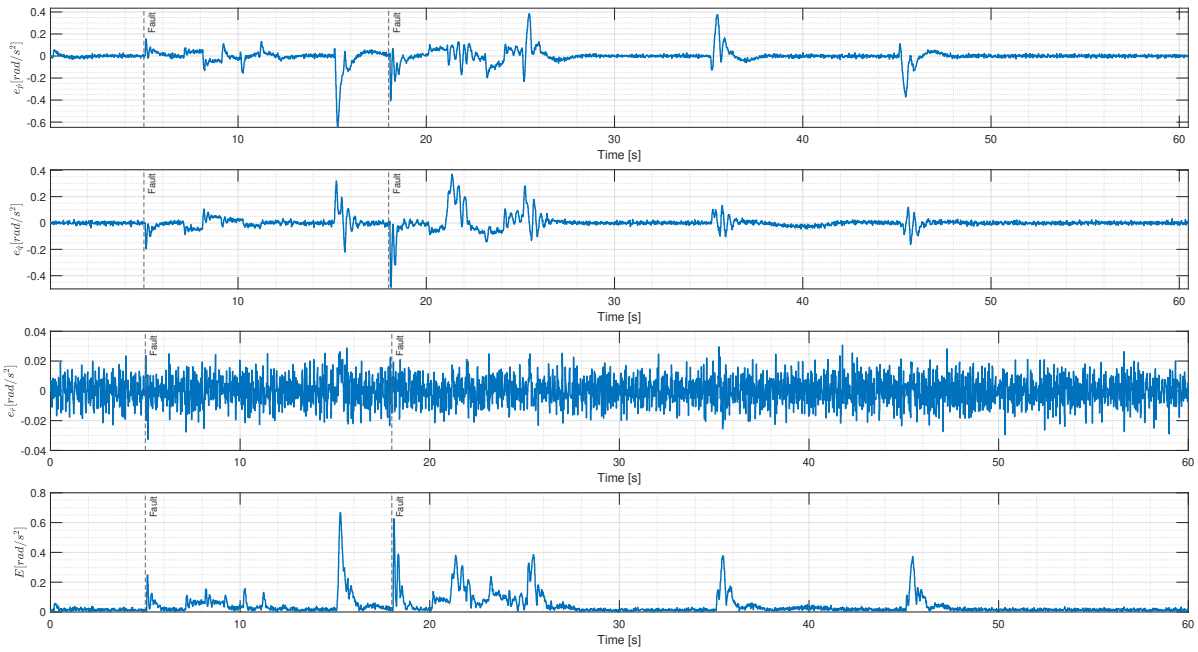

Figure 6.40: Cruise (AFT CG): Innovation

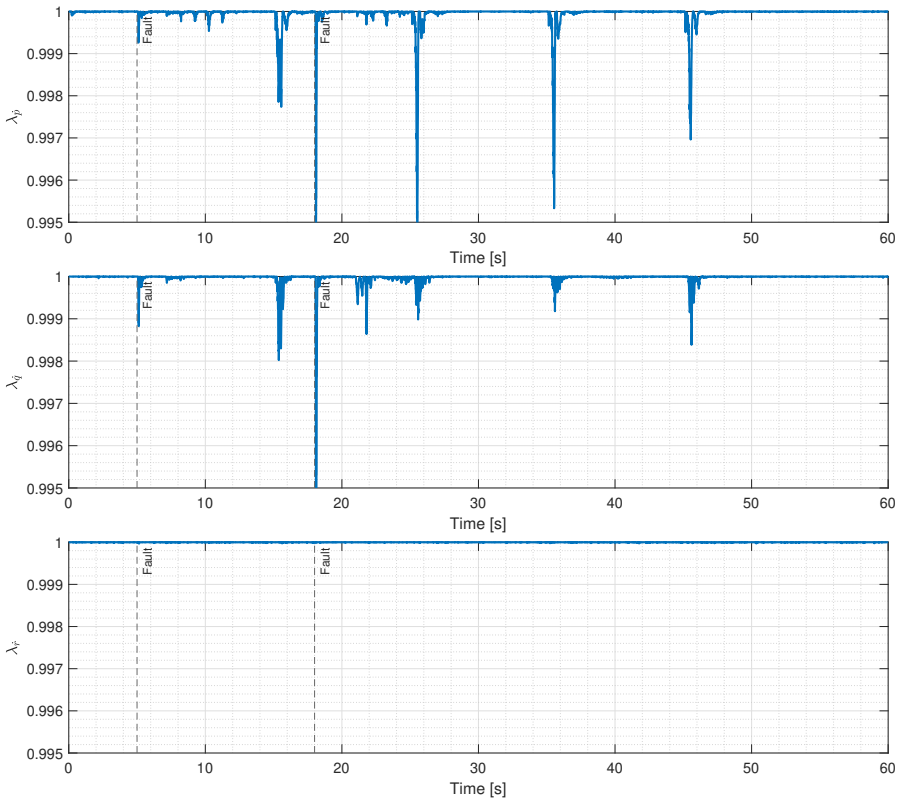

Figure 6.41: Cruise (AFT CG): VFF

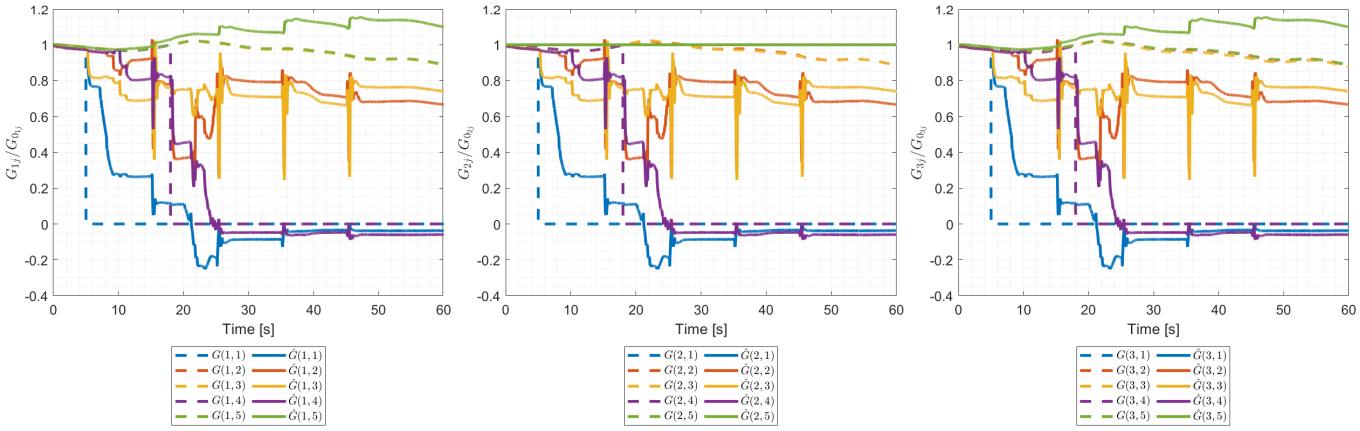

Figure 6.42: Cruise (AFT CG): Control effectiveness adaptation

Part IV

Conclusion & Recommendations

7

Conclusions & Recommendations for Future Work

The research objective of this study is to develop a fault-tolerant flight control system, that can learn and adapt to model uncertainties and faults, while adhering to the stability and handling qualities to safely operate the aircraft. The main research question is defined as:

How can an adaptive control method be applied to the Flight Control System (FCS) of the Flying V for improving its fault tolerance?

To answer the main research question, several sub-questions are formulated to scope and define the research work and objective for the literature research and master thesis project. These research questions are revisited and answered, and thereafter the conclusion with the answer of the main research question is given (7.1). At last, recommendations for future work are given (7.2).

7.1. Conclusion

In this section, several questions, where some have been answered in Chapter 5, are further expanded upon with the insights gained during the research.

1. What are the results and lessons from previous research on developing the FCS for the Flying V?
   (a) What is the current state of handling qualities of the Flying V?
      - The current state of handling qualities of the Flying V have been established on the new aerodynamic model where at the respective flight conditions the bare-frame eigenvalues have been examined and experimentally simulated with disturbances from its steady-state trim, revealing unstable lateral modes and marginally stable longitudinal modes where the short period quickly damps, but the phugoid is underdamped and remains oscillatory, the lateral excitation reveals a Dutch roll that's stable, but the dynamics diverge due to the unstable spiral.
      - The augmented aircraft fulfils the Level 1 flying qualities with respect to the dynamic modes and handling criteria used in previous researches have been applied again, with the bandwidth criterion not being satisfied for level 1 flying qualities. The CAP criterion has been fulfilled partially, as the time delay is within Level 1 and Level 2 flying qualities at the evaluated flight conditions. The Gibson dropback criterion is met for the Appproach flight condition, whereas the other flight conditions, Takeoff and Cruise, aren't satisfied.
   (b) What are the latest developments in aerodynamic modelling for the Flying V?
      - During this research, updated aerodynamic models have been provided, which incorporate additional states and control surfaces than used in this research, whereby the nonlinearity of the aerodynamic model is further defined. This research incorporated the first iteration of this newer model with a simulation model that independently commands

each elevon instead of ganged control surfaces, however the model is still defined with linear control surface effectiveness estimations

(c) What is the current state of the Flying V simulation model?
- The developed model in this research has updated tuning scripts and a new aerodynamic model, and fault injections or on-board model mismatches. Moreover, the actuator dynamics were updated as the previous simulations models used actuator dynamics of a highly agile aircraft, and this was adjusted to be more in line with commercial passenger aircrafts. The Flight Envelope Protection and Control Allocation in previous research were not enabled in this research.

(d) What assumptions and uncertainty are present in the simulation model of the Flying V?
- There is no engine simulation model that computes the thrust at the various flight condition, but it is computed to achieve the necessary trim at the flight condition.
- The mass, weight, and moment of Inertia of the aircraft remains constant during the simulation.
- The moment of inertia matrix is not updated for this newer geometry and is a source of uncertainty.
- It is assumed that the structural faults do not influence any other aerodynamic parameters and constants.
- Zero wind and perfect atmosphere assumption in the simulation model.

(e) What are the specifications and requirements that apply to an FCS with an adaptive control method?
- The same specifications and requirements used in previous research of Nonlinear Incremental Dynamic Inversion (INDI) have been applied, whereby the outer loop reference controllers are tuned with the INDI in the inner loop for rate control.

2. What evaluation metrics are suitable to assess the adaptive control method for the FCS?
   (a) What are the flying & handling qualities criteria, which have been evaluated for the FCS?
   - The same specifications and requirements used in previous research [23] have been applied for the tuning of the outer loop gains, but no evaluation of the handling quality with adaptation have been performed.

   (b) What assessment for evaluating model parameter uncertainties have been performed?
   - Structural faults have been incorporated as a scaling parameter with respect to the aerodynamic parameters of the control surfaces.

3. What advancements have there been in the applications of nonlinear & adaptive methods?
   (a) What methods have been implemented for fault-tolerant control?
   - This research has incorporated adaptation in the inner loop, where the on-board model is adapted online with Recursive Least Squares.

4. How does the selected adaptive method satisfy the requirements for the Flying-V FCS?
   (a) How does the adaptive FCS compare in tracking qualities to a non-adaptive FCS?
   - The FCS with adaptation achieves lower Root Mean Square Error (RMSE) for the respective tracking references, but its adaptation also leads to higher control activity since the adaptation leads to an underestimation of the control effectiveness.

   (b) How does the adaptive FCS cope with faults compared to the non-adaptive FCS?
   - At the analysed flight conditions the FCS with adaptation is able to appropriately adjust for faults, by reconfiguring and adapting the on-board model. The algorithm does not estimate the true parameters from the dynamics, but adapts the parameters such that the desired angular acceleration can be met.

To answer the main research question and conclude the research, the objective of this research was to incorporate a fault-tolerant FCS for the Flying-V and thereby improve its fault tolerance. The method applied in this research was to use an adaptive control method, where an adaptive inner loop rate control law is designed with INDI. The adaptation mechanism is to adapt and update the control effectiveness parameters with RLS. With adaptation, it was shown that adaptive INDI improves the tracking response and when faults or on-board model mismatches are introduced, it can maintain better performance. This improves the fault tolerance of the FCS and leads to further advancements of FCS for the Flying V.

7.2. Recommendations

As outlined in the previous section, a fault-tolerant FCS with adaptive INDI has been implemented, which leads to improved tracking performance. However, improvements can still be incorporated in the method used, the assessment of its fault tolerance and other improvements regarding the simulation model, gain tuning and optimisation and handling quality.

The current estimation method utilizes a correction parameter to update the control effectiveness model, however, this model is a non-physical parameters solely dependent on a single variable for its estimation. Further studies can be conducted to investigate if more variables or a different model can be applied to improve the control effectiveness estimations. This is especially important as future aerodynamic models can contain non-linear estimations and the current model becomes more limited.
Further research can also investigate on Control Allocation (CA) with the aim of making optimal use of the adapted control effectiveness, where a comprehensive analysis on this aspect can be conducted to ensure appropriate distribution of control commands when saturated or in case of complete loss of effectiveness. This is also related to the control surface excitation to enrich dynamics and improve the estimation, while minimizing the disturbance on the tracking task.

The analysed fault cases are limited to structural faults which lead to control effectiveness reduction, but further analysis towards actuator faults and sensor faults or combined faults are of interested and thus necessitate more investigation and analysis to assess the fault-tolerant FCS. This can also be cases at Takeoff and One Engine Inoperative (OEI) cases.
Future evaluations can also investigate how uncertainties related to time delays, higher noise or disturbances affect the adaptation. Moreover, the Flight Envelope Protection (FEP) is not incorporated, and future research can analyse how the updated on-board model affects the FEP.

The optimization was performed with the *PatternSearch* method in MATLAB with an objective function that evaluates the handling qualities and tracking performance concurrently. Upon completion of the gain tuning, it was observed that not all handling qualities are confidently met and some tracking quality specifications. The bandwidth criterion is not met for all flight conditions and the handling quality constraints have been mostly superficial, where the boundaries are incorporated as soft-constraints to that could be exceeded. Future research can improve the optimisation and meet the handling quality criterions.

The simulation model applied various assumptions, such as zero wind and perfect atmosphere assumptions, and future research can focus on incorporating more realistic dynamics and combine that with faults. Additionally, the mass model and inertia is remained constant, with the latter still obtained from an older geometry model. Further updates and uncertainty analysis should be evaluated.
Moreover, the tracking reference used in this research is a short simulation and is not assessed against more complex manoeuvres to meet compliance against CS-25. At last, no piloted simulator tests were performed, and future research can also evaluate the performance with and without adaptation.

References

[1] E. van der Sman, B. Peerlings, J. Kos, R. Lieshout, and T. Boonekamp, *Destination 2050*. Report, Netherlands Aerospace Centre NLR, 2021. Available: https://www.destination2050.eu/wp-content/uploads/2021/03/Destination2050_Report.pdf.

[2] F. Faggiano, R. Vos, M. Baan, and R. van Dijk, "Aerodynamic Design of a Flying V Aircraft," *17th AIAA Aviation Technology, Integration, and Operations Conference*, Jun. 2017. doi: 10.2514/6.2017-3589.

[3] R Martínez-Val, E Pérez, P Alfaro, and J Pérez, "Conceptual design of a medium size flying wing," *Proceedings of the Institution of Mechanical Engineers, Part G: Journal of Aerospace Engineering*, vol. 221, no. 1, pp. 57–66, Jan. 2007, issn: 0954-4100. doi: 10.1243/09544100JAERO90.

[4] F. Afonso *et al.*, "Strategies towards a more sustainable aviation: A systematic review," *Progress in Aerospace Sciences*, Feb. 2023, issn: 03760421. doi: 10.1016/j.paerosci.2022.100878.

[5] J. Benad, *DPMAregister | Originaldokument - DE102014201040A1*, Jul. 2015. Available: https://register.dpma.de/DPMAregister/pat/PatSchrifteneinsicht?docId=DE102014201040A1.

[6] J. Benad, "The Flying V - A new Aircraft Configuration for Commercial Passenger Transport," Deutsche Gesellschaft für Luft- und Raumfahrt, Nov. 2015. doi: 10.25967/370094.

[7] J Benad and R. R. Vos, "Design of a Flying V Subsonic Transport," Sep. 2022. Available: https://www.icas.org/ICAS_ARCHIVE/ICAS2022/data/preview/ICAS2022_0358.htm.

[8] F. Faggiano and R. Vos, *Aerodynamic Design Optimization of a Flying V Aircraft*. MSc. Thesis, Delft University of Technology, 2016. Available: https://resolver.tudelft.nl/uuid:0b1472a5-3aad-433c-9a64-242c84b114fd.

[9] W. Oosterom and R. Vos, "Conceptual Design of a Flying-V Aircraft Family," in *AIAA AVIATION 2022 Forum*, Reston, Virginia: American Institute of Aeronautics and Astronautics, Jun. 2022, isbn: 978-1-62410-635-4. doi: 10.2514/6.2022-3200. Available: https://arc.aiaa.org/doi/10.2514/6.2022-3200.

[10] L. A. van Der Schaft, R Vos, and J. M. J. F. van Campen, *Development, Model Generation and Analysis of a Flying V Structure Concept*. MSc. Thesis, Delft University of Technology, 2017. Available: http://resolver.tudelft.nl/uuid:d9c9c02f-d67a-4e3c-93a7-eb20ed67cd03.

[11] M. Claeys, R. Vos, C. Kassapoglou, K. Bender, and J. Clausen, *Flying V and Reference Aircraft Structural Analysis and Mass Comparison*. MSc. Thesis, Delft University of Technology, 2018. Available: http://resolver.tudelft.nl/uuid:ee7f2ecb-cdb6-46de-8b57-d55b89f8c7e6.

[12] D. J. Leith and W. E. Leithead, "Survey of gain-scheduling analysis and design," *International Journal of Control*, vol. 73, no. 11, pp. 1001–1025, Jul. 2000, issn: 00207179. doi: 10.1080/002071700411304. Available: https://www.tandfonline.com/doi/abs/10.1080/00207170041304.

[13] G. Stein, D. Bugajski, R. Hendrick, and G. Stein, "Dynamic inversion: An evolving methodology for flight control design," *International Journal of Control*, vol. 59, no. 1, pp. 71–91, 1994, issn: 13665820. doi: 10.1080/00207179408923070. Available: https://www.tandfonline.com/action/journalInformation?journalCode=tcon20.

[14] J. J. E. Slotine and W Li, *Applied Nonlinear Control*. Prentice-Hall, 1991, isbn: 9780130408907. Available: https://api.semanticscholar.org/CorpusID:106519536.

[15] L. Sonneveldt, *Adaptive backstepping flight control for modern fighter aircraft.* Doctoral Thesis, Delft University of Technology, 2010, isbn: 9789085705734. Available: https://resolver.tudelft.nl/uuid:a21d2cc6-9924-4018-9387-60527fb27d4b.

[16] J. J. Harris and J. R. Stanford, “F-35 flight control law design, development and verification,” *2018 Aviation Technology, Integration, and Operations Conference*, 2018. doi: 10.2514/6.2018-3516. Available: https://arc.aiaa.org/doi/10.2514/6.2018-3516.

[17] D. G. Canin, J. K. McConnell, and P. W. James, “F-35 high angle of attack flight control development and flight test results,” *AIAA Aviation 2019 Forum*, pp. 1–29, 2019. doi: 10.2514/6.2019-3227. Available: https://arc.aiaa.org/doi/10.2514/6.2019-3227.

[18] S. Wang, *Incremental sliding mode flight control*. Doctoral Thesis, Delft University of Technology, 2019. Available: https://resolver.tudelft.nl/uuid:c8259a08-bbee-4af0-b570-1350a2dd8d89.

[19] S. Sieberling, Q. P. Chu, and J. A. Mulder, “Robust Flight Control Using Incremental Nonlinear Dynamic Inversion and Angular Acceleration Prediction,” *Journal of Guidance, Control, and Dynamics*, vol. 33, no. 6, pp. 1732–1742, Nov. 2010, issn: 0731-5090. doi: 10.2514/1.49978.

[20] P. J. Acquatella, *Robust Nonlinear Spacecraft Attitude Control an Incremental Backstepping approach*. MSc. Thesis, Delft University of Technology, 2011. Available: https://resolver.tudelft.nl/uuid:a56090a3-bbce-404b-8e4b-d0e9050b518a.

[21] P. Acquatella Bustillo, *Robust nonlinear attitude control of aerospace vehicles: An incremental nonlinear control approach*. Doctoral Thesis, Delft University of Technology, 2020, isbn: 978-94-6421-120-7. doi: 10.4233/uuid:99d82992-080c-4c5d-8d40-4e62e62285c0.

[22] S. van Overeem, *Modelling, Control, and Handling Quality Analysis of the Flying-V*. MSc. Thesis, Delft University of Technology, 2022. Available: https://resolver.tudelft.nl/uuid:7fd04eec-41d4-4967-b246-89fdfac2446e.

[23] J. Stougie, *Incremental Nonlinear Dynamic Inversion Control with Flight Envelope Protection for the Flying-V*. MSc. Thesis, Delft University of Technology, 2022. Available: https://resolver.tudelft.nl/uuid:5d0a883c-bf58-4507-b688-6abccdca4842.

[24] R. C. van ’t Veld, *Incremental Nonlinear Dynamic Inversion Flight Control*. MSc. Thesis, Delft University of Technology, Sep. 2016. Available: https://resolver.tudelft.nl/uuid:f85a9c88-7bdb-42cd-a01c-aa85251d365c.

[25] Y. Kumtepe, E. van Kampen, and T. Pollack, *Flight Control Design Using Hybrid Incremental Nonlinear Dynamic Inversion*. MSc. Thesis, Delft University of Technology, 2020. Available: https://resolver.tudelft.nl/uuid:755193c5-9a83-47bc-a904-bfb0f2a4579a.

[26] T. Pollack and E.-J. van Kampen, “Robust Stability and Performance Analysis of Incremental Dynamic Inversion-based Flight Control Laws,” in *AIAA SCITECH 2022 Forum*, Reston, Virginia: American Institute of Aeronautics and Astronautics, Jan. 2022, isbn: 978-1-62410-631-6. doi: 10.2514/6.2022-1395.

[27] E. J. J. Smeur, Q. Chu, and G. C. H. E. de Croon, “Adaptive Incremental Nonlinear Dynamic Inversion for Attitude Control of Micro Air Vehicles,” *Journal of Guidance, Control, and Dynamics*, vol. 39, no. 3, pp. 450–461, Mar. 2016, issn: 1533-3884. doi: 10.2514/1.G001490.

[28] Boeing Commercial Airplanes, *Statistical Summary of Commercial Jet Airplane Accidents: Worldwide Operations 1959-2022*. Seattle, Washington: The Boeing Company, 2023. Available: https://www.boeing.com/content/dam/boeing/boeingdotcom/company/about_bca/pdf/statsum.pdf.

[29] L. G. Sun, *Model and sensor based nonlinear adaptive flight control with online system identification*. Doctoral Thesis, Delft University of Technology, 2014. Available: https://resolver.tudelft.nl/uuid:89455d9a-fb38-42bf-b1db-03a8a5104bcf.

[30] A. Jürisson, *Optimal trajectory tracking control design*. MSc. Thesis, Delft University of Technology, 2018. Available: https://resolver.tudelft.nl/uuid:19d69477-f1f7-4c53-82a5-0b9bf8e8a57f.

[31] D. Hanover, P. Foehn, S. Sun, E. Kaufmann, and D. Scaramuzza, “Performance, Precision, and Payloads: Adaptive Nonlinear MPC for Quadrotors,” 2021. doi: 10.1109/LRA.2021.3131690. Available: https://youtu.be/8oB1rG5iYc4.

[32] S. Sun, A. Romero, P. Foehn, E. Kaufmann, and D. Scaramuzza, “A Comparative Study of Nonlinear MPC and Differential-Flatness-based Control for Quadrotor Agile Flight,” 2022. Available: https://youtu.be/SEZJ-OIR8Bo.

[33] B. Rubio Pascual, *Engine-Airframe Integration for the Flying-V*. MSc. Thesis, Delft University of Technology, 2018. Available: https://resolver.tudelft.nl/uuid:75be27a7-6fd4-4112-a600-45df2999758f.

[34] T. Cappuyns, *Handling Qualities of a Flying V Configuration*. MSc. Thesis, Delft University of Technology, 2019. Available: https://resolver.tudelft.nl/uuid:69b56494-0731-487a-8e57-cec397452002.

[35] C. Donlan, “An interim report on the stability and control of tailless airplanes,” 1944. Available: https://ntrs.nasa.gov/citations/20050241739.

[36] G. Vugts, *Assessing the Longitudinal Handling Qualities of the Flying V by Pilot Evaluation*. MSc. Thesis, Delft University of Technology, 2022. Available: https://resolver.tudelft.nl/uuid:89c5ef4c-5e13-4af6-bafc-71e4e9a3375c.

[37] N. A. Johnson, *Effect of Winglet Integration and Rudder Deflection on Flying V Aerodynamic Characteristics*. MSc. Thesis, Delft University of Technology, Jan. 2021. Available: https://resolver.tudelft.nl/uuid:b664ae03-846f-4ad3-849a-c081a32260ad.

[38] S. van Empelen, *Engine Integration of the Flying V*. MSc. Thesis, Delft University of Technology, 2020. Available: https://resolver.tudelft.nl/uuid:c519caf8-0eba-4633-a4f9-be37684417a8.

[39] N. van Luijk, *Constrained Aerodynamic Shape Optimisation of the Flying V Outer Wing*. MSc. Thesis, Delft University of Technology, 2023. Available: http://resolver.tudelft.nl/uuid:fc2bbe10-6796-4337-81cc-5971b324d50e.

[40] A. A. Amur, *Multi-objective Aerodynamic Assessment and Optimization of Winglets for the Flying-V Aircraft Configuration*. MSc. Thesis, Delft University of Technology, 2023. Available: https://resolver.tudelft.nl/uuid:d4428b69-93e7-4149-970e-16572ae5f111.

[41] S Nolet, *Improving the Flying V Directional Control Power by the Implementation of Split Flaps*. MSc. Thesis, Delft University of Technology, 2023. Available: https://resolver.tudelft.nl/uuid:18847b0d-597d-4539-968f-ebc8a14c905e.

[42] S. Eftekhar, *High Lift Split Flaps for the Flying-V*. MSc. Thesis, Delft University of Technology, 2024. Available: http://resolver.tudelft.nl/uuid:0ad3c088-b6a6-472b-b60b-4b424a08e15c.

[43] W. J. Oosterom, *Flying-V Family Design*. MSc. Thesis, Delft University of Technology, 2021. Available: https://resolver.tudelft.nl/uuid:9e8f9a41-8830-405d-8676-c46bf6b07891.

[44] Y.A. Laar, *Aerodynamic Design of a Flying V Aircraft in Transonic Conditions*. MSc. Thesis, Delft University of Technology, 2023. Available: https://resolver.tudelft.nl/uuid:591093b2-5cdc-41c5-b564-3786f43d51db.

[45] M. J.A. *et al.*, *Flight Dynamics: Lecture Notes AE3202*. 2013.

[46] A. Raju Kulkarni, G. La Rocca, L. Veldhuis, and G. Eitelberg, “Sub-scale flight test model design: Developments, challenges and opportunities,” *Progress in Aerospace Sciences*, Apr. 2022, issn: 03760421. doi: 10.1016/j.paerosci.2021.100798.

[47] R. V. Jategaonkar, *Flight Vehicle System Identification: A Time-Domain Methodology*, Second Edition. American Institute of Aeronautics and Astronautics, Inc., Feb. 2015. doi: 10.2514/4.102790.

[48] R. A. Viet, *Analysis of the flight characteristics of a highly swept cranked flying wing by means of an experimental test*. MSc. Thesis, Delft University of Technology, 2019. Available: https://resolver.tudelft.nl/uuid:90de4d9e-70ae-4efc-bd0a-7426a0a669c3.

[49] M. Palermo, *The Longitudinal Static Stability and Control Characteristics of a Flying V Scaled Model*. MSc. Thesis, Delft University of Technology, 2019. Available: https://resolver.tudelft.nl/uuid:6286f9e2-c24a-430c-a4fa-9fb67b9558b4.

[50] A. Ruiz Garcia, *Aerodynamic Model Identification of the Flying V using Wind Tunnel Data*. MSc. Thesis, Delft University of Technology, 2019. Available: https://resolver.tudelft.nl/uuid:79e01f29-1789-4501-8556-ca2bcf06f3ab.

[51] A. Ruiz-García, R. Vos, and C. C. de Visser, "Aerodynamic model identification of the flying V from wind tunnel data," *AIAA AVIATION 2020 FORUM*, vol. 1 PartF, 2020. doi: 10.2514/6.2020-2739.

[52] K. Siemonsma, *Aerodynamic Model Identification of the Flying-V Using Flight Data*. MSc. Thesis, Delft University of Technology, 2022. Available: https://resolver.tudelft.nl/uuid:3cf35fb2-4fe7-49d7-9076-068c44fb2016.

[53] A. Ruiz Garcia, M. Brown, D. Atherstone, N. v. Arnhem, and R. Vos, "Aerodynamic Model Identification of the Flying V from Sub-Scale Flight Test Data," in *AIAA SCITECH 2022 Forum*, American Institute of Aeronautics and Astronautics, Jan. 2022, isbn: 978-1-62410-631-6. doi: 10.2514/6.2022-0713.

[54] Anonymous, *Flying qualities of piloted aircraft*, MIL-STD-1797A, Department of Defense Interface Standard, originally issued January 30, 1990., 1990.

[55] M. V. Cook, *Flight Dynamics Principles: A Linear Systems Approach to Aircraft Stability and Control*. Elsevier, Nov. 2012, pp. 1–575, isbn: 9780080982762. doi: 10.1016/C2010-0-65889-5.

[56] D. E. Bossert, S. L. Morris, W. F. Hallgren, and T. R. Yechout, *Introduction to Aircraft Flight Mechanics*. Blacksburg ,VA: American Institute of Aeronautics and Astronautics, Jan. 2003, isbn: 978-1-56347-577-1. doi: 10.2514/4.862069.

[57] T. Lombaerts, Q. Chu, J. Mulder, and D. Joosten, "Modular flight control reconfiguration design and simulation," *Control Engineering Practice*, vol. 19, no. 6, pp. 540–554, Jun. 2011, issn: 09670661. doi: 10.1016/j.conengprac.2010.12.008.

[58] R. P. Harper and G. E. Cooper, "Handling qualities and pilot evaluation," *https://doi.org/10.2514/3.20142*, vol. 9, no. 5, pp. 515–529, May 2012, issn: 07315090. doi: 10.2514/3.20142.

[59] S. Joosten, *Piloted Assessment of the Lateral-Directional Handling Qualities of the Flying-V*. MSc. Thesis, Delft University of Technology, 2022.

[60] R. Torelli, *Piloted simulator evaluation of low speed handling qualities of the Flying-V*. MSc. Thesis, Delft University of Technology, 2022. Available: https://resolver.tudelft.nl/uuid:b68bb437-8a44-4e88-b331-4bd9b74c547c.

[61] G. Vugts, O. Stroosma, R. Vos, and M. Mulder, "Simulator Evaluation of Flightpath-oriented Control Allocation for the Flying-V," in *AIAA SCITECH 2023 Forum*, Reston, Virginia: American Institute of Aeronautics and Astronautics, Jan. 2023, isbn: 978-1-62410-699-6. doi: 10.2514/6.2023-2508. Available: https://arc.aiaa.org/doi/10.2514/6.2023-2508.

[62] J. Roskam, *Airplane Flight Dynamics and Automatic Flight Controls Part II*. DARcorporation, 1998, isbn: 1-884885-18-7.

[63] B. L. Stevens, F. L. Lewis, and E. N. Johnson, "Aircraft control and simulation : dynamics, controls design, and autonomous systems," 2015. Available: https://www.wiley.com/en-us/Aircraft+Control+and+Simulation%3A+Dynamics%2C+Controls+Design%2C+and+Autonomous+Systems%2C+3rd+Edition-p-9781118870983.

[64] I. Matamoros and C. C. de Visser, "Incremental Nonlinear Control Allocation for a Tailless Aircraft with Innovative Control Effectors," in *2018 AIAA Guidance, Navigation, and Control Conference*, Kissimmee, Florida: American Institute of Aeronautics and Astronautics, Jan. 2018, isbn: 978-1-62410-526-5. doi: 10.2514/6.2018-1116.

[65] M. Li, J. Li, Y. Tang, and S. Sun, "An Extended INDI Approach and Application to Pitch Rate Control Laws Design of an Aircraft," in *AIAA AVIATION 2021 FORUM*, Reston, Virginia: American Institute of Aeronautics and Astronautics, Aug. 2021, isbn: 978-1-62410-610-1. doi: 10.2514/6.2021-3005.

[66] W. Durham, K. A. Bordignon, and R. Beck, *Aircraft Control Allocation*. Wiley, Dec. 2016, isbn: 9781118827796. doi: 10.1002/9781118827789.

[67] T. Lombaerts, G. Looye, J. Ellerbroek, and M. R. y. Martin, “Design and Piloted Simulator Evaluation of Adaptive Safe Flight Envelope Protection Algorithm,” *Journal of Guidance, Control, and Dynamics*, vol. 40, no. 8, pp. 1902–1924, Aug. 2017, issn: 0731-5090. doi: 10.2514/1.G002525.

[68] E. Field, *The application of a C* flight control law to large civil transport aircraft*. College of Aeronautics, Cranfield Institute of Technology, 1993, vol. 9303.

[69] C. FAVRE, “Fly-by-wire for commercial aircraft: the Airbus experience,” *International Journal of Control*, vol. 59, no. 1, pp. 139–157, Jan. 1994, issn: 0020-7179. doi: 10.1080/00207179408923072.

[70] F. Grondman, G. Looye, R. O. Kuchar, Q. P. Chu, and E.-J. van Kampen, “Design and Flight Testing of Incremental Nonlinear Dynamic Inversion-based Control Laws for a Passenger Aircraft,” in *2018 AIAA Guidance, Navigation, and Control Conference*, Reston, Virginia: American Institute of Aeronautics and Astronautics, Jan. 2018, isbn: 978-1-62410-526-5. doi: 10.2514/6.2018-0385.

[71] M. Krstic, P. V. Kokotovic, and I. Kanellakopoulos, *Nonlinear and Adaptive Control Design*, 1st. USA: John Wiley & Sons, Inc., 1995, isbn: 0471127329.

[72] R. Sepulchre, M. Janković, and P. V. Kokotović, *Constructive Nonlinear Control* (Communications and Control Engineering). London: Springer London, 1997, isbn: 978-1-4471-1245-7. doi: 10.1007/978-1-4471-0967-9.

[73] P van Gils, *Adaptive Incremental Backstepping Flight Control*. MSc. Thesis, Delft University of Technology, May 2015. Available: https://resolver.tudelft.nl/uuid:f62ac38d-5101-4230-ad90-d54543c1f1b8.

[74] J. A. Farrell, M. Polycarpou, M. Sharma, and W. Dong, “Command filtered backstepping,” in *2008 American Control Conference*, IEEE, Jun. 2008, pp. 1923–1928, isbn: 978-1-4244-2078-0. doi: 10.1109/ACC.2008.4586773.

[75] E. R. v. Oort, *Adaptive backstepping control and safety analysis for modern fighter aircraft.* Doctoral Thesis, Delft University of Technology, 2011. Available: https://resolver.tudelft.nl/uuid:68fd89ff-aad6-4ad8-b280-d2fe8b500d48.

[76] W. van Ekeren, *Incremental Nonlinear Flight Control for Fixed-Wing Aircraft*. MSc. Thesis, Delft University of Technology, 2016.

[77] S. H. Kim, H. Cho, and D. Jung, “Robust Path Following Control Via Command-Filtered Backstepping Scheme,” *International Journal of Aeronautical and Space Sciences*, vol. 22, no. 5, pp. 1141–1153, Oct. 2021, issn: 20932480. doi: 10.1007/s42405-021-00395-7.

[78] P. Smith and A. Berry, “Flight test experience of a non-linear dynamic inversion control law on the VAAC harrier,” *Atmospheric Flight Mechanics Conference*, 2000. doi: 10.2514/6.2000-3914.

[79] B. Bacon and A. Ostroff, “Reconfigurable flight control using nonlinear dynamic inversion with a special accelerometer implementation,” in *AIAA Guidance, Navigation, and Control Conference and Exhibit*, Reston, Virigina: American Institute of Aeronautics and Astronautics, Aug. 2000, isbn: 978-1-62410-301-8. doi: 10.2514/6.2000-4565.

[80] P. Lu, E.-J. van Kampen, and Q. P. Chu, “Robustness and Tuning of Incremental Backstepping Approach,” in *AIAA Guidance, Navigation, and Control Conference*, Kissimmee, Florida: American Institute of Aeronautics and Astronautics, Jan. 2015, isbn: 978-1-62410-339-1. doi: 10.2514/6.2015-1762.

[81] P. Lu and E. van Kampen, “Active fault-tolerant control system using incremental Backstepping approach,” *AIAA Guidance, Navigation, and Control Conference 2015, MGNC 2015 - Held at the AIAA SciTech Forum 2015*, 2015. doi: 10.2514/6.2015-1312.

[82] T. Keijzer, G. Looye, Q. P. Chu, and E.-J. van Kampen, “Design and Flight Testing of Incremental Backstepping based Control Laws with Angular Accelerometer Feedback,” in *AIAA Scitech 2019 Forum*, Reston, Virginia: American Institute of Aeronautics and Astronautics, Jan. 2019, isbn: 978-1-62410-578-4. doi: 10.2514/6.2019-0129.

[83] D. Ignatyev, H.-S. Shin, and A. Tsourdos, “Gaussian Process Adaptive Incremental Backstepping Flight Control,” in *AIAA SCITECH 2022 Forum*, Reston, Virginia: American Institute of Aeronautics and Astronautics, Jan. 2022, isbn: 978-1-62410-631-6. doi: 10.2514/6.2022-2032.

[84] C. Kim, C. Ji, G. Koh, and N. Choi, "Review on Flight Control Law Technologies of Fighter Jets for Flying Qualities," *International Journal of Aeronautical and Space Sciences*, vol. 24, no. 1, pp. 209–236, Feb. 2023, issn: 20932480. doi: 10.1007/s42405-022-00560-6.

[85] T. J. J. Lombaerts, *Fault Tolerant Flight Control*. Doctoral Thesis, Delft University of Technology, 2010. Available: https://resolver.tudelft.nl/uuid:538b0174-fe84-43af-954d-02f256b2ec50.

[86] P. Smith and A. Berry, "Flight test experience of a non-linear dynamic inversion control law on the VAAC Harrier," in *Atmospheric Flight Mechanics Conference*, Reston, Virigina: American Institute of Aeronautics and Astronautics, Aug. 2000. doi: 10.2514/6.2000-3914.

[87] E. Smeur, *Incremental Control of Hybrid Micro Air Vehicles*. Doctoral Thesis, Delft University of Technology, 2018, isbn: 978-94-6186-973-9. doi: https://doi.org/10.4233/uuid:23c338a1-8b34-40a6-89e9-997adbdafd75. Available: https://doi.org/10.4233/uuid:23c338a1-8b34-40a6-89e9-997adbdafd75.

[88] P. Lu, E.-J. van Kampen, C. de Visser, and Q. Chu, "Aircraft fault-tolerant trajectory control using Incremental Nonlinear Dynamic Inversion," 2016. doi: 10.1016/j.conengprac.2016.09.010. Available: http://dx.doi.org/10.1016/j.conengprac.2016.09.010.

[89] J. Chang, R. De Breuker, and X. Wang, "Discrete-time Design and Stability Analysis for Nonlinear Incremental Fault-tolerant Flight Control," in *AIAA SCITECH 2022 Forum*, Reston, Virginia: American Institute of Aeronautics and Astronautics, Jan. 2022, isbn: 978-1-62410-631-6. doi: 10.2514/6.2022-2034.

[90] P. Kanhai, *Adaptive control with Multivariate B-Splines and INDI*. MSc. Thesis, Delft University of Technology, 2022. Available: https://resolver.tudelft.nl/uuid:fdd8e2fa-1372-4f79-aa05-6ab152e848e1.

[91] B Smit, *Adaptive Incremental Nonlinear Dynamic Inversion for Consistent Pitch Rate Control*. MSc. Thesis, Delft University of Technology, Mar. 2021. Available: https://resolver.tudelft.nl/uuid:3014e195-28c7-49e9-9e29-1e468d045325.

[92] J. Chang, R. De Breuker, and X. Wang, "Active Fault-Tolerant Incremental Sliding-Mode Flight Control Against Control Reversal," *Journal of Guidance, Control, and Dynamics*, vol. 45, no. 12, pp. 2411–2420, Dec. 2022, issn: 0731-5090. doi: 10.2514/1.G006690.

[93] L. T. Nguyen, M. E. Ogburn, W. P. Gilbert, K. Kibler, P. W. Brown, and P. L. Deal, "Simulator study of stall/post-stall characteristics of a fighter airplane with relaxed longitudinal static stability," National Aeronautics and Space Administration, 1979. Available: https://ntrs.nasa.gov/citations/19800005879.

[94] T. Pollack and E.-J. van Kampen, "Robust Stability and Performance Analysis of Incremental Dynamic Inversion-based Flight Control Laws," in *AIAA SCITECH 2022 Forum*, Reston, Virginia: American Institute of Aeronautics and Astronautics, Jan. 2022, isbn: 978-1-62410-631-6. doi: 10.2514/6.2022-1395. Available: https://arc.aiaa.org/doi/10.2514/6.2022-1395.

[95] Anonymous, "Flight control design–best practices," NATO Research and Technology Organization (RTO), 2000.

[96] D. Atmaca and E.-J. van Kampen, "Fault Tolerant Control for the Flying-V Using Adaptive Incremental Nonlinear Dynamic Inversion," in *AIAA SCITECH 2025 Forum*, Reston, Virginia: American Institute of Aeronautics and Astronautics, Jan. 2025, isbn: 978-1-62410-723-8. doi: 10.2514/6.2025-0081.

[97] M. R. van Der Toorn, *Flying-V Family Design for Stability & Control*. MSc. Thesis, Delft University of Technology, 2022. Available: https://resolver.tudelft.nl/uuid:c9c1ded2-a0a0-4e95-9d81-5d93e9f54ad2.

[98] S. Asaro and R. Vos, "Synthesis of the Aerodynamic Model of a Flying Wing Aircraft," in *AIAA SCITECH 2025 Forum*, Reston, Virginia: American Institute of Aeronautics and Astronautics, Jan. 2025, isbn: 978-1-62410-723-8. doi: 10.2514/6.2025-0852.

[99] T.J.J. Traas, *Hybrid INDI with enhanced FEP*. MSc. Thesis, Delft University of Technology, 2024. Available: https://resolver.tudelft.nl/uuid:1c3fb8d1-4e7a-4bda-8ce0-537a69fe64f8.

[100] S. van Overeem, X. Wang, and E.-J. van Kampen, “Modelling and Handling Quality Assessment of the Flying-V Aircraft,” in *AIAA SCITECH 2022 Forum*, Reston, Virginia: American Institute of Aeronautics and Astronautics, Jan. 2022, isbn: 978-1-62410-631-6. doi: 10.2514/6.2022-1429.

[101] J. Stougie, T. Pollack, and E.-J. van Kampen, “Incremental Nonlinear Dynamic Inversion control with Flight Envelope Protection for the Flying-V,” in *AIAA SCITECH 2024 Forum*, Reston, Virginia: American Institute of Aeronautics and Astronautics, Jan. 2024, isbn: 978-1-62410-711-5. doi: 10.2514/6.2024-2565.

[102] A. NADZIEJKO, J.-P. Ponchaud, A. Moutinho, S. Saboo, and H.-S. Shin, “Benchmark requirements & performance metrics,” Cranfield University, INCEPTION, 723515-INCEPTION-D2.5, 2018.

[103] T. Pollack, S. Theodoulis, and E. van Kampen, “Commonalities between robust hybrid incremental nonlinear dynamic inversion and proportional-integral-derivative flight control law design,” *Aerospace Science and Technology*, 2024, issn: 12709638. doi: 10.1016/j.ast.2024.109377.

[104] D. BISCHOFF, “THE CONTROL ANTICIPATION PARAMETER FOR AUGMENTED AIRCRAFT,” NAVAL AIR DEVELOPMENT CENTER WARMINSTER PA AIRCRAFT and CREW SYSTEMS TECHNOLOGY DIRECTORATE, 1981.

[105] D. A Kivioja, *Comparison of the Control Anticipation Parameter and the Bandwidth Criterion During the Landing Task*. Thesis, . Air Force Institute of Technology, Wright-Patterson AFB, 1996, vol. AFIT/GAEJENY/96M-2.

[106] Anonymous, *Flight control systems – design, installation, and test of piloted aircraft*, MIL-DTL-9490E, Department of Defense Detail Specification, issued April 22, 2008., 2008.

[107] D. G. Mitchell and R. H. Hoh, “Low-Order Approaches to High-Order Systems: Problems and Promises,” *Journal of Guidance, Control, and Dynamics*, vol. 5, no. 5, pp. 482–489, Sep. 1982, issn: 0731-5090. doi: 10.2514/3.56195.

[108] D. G. Mitchell, D. H. Klyde, R. H. Hoh, and B. L. Aponso, “Proposed incorporation of mission-oriented flying qualities into mil-std-1797a,” Wright Laboratory, Wright-Patterson Air Force Base, OH, USA, WL-TR-94-3162, 1994.

[109] Anonymous, “Flying Qualities of Piloted Aircraft MIL-F-8785C,” 1982.